CHARACTERIZATION OF OROGRAPHIC CLOUD AND PRECIPITATION FEATURES OVER SOUTHERN BAFFIN ISLAND AND SURROUNDING AREA

by

Shannon Elizabeth Fargey

A THESIS

SUBMITTED TO THE FACULTY OF GRADUATE STUDIES OF

THE UNIVERSITY OF MANITOBA

IN PARTIAL FULFILMENT OF THE REQUIREMENTS OF

DOCTOR OF PHILOSOPHY

DEPARTMENT OF ENVIRONMENT AND GEOGRAPHY

UNIVERSITY OF MANITOBA

WINNIPEG, MANITOBA

ABSTRACT

Improved characterization of cloud and precipitation features are required to understand the impact of a changing climate in high latitude regions and accurately represent these features in models. The importance of cold season precipitation to regional moisture cycling and our limited understanding of orographic cloud and precipitation processes in the Arctic provide the motivation for this research. Using high-resolution datasets collected during the Storm Studies in the Arctic (STAR) field project autumn 2007, this thesis examines cloud and precipitation features over southern Baffin Island in Nunavut.

Cloud and precipitation features were shown to differ over orography compared to the adjacent ocean regions upstream through the influence of multiple factors. Gravity waves, terrain shape, atmospheric stability and atmosphere-ocean exchanges were all associated with precipitation enhancement. In addition, factors that reduce precipitation were identified, including high sea ice extent, low-level blocking in the upstream environment and sublimation. The nature of hydrometeors was variable and accretion and aggregation were found to be important determinants of whether precipitation reached the ground over the orography.

The processes controlling a small accumulation snowfall event over southern Baffin Island were found to be complex, representing a significant challenge for predicting and modelling. Several factors were shown to collectively produce the event including low-level convection over adjacent ocean regions, strong upslope flow over the terrain, and the passing of a weak trough. Analysis of the Global Environmental Multi-scale limited area model (GEM-LAM 2.5) revealed that upstream convection and upslope

processes were affected by model errors. Consequently, precipitation onset was delayed and total modelled accumulation was 50% less than observations.

Further evaluation of a numerical weather prediction model during STAR cases provided descriptions of model errors and proficiencies for different synoptic forcing and surface environments. Overall the model overestimated temperature, with the exception of profiles over sea ice where difficulties representing temperature inversions resulted in both positive and negative bias in the vertical profile. The model generally over-predicted moisture, but this was not consistent. Over open water, standard errors for moisture were much larger for cyclonically driven events compared to weakly forced events and in a high sea ice cover environment the model showed a greater tendency to underestimate moisture content. In some profiles the model also had difficulty with moisture over land in dry layers (too dry). Wind speed was frequently underestimated, weakening upslope processes below terrain height and errors in wind direction were large at times. Cloud-tops were usually too high and cloud-bases too low. In cases where multiple cloud layers were present, this feature was well represented, but dry layer depth did not always match observations. Model errors were shown to have implications for cloud and precipitation production and their forecast. Based on evidence from the four case studies, results confirm regional variation in GEM-LAM 2.5 performance in the Arctic, along with variability in its ability to characterize high and mid-latitudes mountainous environments.

ACKNOWLEDGEMENTS

I would like to take the opportunity to thank several people who helped and encouraged me to realize this work.

I express most of my gratitude to my supervisor Dr. John Hanesiak for his patience, support and assistance over the many years it took me to complete this work. I also wish to express my appreciation to Dr. Ronald Stewart for his support. Both of you were always willing to discuss my work and offer invaluable expertise on the subject matter. Thank you for creating an exceptional learning environment for your students. I would also like to thank Dr. Trish Stadnyk for all of her helpful advice and feedback as a member of my advisory committee.

I also express my sincere gratitude to Dr. William Henson for sharing his ideas and advice with me. His continued encouragement helped me succeed. I am glad to have such a great colleague and friend.

This research would not have been possible without the hard work and dedication of the National Research Council and Environment Canada aircraft personnel during the STAR project. A special thank you is extended to Walter Strapp and Dr. Mengistu Wolde for their contributions to this research. I would also like to thank the many STAR collaborators and students. It was a pleasure working with you all. I am especially grateful for the help provided by Ron Goodson and Dr. George Liu.

There are many office mates, fellow students, research associates, post-doctoral fellows and staff at the Centre for Earth Observation Science and in the Department of Environment and Geography at the University of Manitoba, past and present that I would like to acknowledge. Your support through insightful discussions and/or laughter has helped me complete this work. In particular without the support of Lauren Candlish, Dr. Matthew Asplin, Teresa Fisico, Dr. John Iacozza and Robyn Dyck this dissertation would not exist.

I would like also like to thank the different funding agencies that allowed me to pursue this education and publish my work. They include the Canadian Foundation for

Climate and Atmospheric Sciences (CFCAS), the National Research Council of Canada, the Natural Sciences and Engineering Research Council of Canada (NSERC) Post-Graduate Scholarship (PGS-D), the University of Manitoba Graduate Fund (UMGF) and the Northern Studies Training Program (NSTP) grant. Additional funding was provided by the University of Manitoba Graduate Travel Award, the Canadian Meteorological and Oceanographic Society (CMOS) Travel Award, the American Meteorological Society (AMS) Travel Award, and the UK Polar Network Travel Award to present my research at major conferences. Funding for publishing my second manuscript was generously provided to me by AMEC.

Personally I wish to thank my family and friends who supported me while I completed my dissertation, it would have been impossible to finish without you. I would like to thank my parents for always believing in me and teaching me to strive to achieve my goals. You show endless support for everything that I do (big and small) … I am lucky to have both of you.

To Randy, thank you for your love, encouragement and support through this lengthy process. I look forward to our many adventures yet to come …

DEDICATION

This thesis is dedicated to my grandmother Audrey Vera Shaw.

You inspired me to work hard, you encouraged me every step of the way, and you taught me to be grateful for the opportunities that I have been given.

TABLE OF CONTENTS

LIST OF TABLES

LIST OF FIGURES

LIST OF ABBREVIATIONS

2DC	two-dimensional cloud
2DP	two-dimensional precipitation
AMAP	Arctic Monitoring and Assessment Programme
ASL	above mean sea level
AVAPS	Advanced Very High Resolution Radiometer
AVHRR	Airborne Vertical Atmospheric Profiling System
BASE	Beaufort and Arctic Storms Experiment
BMS	bulk microphysical scheme
CAPE	convective available potential energy
CCL	cloud condensation level
CFAD	Contour Frequency Altitude Diagram
CIS	Canadian Ice Service
CISDA	Canadian Ice Service digital archive
COAST	Coastal Observation and Simulation with Topography Project
CV-580	Convair-580 Research Aircraft
DEM	Digital Elevation Model
DFIR	Double Fence Intercomparison Reference
EC	Environment Canada
FIRE-ACE	First International Satellite Cloud Climatology Project Regional Experiment – Arctic Cloud Experiment
Fr	Froude number
GCM	Global Climate Model
GEM	Global Environmental Multi-scale Model
GEM-LAM 2.5	Global Environmental Multi-scale Limited Area Model 2.5 km resolution
GEWEX	Global Energy and Water Cycle Experiment
GPM	Global Precipitation Mission
GPS	Global Positioning System
ICE	Sea ice with concentration greater than or equal to 8/10s
IMPROVE	Improvements of the Microphysical Parameterizations through Observational Verification Experiments
IN	ice nuclei
IOP	Intensive observation period
IPCC	Intergovernmental Panel on Climate Change
IWC	ice water content
LCL	lifting condensation level
LD	Land
LD-ICE	Land with sea ice with concentration greater than or equal to 8/10s upstream
LFC	level of free convection
LPM	Thies Clima Laser Precipitation Monitor
LWC	liquid water content
MAP	Mesoscale Alpine Programme

M-PACE	Mixed-Phase Arctic Cloud Experiment
NARR	North American Regional Reanalysis
NCEP	National Centers for Environmental Prediction
NOAA	National Oceanic and Atmospheric Administration
NRC	National Research Council of Canada
OW	Open water
P	pressure
PPI	Doppler Plan Position Indicator
PMS	Particle Measuring System
RCM	Regional Climate Model
RHI	Range Height Indicator
RID	Rosemont Ice Detector
SCAPE	surface-based convective available potential energy
SCPP	Sierra Cooperative Pilot Project
Se	Standard error
SHEBA	Surface Heat Budget of the Arctic
SNOW-V10	Science and Nowcasting of Olympic Weather for Vancouver 2010 project
STAR	Storm Studies in the Arctic field project
T	temperature
Td	dew-point temperature
TWC	total water content
WBF	Wegener-Bergeron-Findeison process
WISP	Winter Icing and Storms Project

USE OF COPYWRITED MATERIAL

Chapter 2

Chapter 3

Chapter 3 of this thesis is reproduced with minor modifications from Fargey et al. [2014 Aircraft Observations of Orographic Cloud and Precipitation Features over Southern Baffin Island, Nunavut, Canada *Atmosphere*-Ocean *52 (1), 54-76* doi:10.1080/07055900.2013.855624], © Taylor & Francis Publishing. Reprinted with permission.

Chapter 4

Chapter 4 of this thesis is reproduced with minor modifications from Fargey et al. [2014, Characterization of an unexpected snowfall event in Iqaluit, Nunavut and surrounding area during the Storm Studies in the Arctic field project. *Journal of Geophysical Research – Atmospheres, 119* (9), *5492-5511 doi:10.1002/2013JD021176*] © American Geophysical Union. Reprinted with permission.

CHAPTER 1: INTRODUCTION

1.1 Motivation

Considerable attention has been directed toward understanding the impact of increasing temperatures in high latitude regions in recent decades. Although the net effect of warming in the Arctic remains unclear, any change will likely have a profound influence on the hydrological cycle. In the current century Arctic precipitation, an essential component of the hydrological cycle, is expected to increase with the largest projected changes to occur in the cold season (autumn and winter) [*AMAP,* 2011]. Other anticipated changes include an increased tendency for more severe storms, changes in the timing and phase of precipitation seasonally, and increase in cloud cover [*IPCC*, 2013] all of which will influence regional moisture cycling. These changes will also impact local ecosystems as well as have an effect on many communities scattered across the region.

There is already some evidence that precipitation has increased at latitudes above 60°N over the past few decades, however this trend is somewhat uncertain because of the limited number of monitoring stations, particularly in Canada [*IPCC*, 2013]. Due to the challenges and cost of data collection in the north, stations are typically located in easily accessible coastal, low elevation topographies with uneven spatial coverage [*Serreze, Barrett, & Lo,* 2005]. This has resulted in significant knowledge gaps. As a result, the *Arctic Monitoring and Assessment Programme (AMAP)* [2011] highlighted a need for more robust observations for monitoring and model improvement.

Arctic clouds, precipitation and storms have been the focus of previous studies. The formation of snow crystals has been investigated in the western Canadian Arctic since the late 1970s [*Kikuchi & Kajikawa*, 1979; *Magono & Kikuchi*, 1980; *Kikuchi & Taniguchi*, 1990]. More recently, results from the Beaufort and Arctic Storms Experiment (BASE) characterized the cloud and precipitation features, along with the evolution of storms occurring over the Beaufort Sea and the Mackenzie River Basin regions [*Hanesiak, Stewart, Szeto, Hudak, & Leighton*, 1997; *Asuma et al*., 1998; *Burford & Stewart*, 1998; *Hudak & Young*, 2002; *Stewart et al*., 2004]. The microphysical and optical properties of clouds in the Arctic were studied in detail during the First International Satellite Cloud Climatology Project (ISCCP)/Regional Experiment - Arctic Cloud Experiment (FIRE-ACE) [*Curry et al.,* 2000; *Morrison, Zuidema, McFarquhar, Bansemer, & Heymsfield,* 2011], the Mixed-Phased Arctic Cloud Experiment (M-PACE) [*Verlinde et al.,* 2007] and the Surface Heat Budget of the Arctic (SHEBA) [*Uttal et al*., 2002; *Shupe, Matrosov, & Uttal*, 2006] using data mostly collected west of the Canadian Archipelago. Further study of the role of cloud systems in the water cycle was achieved during the Mackenzie Global Energy and Water Cycle Experiment (GEWEX) Study [*Stewart, Szeto, Reinking, Clough, & Ballard,* 1998; *Asuma et al.,* 2000]. Despite these substantial research efforts uncertainties continue especially in the less studied eastern Canadian Arctic.

The eastern Canadian Arctic contains significant topography, which has been shown to play an important role in the production and intensification of cloud systems and precipitation [*Intihar & Stewart*, 2005; *Serreze & Barry,* 2005; *Laplante, Stewart, & Henson*, 2012]. Greater than normal precipitation has been observed in regions where orographic lifting occurs, not only influencing the hydrological cycle [*Walsh, Zhou, Portis, & Serreze,* 1994], but also the radiation budget and regional climate [*Serreze &*

Barry, 2005]. However, studies characterizing snowfall and clouds over high latitude orography remain limited, so our current understanding of orographic precipitation processes and cloud structure has largely come from mid-latitude research [*Hobbs,* 1975; *Smith,* 1979; *Rasmussen et al*., 1992; *Bond et al*., 1997; *Stoelinga et al*., 2001; *Rotunno & Houze*, 2005; *Isaac et al*., 2012; among others]. Although valuable, these studies may not fully represent the processes observed in high latitude regions.

With these overarching issues providing the motivation, it is clear that improved characterization of cloud and precipitation features are required to better understand the impact of a changing climate on the hydrological cycle. Of particular importance is the need to focus on the eastern Canadian Arctic, which contains complex topographies and remains less studied, and investigate cold season precipitation, which is expected to undergo considerable changes.

1.2 Thesis objectives

Given the importance of cold season precipitation and our limited understanding of orographic cloud and precipitation processes in the Arctic, the overarching goal of this thesis is to better understand the physical processes associated with orographic cloud and precipitation in a high latitude mountainous region, with the purpose of providing improved details required by models. This thesis is organised as a series of three research sections that investigate the following objectives:

1. Identify characteristics of orographic clouds and precipitation using high-resolution data collected on southern Baffin Island, Nunavut and surrounding

areas during the Storm Studies in the Arctic (STAR) field project, in autumn 2007.

2. Examine how cloud and precipitation features are modified over the orography compared to the adjacent ocean regions upstream of the terrain, in addition to differences associated with variable event forcing and sea ice extent.
3. Identify factors that influence the characteristics of cloud and precipitation over the orography in the study region.
4. Evaluate the proficiency of a limited area numerical weather prediction model, the Canadian Global Environmental Multi-Scale model 2.5 km resolution (GEM-LAM 2.5), in its ability to characterise the environment of the study region.
5. Gain insight into why some precipitation events are not well forecast by the limited area model (GEM-LAM 2.5).

1.3 Thesis outline

This thesis is comprised of six chapters. The first Chapter, places the topic of this thesis into a broader scientific context. The second Chapter describes the importance and current state of knowledge of cold season orographic precipitation and the various controlling physical processes involved through a comprehensive literature review. The remainder of the thesis is composed of three research papers, each of which makes up an individual chapter.

The first research paper (Chapter 3) analyzes factors that influence cloud and precipitation over the orography of southern Baffin Island. Specifically, three case studies are examined, which provide the basis for identifying the general characteristics of cloud and precipitation in the study region, how these features are modified over the orography and vary with synoptic and sea ice conditions. This work addresses objectives 1, 2, and 3. This work has been peer-reviewed and published in *Atmosphere-Ocean*.

Fargey, S., Hanesiak, J., Stewart, R., and Wolde, M. (2014). Aircraft observations of orographic cloud and precipitation features over southern Baffin Island, Nunavut, Canada. *Atmosphere-Ocean, 52,* 54-76. doi:10.1080/07055900.2013.855624

The second research paper (Chapter 4) characterizes an unexpected high latitude snowfall event over Iqaluit, Nunavut and the surrounding area. The mechanisms that led to the event are examined in detail, providing some insight as to why it was not well forecasted by the Canadian operational limited area model. This work primarily addresses objectives 3, 4 and 5. This work has been peer-reviewed and published in *Journal of Geophysical Research – Atmospheres*.

Fargey, S., Henson, W, Hanesiak, J., and Goodson, R. (2014). Characterization of an unexpected snowfall even in Iqaluit, Nunavut and surrounding area during the Storm Studies in the Arctic field project. *Journal of Geophysical Research – Atmospheres, 119,* 5492-5511. doi: 10.1002/2013JD021176

The third research paper (Chapter 5) evaluates the accuracy of the Canadian operational limited area model during four STAR case studies. Descriptions of model errors and proficiencies are examined for different synoptic forcing and surface environments, including orography, open water and sea ice. The skill of the model is also discussed in the context of its ability to accurately represent clouds and precipitation features. This work predominantly addresses objective 4 and 5, and has been prepared for submission to *Arctic.*

Fargey, S., Hanesiak, J., and Goodson, R. An evaluation of vertical profiles using a limited area numerical weather prediction model over southern Baffin Island and surrounding area during autumn 2007.

In the final Chapter (6) of this thesis, key findings from the three research papers (Chapters 3, Chapter 4 and Chapter 5) are summarized, limitations and future work are discussed, and the concluding remarks of this body of work are presented.

This thesis also contains three appendices. Appendix A describes the contributions of collaborating authors to the work presented in Chapters 3, Chapter 4 and Chapter 5. Appendix B contains supplemental figures used in the analysis for Chapter 5. Appendix C of this thesis lists contributions made as a co-author to publications and technical reports, along with a list of conference presentations during my time as a Ph.D. student at the University of Manitoba.

Overall this thesis will make a significant contribution to improve the understanding of the physical processes associated with orographic precipitation in high latitude mountain environments, as well as provide a number key observations of cloud and precipitation features required by models.

1.4 References

Arctic Monitoring and Assessment Programme (AMAP). (2011). Snow, Water, Ice and Permafrost in the Arctic (SWIPA): Climate Change and the Cryosphere. Oslo, Norway. 538 pages.

Asuma, Y., Iwata, S., Kikucki, K., Moore, G.W.K., Kimura, R., and Tsuboki, K. (1998). Precipitation Features Observed by Doppler Radar at Tuktoyaktuk, Northwest Territories, Canada, during the Beaufort and Arctic Storms Experiment. *Monthly Weather Review, 125,* 2384-2405.

Asuma, Y., Inoune, Y., Kikuchi, Y.K., Kajiokawa, M., Sata, N., and Hayaska, T. (2000). Wintertime precipitation behavior in the western Canadian Arctic region. *Journal of Geophysical. Research, 105, D11,* doi:10.1029/1999JD901124

Bond, N.A., Mass, C.F., Smull, B.F., Houze, R.A., Yang, M.-J., Colle, B.A., Braun, S.A., Shapiro, M.A., Colman, B.R., Neiman, P.J., Overland, J.E., Neff, W.D., and Dolye, J.D. (1997). The coastal observation and simulation with topography (COAST) experiment. *Bulletin of the American Meteorological Society, 78,* 1941-1955.

Burford, J.E. and Stewart, R.E. (1998). The sublimation of falling snow over the Mackenzie River Basin. *Atmospheric Research, 49*, 289-214.

Curry, J.A. Hobbs, P.V., King, M.D., Randall, D.A., Minnis, P., Isacc, G.A., Pinto, J.O., Uttal, T., Bucholtz, A., Cripe, D.G., Gerber, H., Fairall, C.W., Garrett, T.J., Hudson, J., Intrier, I., J.M., Jakob, C., Jensen, T., Lawson, P., Marcotte, D., Nguyen, L., Pilewskie, P., Rangno, A., Rogers, D.C., Strawbridge, K.B., Valero, F.P.J., Williams, A.G., and Wylie, D. (2000). FIRE Arctic Clouds Experiment. *Bulletin of the American Meteorological Society*. 81, 5–29.

Hanesiak, J., Stewart, R.E., Szeto, K., Hudak, D., and Leighton, H. (1997). The structure, water budget, and radiational features of a high-latitude warm front. *Journal of Atmospheric Sciences, 12*, 1553–1573.

Hobbs, P.V. (1975). The nature of winter clouds and precipitation in the Cascade Mountains and their artificial seeding. Part 1: natural conditions. *Journal of Applied Meteorology. 14,* 783-804.

Hudak, D.R. and Young, M.C. (2002). Storm climatology of the southern Beaufort Sea. *Atmosphere-Ocean, 40,* 145-158.

Intihar, M.R. and Stewart, R.E. (2005). Extratropical cyclones and precipitation within the Canadian archipelago during the cold season. *Arctic, 58,* 162-174.

IPCC. (2013). Climate Change 2013: The Physical Science Basis. Contribution of Working Group I to the Fifth Assessment Report of the Intergovernmental Panel on Climate Change [Stocker, T.F., D. Qin, G.-K. Plattner, M. Tignor, S.K. Allen, J. Boschung, A. Nauels, Y. Xia, V. Bex and P.M. Midgley (eds.)]. Cambridge University Press, Cambridge, United Kingdom and New York, NY, USA, 1535 pp.

Isaac G.A., Joe, P. Mailhot, J., Bailey, M., Belair, S., Boudala, F., Brugman, M., Campos, E., Carpenter, R., Crawford, R.W., Cober, S., Denis, B., Doyle, C., Reeves, H., Gultepe, I., Heiden, T., Heckman, I., Huang, L., Milbrandt, J.A., Mo, R., Rasmussen, R., Smith, T., Stewart. R.E., and Wang, D. (2012). Science of nowcasting Olympic weather for Vancouver 2010 (SNOW-V10): A world weather research programme project**.** *Pure and Applied Geophysics, 169*, doi:10.1007/s00024-012-0579-0

Kikuchi, K. and Kajikawa, M. (1979). Comments on V-shaped snow crystals observed in Arctic Canada. *Journal of the Meteorological Society of Japan*, *57*, 484-487

Kikuchi, K. and Taniguchi, T. (1990). Relation between the center nucleus of snow crystals and aerosols particles in Arctic Canada. *Jour. Fac. Sci. Hokkaido Univ. Ser. 8,* 415-435.

Laplante, A., Stewart, R., and Henson, W. (2012). Characterization of cloud and precipitation features over southern Baffin Island and adjacent areas during STAR. *Atmosphere-Ocean*, *50*, 54-69. doi:10.1080/07055900.2011.646535.

Magono, C. and Kikuchi, K. (1980). Some observations of snowfall and meteorological conditions in Arctic Canada. *Monthly Weather Review, 108,* 1656-1664.

Morrison, H., Zuidema, P., McFarquhar, G.M., Bansemer. A., and Heymsfield, A.J. (2011). Snow microphysical observations in shallow mixed-phase and deep frontal Arctic cloud systems. *Q. J. R. Meteorol. Soc.,* 137: 1589–1601.

Rasmussen, R., Poliovich, M., Sand, W., Stossmeister, G., Bernstein, B., Elmore, K., Marwitz, J., McGinley, J., Smart, J., Westwater, E., Standkov, B.B., Pielke, R., Rutledge, Wesley, S.D., Powell, N., and Burrows, D. (1992). Winter Icing and Storms Project (WISP). *Bulletin of the American Meteorological Society, 73*, 951–974.

Rotunno, R. and Houze, R.A. (2007). Lessons on orographic precipitation from the Mesoscale Alpine Programme. *Quarterly Journal of the Royal Meteorology Soc*iety, *133,* 811–830.

Serreze, M.C. and Barry, R.G. (2005). The Arctic Climate System. Cambridge University Press. Cambridge, England, UK. 385 pages.

Shupe, M.D., Matrosov, S.Y., and Uttal, T. (2006). Arctic mixed-phase cloud properties derived from surface-based sensors at SHEBA. *Journal of Atmospheric Sciences, 63*, 697-711.

Smith, R.B. (1979). The influence of mountains on the atmosphere. *Advanced Geophysics, 21***,** 187-230.

Stewart, R.E., Szeto, K.K., Reinking, R.F., Clough, S.A., and Ballard, S.P. (1998). Midlatitude cyclone cloud systems and their features affecting large scales and climate, *Reviews of Geophysics*. 36, 245-273.

Stewart, R.E., Burford, J.E., Hudak, D.R., Currie, B., Kochtubajda, B., Rodriguez, P., and Liu, J. (2004). Weather systems occurring over Fort Simpson, Northwest Territories, Canada, during three seasons of 1998–1999: Part 2. Precipitation features. *Journal of Geophysical Research, 189,* 1984-2012.

Stoelinga, M.T. Hobbs, P.V., Mass, C.V., Locatelli, J.D., Colle, B.A. Houze, R.A., Rangno, A.L., Bond, N.A., Smull, B.F., Rasmussen, R.M., Thompson, G., and Colman, B.R. (2003). Improvement of microphysical parameterization through observational verification experiment (IMPROVE)**.** *Bulletin of the American Meteorological Society, 84,* 1807–1826.

Uttal, T.U., Curry, J.A., McPhee, M.G., Perovich, D., Moritz, R.E., Maslanik, J.A., Guest, P.S., Stern, H.L., Moore, J.A., Turenne, R., Hieberg, A., Serreze, M.C., Wylie, D.P., Persson, O.G., Paulson, C.A., Halle, C., Morison, J.A., Wheeler, P.E., Makshtas, A., Welch, A., Shupe, M.D., Intrieri, J.M., Stamnes, K., Lindsey, R.W., Pinkel, R., Pegau, W.S., Stanton, T.P., and Grenfeld, T.C. (2002). Surface heat budget of the Arctic Ocean *Bulletin of the American Meteorological Society, 82***,** 255-275.

Verlinde, J., Harrington, J.Y., McFarquhar, G.M., Yannuzzi, V.T., Avramov, A., Greenberg, S., Johnson, N., Zhang, G., Poellot, M.R., Mather, J.H., Turner, D.D., Eloranta, E.W., Zak, B.D., Prenni, A. J., DanieL, J.S., Kok, G.L., Tobin, D.C., Holz, R., Sassen, K., Spangenberg, D., Minnis, P., Tooman, T. P., Ivey, M.D., Richardson, S.J., Bahrmann, C P., Shupe, M., Demott, P. J., Heymsfield, A.J., and Schofield, R. (2007). The mixed-phase Arctic cloud experiment. *Bulletin of the American Meteorological Society*, *88,* 205-222.

Walsh, J.E., Zhou, X., Portis, D., and Serreze, M.C. (1994). Atmospheric contribution to hydrological variations in the Arctic. *Atmosphere-Ocean, 34,* 733-755.

CHAPTER 2: BACKGROUND AND LITERATURE REVIEW

This chapter describes the importance and current state of knowledge of cold season orographic precipitation and the various controlling physical processes involved with an emphasis on high latitude environments whenever possible.

2.1 Introduction

Orographic precipitation is precipitation that is either induced, or enhanced, by the lifting of air over an orographic barrier such as a mountain range [*Smith,* 1979]. Orographic lifting has been identified as an important mechanism for the production and intensification of precipitation in both synoptic and local storm systems [*Houze,* 1993; *Smith,* 2006] and it is a critical component of the hydrological cycle, with greater than normal precipitation totals observed in regions where orographic lifting occurs [*Serreze & Barry,* 2005] (Figure 2.1). Clouds associated with orographic precipitation also influence the high latitude radiation budget and regional climate [*Serreze & Barry,* 2005]. Depending on height and microphysical composition, orographic clouds either increase the backscatter of solar radiation, resulting in a cooling effect, or absorb and re-emit thermal radiation of land or ocean origin, resulting in a warming effect.

Figure 2.1: Mean annual precipitation (mm) based on available bias-adjusted data sources. Contour intervals are 100 mm (solid for amounts up to 600 mm) and 200 mm (dotted for amounts 800 mm and greater) (From Serreze & Barry, 2005 © Cambridge University Press. Reproduced with permission)

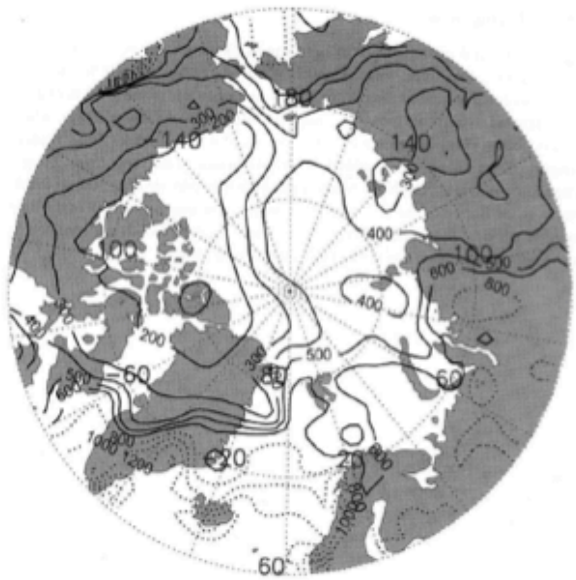

Despite the recognized importance that orography has on precipitation and radiative processes, the meteorology of most mountain areas - particularly at high latitudes - are poorly understood [*Intihar & Stewart,* 2005]. This is largely attributable to the challenges in data collection. Weather stations are sparse, uneven in spatial coverage, and declining in number over the last decade [*Serreze, Barrnett, & Lo,* 2005]. Stations are typically located in easily accessible valley or coastal settings, and not in high elevation topographies. Furthermore, orographic precipitation amounts are subject to error due to significant losses from wind effects incurred during the measurement process. Errors in precipitation amount measured at high latitude stations range from 50 to 100% [*Serreze & Barry,* 2005]. Precipitation data from remote sensing platforms, such as ground, airborne, or spaceborne radar, represent their own challenges. The distribution of ground radars at high latitudes is uneven and regionally specific, with no permanent radar systems in the Canadian Arctic. While airborne radars are becoming an increasingly common tool for investigating precipitation processes in poorly accessible areas, high latitude data remain limited due to cost and accessibility. Spaceborne radar is also an effective tool that provides greater spatial and long-term temporal coverage compared to airborne radar studies, though further validation of satellite-derived precipitation is required [*de Boer et al.,* 2008].

There are large uncertainties in modelled scenarios of meteorological features such as snowfall and clouds in regions where orographic lifting occurs [*IPCC*, 2013]. Operational and climate model uncertainties are due in part to a lack of validation observations, but also to the coarse horizontal and vertical model scales relative to topographic features. The typical horizontal resolution of a Global Circulation Model (GCM) is 2.5° in latitude, with a fine-mesh embedded model of 1° resolution, resulting in a smoothed representation of topography. As such, mean elevations are lowered and details of valley-ridge systems are lost [*Barry,* 2008]. The Canadian Global Environmental Multi-Scale (GEM) operational model operates at 15 km regional and 2.5 km limited area model (GEM-LAM) grid cell resolutions, have mountain grid scales that are too coarse to adequately resolve complex interactions between ambient flow and topography occurring at finer scales [*Zadra, Roch, Laroche, & Charron,* 2003]. Modelling orographic precipitation in high latitude environments is further challenged by model parameterizations for clouds, radiation, and precipitation producing mechanisms developed for regions with thermodynamic characteristics that are not representative of a high latitude system [*Lachlan-Cope*, 2010].

This chapter outlines the importance and current state of knowledge of cold season (October to April) orographic precipitation, and describes the physical processes that control orographic precipitation in a high latitude polar environment (>60° north and south). Section 2.2 describes the basic dynamic, thermodynamic, and microphysical processes involved in the formation of orographic precipitation. In section 2.3, the atmospheric flow response to orographic barriers, as well as how the shape of the topography and incoming flow characteristics control orographic precipitation magnitude and distribution, are described. This chapter will conclude with a summary of the unresolved challenges associated with orographic precipitation data collection methods and modelling, which are required to more accurately represent orographic precipitation processes in operational and climate models.

2.2 Formation of orographic precipitation

The formation of orographic precipitation can be broken down into three main components: (1) large-scale flow towards a topographic barrier; (2) orographic lifting of (1), which cools the air to saturation and initiates condensation; and (3) conversion of condensate to precipitation particles through microphysical processes [*Rotunno & Houze,* 2007].

These factors constitute a general framework for orographic precipitation formation, but in reality the interactions of the above processes are complex and can vary substantially from one situation to the next depending on ambient atmospheric conditions (flow strength, stability, moisture, temperature) and terrain geometry (mountain height, and width). The interaction of these parameters and their influence on orographic precipitation will be discussed in more detail in section 2.3. The purpose of this section is to review the basic processes involved in cloud and precipitation formation over topography.

2.2.1 Atmospheric motion

The atmosphere must be in motion for it to be modified by topography. Circulation patterns, on a wide variety of scales, are driven by differential heating (the distribution of solar radiation) between low (excess) and high latitudes (deficit) [*Serreze & Barry*, 2005].

The movement of air in the atmosphere is described by Newton's second law of motion, which can be written to represent the forces that affect the motion of a unit mass of air, via equation 2.1:

$$\frac{Dv}{Dt} = -\frac{1}{\rho}\nabla p - fk \times v - gk + F \tag{2.1}$$

where *t* is time, and *v* is the three-dimensional wind velocity of an air parcel (v = ui +vj + wk, where i, j, and k are unit vectors in the x, y, and z directions) [*Houze,* 1993]. The total derivative is the time derivative following an air parcel ($D/Dt=(\partial/\partial t)+v\cdot\nabla$) through the atmosphere.

The pressure gradient force (PGF), the first term in equation 2.1, where ρ is air density and *p* is air pressure, sets the air into motion, causing it to move from an area of high to low pressure. The ∇ is the three-dimensional gradient operator, shown in equation 2.2 [*Houze,* 1993]:

$$\nabla p = \frac{\partial p}{\partial x} i + \frac{\partial p}{\partial y} j + \frac{\partial p}{\partial z} k \tag{2.2}$$

Air flowing across a pressure gradient is further subject to external forces, which modify its direction of flow. The Coriolis force ($f = 2 \cdot \Omega \cdot \sin(\phi)$), the second term in equation 2.1, describes the influence of the Earth's rotation on moving air, where $2{\cdot}\Omega = 1.458 \times 10^{-4}\ s^{-1}$ is the angular velocity of the Earth and ϕ is the latitude angle [*Houze*, 1993]. The Coriolis force deflects air motion to the right (left) in the northern (southern) hemisphere and is strongest at the poles. The gravitational acceleration force (g) is the third term in equation 2.1. It represents the true gravitational acceleration (g*), which draws all elements of mass towards the Earth's centre of mass and the centrifugal force ($\Omega^2 R_A$), where Ω is the rotation rate and R_A is the distance from the axis of rotation. The last force represented in equation 2.1 is friction. At the Earth's surface the air experiences frictional resistance (drag), thus acting to counteract forward momentum. When horizontal winds flow over roughness elements along the surface, drag slows the wind near the surface relative to the wind aloft, creating vertical wind shear. Wind shear produces eddies that exchange momentum and energy vertically. The greater the height that the roughness elements protrude from the surface, and the greater the horizontal wind speed, the greater the resulting wind shear and vertical flux of horizontal momentum. The frictional force (F) is given by equation 2.3:

$$F = -\frac{1}{\rho} \cdot \frac{\partial \tau}{\partial z} \tag{2.3}$$

where, τ represents the vertical component of shear stress (the applied force per unit area) [*Wallace & Hobbs,* 2006].

Now that an air mass is in motion, it must have sufficient kinetic energy input in order to rise against the force of gravity and be lifted over a topographic barrier, or otherwise be blocked by that barrier. This determined by the strength of flow and the stability of the atmosphere in relation to the characteristics of the topography (height, width). Typically, the Froude number (*Fr*) is used as an indicator for the tendency of air to flow over or around an obstacle, equation 2.4:

$$Fr = \frac{U}{Nh^{1/2}} \tag{2.4}$$

where *U* is the wind speed, *h* is the height of the mountain [*Barros & Lettenmaier*, 1994]. *N* is the Brunt-Vaisala frequency, via equation 2.5:

$$N_{BV} = \sqrt{\left(\frac{g}{T_v} \cdot \frac{\Delta\theta_v}{\Delta z}\right)} \tag{2.5}$$

where *g* is acceleration of gravity, T_v is virtual temperature, θ_v is virtual potential temperature and *z* is height [*Stull*, 2000]. For relatively dry air it is often assumed that T_v is equal to temperature and, θ_v is equal to potential temperature [*Stull,* 2000]

The Froude number is interpreted as the ratio of kinetic energy of air encountering a barrier to the potential energy necessary to cross over the barrier. A large (small) *Fr* results from strong (weak) cross-barrier flow and low (strong) static stability and infers that flow over the barrier will be lifted (blocked).

2.2.2 The ideal gas law

The fundamental empirical and theoretical law that underlies all atmospheric sciences is the ideal gas law (equation 2.6) from *Tsonis* [2002]:

$$\mathrm{PV} = \mathrm{nR^*T} \quad or \quad \mathrm{P} = \rho RT \tag{2.6}$$

In its classical form (left), *P* is pressure, *V* is volume, n is the number of moles of a gas, R^* is the gas law constant 8.314 J·K^{-1}mol^{-1}, and *T* is temperature. The equation on the right is more common in atmospheric sciences, where R is derived from R^*, where $R=(R^*/M_m)$ and M_m is the molar mass of the gas (or mixture of gases). The ideal gas law is the equation of state that explains the thermodynamic behaviour of atmospheric gases and relates P, T and V.

2.2.3 Mechanisms of orographic precipitation production

Orographic lifting of air over a barrier will form clouds and precipitation through three primary generation mechanisms: upslope condensation, convection, and the seeder-feeder process [*House,* 1993]. The basic mechanisms of orographic precipitation production rarely act independently, but are discussed individually to better understand their unique contributions.

2.2.3.1 Upslope condensation

The simplest conceptual model of orographic formation is by upslope lifting and condensation (Figure 2.2). Using the concept of the ideal gas law from the previous section and the first law of thermodynamics, which states that energy, can neither be created nor destroyed [*Tsonis*, 2002]; the development of orographic cloud systems and precipitation can be understood. A parcel of unsaturated air is forced to rise over terrain, causing it to expand, due to the lower ambient air pressure, and cool. Under the assumption that no heat is lost from the parcel to the surrounding environment it ascends adiabatically at Γ_{dry} (9.8°C km^{-1}), where Γ_{dry} is equal to g/cp, cp is the specific heat capacity of dry air at constant pressure. The parcel of air will become saturated when the partial pressure of water vapour within it reaches a critical value known as the saturation vapour pressure. Because the cloud can consist of suspended liquid drops and ice crystals, saturation vapour pressure must be considered with respect to water and ice. Saturation vapour pressure (e_s) is given by the Clausius-Clapeyron relationship, via equation 2.7 [*Stull,* 2000]:

$$e_s = 0.611 \cdot exp\left[\frac{L}{\Re_v} \cdot \left(\frac{1}{T_0} - \frac{1}{T}\right)\right] \tag{2.7}$$

where $\Re_v$ is the gas constant for water vapour (461.5 J·K^{-1}·kg^{-1}), T_0 = 273 K, and T is ambient temperature in Kelvin. When considering saturation vapour pressure with respect to water, L in equation 2.7 is the latent heat of vaporization over water L_v = 2.5 x 10^6 J kg^{-1}. When considering saturation with respect to ice, L in equation 2.7 is the latent heat of deposition L_d = 2.83 x 10^6 J kg^{-1}. Once saturated, water vapour will begin to condense into either liquid drops or ice crystals, forming clouds (Figure 2.2). This height in the atmosphere is called the lifting condensation level (LCL).

Figure 2.2: Illustrations of different mechanisms of orographic precipitation. (left) stable upslope ascent; (middle) partial blocking of an impinging air mass; and (right) seeder-feeder mechanism (From Roe, 2005. Reprinted with permission from the Annual Review of Earth and Planetary Sciences, Volume 33 © 2005 by Annual Reviews, http://www.annualreviews.org).

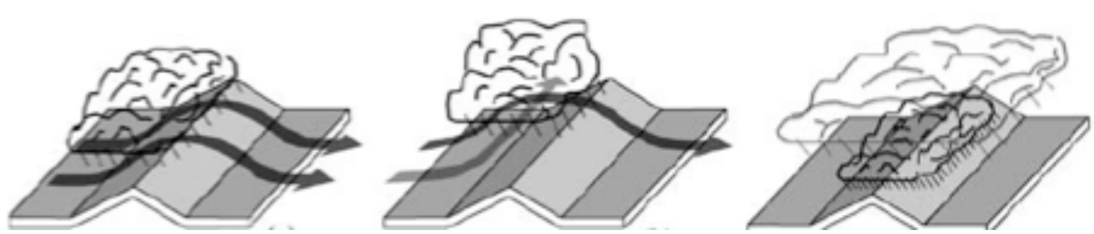

As the parcel continues to rise in the atmosphere, the pressure decreases, the volume expands, while simultaneously the T and e_s continue to decrease. The lifting of a saturated parcel results in cooling at a lesser rate, the saturated-adiabatic lapse rate Γ_m, due to the release of latent heat, which partially offsets cooling. The Γ_m (equation 2.8) is not constant and varies greatly with temperature and humidity content in the atmosphere [*Stull,* 2000]:

$$\Gamma_m = g \frac{1+\frac{L_v r_v}{RT}}{cp+\frac{{L_v}^2 r_v \varepsilon}{RT^2}} \tag{2.8}$$

where r_v is the mixing ratio of water vapour, ε is the ratio of the gas constants for dry air and water vapour Rd/Rv = 0.622 g g^{-1}.

When -20°C ≤ T ≤ 0°C, $\Gamma_{dry} \approx \Gamma_m$ as cold clouds do not produce as much liquid water as warm clouds (equation 2.7). Average Γ_m in cold clouds has been estimated to be between 7.0 °C km^{-1} and 8.0°C km^{-1} [*Barry*, 2008].

The amount of condensation for saturated air, subject to orographic lifting, will be dependent on: (1) the lifting depth; (2) the amount of air lifted; (3) the moisture content and (4) the speed of the rising air. This relationship is described in equation 2.9 [*Barry,* 2008]:

$$c = \int_z \ pw \frac{dr_s}{dz} dz \tag{2.9}$$

where c is the condensation rate, r_s is the saturation mixing ratio - the ratio of the mass of water vapour in a given volume of air that is saturated, to the mass of dry air - and w is the vertical velocity. Thus the condensation rate will decrease with decreasing temperatures and increasing altitude [*Wallace & Hobbs,* 2006].

Nucleated cloud particles grow through various microphysical processes (see section 2.3). When they reach a critical size or weight, where the internal updrafts of the cloud can no longer support particle suspension, they fall as precipitation [*Reinking & Boatman,* 1986].

2.2.3.2 Convection

If the air parcel rising over the terrain is orographically lifted above the level of free convection (LFC), the parcel then becomes less dense than its surroundings and continues to rise convectively. Convective cells usually enhance condensation processes locally and can produce greater amounts of super-cooled water, leading to increased growth rates of ice particles [*Houze & Medina,* 2005]. Convective cells formed by orographic uplift are usually embedded with a larger-scale process such as the lifting of fronts during the cold season [*Medina & Houze,* 2005], although they can also be an isolated feature [*Houze,* 1993]. During the high latitude cold season, convective cells can also form over open water in coastal regions [*Hanesiak et al.,* 2010]. Depending on the large-scale flow regime, these features can further interact with topography. The importance of embedded convective cells in orographic precipitation systems will be discussed in detail in sections 2.3.2 and 2.3.3.

2.2.3.3 Seeder-feeder

The seeder-feeder mechanism was originally proposed to explain the amplification of precipitation over hills that were too small to generate precipitation themselves because the air would traverse the barrier too quickly for hydrometeors to form alone [*Bergeron,* 1949]. In this instance the seeder-feeder process occurs when you have multiple cloud layers, referring to the presence of an upper-level cloud, not formed by orographic lifting, and a smaller shallower cloud produced from upslope ascent over topography [*Houze*, 1993]. Enhancement occurs as precipitation from an upper-level cloud (seeder) falls through the lower-level shallow orographic cloud (feeder) (Figure 2.2). Precipitation particles from the seeder cloud and collects cloud water as they pass through the feeder cloud or aggregate with other particles, which can results in more enhanced and larger precipitation particles then would have occurred in absence of the shallow orographic cloud. The second usage in the literature of a seeder-feeder mechanism relates to the presence of embedded convective cells within a larger-scale precipitating cloud. Under these conditions the cloud can be considered to have a seeder region (embedded convective cells) and a feeder region (remainder of the cloud) [*Roe,* 2005]. The small-scale convection produces particles, which then fall through the cloud and grow through aggregation and accretion processes.

In *Bergeron* [1949], the seeder-feeder process was shown to be particularly important in orographic precipitation enhancement in Norway. Low-level winds were observed to pick up significant moisture upstream when travelling over the ocean. The warm moist air becomes saturated and can produce thick low-level clouds as it ascends over the cold boundary layer air trapped in fjords. When precipitation from a larger synoptic scale system passes over the region, precipitation is enhanced.

2.2.4 Microphysical processes

Several microphysical processes, i.e. pathways and interactions, influence the formation and growth of cloud ice and cloud water particles, as well as the distribution of condensation as precipitation over the landscape. This section outlines growth processes of precipitation particles in cold clouds (≤ 0°C), either ice (glaciated clouds) or mixed-phase (a combination of supercooled water drops and ice crystals) because they have both been identified to be present during the high latitude cold season [*Curry, Rossow, Randall, & Scharamm,* 1996]. The dominant form of precipitation in orographic precipitation events during the cold season is solid, but during the shoulder seasons, rain and freezing rain or freezing drizzle events can occur [*Gascon, Stewart, & Henson*, 2010].

2.2.4.1 Nucleation of cloud particles

Cloud particles, known as *hydrometeors*, form when the atmosphere becomes saturated through a process called nucleation, which is distinguished as either homogenous or heterogeneous. Homogeneous nucleation occurs without the presence of an aerosol or containment particles (AP), a process which is impossible in natural warm clouds (≥ 0°C) because of the unrealistic levels of supersaturation required for vapour to condense without AP. Conversely, homogeneous nucleation of liquid drops can occur in cold clouds when T ≤ -40°C. Ice embryos, clusters of ~250 molecules at -40°C, form when water molecules become aligned and bond with the specific orientations. At this point the water drops will spontaneously freeze forming an ice nuclei (IN) [*Stull,* 2000].

In cold clouds, IN may be any AP that serves as a nucleus for the formation of ice crystals. Heterogeneous nucleation of IN at temperatures occurs by several modes, including: (1) deposition; (2) condensation freezing; (3) immersion; and (4) contact [*Pruppacher & Klett,* 2000].

- *Deposition mode* occurs when water vapour is absorbed directly on an IN;

- *Condensation freezing* occurs when a cloud condensation nuclei (CCN) acts to form a drop and at some point in the condensation process the drop freezes;
- *Immersion mode* occurs when an IN becomes immersed in a water drop at temperatures warmer than 0°C. Freezing in initiated when the temperatures drop sufficiently low; and
- *Contact mode* occurs when a supercooled water droplet comes in contact with an IN and immediately initiates the ice phase particle.

Cloud particles can also form from secondary processes not involving nucleation, called *ice enhancement*. Ice enhancement can result from: (1) rime/splintering; (2) drop shattering; and (3) fragmentation of existing ice crystals [*Rangno & Hobbs,* 2001].

- *Splintering* occurs when supercooled drops collide with an ice particle and freezes symmetrically inward so that unfrozen water drop remains trapped beneath the shell. As the internal drop freezes and expands it exerts significant pressure, which can cause it to shatter into numerous ice splinters
- *Drop shattering* occurs when isolated supercooled drops > 50 μm begins to freeze symmetrically inward so that unfrozen water drop remains trapped beneath the shell. When the internal drop begins to freeze and expand, it can cause the frozen drop to shatter into numerous pieces; and
- *Fragmentation* occurs as a result of collisions between ice crystals (either crystal-crystal or crystal-liquid drop) in the cloud causing part, or all, of a particle to break.

2.2.4.2 Growth by deposition

Deposition refers to the growth of an ice particle by diffusion of a vapour from the ambient environment or water particle to the ice particle. This process is the fundamental method of growth in cold clouds. This process occurs as a result of the lower e_s of ice relative to water at the same temperature, which means that ice crystals will grow from the vapour phase at a lower humidity than water would in the same environment (Figure 2.3) [*Stull,* 2000].

Figure 2.3: (left) Saturation vapour pressure over flat surfaces of pure liquid water and ice at temperatures below 0°C. The inset shows the difference between saturation vapour pressures over water and ice; and (right) Enlargement from inset (saturation vapour pressure vs. temperature), illustrating the WBF ice growth process of a rising air parcel. Spheres represent cloud water droplets and hexagons represent ice crystals. Small arrows indicated movement of water vapour. (From Stull, 2005 © Brooks/Cole. Reproduced with permission)

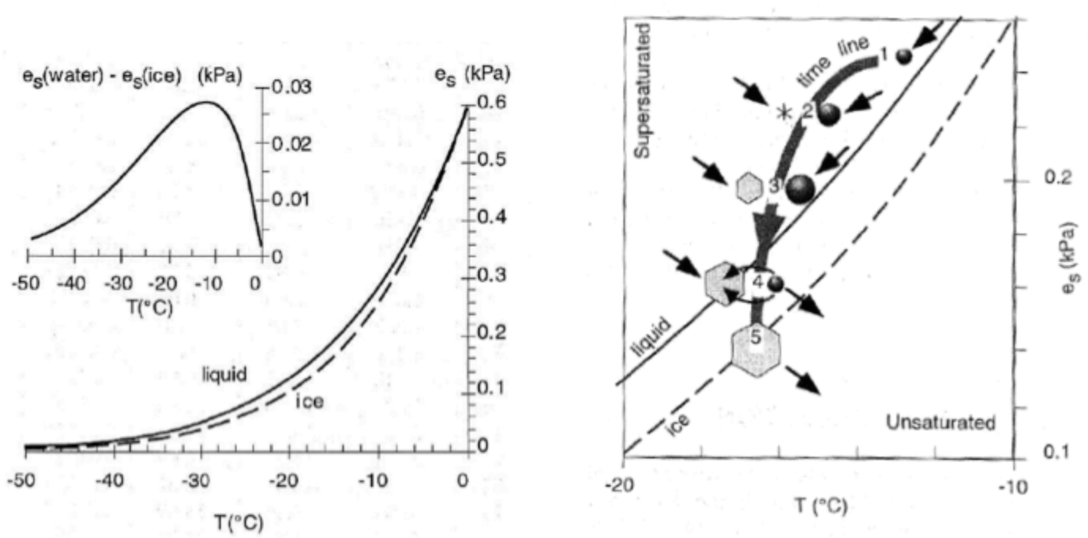

When the difference in vapour pressure causes water vapour molecules to move (diffuse) from the liquid drops to ice crystals, this process can be called the Wegener-

Bergeron-Findeisen (WBF) process. At position 4 along the timeline shown in Figure 2.3, the relative humidity is below 100% with respect to water, which results in evaporation of the liquid drop. The ice crystal will continue to grow by diffusion because the air is still saturated with respect to ice. The ice crystal grows at the expense of liquid drop until the drop has disappeared, the ice crystal has fallen out of the cloud, or the ambient environmental conditions become unsaturated and the ice crystal begins to sublimate (position 5 in timeline of Figure 2.3). The largest difference between the e_s of water and ice occurs between the temperature range of -8°C and -16°C (Figure 2.3), therefore the effect of growth by the WBF process will be greatest between these temperatures.

Once an ice particle has been nucleated and growth is initiated, the ice crystal continues to grow by deposition into a variety of shapes, termed *habits*. In 1966, *Magono and Lee* proposed a meteorological classification using the temperature and vapour supply to define various types of natural ice habits. Observations in both laboratory experiments and natural clouds are in good agreement with the Magono-Lee diagram [*Pruppacher & Klett,* 2000], particularly with respect to the behaviour of ice crystals at -18°C ≥ T ≤ 0°C. However, some minor deviations of ice crystal habits have been observed at T < -20°C due to the presence of irregularly shaped polycrystalline ice crystals [*Bailey & Hallet,* 2009]. Based on this observation, *Bailey and Hallet* [2009] provided some additions to and revised the *Magono and Lee* [1966] diagram (Figure 2.4).

Figure 2.4: Temperature and humidity conditions for the growth of natural snow crystals of various types. Habit diagram, in pictorial format, for atmospheric ice crystals derived from laboratory results and CPI images gathered during AIRS II and other field studies (From Bailey & Hallett, 2009 © American Meteorological Society. Used with permission).

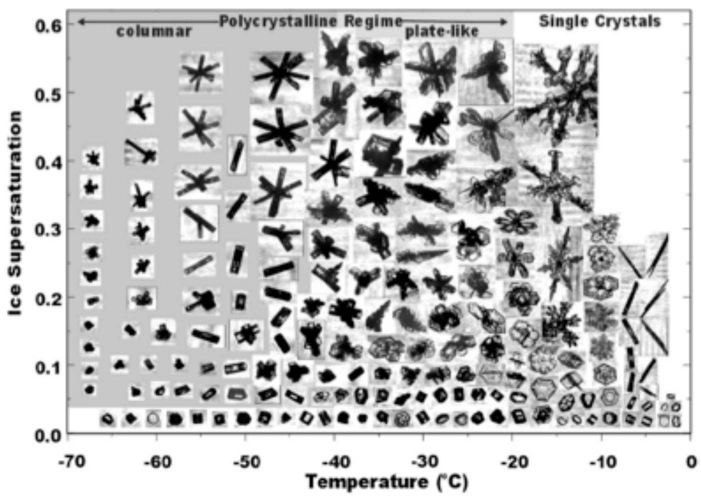

<u>2.2.4.3 Growth by accretion (riming)</u>

Growth by accretion occurs in mixed phase clouds when an ice crystal collides with a supercooled liquid droplet, causing it to freeze on impact. The additional ice collected on the particle during collisions is called *rime*. Concurrent with growth is an increase in particle density and the evolution of its shape. Particles can be denoted as being lightly, moderately, to densely rime covered. When the original particle shape is no long recognizable, the ice particle is termed *graupel*, or *snow pellet*. The ability of any ice crystal to grow by this process is determined by the size and shape of the crystal, the size of the supercooled drops it encounters and the fall velocity [*Harimaya,* 1975].

Research has shown that ice crystals usually grow to a critical size (dependant on particle habit) by deposition before they can further grow by riming [*Hobbs, Chang, & Locatelli,* 1971; *Harimaya,* 1975]. For example, in *Harimaya* [1975] riming did not occur until plate particles reached a size of ~150 μm, while the onset of riming did not occur until dendrites reached a size of ~800 μm. The onset of riming is also related to the diameter of the supercooled water drops. Drops in the range of 10-80 μm are most commonly observed on ice crystals. Drops smaller and larger are generally absent. An increase of rime on an ice crystal will increase the mass of the particle. *Locatelli & Hobbs* [1974] investigated fall speeds of ice crystals and found that fall speeds have tendency to increase with an increase in mass, increase in size and increase in the degree of riming.

Figure 2.5 Hydrometeor trajectories of ice particles grown by riming and deposition and by deposition alone over multi-scale terrain, where A-B denotes starting positions; three trajectories correspond to a specified ice particle concentration (1 (·····), 25 (----) and 100 (—) L^{-1}); (c) same as (b) but trajectories over simple terrain (From Hobbs et al., 1973 © American Meteorological Society. Used with permission).

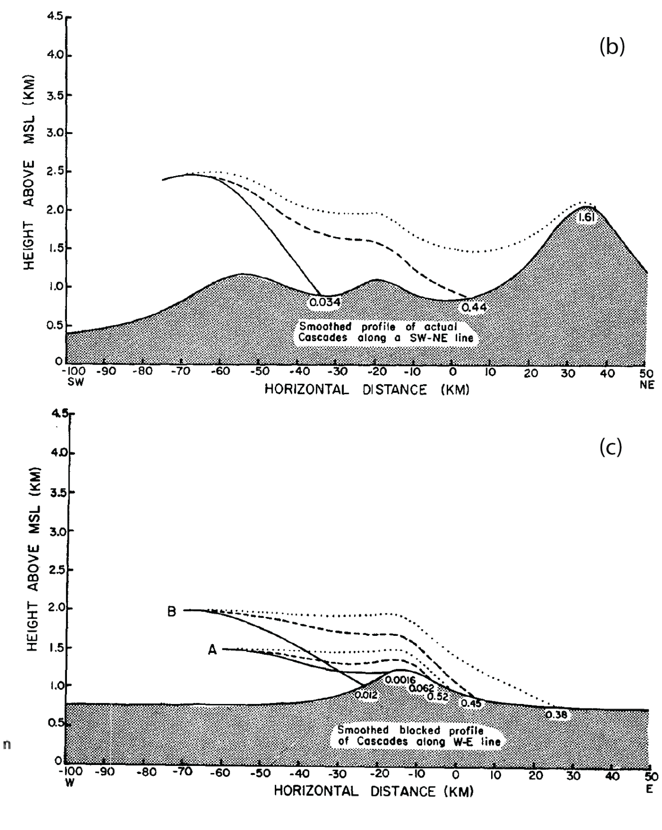

2.2.4.4 Growth by aggregation

Ice particles grow by aggregation when one or more particles collide. Whether or not particles will adhere when they collide, is determined by the shape of the hydrometeor, the temperature and the terminal velocity [*Pruppacher & Klett,* 2000]. The *collection efficiency* can be used as a dimensionless measure of the tendency for the collision of particles and/or the collection, the aggregation, of particles.

Hydrometeors such as dendrites have intricate details on their branches, and have a tendency to adhere to other crystals when they become entwined on collision, whereas two plates have a tendency to rebound away from each other if they collided. With respect to temperature, the success of particle aggregation has been found to greatly increase if the temperatures are > -5°C, at which time the surfaces of the ice particles become 'sticky'. *Hobbs et al.* [1974] found that the probability of occurrence of aggregates decreases with decreasing temperatures, exhibiting a local maximum near the dendrite growth region (Figure 2.5). Aggregates have generally been observed fallout faster than a single crystal of the same habit because of the increase in particle density [*Locatelli & Hobbs*, 1974], which results in different fallout velocities in the cloud, allowing for an increase in possible collisions between particles. The collection efficiency has been found to increase with increasing crystal size, which increases the likelihood for particle interactions and decrease when particles in the cloud approach similar fall velocities. At this time they are not likely to collide with each other [*Pruppacher &Klett,* 2000].

2.2.4.5 On the influence of ice nuclei concentration

The concentration of IN can affect the number of hydrometeors that form and their evolution in the cloud [*Roe,* 2005]. By increasing the IN concentration, cloud particles are smaller, more numerous, and exhibit slower growth rates. As a result, they are less dense, have slower fall speeds, and more likely to be advected over the crest of the mountain into the lee-side (Figure 2.5c) [*Hobbs, Easter, & Fraser,* 1973]. Lower IN concentrations promote growth of individual particles at a faster rate than if more IN were present. This implies that growth processes such as accretion, and aggregation can occur faster once particles became large enough, thereby increasing particle mass, fall out time and speeds. In a modeled trajectory analysis, *Hobbs et al.* [1973] observed that rimed particles had a greater tendency to fallout on windward slopes. Over multi-scale terrain (Figure 2.5c), the addition of successive ridges produces secondary updraft regions that further promotes growth and advection beyond trajectories observed in Figure 2.5b.

2.2.4.6 Particle habit observations at high latitudes

Observations of particle habits are important for characterizing orographic precipitation regionally. Knowledge of particle habit has implications for inferences from remote sensing instrumentation and modelling (further discussed in section 2.4). Some observations of high latitude habits are summarized here.

The microphysical properties of cold season precipitation were investigated on the Antarctic plateau by *Lawson et al.* [2006]. They found that that 30% of ice crystals were rosette shaped (combination bullets); 45% were columns, thick plates, and plates; and

25% were irregularly shaped. *Walden, Warren and Tuttle* [2003] observed similar distributions of particle habits in the winter of 1993. Higher accumulation precipitation events were attributed to the presence of combination bullets, and 'diamond dust' events were associated with columns and plates.

In contrast, *Korolev, Isaac and Hallett* [1999] found that irregularly shaped ice crystals accounted for > 95% of particle shapes in the Arctic. They showed that the high concentrations of irregularly shaped particles were in part due: (1) to the presence of polycrystalline particles, consisting of combinations of different habits growing in different directions; (2) particles that had been subject to partial sublimation altering their shape; and (3) heavily rimed dendrites and dendrites with some imperfections. It is unknown from this study if they started as irregularly shaped or began as a pristine crystal and were modified by other processes. It is worth mentioning that observations by *Korolev et al.* [1999] are from the western Canadian Arctic, where no orographic lifting occurred. However, the study contains valuable information about particle habits in the Arctic and it is worth mentioning. Some similarities can be drawn from this study to ones where orographic lifting has occurred.

Rimed particles and aggregates of multiple habits were observed in storms over Baffin Island in the eastern Canadian Arctic [*Roberts, Nawri, & Stewart,* 2008; *Henson, Stewart, & Hudak,* 2011]. Fragments of rimed dendrites and other habits were identified, indicating particle collisions and fragmentation were occurring in the atmosphere. Although rime on particles was common in studies by both *Roberts et al.* [2008] and *Henson et al.* [2011] pristine crystals were also observed, indicating that the presence of supercooled water was not continuous throughout growth regions. Unrimed polycrystalline particles (such as bullet rosettes and combination columns), like ones observed by both *Korolev et al.* [1999] and *Lawson et al.* [2006] were also observed.

2.3 Physical controls of orographic precipitation

This section outlines the atmospheric flow response to orographic barriers (mountains), and how the shape of topography and incoming flow characteristics control orographic precipitation processes – growth, magnitude, and distribution. Generalized relationships between orographic precipitation processes and idealized mountain geometries and atmospheric flows, derived from meso-scale modeling studies, are integrated with results from intensive observational studies.

Our current understanding of these relationships is largely based on research focused on mid-latitudes (the Cascade Project (1975), Sierra Cooperative Pilot Project (1986), Winter Icing and Storms Project (1992), among others), with limited research directly pertaining to orographic precipitation at high latitudes. Significant recent contributions to the literature were borne out of research on orographic precipitation events conducted during the Meso-scale Alpine Programme (MAP) in the European Alps (1999), and the Improvements of Microphysical Parameterizations through Observational Verification Experiments (IMPROVE-II) in the Pacific-Northwest Cascade Mountains (2001).

Work studying cloud systems and the evolution of storms and precipitation processes in high latitudes have been completed over the Beaufort Sea [*Hanesiak. Stewart, Szeto, Hudak, & Leighton,* 1997; *Stewart, Szeto, Reinking, Clough, & Ballard,* 1998; *Hudak & Young*, 2002] and the Mackenzie Basin [*Stewart et al.,* 1998; *Asuma et* *al.,* 2000], which were carried out over relatively flat terrain in the western Canadian Arctic. Recent work during the Storm Studies in the Arctic (STAR) project in the eastern Canadian Arctic [*Hanesiak et al.,* 2010], combined with orographic observations from smaller research projects conducted in Antarctica and Norway [*Reuder, Fagerlid, Barstad, & Sandvik,* 1997; *Lachlan-Cope,* 2010] form the basis of the high latitude research presented here.

2.3.1 Atmospheric conditions and mountain geometry

Incoming, cross-barrier, atmospheric flow strength is an important control on the amount and distribution of orographic precipitation over topography. Observational studies have shown a near-linear dependence of precipitation totals with wind speed in both middle [*Neiman, Ralph, White, Kingsmill, & Persson,* 2002] and high latitude winter storms [*Nordø & Hjortnæs*, 1966] over mountains. Modelling studies by *Jiang and Smith* [2003] and *Colle* [2004] also observed this general relationship, where a stronger dependence was observed when mountain heights were greater than 1500 m. Using a two-dimensional meso-scale model and a constant barrier height of 1500 m, *Colle* [2004] demonstrated the sensitivity of orographic precipitation distribution to wind speed (Figure 2.6a). He found that for light winds (5 to 10 m s^{-1}), precipitation formed over the windward slope and precipitated out there, whereas for strong winds (15 to 20 m s^{-1}), more precipitation advected over the crest into the lee of the mountain. This is expected because snow aloft is more susceptible to being transported over a crest than liquid precipitation under high winds, because of its lower density [*Reuder, et al.,* 2007] and hence the fall speed.

The dominant precipitation phases and growth mechanisms are affected by the atmospheric temperature profile, in particular freezing levels. *Colle* [2004] found that when the freezing level of the atmosphere was raised (see FL750, FL500 in Figure 2.6a) the precipitation efficiency, defined as the ratio of surface precipitation fallout to the precipitation generated aloft in the same region, increased. The large precipitation efficiency for these cases was related to increased generation of rain, which subsequently fell out more rapidly on the windward slopes than would snow. Based on simulations by *Kirshabum & Smith* [2008], lowering temperatures throughout the atmospheric profile yields ice vapour deposition and riming processes that convert a greater fraction of the water vapour in an airflow into precipitation than for comparable warm-rain processes.

Figure 2.6:(a) Windward slope precipitation efficiency for a 1500 m barrier as a function of wind speeds for a modelling study. (For reference: N=0.01 (stable), N=0.05 (unstable), L=50 km (half length), L=25 km (half length)). (From Colle, 2004 © American Meteorological Society. Used with permission) and (b) Plot of maximum precipitation rate versus mountain height. Symbols related to different experiment runs (various controlling mechanisms also listed). (From Jiang & Smith, 2003 © American Meteorological Society. Permission for reprint pending); (c) Average precipitation (mm) (100km upstream of crest to 52 km in the less) vs wind speed for various mountain heights (stable atmospheric conditions); (d) same as (c) but in reduced stability conditions (From Colle, 2004 © American Meteorological Society. Used with permission).

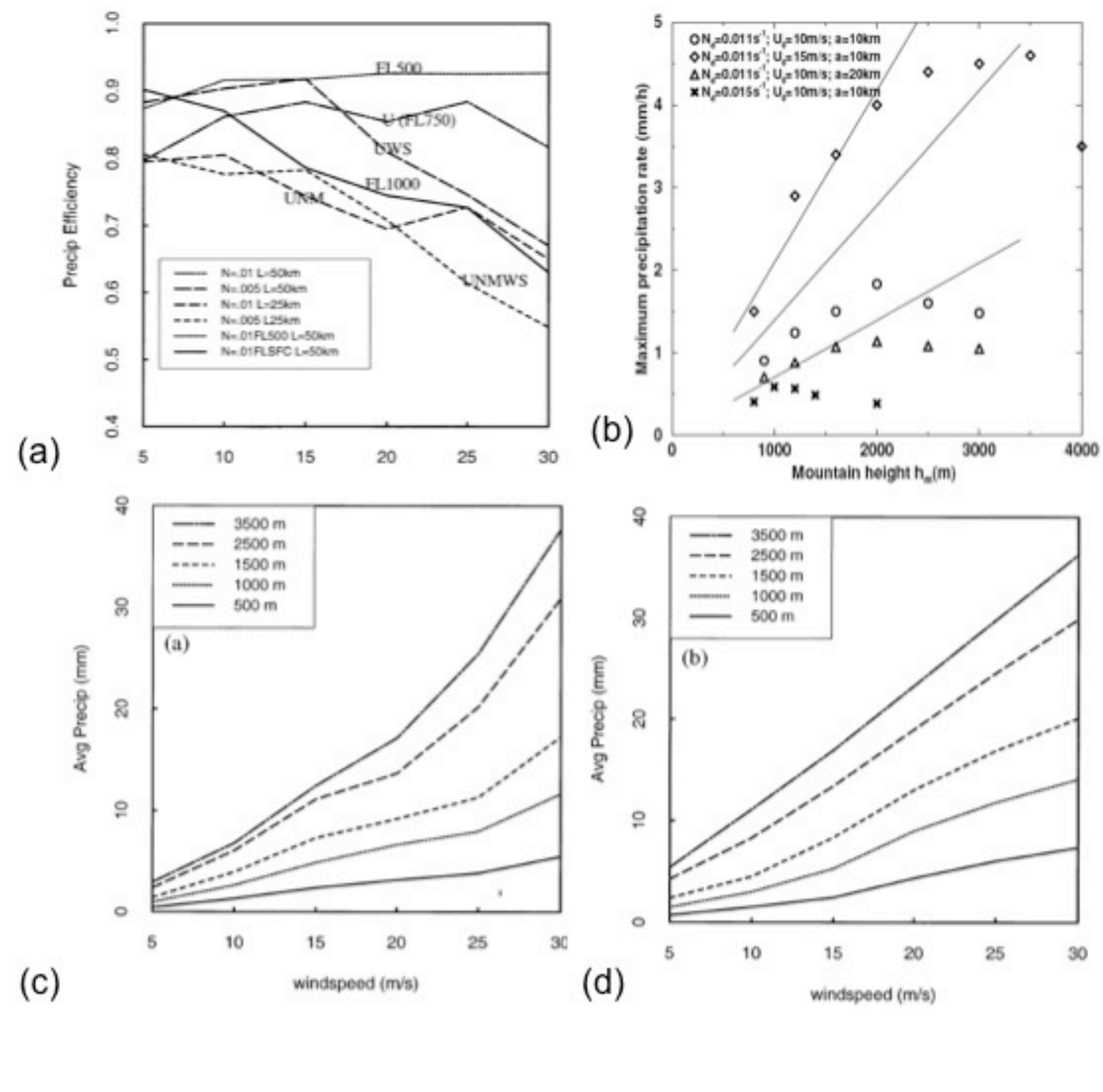

Moisture supply and atmospheric stability are also two important atmospheric controls on orographic precipitation. In its basic form, moisture supply is limited by temperature (equation 6), under very cold conditions; the low-level moisture supply can be limited thereby reducing orographic precipitation [*Wallace & Hobbs*, 2006]. In stable conditions the ability of air to flow over a barrier can be a limiting factor by reducing condensation processes [*Colle*, 2004]. In cases where unstable air or conditionally unstable air traverses a barrier, more precipitation has been observed in both modelling (Figure 2.6c and 2.6d) and observation studies [*Medina & Houze,* 2005].

Mountain shape, simply its height and width, affects orographic precipitation in a manner that is interconnected with atmospheric conditions, though generalities specific to the influence of shape on orographic precipitation growth and distribution can be made. It was previously mentioned that high latitude regions with topography receive more precipitation annually then regions associated with low elevations. To provide some perspective, the largest elevations in high latitude regions (> 60°N) can range from 4000 to 6000 m in Greenland, the Antarctic Plateau and Alaska, to more moderate elevations of 700 to 2500 m in the Scandinavian countries, the eastern Canadian Arctic, and Siberia [*Barry*, 2008].

Jiang [2003], *Colle* [2004] and *Barsted and Smith* [2005] have all identified that orographic precipitation increases with mountain height (Figure 2.6b, 2.6c, 2.6d). However, this relationship only holds until height becomes too large for the flow regime, and low-level blocking occurs. Blocking reduces the amount of airflow ascending the barrier and reduces condensation and precipitation processes. Blocking also affects flow dynamics and microphysical growth processes (discussed further in section 2.3.2).

Mountain width, lateral distance from base to crest, influences the advective timescale. An increase in mountain width increased the time allowed for hydrometeor formation and precipitation, also significantly influences precipitation growth processes such as accretion and aggregation. *Jiang and Smith* [2003] observed that narrow mountains are associated with steeply sloped terrain, resulting in strong updrafts and enhanced growth. Whether this results in increased orographic precipitation amount is further dependent on the speed of the microphysical growth processes occurring in the cloud. A narrow mountain means that there is less time for the condensate to precipitate out before being advected over the crest into the lee. Ice particles carried to the lee-side are more likely subject to loss by sublimation [*Colle,* 2004]. Simulations by *Jiang and Smith* [2003] and *Kirshbaum and Smith* [2008] showed greater precipitation for mountains with a larger width, at constant height.

Further to mountain shape is its orientation in relation to prevailing winds and/or dominant storm tracks, shown in a high latitude observational study to be a key determinant of precipitation amount [*Smith,* 1979]. For example, accumulation studies over the Antarctic Peninsula have revealed that the western side has significantly more precipitation than the east. This is primarily because the prevailing westerly flow forces air masses to rise over the topography resulting in upslope precipitation [*Miles, Marshall, McConnell, & Aristarian,* 2008; *Knuth, Tripoli, Thom, & Weidner*, 2010]. Orientation is a significant variable whose influence is often overlooked when defining general relationships between mountain shape and precipitation amount, such as in *Jiang* [2003] and *Barstad and Smith* [2005]. The distribution of precipitation on the lee side of slopes (the rain-shadow effect) may be substantially less than what was observed at similar elevations on windward slopes.

2.3.2 Low-level blocking

Orographic precipitation growth and distribution have been found to be strongly dependent on whether or not low-level atmospheric flow undergoes blocking, or remains unblocked, freely flowing over terrain [*Smith,* 1979]. Low-level blocking has itself been linked to large mountain height [*Colle,* 2004], weak cross-barrier flow strength [*Jiang,* 2003] and strong stability in the lower atmosphere [*Medina & Houze*, 2005].

The influence that low-level blocking has on the microphysical growth mechanisms, as well as the distribution of orographic precipitation, is best illustrated by presenting results from two separate MAP case studies associated with troughs passing over the Alps during the winter of 1999 [*Medina & Houze*, 2003]. The large-scale dynamics of each storm were variable, one with weak stability and strong-cross barrier flow at all levels (Case A) and the other with strong stability and weaker cross-barrier flow (Case B). For Case A, airflow associated with a trough easily rose over the steeply sloped terrain at all levels, with the strong upward motion triggering small regions of convection. Convection then enhanced ice crystal growth over a major peak and increased orographic precipitation on the windward side of the range, particularly in the lower regions. Outside of the convective regions, ice particles continued to grow by deposition because of the strong forced ascent of the airflow over the terrain, and precipitated out over the upper regions on the windward slopes, with some spill over into the lee. A reflectivity cross section during this event is shown in Figure 2.7a, where a convective-like echo structure can be easily identified over the first peak, i.e. where the horizontal gradient of elevation first becomes large. Conversely, for Case B the stable conditions made it difficult for the low-level flow to rise over the barrier (blocking) and impossible for embedded convection to form (Figure 2.7b). This, combined with cooler conditions (implying lower e_s), led to lower precipitation amounts compared Case A. In addition, most of the orographic precipitation was confined to the windward slopes in Case B because of the weak wind speeds associated with this event.

Figure 2.7: 3-hour mean reflectivity cross-section from S-band polarized radar during MAP for two cases, September 1999 and October 1999, respectively: (a) No low-level blocking; and (b) low-level blocking. Topography highlighted in green. (From Medina & Houze 2003 © John, Wiley & Sons Publishing. Reproduced with permission).

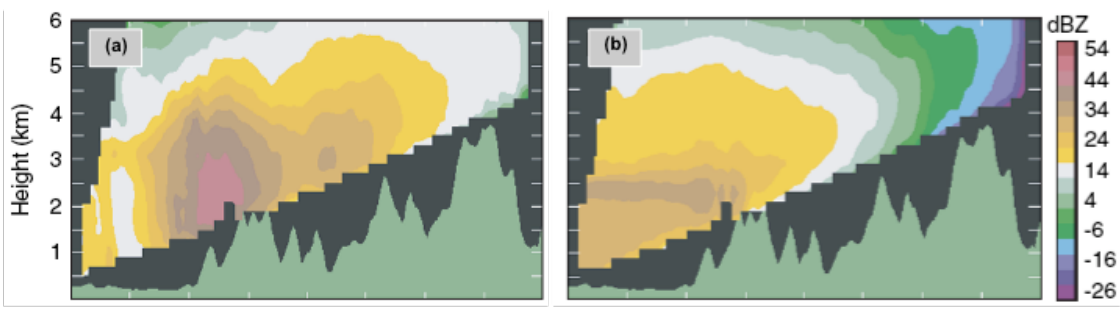

Low-level blocking has also been observed to mechanically produce small-scale convection and enhancement of orographic precipitation along a layer of wind shear that can form above the blocked flow [*Houze & Medina,* 2005]. *Houze and Medina* [2005] observed that the cellular motion favoured the growth of particles by aggregation, with some riming from enhanced cloud water content in the small convective updrafts. *Houze* [1993] also noted that blocked air could also be a possible enhancement mechanism for orographic precipitation by increasing the advective time scale of growth and precipitation fallout. He found that the blocked airflow essentially becomes an extension of the mountain width upstream. The widening effect allows more time for microphysical processes in the cloud, both growth and fallout to occur on the windward slope. *Colle* [2004] found that this process increased the precipitation efficiency over the windward slope, and altered the distribution, with greater precipitation likely in the lower regions of the windward slope. However, understanding the importance of these processes in acting to enhance precipitation requires further observational study.

The influence of low-level blocking on orographic precipitation amount has not been investigated at high latitudes. The frequent occurrence of low-level temperature inversions and corresponding strong stability in the lower atmosphere [*Serreze & Barry*, 2005] implies that this may be commonly observed feature. A stable atmosphere will reduce the ability of low-level airflow to ascend an orographic barrier and, as a result, there is a decoupling of low-level flows from the flow aloft. This process has been observed during an investigation of a strong wind event over Baffin Island [*Deacu, Zadra, & Hanesiak,* 2010], but the effect of blocking on precipitation was not discussed.

2.3.3 Embedded convection

Small-scale, embedded convection initiated by orographic lifting, as introduced in section 3.2, significantly influences the dominant microphysical processes occurring in orographic clouds [*Medina & Houze,* 2003]. Convective cells provide locally strong updrafts, which vertically redistribute moisture, producing high concentrations of cloud liquid water [*Yuter & Houze,* 2003], and increasing the growth time for particles aloft

[*Colle,* 2004]. *Woods, Stoelinga, Locatelli and Hobbs* [2005] detailed the particle habit and growth processes occurring during the passage of a cyclone, containing embedded convective towers, using an aircraft-based particle imaging system over the Cascades, during IMPROVE-II. Pristine plates, assemblages of sectors and capped columns were observed in the upper-level baroclinic zone, indicating that particle growth by vapour diffusion dominates in upper levels. In lower levels, a rapid shift to rimed crystals associated with orographically induced convective clouds composed of dendrites, aggregates of dendrites, and composites of needles and, eventually, graupel was observed. A comparison of the particle size spectrum with height prior-to, and after, the initiation of convection shows that, once convection begins, larger particles occur in higher concentrations [*Woods, et al.,* 2005]. This suggests a shift in the growth mechanisms, and an increase in accretion and aggregation, relative to deposition associated with convection. Outside of convective cells, deposition was found to remain the dominant microphysical growth process, and the particle spectrum showed a higher concentration of smaller particles [*Wood et al.,* 2005].

Reflectivity values from an X-band Doppler radar suggest that during a major Arctic precipitation event, embedded convection likely occurred [*Henson et al.,* 2011]. Photographs of hydrometeors taken at the surface indicate that snow mainly fell as graupel and large aggregates of rimed needles and dendrites. During this event, the largest accumulations and highest precipitation rates over the entire STAR project were observed identifying the potential importance that small-scale embedded convection may have for regional precipitation amounts in Arctic orographic locations such as over Baffin Island.

2.3.4 Gravity waves

Gravity waves, induced by strong vertical motion by orographic lifting, have been found to significantly influence condensation and precipitation processes [*Reinking, Snider, & Coen,* 2000; *Garverts, Smull, & Mass,* 2007; *Jiang,* 2007]. Air forced over topography is counteracted by gravitational forces in the atmosphere, resulting in the formation of small wave structures within the circulation called gravity waves [*Stull,* 2000]. These waves may propagate away from the source (horizontally and/or vertically), become trapped, or decay [*Roe,* 2005]. Mountain geometry plays an influential role, as multiple ridge systems act to either enhance or suppress wave motion based on mountain height, distance between peaks, and depth of valley systems [*Jiang,* 2007]. Strong gravity waves produced by airflow over the first peak of a windward slope have been found to significantly enhance precipitation over the subsequent ridges by directly increasing condensation rates and enhancing snow generation aloft [*Reinking et al*., 2000].

This importance of storm-embedded gravity waves as a mechanism for orographic precipitation enhancement is clearly seen in a study by *Garvert et al.* [2007]. During the IMPROVE-II project, they observed that the interaction of the low-level cross-barrier flow along the windward slopes of the Cascades resulted in wave motions and enhanced precipitation parallel to mountain ridges. As Figure 2.8a illustrates, positive vertical perturbations, shown as the enhancement of radar reflectivity values, denotes increased precipitation rates triggered by the ascent. Modelled precipitation type and cloud liquid water mixing ratios for this case, to supplement observations from the aircraft radar, reveal complex microphysical interactions produced by the strong vertical velocities (Figure 2.8b). Localized pockets of vertical motion and increased cloud water content aloft resulted in the formation of graupel in the model, implying increased particle growth by riming.

Figure 2.8: (a) Doppler velocity (contours) overlaid on radar reflectivity (shaded) from aircraft; and (b) Modelled precipitation overlaid on modelled cloud water content (From Garvert et al., 2007 © American Meteorological Society. Used with permission).

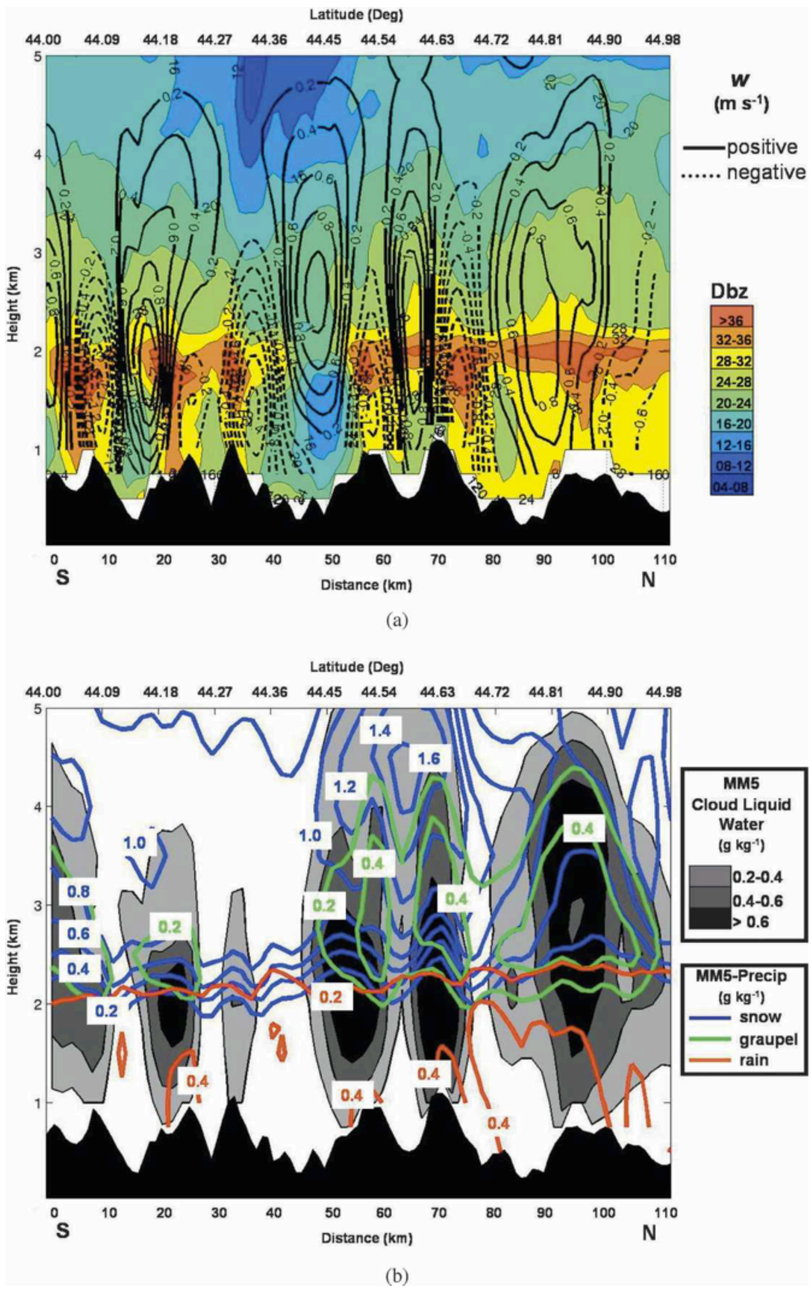

2.3.5 Sublimation

Sublimation below the cloud base, and between multiple cloud layers (up to 4 or 5 cloud layers have been identified in the Canadian Arctic during precipitation events) leads to a reduction in the precipitation that reaches the surface, even if microphysical processes aloft are efficient at precipitation production [*Stewart et al.,* 2004; *Roberts et al.,* 2008; *Henson et al.,* 2011]. In high latitude environments during the cold season, the persistence of low ambient temperatures, low moisture supply and the predominant presence of solid precipitation (lower fall speeds compared to liquid drops) means that the probability that precipitating ice crystals will sublimate before they reach the ground is high [*Burford & Stewart*, 1998]. Mass loss of particles from sublimation has been found to be greatest in the warmest and driest environments and lowest in environments that were cold and moist [*Stull,* 2000]. With respect to fall speeds, lower terminal velocities result in more time for sublimation processes to occur during descent [*Burford & Stewart*, 1998].

In 1998, *Burford and Stewart* investigated sublimation in the Mackenzie Basin in the western Canadian Arctic in September and October of 1994. An important observation was the relatively large magnitude of mass loss at relative humidity of 70% and greater, where sublimation losses ranged from 20 to100%, -20°C ≥ T ≤ 0°C. On average they found that sublimation loss was 50% in the region. Sublimation was found to be in part dependant on particle type. For surface precipitation rates of 1 mm hr^{-1}, relative humidity conditions of 70%, at temperatures of -20°C and with cloud base near 1 km, sublimation rates were observed to be as high as 100% for unrimed dendrites and aggregates of dendrites, and between 65 to 70% for rimed dendrites and aggregates of plates.

In the eastern Canadian Arctic, *Henson et al.* [2011] observed that, during major precipitation events over Baffin Island, there were periods when radar reflectivity patterns suggested precipitation aloft, despite no precipitation reaching the surface, which suggests hydrometeors were sublimating as they fell. Furthermore, *Henson et al.* [2011] identified that a major difference between precipitation efficiency in high latitude and mid-latitude observations is enhanced loss of precipitation to sublimation at the surface or in dry layers aloft in polar regions.

The process of sublimation will also moisten, and cool the sub-cloud layer during the phase change. Subsequent falling particles after time will undergo less mass loss and have an increased fall depth. In the Mackenzie Basin, *Burford and Stewart* [1998] found that the dry layer beneath precipitating clouds requires timescales of hours before it may become saturated from sublimation alone. The cooling of the atmosphere through sublimation can also lead to localized dynamical circulations and flow reversals down the mountain slopes [*Roe*, 2005].

2.3.6 Frontal interaction with topography

A recent study investigated the climatology of major cold season precipitation (> 9.5 mm) over Baffin Island and showed that there was strong relationship with frontal structures. *Gascon et al.* [2010] observed that: 56% of major precipitation events were associated with the passing of warm fronts; 8% the passage of a cold front; and 35% of events were not associated with an analyzed front. This work emphasizes the importance of large-scale systems on precipitation events in the region. Unfortunately, detailed analysis of the evolution of frontal systems in high latitudes is lacking, particularly with respect to modification of the system during the passage over topography. In 1997, *Hanesiak et al.* used a research aircraft and other field observations during the Beaufort and Arctic Storms Experiment (BASE) to investigate the structure of a warm front over the western Canadian Arctic. They observed that the overall structure of the warm-front was similar to mid-latitude events, but notable differences were that the warm front contained a < 0°C profile across the frontal region, was characterized by a weak and steep formal zone, precipitation was light and fell exclusively as snow. *Szeto, Stewart and Hanesiak* [1997] showed that such systems can either be very efficient at converting water vapour into precipitation or very inefficient, where differences arose in part from latitudinal effects. They found that high latitude synoptic systems are generally shallow and have smaller horizontal scales, colder temperatures, limited moisture availability and strong static stability.

Numerous studies have characterized the structure, associated precipitation patterns and the modification as frontal storm systems interact with topography in the mid-latitudes [*Hobbs et al.*, 1971; *Egger & Hoinka*, 1992; *Medina & Houze*, 2003; *Woods et al.,* 2005]. Their research has shown that orography irreversibly modifies the thermodynamic properties of the impinging air mass associated with the front as it passes over a mountain range [*Smith et al.,* 2003]. The forced ascent over the barrier results in: the distortion of the temperature structure through adiabatic processes, modification of the vertical distribution of moisture, in addition to some fraction of the moisture being depleted by enhanced condensation and precipitation rates occurring in uplift regions

[*Rotunno & Houze*, 2007]. As the frontal system crosses the mountain range orographic lifting enhances microphysical processes above and beyond that produced by the frontal systems dynamics alone, often resulting in more precipitation at the surface [*Houze & Medina*, 2005]. The airflow associated with the front will likely travel into the lee-side of the range warmer and drier than the incident airstream [*Kirshbaum & Smith*, 2008]. Dynamically the approaching circulation is usually weakened or retarded depending on the mountain shape [*Peng, Powell, Williams, & Jeng,* 2001]. Upstream blocking and discontinuous frontal propagation can occur when a weak front encounters topography. Conversely, strong fronts crossing over these mountains were shown to only be weakly retarded and continuously propagated over the terrain [*Dickenson & Knight*, 1999]. The interaction of a front with topography has been found to change precipitation amount and distribution associated with the baroclinic weather system [*Smith*, 2006].

2.3.7 Summary

There are various physical processes involved in controlling the formation and distribution of orographic precipitation in high latitudes. Precipitation is dependant on the complex interactions between large-scale atmospheric flow towards a barrier, the interaction of the ambient flow with the orographic barrier, and the microphysical processes that occur. Section 2.3 outlined the ways in which the atmospheric flow can respond to orographic barriers, and how the shape of the topography and incoming flow characteristics control precipitation magnitude and distribution. These results have been summarized here:

- *Mountain shape (height and width)*: (1) Linear theory of orographic precipitation suggests that as mountain height increases, precipitation will increase, until the mountain becomes too high and blocking occurs; (2) wider mountains (increased lateral distance from base to crest) in general receive more orographic precipitation than mountains with a smaller width of the same height, unless strong updrafts associated with a the steeper slope are more efficient at precipitation production and fallout; and (3) orographic precipitation increases if the mountain is oriented against the prevailing winds.
- *Atmospheric conditions:* (1) An approximate linear relationship between orographic precipitation and wind speed can be observed; (2) as wind speeds increase, more precipitation will be advected to the lee-side of the mountain, which may reduce overall orographic precipitation amount if there are losses from sublimation; (3) an increase in the freezing level in temperature profile could result in more precipitation to fall out as rain on windward slopes and more ice particles loft to be advected into to the lee-side of the mountain; (4) increase moisture supply can increase orographic precipitation if the microphysical processes are sufficient to create precipitation sized particles; and (5) under reduced atmospheric stability, orographic precipitation will increase.
- *Low-level blocking:* (1) occurs most often when a mountain is high, there is a weak cross-barrier flow, and strong stable atmosphere; (2) usually results in gentle and gradual ascent of airflow aloft, where particles grow by deposition; (3) if a layer of wind shear forms, small-scale convection can be induced above the blocked lower air, in these cases precipitation distribution is more upstream of the crest; and (4) blocked

air in the lower-levels can increase the advected time scale by becoming an extension of the barrier upstream to the incoming flow.

- *Embedded convection:* (1) associated with locally strong updrafts, redistribute moisture vertically, increase the time that particles spend aloft, as a result, accretion and aggregation become important microphysical growth processes; and (2) total orographic precipitation is likely to increase over the entire mountain range, enhanced amounts can be associated with the region where convection was initiated.
- *Gravity waves:* (1) induced wave motion enhances condensation and precipitation processes over orography; and (2) mountain geometry is very important for wave formation, multiple ridge systems can act to enhance or suppress wave motion.
- *Sublimation:* commonly observed in high latitudes: (1) can reduce precipitation that reaches the surface, even when relative humidity is greater than 70%; (2) loss from sublimation is estimated at 50% for high latitude precipitation events in the Canadian Arctic and (3) cooling associated with sublimation can create localized downdraft and flow reversals on mountain slopes.
- *Frontal interaction with topography:* major precipitation events over Baffin Island have been linked to the passage of weather systems associated with fronts.

2.4 Challenges in data collection and modelling

Orographic lifting has been identified as an important influence on regional precipitation, enhancing precipitation associated with both synoptic and local storm systems, and by influencing the its distribution, nonetheless it has not been studied in great detail. Limitations in our current understanding can in part be related to challenges in data collection and modelling.

2.4.1 Data collection challenges

Data acquisition in high latitudes is challenging. The frequency of observations from surface instrumentation and aircrafts is substantially lower, relative to mid-latitude regions, due to remoteness, harsh climates, variable surface environments, and high maintenance costs [*Serreze & Barry*, 2008]. To better characterize precipitation requires enhanced observations at the surface by gauges, ground-based radars, macro-photography and other special surface instrumentation that can provide data on amount and microphysical composition of orographic precipitation such as shape, particle size, concentration and phase. Acquiring such data is difficult, particularly in the lower regions of the atmosphere. Some of the specific challenges to data collection of orographic precipitation characteristics include, but are not limited to: the number of gauge measurements; ground clutter and blocking of radar; satellite sampling resolution, and aircraft sampling heights.

2.4.2 Instrument accuracy

Instrument accuracy and the main sampling limitations of key instrumentation used in this thesis (Chapter 3, Chapter 4 and Chapter 5) are outlined in this section. This is by no means an exhaustive list of data collected during the STAR field project [*Hanesiak, et al*. 2010] or the data that can be used to examine these critical features, but is relevant to the research presented in this thesis.

2.4.2.1 Precipitation gauge measurements

The most common, and widely distributed instrument to measure precipitation is a precipitation gauge. They vary is design, from a simple standard gauge, to a more complicated instrument such as a weighing-type gauge. A standard gauge consists of an outside container that holds a removable funnel, which empties into an inner graduated cylinder (liquid precipitation only) [*Ahrens, Jackson & Jackson*, 2012]. This type of gauge requires an observer to maintain and monitor the measurements at regular intervals. In contrast, a weighing-type gauge has an automatic recording system, resulting in an efficient way to gather continuous data from remote locations without having to visit the site immediately after a precipitation event. The amount is determined by collecting precipitation (liquid and solid) into a bucket on a sensitive load platform, with a vibrating wire transducer. The result is a frequency output, which is a direct function of the applied tension on the wire and can be translated into a quantitative precipitation measurement [*Ahrens, et al.*, 2012].

The main source of error in precipitation gauge measurements comes from wind [*Goodison, Louie, & Yang*, 1998; *Duchon & Essenberg*, 2001; *Smith*, 2008]. Turbulent airflow around and over the gauge affects the catch efficiency by altering particle fall trajectories. Wind effects are introduced by either mounting a gauge above ground or without a proper shield and usually results in an under-catch of true precipitation at the surface. This problem is enhanced for solid precipitation, due in part to the slower fall speeds. In 2008, *Smith* performed an experiment on the catch efficiency of gauge measurements using two different shield types, an Alter shield (current standard configuration in the Canadian Reference Climate Station network) and a more advanced octagonal Double Fence Intercomparison Reference (DFIR) shield. He found that the catch efficiency of the gauge with the double-fenced enclosure was improved by 50% over the Alter shield. The author commented that accurately measuring snowfall is still an ongoing challenge, but the double-fenced enclosure offers greater protection from wind related errors.

During STAR, ground based measurements of precipitation were collected using a Geonor 200B all-weather gauge situated inside an octagonal DFIR shield, minimizing wind effects [*Sevruk et al.,* 2008; *Smith,* 2008]. This gauge has a sensitively of 0.05 mm and 0.1 mm resolution. In conjunction with gauge measurements, a Thies Clima Laser Precipitation Monitor (LPM) provided information about precipitating hydrometeors. The LPM detects and discriminates the different precipitation types such as drizzle, rain, hail, snow, snow grains, graupel (small hail / snow pellets), and ice pellets. The LPM detailed concentration and particle size distributions, for intervals from 125 to 8000 μm during precipitation events [*Fargey et al.,* 2008]. The LPM is reported to have >97% accuracy of precipitation type when compared to results from an observer. The instrument can detect precipitation with a minimum intensity of 0.005 mm hr^{-1} (drizzle).

2.4.2.2 Doppler radar measurements

Remote sensing instruments such as radars have become important tools for estimating cloud and precipitation characteristics. The development of radar was more for tactical warfare than meteorology, but its application soon became invaluable when investigating weather processes [*Rinehart,* 2004]. Radar measurements can be from ground-based, airborne or spaceborne instrumentation, their use varies from region to region. Currently no permanent meteorological radars can be found in northern Canada, but during the last few decades organized research projects have set-up portable radar systems, and used aircraft measurements. Airborne radar is becoming an increasing common tool to investigate precipitation processes over poorly accessible areas, such as the Arctic and over mountain ranges, due to their uniquely elevated location and vertical sampling strategies [*Bousquet & Smull*, 2003].

Radar operates by transmitting microwave signals (electromagnetic energy pulse) towards the cloud (or scene of interest). Cloud particles scatter back a portion of the transmitted energy to the radar's receiver. The strength (detection) and the time delay (ranging) of the return signal (echo), provides inferred information about the cloud particle size and distance from the radar [*Rinehart,* 2004]. Weather radars use the microwave portion of the electromagnetic spectrum, and can vary in wavelength between 1 mm to 1 m depending on what environmental feature is being investigated by the user. Short-wavelength (mm) radar is well suited for detailed monitoring of clouds, while larger (cm) wavelength radars are more suited for precipitation and severe weather [*Moran et al.,* 1998]. Because the millimeter wavelengths used by cloud radars (W and Ka-band) are approximately an order of magnitude shorter than those used by precipitation detection radars (X and S-band) they can detect small cloud particles and provide microphysical details of precipitating and non-precipitating clouds.

During STAR a ground-based X-band Doppler radar, owned and operated by Environment Canada, was deployed in Iqaluit. The radar has a peak power of 25 kW and a beam width of 2.5°, with an operational radius of approximately 50 km. Its normal operating procedure repeated every 15 minutes, involved volume scans, Range Height

Indicators (RHIs), Doppler Plan Position Indicator (PPI) scans on selected azimuths and was operated in vertical stare mode. For the STAR campaign it was configured for a pulse duration during was 0.4 μs, and pulse repetition frequency of 2000 s^{-1}. The range resolution was 50 m and the minimum detectable signal of the radar is 17 dBZ at 1 km [*Hudak & Nissen*, 1996; *Henson et al.*, 2011].

An aircraft onboard profiling radar system was also used. The National Research Council of Canada (NRC) Convair-580 (CV-580) research aircraft, instrumented by Environment Canada and the NRC, used a 95 GHz (3.2 mm wavelength) cloud profiling radar system (W-band) with a 0.7° beam width and 30 to 60 m vertical resolution that provided continuous and simultaneous reflectivity cross sections above and below the aircraft from upward and downward pointing fixed antennae. To remove ground contamination, terrain masks were applied. Once the aircraft motion was removed, doppler velocity measurements were accurate within ±0.3 m s^{-1} [*Wolde*, 2009, personal communication].

Complex topography results in data challenges for radar systems. Ground based radar stations must be located so that the line of sight of the beam is not blocked by the orography. In addition, no data are available from valley-ridge structures over mountains because of screening, which is clearly illustrated in Figure 2.9. Aircraft and satellite radar also suffer from ground clutter, resulting in observations below ~250 m for aircraft radars and ~1 km above terrain for satellite radars unusable [*Marchand, Mace, Ackerman, & Stephans*, 2008]. These limitations reduce available data on orographic precipitation characteristics and growth processes in the lower attitude near of the terrain, which have been found to be important for orographic production [*Woods, Stoelinga, & Locatelli,* 2007].

Although the spatial area investigated is greatly expanded and remote locations may be better served through the use of satellite technologies, their sampling resolutions must also be considered. CloudSat (operational since 2006), carries a cloud profiling radar, has a sampling resolution of 1.4 km by 2.5 km and a vertical resolution of approximately 250 m [*Stephen et al.*, 2002]. The Global Precipitation Mission (GPM) (launched March 2014) carries a precipitation profiling radar with a 5 km by 5 km horizontal sampling resolution and a 250 to 500 m vertical resolution. Both satellite resolutions are larger than ideal for sampling precipitation processes; and with respect to the GPM satellite, the minimum reflectivity that can be detected is 12 dBZ [*Hou et al.,* 2013]. Based on low reflectivities that were commonly observed during STAR project indicate that precipitation would remain undetected by this radar [*Henson et al.,* 2011].

2.4.2.3 Upper air and dropsonde measurements

Upper air measurements were collected using Vaisala RS92-SGP units. Sounding temperature, relative humidity, pressure and wind data were recorded at 10-second intervals, with accuracies of ±1.0 hPa for pressure, ±0.5°C for temperature, < 5% for relative humidity, 10 m horizontal position uncertainty, 0.15 m s^{-1} wind speed measurement uncertainty, and 2° directional measurement uncertainty [*Vaisala*, 2013].

The CV-580 was also equipped with remote temperature, humidity, and wind profiling below the aircraft using an Airborne Vertical Atmospheric Profiling System (AVAPS; GPS dropsonde system). The dropsonde units were modified RD-93 type, where thermodynamic and wind data are recorded at 0.5 s intervals (vertical resolutions of approximately 5 m), with accuracy of: 1.0 hPa for pressure, ±0.2°C for temperature, < 0.5 m s^{-1} wind speed measurement uncertainty and 2° directional measurement uncertainty and < 5% for relative humidity [*Hock & Franklin,* 1999].

2.4.2.4 Aircraft meteorological sensors and microphysical instrumentation

The aircraft was also equipped with a variety of cloud spectrometers, including Particle Measuring System (PMS) two-dimensional cloud (2DC) and precipitation (2DP) imaging probes to estimate particle concentrations for size intervals of 100 to 800 μm and 1000 to 6400 μm respectively. Previous research has revealed substantial errors below for particles < 100 μm measured by the PMS-2DC due to digitization, out of focus oversizing, and speed response issues [*Strapp et al.,* 2001]. Contamination of particle by shattering of ice particles on probe forward surfaces is also an increasing problem below this size [*Korolev et al.*, 2011].

Atmospheric state parameter measurements were collected. They include temperature (*T*), dew point temperature (*Td*), pressure (*P*), and wind fields (speed and direction). Additional parameters, including Nevzorov total water content (TWC) and PMS King liquid water content (LWC) probe (0.05 g m^{-3} sensitivity), as well as data from a Rosemont Icing Detector (RID) (mV) were collected. The Nevzorov probe is a constant temperature hot-wire instrument consisting of two sensors, one for LWC and one for TWC. The threshold sensitivity to water and ice was estimated at 0.003 to 0.005 g m^{-3}.

2.4.3 Modelling challenges

Realistic modelling of orographic precipitation entails consideration of both cloud microphysics and circulation dynamics over a wide range of time and spatial scales, and requires detailed knowledge of complicated processes upstream, over, and downwind of complex terrain [*Barros & Lettenmainer*, 1994]. Models of orographic precipitation processes can range from simple statistical regressions [*Nordo & Hjortnaes*, 1966; *Basist & Bell*, 1994] to sophisticated, prognostic, meso-scale models, which integrate the full dynamic equations of motion over time [*Smith et al.,* 2003]. For the latter, bulk microphysical parameterization schemes (BMS) are typically included to represent complex processes through simplified equations [*Lin et al.,* 1983]. BMS contain a range of assumptions, such as the density and habit of ice hydrometeors, number concentrations of cloud drops and IN, as well as the collection efficiencies of riming and aggregation processes. Currently, most BMS contain six classes of hydrometeors: cloud water; cloud ice; snow; rain; and graupel [*Brown & Swann*, 1997]. Some key challenges facing accurate modelling of orographic precipitation are: (1) model resolution; (2) limited high-resolution data to validate model performance; and (3) snow representations in microphysical schemes.

- *Resolution:* The horizontal and vertical resolution of operational and climate models are too coarse to adequately resolve complex interactions between ambient flow and topography occurring at finer scales; and a smoothed representation of topography in mountain grids will determine dominant microphysical growth processes, which may not represent what is actually occurring over highly irregular real orography. This also means that discrepancies between model and observations may be partially attributed to the observational scale used in comparisons (station versus grid point).

- *Limited data to evaluate model performance*: orographic precipitation in models is often evaluated using observations of individual storms [*Garverts et al.,* 2005] or climatological distribution [*Colle, Westrick, & Mass,* 1999], due to aforementioned challenges in acquiring data in complex terrain. With appropriate optimization of parameters, models are generally able to achieve a good match with observed precipitation rates at scales of 10s of km though model skill can vary widely between storms, and when the same model is applied to a different mountain range [*Barros & Lettenmaier*, 1994]. Higher resolution data are required to reduce assumptions or oversimplifications. However, errors in measurements (instrument accuracy) is also a large source of model error that can propagate through simulations and results in poor model calibration.
- *Microphysical parameterization schemes*: BMS typically represent snow as a spherical particle of given density, and an assumed fall velocity, both of which do not accurately represent reality. Habit dependent *mass–diameter* and *velocity–diameter* relationships for snow particles can be substituted to improve representation of orographic precipitation in models [*Wood et al.*, 2007], though this requires further work on establishing the applicable bounds. Range-by-range calibration based on observed microphysical relationships may be required in order to improve region-specific orographic precipitation modelling.

2.4.4 GEM-LAM 2.5 configuration

In Chapters 4 and 5 of this thesis, the limited area version (2.5 km resolution) of the Global Environmental Multi-scale limited area model (GEM-LAM 2.5) was run in experimental mode to investigate model accuracy in the study region during case studies. The following section briefly summarizes the model's configuration and can be used as reference in upcoming chapters.

The GEM-LAM 2.5 is non-hydrostatic and uses semi-implicit, semi-Lagrangian time integration. There are 58 vertical sigma-pressure levels up to 10 hPa. For specific analysis objectives, the model can be run in experimental operational mode [*Erfani et al*., 2006]. The initial and boundary conditions are extracted for the hourly output of the GEM regional model (15 km resolution), with initial conditions derived from the global forecasting system of the CMC and integrated for at least 48-hours [*Côté, Gravel, Méthot, Patoine, Roch, & Staniforth*, 1998; *Mailhot et al*. 2006]. Physical parameterizations include a unified cloudiness-turbulence scheme for the planetary boundary layer [*Belair, Mailhot, Girard, & Vaillancourt,* 2005]; a radiation scheme [*Garand & Malihot*, 1990]; and a shallow convection scheme [*Belair et al*., 2005]. The explicit moisture scheme in the model uses cloud ice as a prognostic resolvable variable assuming that the grid cell is completely filled with hydrometeors [*Mailhot*, 1994]. Generation of cloud water (ice) occurs when air is super-saturated with respect to water (ice). For cloud ice generation (T ≤ 0°C), the condensation rate (Q) is given by:

$$Q = \min \left\{ \begin{matrix} \dfrac{M_0 n_c}{\rho \Delta t} \\ \dfrac{q_v - q_{vs}}{\Delta t} \end{matrix} \right\}$$

where M_0 is the initial mass of cloud ice crystals and n_c is the concentration of cloud ice. The q_{vs} term is the saturation mixing ratio of water vapour with respect to ice. Cloud ice sublimates when the air is sub-saturated with respect to ice and growth by deposition occurs when relative humidity is greater than 100% [*Mailhot*, 1994].

In the version of the model used in this thesis, cloud microphysical processes and precipitation were parameterized using the Kong-Yau microphysical scheme [*Kong & Yau*, 1997], which represents solid precipitation as spherical particles with a prescribed constant density, with two ice-phases: a hybrid pristine ice-snow and a graupel category. In the scheme, the important microphysical processes related to ice phase wintertime precipitation include nucleation, deposition and sublimation, freezing, riming, accretion and aggregation, which were discussed in section 2.2.4.

Figure 2.9 illustrates the relationship between the microphysical processes in the scheme, where the terms q_v, q_c, q_r and q_i are water vapour, cloud water, rain water and ice or snow, respectively. For the purposes of this thesis, focus in this section is on the ice-phase microphysical processes. Ice can grow, by riming (*CLci*), accretion of small raindrops by ice particles (FR_{ri}), deposition nucleation on active IN to form initial ice (NU_{vi}), and deposition of water vapour (VD_{vi}). Ice particles can be reduced by sublimation of water vapour (VD_{vi}) in subsaturated conditions, or by the melting of ice particles to form rain (ML_{ir}). In this scheme, a single ice phase field is forecasted, no explicit size spectrum is calculated and ice aggregation is not explicitly parameterized [*Kong & Yau*, 1997].

Figure 2.9: Schematic of the microphysical processes in the Kong-Yau scheme (from Kou & Yau, 1997). From Kong & Yau, 1997 © Taylor & Francis Publishing. Reproduced with permission.

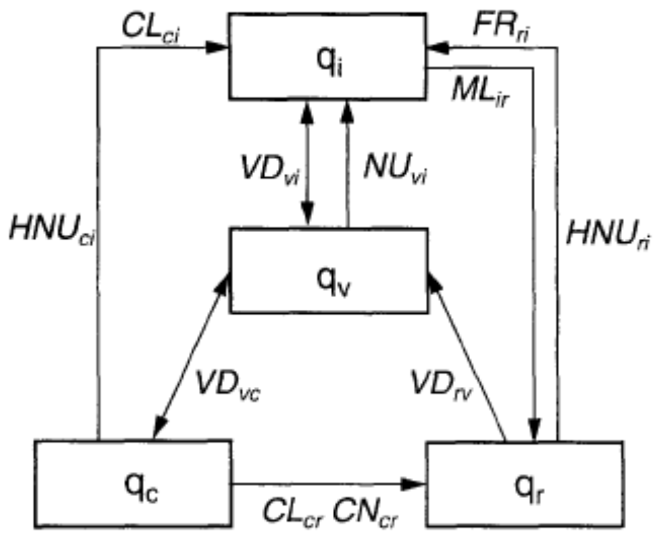

- Deposition nucleation on active IN to form initial ice *(NU_{vi})* occurs when $T < T_o$ -5°C and when the air is saturated with respect to water.
- Homogeneous nucleation (HNU_{ci} and HNU_{ri}) occur when $T <$ -40°C
- The growth (loss) rates of ice particles through deposition (sublimation) are determined by the water vapour diffusion rate in the surrounding air and the condition for thermodynamic equilibrium. The bulk deposition (sublimation) rate is calculated by equation 2.10 [*Kong & Yau*, 1997]:

$$VD_{vi} = \frac{1}{\rho}\int_0^\infty \left(\frac{dm_i}{dt}\right)_{VD} N_i(D_i)dD_i \qquad (2.10)$$

where $(dm_i/dt)_{VD}$ is the rate of change of mass of a single ice particle by deposition or sublimation.

- Growth of a single ice particle by riming (*CLci*) occurs when the environment is supersaturated with respect to ice, $q_c \geq 10^{-5}$ g g^{-1} and $D_i \geq 200$ μm.

- Contact freezing (*FR_{ri}*) occurs in a cloud where supercooled raindrops and ice crystals coexist in the model environment ($T < T_0$, $q_i > 0$) and uses a probability function that a supercooled rain drop of diameter *D* captures an ice crystal of any size per unit time and deposition of water vapour *(VD_{vi})*.
- When ice particles fall into a layer with $T > T_0$ melting of ice particles occurs to form rain *(ML_{ir})* instantaneously.

The model surface component uses a set mosaic approach with four surface types: land, open water, sea ice and glaciers [*Erfani et al*., 2006]. The sea ice fraction in the regional model is updated with weekly Canadian Ice Service data, which are interpolated to model resolution. The generalization to model resolution means small-scale features such as leads are not considered.

2.5 Summary and concluding remarks

The purpose of this chapter was to discuss the importance and current state of knowledge of cold season orographic precipitation with an emphasis on high latitudes. The formation of orographic precipitation was shown to be dependent on the characteristics of large-scale flow towards a topographic barrier, orographic lifting which cools the air to saturation and initiates condensation and the conversion of condensate to precipitation particles through microphysical processes. The amount and distribution of precipitation was shown to vary based on ambient atmospheric conditions (cross-barrier flow strength, stability, moisture, temperature) and terrain geometry (mountain height and width).

Many aspects of the basic mechanisms responsible for orographic precipitation are known: however multiple interacting processes, operating on a wide variety of scales, make the prediction of precipitation in complex terrain challenging. Meso-scale models, with sophisticated cloud and precipitation parameterizations, have been used to further advance understanding of cold season orographic precipitation processes and events across mountainous terrain. This body of research has provided insights into the complexity and variety of interactions between the atmosphere and orography, and has had some success simulating orographic precipitation. A significant portion of our knowledge of orographic precipitation is derived from mid-latitude observations with limited research directly pertaining to orographic precipitation at high latitudes. Some similarities have been identified between precipitation in mid- and high latitudes, but there are also many unique features more specific to high latitudes that will influence the formation and distribution of orographic precipitation, which may not be properly characterized in model parameterization schemes developed from mid-latitude observations. In high latitude environments temperatures are typically below 0°C from late fall until spring, making snow the dominant form of precipitation, the lower atmosphere is normally characterized by a strong static stability, low moisture supply, and a seasonally frozen surface. Sublimation also has been shown to reduce precipitation that reaches the surface.

An improved understanding of orographic precipitation at high latitudes necessitates the collection of high-resolution data as part of intensive, dedicated, field programmes strongly focused on cold season orographic precipitation events. Through the integration of field-based observations with properly validated remote sensing data, as well as regionally focused modelling studies based on microphysical parameterizations specific to high latitude environments, will ultimately lead to an improved understanding of cold season orographic processes and the importance of orographic precipitation in the context of a changing climate.

2.6 References

Ahrens, C.D, Jackson, P., and C. Jackson. Meteorology Today: an introduction to weather, climate, and environment (1st Canadian Edition). Nelson Education Ltd., Toronto, Ontario, Canada. 615 pages.

Asuma, Y., Inoune, Y., Kikuchi, Y.K., Kajiokawa, M., Sata, N., and, Hayaska, T. (2000). Wintertime precipitation behaviour in the western Canadian Arctic region. *Journal of Geophysical Research, 105, D11,* doi:10.1029/1999JD901124.

Asuma, Y., Iwata, S., Kikucki, K., Moore, G.W.K., Kimura, R., and Tsuboki, K. (1998). Precipitation Features Observed by Doppler Radar at Tuktoyaktuk, Northwest Territories, Canada, during the Beaufort and Arctic Storms Experiment. *Monthly Weather Review. 125,* 2384-2405.

Bailey, M. P. and Hallett, J. (2009): A Comprehensive Habit Diagram for Atmospheric Ice Crystals: Confirmation from the Laboratory, AIRS II, and Other Field Studies. *Journal of Atmospheric Sciences, 66,* 2888–2899.

Barros, A.P. and Lettenmaier, D.P. (1994). Dynamic Modeling of Orographically Induced Precipitation. *Review of Geophysics*, *32*, 265-284.

Barry, R.G. (2008). Mountain Weather and Climate. Cambridge University Press, Cambridge, UK. 506 pages.

Barstad, I. and Smith, R.B. (2005). Evaluation of an orographic precipitation model. *Journal of Hydrometeorology, 6,* 85-99.

Basist, A. and Bell, G.B. (1994). Statistical Relationship between Topography and Precipitation Patterns. *Journal of Climate*, *7*, 1305-1315.

Bech, J., Gjertsen, U., and G. Hasse (2007). Modelling weather radar beam propagation and topographical blockage at northern high latitudes. *Quarterly Journal of the Royal Meteorological Society, 133,* 1191-1204.

Belair, S., Mailhot, J., Girard, J., and Vaillancourt, P. (2005). Boundary layer and shallow cumulus clouds in a medium-range forecast of a large-scale weather system. *Monthly Weather Review, 133,* 1938–1960. doi:10.1175/MWR2958.1.

Bergeron, T. (1949). The problems of artificial control of rainfall on the globe II: The coastal orographic maxima of precipitation in autumn and winter. *Tellus. 1,* 15-32.

Brown, P.A. and Swann, H.A. (1997). Evaluation of key parameters in three-dimensional cloud model simulations using aircraft and multi-parameter radar data. *Quarterly Journal of the Royal Meteorological Society, 123,* 2245-2275.

Bousquet, O., and Smull, B.F. (2003). Airflow and precipitation fields within deep alpine valleys observed by airborne Doppler Radar. *Journal of Applied Meteorology. 42,* 1497-1513.

Brynjólfsson, S. and Ólafsson, H. (2009). Precipitation in the Svarfaðardalur region, North Iceland. *Meteorology and Atmospheric Physics*. *103,* 57-66.

Burford, J.E. and Stewart, R.E. (1998). The sublimation of falling snow over the Mackenzie River Basin. *Atmospheric Research, 49*, 289-214.

Colle, B.A. (2004). Sensitivity of orographic precipitation to changing ambient conditions and terrain geometrics: An idealized modelling perspective. *Journal of Atmospheric Science, 61,* 588-608.

Colle, B. A., Westrick, K. J., and Mass, C.F. (1999). Evaluation of the MM5 and Eta-10 precipitation forecasts over the Pacific Northwest during the cool season. *Weather and Forecasting*. *14,* 137–154

Cosma, S., Richard, E., and Miniscloux, F. (2002). The role of small-scale orographic features in the spatial distribution of precipitation. *Quarterly Journal of the Royal Meteorological Society, 2,* 75-92.

Côté, J., Gravel, S., Méthot, A., Patoine, A., Roch, M., and Staniforth, A. (1998). The operational CMC-MRB global environmental multiscale (GEM) model. Part I: Design considerations and formulation. *Monthly Weather Review, 126,* 1373-1396

Curry, J.A., Rossow, W.B., Randall, D.A., and Schramm, J.L. (1996). Overview of Arctic cloud and radiation characteristics. *Journal of Climate, 9,* 1731–1764.

Curry, J.A. Hobbs, P.V., King, M.D., Randall, D.A., Minnis, P., Isaac, G.A., Pinto, J.O., Uttal, T., Bucholtz, A., Cripe, D.G., Gerber, H., Fairall, C.W., Garrett, T.J., Hudson, J., IntrierI, J.M., Jakob, C., Jensen, T., Lawson, P., Marcotte, D., Nguyen, L., Pilewskie, P., Rangno, A., Rogers, D.C., Strawbridge, K.B., Valero, F.P.J., Williams, A.G., and Wylie, D. (2000). FIRE Arctic Clouds Experiment. *Bulletin of the American Meteorological Society, 81*, 5–29.

Deacu, D., Zandra. A., and Hanesiak, J. (2010). Simulating wind channelling over Frobisher Bay and its interaction with downslope winds during the 7-8 November 2006 Wind Event. *Atmosphere-Ocean. 48*, 101-121. doi:10.3137/AO1109.2010.

De Boer, G., Tripoli, G.J., and Eloranta, E.W. (2008). Preliminary comparison of CloudSAT derived microphysical quantities with ground-based measurements for mixed-phase cloud research in the Arctic. *Journal of Geophysical Research –Atmosphere,* 113, doi:10.1029/2008JD10029.

Dickinson, M.J. and D.J. Knight (1999). Frontal Interaction with Mesoscale Topography. *Journal of Atmospheric Science, 56*, 3544-3559.

Duchon, C.E. and Essenberg, G.R. (2001). Comparitve rainfall observations from pit and above ground rain gauges with and without wind shields. *Water Resource Research. 37*, 3253-3263.

Egger, J. and Hoinka, K.P. (1992). Fronts and Orography. *Meteorology and Atmospheric Physics*. 48, 3-36.

Erfani, A., Mailhot, J., Methot, A., Gravel, S., Desgagne, M., Plante, A., Sills, D., King, P., and Ashton, A. (2006). The 2.5 km horizontal resolution limited area version of the Global Environmental Multiscale model over southern Ontario and Quebec. *In: Abstracts of 15th International Great Lakes Operational Meteorology Workshop, 25–27 October 2006*, Niagara Falls, Ontario, Canada.

Fargey, S., Hanesiak, J., Liu, G., Gilligan, J., and Stewart, R. (editors) (2008). Storm Studies in the Arctic (STAR) Data Report. Centre for Earth Observation Science, 440 Wallace Building, University of Manitoba, Winnipeg, Manitoba, Canada, 75 pages.

Garand, L. and Mailhot, J. (1990). The influence of infrared radiation on numerical weather forecasts. *In: Proceedings of the seventh Conference on Atmospheric Radiation, 23–27 July 1990*, San Francisco, USA.

Garvert, M.F., Smull, B., and Mass, C. (2007). Multiscale mountain waves influencing a major orographic precipitation event. *Journal of Atmospheric Sciences, 64,* 711-737.

Gascon, G., Stewart, R.E., and Henson, W. (2010). Major cold-season precipitation events at Iqaluit, Nunavut. *Arctic. 63,* 327–337.

Goodison, B.E., Louie, P. and D. Yang. (1998) WMO solid precipitation measurement intercomparison: Final report. World Meteorological Organization, Instruments and Observing Methods Rep. 67, WMO/TD 872, 318 pp.

Gultepe, I., Issac., G.A., and Cober, S.G. (2001). Ice Crystal Number Concentration versus Temperature for Climate Studies. *International Journal of Climatology, 21,* 1281-1302.

Hanesiak, J., Stewart, R.E., Szeto, K., Hudak, D., and Leighton, H. (1997). The structure, water budget, and radiational features of a high-latitude warm front. *Journal of Atmospheric Sciences, 12***,** 1553–1573.

Hanesiak, J., Stewart, R.E., Taylor, P., Moore, K., Barber, D., McBean, G., Strapp, J.W. Wolde, M., Goodson, R., Hudson, E., Hudak, D., Scott, J., Liu, G., Gilligan, J., Biswas, S., Desjardins, D., Dyck, R., Fargey, S., Field, R., Gascon, G., Gordon, M., Greene, H., Hay, C., Henson, W., Hochheim, K., Laplante, A., Martin, R., Melzer, M.A., and Zhang, S. (2010). Storm Studies in the Arctic: The meteorological field project. *Bulletin of the American Meteorological Society, 91,* 47-68. doi:10.1175/2009BAMS2693.1

Harimaya, T. and Sato, M. (1989). Measurements of the Riming Amount on Snowflakes. *Journal of the Faculty of Science, Hokkaido University Series 7, Geophysics*. *8*, 355-366.

Harimaya, T. (1975). The riming properties of snow crystals. *Journal of the Meteorological Society of Japan.* 53, 384-392.

Henson, W., Stewart, R., and Hudak, D. (2011). Vertical reflectivity profiles of precipitation over Iqaluit, Nunavut during Autumn 2007. *Atmospheric Research*, *99*, 217-229. doi: 10.1016/j.atmosres.2010.10.009.

Hobbs, P.V., Easter, R.C., and Fraser, A.B. (1973). A Theoretical Study of the Flow of Air and Fallout of Solid Precipitation Over Mountainous Terrain: Part II Microphysics. *Jounral of Atmospheric Sciences, 30*, 813-824.

Hobbs, P.V., Chang, S., and Locatelli, J.D. (1974). The dimensions and Aggregation of Ice Crystals in Natural Clouds. *Journal of geophysical Research, 79,* 2199-2206.

Hobbs, P.V. (1975). The nature of winter clouds and precipitation in the Cascade Mountains and their artificial seeding. Part 1: natural conditions. *Journal of Applied Meteorology, 14***,** 783-804.

Hou, A.Y., Kakar, R.K., Neeck, S., Azibarizin, A.A., Kummerow, C.D., Kojima, M., Oki, R., Nakamura, K., and Iguchi, T. (2013). The Global Precipitation Measurement (GPM) mission. *Bulletin of the American Meteorological Society,* Advance online publication. doi: 10.1175/BAMS-D-13-00164.1.

Houze, R.A. (1993). Cloud Dynamics. International Geophysics Series, Volume 53. Academic Press, Inc. San Diego, CA, USA. 573 pages.

Houze, R.A, James, C.N., and Medina, S. (2001). Radar observations of precipitation and airflow on the Mediterranean side of the Alps: Autumn 1998 and 1999. *Quarterly Journal of the Royal Meteorological Society, 127***,** 2537-2558.

Houze, R.A. and Medina, S. (2005). Turbulence as a mechanism for orographic enhancement. *Journal of Atmospheric Sciences, 62,* 3599-3623.

Hudak, D.R. and M.C. Young (2002). Storm climatology of the southern Beaufort Sea. *Atmosphere-Ocean, 40,* 145-158.

Hudak, D.R. and R. Nissen (1996). Doppler radar applications in major winter snowstorms. *Atmospheric Research*, *41*, 109-130.

Intihar, M.R. and Stewart, R.E. (2005). Extratropical cyclones and precipitation within the Canadian archipelago during the cold season. *Arctic. 58*, 162-174.

IPCC. (2013). Climate Change 2013: The Physical Science Basis. Contribution of Working Group I to the Fifth Assessment Report of the Intergovernmental Panel on Climate Change [Stocker, T.F., D. Qin, G.-K. Plattner, M. Tignor, S.K. Allen, J. Boschung, A. Nauels, Y. Xia, V. Bex and P.M. Midgley (eds.)]. Cambridge University Press, Cambridge, United Kingdom and New York, NY, USA, 1535 pp.

Jiang, Q. and Smith, R. (2003). Cloud timescales and orographic precipitation *Journal of Atmospheric Sciences, 60,* 1543-1559.

Jiang, Q. (2007). Precipitation over multiscale terrain. *Tellus A*, *59,* 321-335.

Kong, F. and Yau, M.K. (1997). An explicit approach to microphysics in MC2. *Atmosphere-Ocean, 35*, 257-291.

Korolev, A.L., Issac, G.A., and Hallett, J. (1999). Ice Particle habits in Arctic Clouds. *Geophsyical Research Letters, 26*, 1299-1302.

Lachlan-Cope, T. (2010). Antarctic clouds. *Polar Research*, *29*, 150-158.

Lawson, R.P., Baker, B.A, Zmarzly, P., O'Conner, D., Mo, Q., Gayet, J-F., and Shcherbakov, V. (2006). Microphysical and Optical Properties of Atmospheric Ice Crystals at South Pole Station. *Journal of Applied Meteorology and Climatology*, *45*, 1505-1525.

Liu, Y., Farely, R.D., and Orville, H.D. (1983). Bulk Parameterization of a Snow Field in a Cloud Model. *Journal of Climate and Applied Meteorology. 22,* 1065-1092.

Liu, Y., Ackerman, S.T., Maddux, B.C., Key, J.R., and Frey, R.A. (2010). Errors in Cloud Detection over the Arctic Using a Satellite Imager and Implications for Observing Feedback Mechanisms. *Journal of Climate, 23,* 1894-1907.

Locatelli, J. and Hobbs, P.V. (1974). Fall Speeds and Masses of Solid Precipitation Particles. *Journal of Geophysical Research, 79*, 2183-2196.

Mailhot, J. 1994. The Regional Finite-Element (RFE) Model Scientific Description – Part 2: Physics. Meteorological Service of Canada Internal Science Report. Atmospheric Environment Service, Dorval, Quebec. March, 1994.

Mailhot, J., Bélair, S., Lefaivre, L., Bilodeau, B., Desgagné, M., Girard, C., Glazer, A., Leduc, A-M., Methot, A-M., Patoine, A., Plante, A., Rahil, A., Talbot, D., Tremblay, A., Vaillancourt, P., Zadra, A., and Qaddouri, A. (2006). The 15-km version of the Canadian regional forecast system. *Atmosphere-Ocean*, 44, 133-149. doi: 10.3137/ao.440202.

Magono, C. and Lee, C.W. (1966). Meteorological Classification of Natural Snow Crystals. *Journal of the Faculty of Science, Hokkiaido University, Series VII* (Geophysics*), 2,* 1-43.

Magono, C. and Kikuchi, K. (1980). Some observations of snowfall and meteorological conditions in Arctic Canada. *Monthly Weather Review*, *108,* 1656-1664.

Marchard, R., Mace, G.G., Ackerman, T. and Stephens, G.L. (2008). Hydrometeor detection using CloudSat – An Earth orbiting 94-GHz cloud radar. *Journal of Atmospheric and Oceanic Technology, 25*, 519-533.

Medina, S. and Houze, R.A. (2003). Air motions and precipitation growth in Alpine Storms. *Quarterly Journal of the Royal Meteorological Society, 129*, 345-371.

Medina, S., Smull, B.F., Houze Jr., R.A., and Steiner, M. (2005). Cross-Barrier Flow during Orographic Precipitation Events: Results from MAP and IMPROVE. *Journal of Atmospheric Sciences – Special Edition. 62*, 3580-3600.

Miles, G.M., Marshall, G.J., McConnell, J.R., and Aristarian, A.J. (2008). Recent accumulation variability and change on the Antarctic Peninsula from the ERA40 reanalysis. *International Journal of Climatology, 28,* 1409-1422.

Milbrandt, J.A., Yau, M.K., Mailhot, J., Belair, S., and McTaggart-Cowan, R. (2010). Simulation of Orographic Precipitation Event during IMPROVE-2 Part II: Sensitivity to the Number of Moments in the Bulk Microphysics Scheme. *Monthly Weather Review, 138,* 625-642.

Moran, K/P., Matner, B.E., Post, M., Kropfli, R.A., Welsh, D.C. and K.B. Widener. (1998). A unattended cloud-profiling radar for use in climate research. *Bulletin of the American Meteorological Society. 19*, 443-455.

Morrison, H., Zuidema, P., McFarquhar, G.M., Bansemer. A., and Heymsfield, A.J. (2011). Snow microphysical observations in shallow mixed-phase and deep frontal Arctic cloud systems. *Quarterly Journal of the Royal Meteorological Society*, *137,* 1589–1601.

Neiman, P.J., Ralph, F.M., White, A.B., Kingsmill, D.E., and Persson, P.O.G. (2002). The statistical relationship between upslope flow and rainfall in California's coastal mountains: Observations during CALJET. *Monthly Weather Review*, *130,* 1468-1492.

Nordø, J. and Hjortæs, K. (1966). Statistical studies of precipitation on local, national and continental scales. *Geofysikk Publikasjonen, 26*, 1-46.

Peng, M.S., Powell, J.H., Williams, R.T., and Jeng, B-F. (2001). Boundary Layer Effects on Fronts over Topography. *Journal of Atmospheric Sciences, 58,* 2222-2239.

Pruppacher, H.R. and Klett, J.D. (2000). Microphysics of Clouds and Precipitation (2nd Edition). Kluwer Academic Publishers, Norwell, MA, USA. 954 pages.

Rango, A.L. and Hobbs, P.V. (2001). Ice particles in stratiform clouds in the Arctic and possible mechanisms for the production of high ice concentrations. *Journal of Geophysical Research, 106,* 15,065-15,075.

Reinking, R.F. and Boatman, J.F. (1986). Upslope precipitation events. *Mesoscale Meteorology and Forecasting*, 437-471.

Reinking, R.F.; Snider, J.B., and Coen, J.L. (2000). Influences of Storm-Embedded Orographic Gravity Waves on Cloud Liquid Water and Precipitation. *Journal of Applied Meteorology 39,* 733-759.

Reuder, J., Fagerlid, G.O., Barstad, I., and Sandvik, A. (2007). Stord Orographic Precipitation Experiment (STORPEX) and overview of phase I. *Advances in Geosciences*, *10,* 17-23.

Roberts, E., Nawri. N., and Stewart, R.E. (2008). On the storms passing over southern Baffin Island during Autumn 2005. *Arctic,* 61, 309-321.

Roe, G.H. (2005). Orographic Precipitation. *Annual Review of Earth and Planetary Sciences, 33,* 645-671.

Rotunno, R. and Houze, R.A. (2007). Lessons on orographic precipitation from the Mesoscale Alpine Programme. *Quarterly Journal of the Royal Meteorological Society*, *133,* 811–830.

Serreze, M.C. and Barry, R.G. (2005). The Arctic Climate System. Cambridge University Press. Cambridge, England, UK. 385 pages.

Serreze, M.C. and Hurst, C.M. (2000). Representation of mean Arctic precipitation from NCEP-NCAR and ERA Reanalysis. *Journal of Climate, 13,* 182-201.

Sevruk, B., Ondrás, M., and Chvíla, B. (2009). The WMO precipitation measurement intercomparisons. *Atmospheric Research*, 92, 376-380.

Smith, R.B. (1979). The influence of mountains on the atmosphere. *Advances in Geophysics, 21,* 187-230.

Smith, R.B., Jiang, Q., Fearson, M.G., Tabary, P., Dororninger, M., Doyle, J.D., and Benoit, R. (2003). Orographic precipitation and air mass transformation: an alpine example. *Quarterly Journal of the Royal Meteorological Society, 129***,** 433-454.

Smith, R.B., Barstad, I., and Bonneau, L. (2005). Orographic precipitation and the Oregon's climate transition. *Journal of Atmospheric Sciences, 62,* 171-191.

Smith, R.B. (2006). Progress on the theory of orographic precipitation. *Tectonic, Climate and Landscape Evolution: Geological Society of America*, Special Paper 398, 1-16.

Smith, C.D. (2008). Correcting the wind bias in snowfall measurements made with a Geonor T-200B precipitation gauge and alter wind shield. *CMOS Bulletin, 36*, 162-168.

Stephens, G.L., Vane, D.G., Boain, R.J., Mace, G.G., Sassen, K., Wang, Z., Illinwirth, J.,O'Conner, E.J., Rossow, W.B., Durden, S.L., Miller, S.D., Austin, R.T., Benedetti, A., Mitrescu, C., and the Cloudsat Science Team. (2002). The Cloudsat Mission and the A-Train: A New Dimension of Space-Based Observations or Cloud and Precipitation. *Bulletin of the American Meteorological Society, 83,* 1771-1790.

Stewart, R.E., Szeto, K.K., Reinking, R.F., Clough, S.A., and Ballard, S.P. (1998). Midlatitude cyclone cloud systems and their features affecting large scales and climate, *Review of Geophysics, 36,* 245-273.

Stewart, R.E., Burford, J.E., Hudak, D.R., Currie, B., Kochtubajda, B., Rodriguez, P., and Liu, J. (2004). Weather systems occurring over Fort Simpson, Northwest Territories, Canada, during three seasons of 1998–1999: Part 2. Precipitation features. *Journal of Geophysical Research, 189,* 1984-2012.

Stull, R.B. (2000). Meteorology for Scientists and Engineers (2nd Edition). Brooks/Cole, PacificGrove, CA, USA. 502 pages.

Tsonis, A.A. (2002). An Introduction to Atmospheric Thermodynamics. Cambridge University Press, Cambridge, UK. 182 pages.

Vaisala, (2013). Vaisala Radiosonde RS92-SGP brochure. Reference B210358EN-F. Accessed from: www.vaisala.com. Date accessed: April 29, 2014.

Walden, V.P., Warren, S.G., and Tuttle, E., (2003). Atmospheric Ice Crystals over the Antarctic Plateau in Winter. *Journal of Applied Meteorology*, *42,* 1391-1406.

Wallace, J.M. and Hobbs, P.V., (2006). Atmospheric Science: An Introductory Survey (2nd Edition). Academic Press Inc. San Diego, CA, USA. 483 pages.

Wolde, M. (2009). Personal communication. STAR Project, NAWX W-band Doppler Velocity vertical velocity profiles.

Woods, C.P., Stoelinga, M.T., Locatelli, J.D., and Hobbs, P.V. (2005). Microphysical processes and synergistic interactions between front and orographic forcing of precipitation during the 13 December 2001 IMPROVE-2 event over the Oregon Cascades. *Journal of Atmospheric Sciences, 62*, 3492-3519.

Woods, C.P., Storelinga, M.T., and Locatelli, J.D. (2007). The IMPROVE-1 Storm of 1-2 February 2001. Part III: Sensitivity of a Mesoscale Model Simulation to the Representation of Snow Particle Types and Testing of a Bulk Microphysical Scheme with Snow Habit Prediction. *Journal of Atmospheric Science, 64,* 3927-3949.

Yuter, S.E. and Houze, R.A. (2003). Microphysical modes of precipitation growth determined by S-band vertically pointing radar in orographic precipitation during MAP. *Quarterly Journal of the Royal Meteorological Society, 129*, 455–476.

Zadra, A., Roch, M., Laroche, S., and Charron, M. (2003). The subgrid-scale orographic blocking parameterization of the GEM Model. *Atmosphere-Ocean, 41*, 155-170.

CHAPTER 3: AIRCRAFT OBSERVATIONS OF OROGRAPHIC CLOUD AND PRECIPITATION FEATURES OVER SOUTHERN BAFFIN ISLAND, NUNAVUT, CANADA

Shannon Fargey[1], John Hanesiak[1], Ronald Stewart[1], and Mengistu Wolde[2]

[1] Department of Environment and Geography, University of Manitoba, Winnipeg, Manitoba, Canada

[2] Flight Research Laboratory, National Research Council of Canada, Ottawa, Ontario, Canada

Atmosphere-Ocean 52 (1), 54-76

doi:10.1080/07055900.2013.855624

This chapter analyses factors that influence cloud and precipitation over the orography in the south-east Canadian Arctic. Specifically, three case studies are examined, which provide the basis for identifying the general characteristics of cloud and precipitation in the study region, along with how these features are modified over the orography and vary with synoptic and sea ice conditions.

Abstract

This study evaluates cloud and precipitation features over the orography of southern Baffin Island in the south-east Canadian Arctic during the Storm Studies in the Arctic (STAR) field project of autumn 2007. Three case studies provide the basis for a comparative analysis of how cloud and precipitation features are modified over the orography compared to the ocean regions upstream, in addition to the variability of these features over diverse synoptic and sea ice conditions.

Using data collected by a research aircraft with an onboard W-band Doppler radar and microphysical instrumentation, multiple factors were found to play roles in enhancing and/or reducing cloud and precipitation over the orography in the region. Gravity waves, terrain shape, atmospheric stability and atmospheric-ocean exchanges were all associated with precipitation enhancement. In addition, several factors were identified to reduce precipitation, including sublimation, high sea ice extent and low-level blocking in the upstream environment. Accretion and aggregation were identified as important particle growth mechanisms over the orography. By increasing particle density and/or mass, the probability of ice particles precipitating to the surface increased. These results indicate that the complexity of these critical features over terrain in high latitude regions poses considerable challenges for modelling.

3.1 Introduction

Orography plays an important role in the production and intensification of cloud systems and precipitation in high latitude environments and is a critical component of the hydrologic cycle. Climatic changes in high latitude environments are expected to include an increase in precipitation as well as cloud cover in the current century [*IPCC*, 2013], increasing the need to accurately represent critical features such as snowfall and clouds over mountain regions.

Our current understanding of orographic precipitation processes (e.g. particle growth, magnitude, and distribution associated with events) and cloud structure has largely been borne from mid-latitude research. Field datasets collected during the Cascade Project [*Hobbs*, 1975], Sierra Cooperative Pilot Project [SCPP; *Reynolds & Dennis*, 1986], Winter Icing and Storms Project [WISP; *Rasmussen et al.,* 1992], Coastal Observation and Simulation with Topography [COAST; *Bond et al.,* 1997], Improvements of the Microphysical Parameterizations through Observational Verification Experiments [IMPROVE-II; *Stoelinga et al.,* 2001], Mesoscale Alpine Programme [MAP; *Rotunno & Houze,* 2005]; Science and Nowcasting of Olympic Weather for Vancouver 2010 [SNOW-V10; *Isaac et al.,* 2012] among others, have revealed important aspects of precipitation production over orography. These include the effect of gravity waves [*Garverts, Smull, & Mass,* 2007], convective instability [*Yuter & Houze,* 2003; *Woods, Stoelinga, Locatelli, & Hobbs,* 2005], and frontal interaction with topography [*Medina & Houze*, 2003; *Smith et al.,* 2003] under a variety of synoptic conditions.

Orographic precipitation growth and distribution has also been shown to be strongly dependent on whether or not low-level atmospheric flow undergoes blocking, or flows unrestricted over terrain [*Smith,* 1979]. Variable ambient atmospheric conditions (flow strength, stability) and terrain geometry (mountain height, width, orientation) were shown to influence the behaviour of a flow impinging on topography in both observational [*Neiman, Ralph, White, Kingsmill, & Persson,* 2002; *Medina & Houze*, 2003; *House & Medina*, 2005] and modelling studies [*Jiang & Smith,* 2003; *Colle,* 2004; *Barsted & Smith,* 2005]. Whether or not the upstream flow has enough energy to rise over the barrier can be described by the Froude number (*Fr*) [*Houze,* 1993]. During MAP, a high *Fr* (>1) resulted in a strong upslope flow and enhancement of precipitation on windward slopes; flow with a low *Fr* (<1) had a tendency to be blocked and may result in enhanced precipitation upstream of the barrier [*Houze, James, & Median,* 2001; *Medina & Houze,* 2003].

Although valuable, these studies may not fully represent the processes observed in high latitude regions. The Arctic often exhibits sub-freezing temperature profiles and precipitation is more likely to fall exclusively as snow during the cold season. Most precipitation events are associated with low to trace amounts, due in part to sublimation below and between multiple cloud layers [*Burford & Stewart,* 1998; *Stewart et al.,* 2004]. In addition, sea ice extent influences atmospheric moisture availability, cloud formation [*Curry, Rossow, Randall, & Scharamm,* 1996; *Curry et al.,* 2000] and atmospheric stability [*Deacu, Zadra, & Hanesiak,* 2010]. In the autumn, the comparatively warm ocean surface underlying a cold atmosphere will foster instability; whereas stronger stability is common when high sea ice extent limits atmosphere-ocean exchanges. As a result, forecasting and modelling clouds and precipitation in the Arctic remains an ongoing challenge.

Difficulties in data collection and limited numbers of monitoring stations have resulted in significant knowledge gaps over the Arctic [*Hanesiak et al.,* 2010]. Results from recent field programs have begun to characterize cloud structure and microphysical properties in the Arctic but investigation of these features over high latitude orography remains limited. Some examples of Arctic field experiments include the Beaufort and Arctic Storms Experiment [BASE; *Hanesiak. Stewart, Szeto, Hudak, & Leighton,* 1997; *Stewart, Szeto, Reinking, Clough, & Ballard,* 1998; *Hudak & Young,* 2002], Mackenzie Global Energy and Water Cycle Experiment (GEWEX) Study [MAGS; *Stewart et al.,* 1998; *Asuma et al.,* 2000], Mixed-Phase Arctic Cloud Experiment [M-PACE; *Verlinde et al., 2007*], First International Satellite Cloud Climatology Project (ISCCP)/Regional Experiment – Arctic Cloud Experiment [FIRE-ACE; *Morrison, Zuidema, McFarquhar, Bansemer, & Heymsfield,* 2011] and Surface Heat Budget of the Arctic [SHEBA; *Uttal et al.,* 2002]. As well, the Storm Studies in the Arctic field experiment [STAR; *Hanesiak et al.,* 2010] was conducted in 2007 over the southern Baffin Island in the eastern Canadian Arctic.

Progress is being made on many aspects of cloud and precipitation characterization from these projects. A recent study by *Laplante, Stewart and Henson* [2012] using CloudSat information pointed out that clouds were common over southern Baffin Island in autumn, but precipitation was only inferred in 13% of the vertical profiles containing clouds. However, precipitation was inferred to preferentially occur on high terrain. *Laplante et al.* [2012] also noted that, when precipitation occurred, cloud tops were generally higher than the mean value, and were colder and thicker than non-precipitating clouds.

The phase of particles within Arctic cloud varies. Mixed-phase clouds occur in all seasons [*Shupe, Matrosov, & Uttal*, 2006], with liquid often occurring in cloud tops that continually precipitate ice [*Hobbs & Rangno,* 1998; *Curry et al.,* 2000; *McFarquhar et al.,* 2007]. *Korolev, Isaac, Cober, Strapp and Hallett* [2003] investigated the relationship with total water content (TWC), ice water content (IWC) and liquid water content (LWC) and temperature in mixed-phase clouds during spring, autumn and winter, using data from both Arctic (BASE; FIRE-ACE) and mid-latitude regions. On average, TWC and IWC in glaciated clouds decreased from about 0.1 g m^{-3} at -5°C to 0.02 g m^{-3} at -35°C. In mixed phase cloud, LWC was found to decrease from about 0.09 g m^{-3} at -5 °C to 0.01 g m^{-3} at -35 °C. By investigating average IWC as a function of height during three major precipitation events in the eastern Canadian Arctic, *Henson, Stewart and Hudak* [2011] observed that, in mostly glaciated clouds, average IWC increased towards the surface. Peak IWC of 0.3 to 0.5 g m^{-3} occurred at relatively low levels, between 500 and 1250 m in these cases, higher than the IWC measured by *Korolev et al.* [2003]. Differences may be related to air mass source region.

In-cloud, *Korolev, Isaac and Hallett* [1999] found that irregularly shaped ice crystals accounted for 97% of ice particles in the western Canadian Arctic. Particles consisted of faceted polycrystalline particles, combinations of different ice habits (ie. bullets, plates, columns) and particles that had been subjected to partial sublimation altering their shape (ie. smooth curving sides or edges). Particles were evenly distributed throughout all size categories (50 to 2000 μm).

At the surface, the nature of snowfall in the eastern Canadian Arctic has also been found to be quite variable. Surface observations identified that columns, needles, plates and dendrites were common during cyclonic storm events [*Roberts, Nawri, & Stewart,* 2008; *Henson et al.,* 2011]. Precipitation was often associated with accreted and pristine particles simultaneously indicating the presence of supercooled water that was not continuous through the growth regions [*Roberts et al.,* 2008]. In addition, particle fragments and aggregate particles were found, indicating particle collisions [*Henson et al.,* 2011]. In contrast, precipitation events over Fort Simpson in the western Arctic were more often associated with single crystals as opposed to aggregates and major cyclonic systems were associated with broad branched crystals, snow grains, and dendrites [*Stewart et al.,* 1998].

In this chapter, cloud and precipitation features associated with upslope flow over the topography of southern Baffin Island in the south-east Canadian Arctic during STAR are investigated. The objective is to analyse factors that influence cloud and precipitation over the orography in the region. Specifically, three case studies are examined, which provide the basis for an analysis of how cloud and precipitation features are modified over the orography compared to the adjacent ocean regions upstream of the terrain. Using data collected by a research aircraft with an onboard W-band Doppler radar and microphysical instrumentation, such as two-dimensional particle probe imagery the thermodynamic, dynamic and microphysical factors that play active roles in enhancing and/or reducing cloud and precipitation over the orography were assessed.

3.2 Data and methodology

3.2.1 Study area

STAR focused on southern Baffin Island, in the south-east Canadian Arctic (Figure 3.1). The region contains some of the most significant topography in Canada and the highest precipitation in the Canadian Arctic. Three quasi-parallel mountain ranges on individual peninsulas, with a northwest-southeast orientation, create multiple lifting regions for advancing flow and variable surface environments that will influence moisture sources. The western-most is the Meta Incognita Peninsula. It has the smallest, 600 to 700 m above mean sea level (ASL), and most gradually inclined topography. The Hall Peninsula reaches a maximum elevation near 1000 m, with a steeply sloped transition from ocean to land on the eastern side of the range. The highest topography (> 2000 m) is on the Cumberland Peninsula, north of Pangnirtung. Peninsula width also varies, with the narrowest being the Meta Incognita (approximately 125 km), and the Hall and Cumberland Peninsulas somewhat wider (each approximately 200 km).

STAR was conducted in autumn 2007 as the adjacent ocean regions transitioned from mainly open water to sea ice covered, reducing ocean-atmosphere exchanges. *Hanesiak et al.* [2010] pointed out that most regions experienced below average ice cover in the autumn of 2007 except for the mouth of Frobisher Bay that had normal ice conditions.

Figure 3.1: Topographic map of southern Baffin Island in Nunavut (1 km Digital Elevation Model (DEM) resolution). The inset map indicates the location of the study area (red box) within Canada.

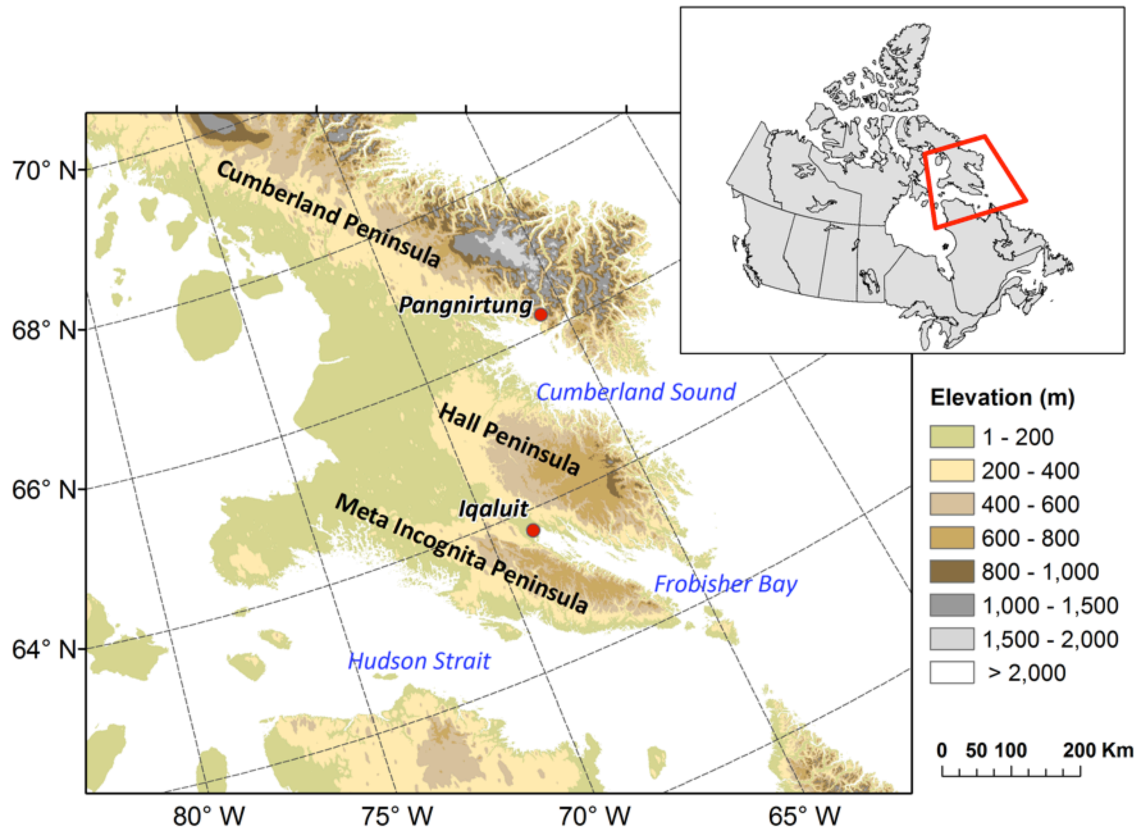

3.2.2 Research aircraft

The National Research Council of Canada (NRC) Convair-580 (CV-580) research aircraft, instrumented by Environment Canada (EC) and the NRC, was used during STAR. The CV-580 used a 95 GHz (3.2 mm wavelength) cloud profiling radar system (W-band) with a 0.7° beam width and 30 to 60 m vertical resolution that provided continuous and simultaneous reflectivity cross sections above and below the aircraft from upward and downward pointing fixed antennae. To remove ground contamination, terrain masks were applied. The aircraft was equipped with a variety of cloud spectrometers, including Particle Measuring System (PMS) two-dimensional cloud (2DC) and precipitation (2DP) imaging probes to estimate particle concentrations for size intervals of 100 to 800 μm and 1000 to 6400 μm respectively, averaged along 10-second (~ 1 km) segments. Particles < 100 μm measured by the PMS-2DC were not used because previous research has revealed substantial errors below this size due to digitization, out of focus oversizing, and speed response issues [*Strapp et al.,* 2001]. Contamination of particle by shattering of ice particles on probe forward surfaces is also an increasing problem below this size [*Korolev et al.*, 2011].

Atmospheric state parameter measurements were collected. They include temperature (*T*), dew point temperature (*Td*), pressure (*P*), and wind fields (speed and direction). Additional parameters, including Nevzorov TWC and PMS King LWC probe (0.05 g m^{-3} sensitivity), as well as data from a Rosemont Icing Detector (RID) (mV) were collected. The Nevzorov probe is a constant temperature hot-wire instrument consisting of two sensors, one for LWC and one for TWC. The threshold sensitivity to water and ice was estimated at 0.003 to 0.005 g m^{-3}. The phase discriminating capabilities of these two sensors are discussed in detail in *Korolev et al.* [2003]. The CV-580 was also equipped with remote temperature, humidity, and wind profiling below the aircraft using an Airborne Vertical Atmospheric Profiling System (AVAPS; GPS dropsonde system). The dropsonde units were modified RD-93 type, where thermodynamic and wind data are recorded at 0.5 s intervals (vertical resolutions of approximately 5 m), with accuracy of: 1.0 hPa for pressure, 0.2°C for temperature, < 0.5 m s^{-1} for wind components and < 5% for relative humidity [*Hock & Franklin,* 1999].

Cloud phase was determined using the RID and techniques developed by *Cober, Isaac and Strapp* [2001]. They demonstrated that differences in the instrument response to ice particles versus water drops could be used to segregate liquid mixed and glaciated cloud regions. Clouds with LWC < 0.01 g m^{-3} cannot be detected with the RID because the mass transfer on the RID sensor from evaporation exceeds that from accretion at such low LWC levels. Visual inspection of particle images from the PMS-2DC and PMS-2DP probes was completed to supplement cloud phase classification to identify glaciated cloud regions.

3.2.3 Additional data sources

Data on sea ice cover were available from the Canadian Ice Service Digital Archive (CISDA). Weekly ice charts were created from an integration of all available real-time sea ice information from various remote sensing satellite sensors, aerial reconnaissance, ship reports, and operational model results [*Howell, Tivy, Yackel, & McCourt,* 2008]. Synoptic and other weather analysis information was obtained from the Environment Canada digital archive (http://www.climate.weatheroffice.ec.gc.ca) as well as real-time archival during STAR. In addition, the National Centers for Environmental Prediction (NCEP) North American Regional Reanalysis (NARR) composites were obtained from the National Oceanic and Atmospheric Administration (NOAA). More information on resolution and accuracy can be found in *Mesinger et al.* [2006].

3.3 Results

To meet the study's objective, a sub-set of available information was evaluated. Of the 14 intensive observation periods (IOPs) during STAR, only three contained data of cloud and precipitation features over orography as well as the associated upstream environment over adjacent ocean regions. The three case studies are *F3* - November 8, 2007 *F5* - November 12, 2007 and *F13* - November 28, 2007 identified by STAR flight number and calendar date. These events were associated with both major cyclonic systems (*F3* and *F5*) and a weak trough (*F13*), all of which resulted in upslope flow over the orography.

Case studies are presented in order of synoptic organization, from most to least developed circulation, to detail forcing fields. Each case study begins with an analysis of the synoptic situation and sea ice extent, followed by a characterization of cloud and precipitation features for both the upstream (adjacent ocean regions) and upslope environment (over orography).

3.3.1 Case study 1: F3 – November 8, 2007

3.3.1.1 Synoptic situation and sea ice extent

Case study 1 (*F3*) is associated with a non-frontal vertically stacked barotropic low pressure system tracking from northern Quebec through Hudson Strait on November 8 (Figure 3.2). The relative position of the low centre resulted in strong easterly to east-south-easterly upslope flow between the surface and 500 hPa and advection of warm air on to the eastern coast of the Hall Peninsula. Sea ice concentrations ranged from < 3/10 (within 50 km of the coast; meaning that combined fractional surface area of all types of ice was less than 30%) to ~8/10 (within 10 km of the coast), thereby not significantly reducing local moisture sources/and or energy exchange prior to lifting over the terrain.

The CV-580 aircraft sampled at multiple levels upstream of the terrain (approximately 25 km from the coast) before flying over the topography of the Hall Peninsula, parallel to the upslope flow (Figure 3.2d). Due to flight restrictions over orography, the CV-580 remained in cloud at a height of 4000 m ASL.

Figure 3.2: F3–8 November 2007 case overview. (a) Sea-level pressure (SLP) (3-hourly NCEP NARR composite) at 0600 UTC with a central pressure of 992 hPa near the flight time; (b) 500 hPa geopotential height (3-hourly NCEP NARR composite) at 0600 UTC; (c) NOAA-17 Advanced Very High Resolution Radiometer (AVHRR) channel 4 image at 0207 UTC; (d) study region—flight track (red line) and data information (i.e., dropsonde (filled yellow circles), radar profile location (black line), and direction of aircraft (blue arrows)). The letters are used as reference locations in upcoming figures. The white dot in panels (a), (b), and (c) indicates the location of Iqaluit, Nunavut, and the red box indicates the case study region of interest (d).

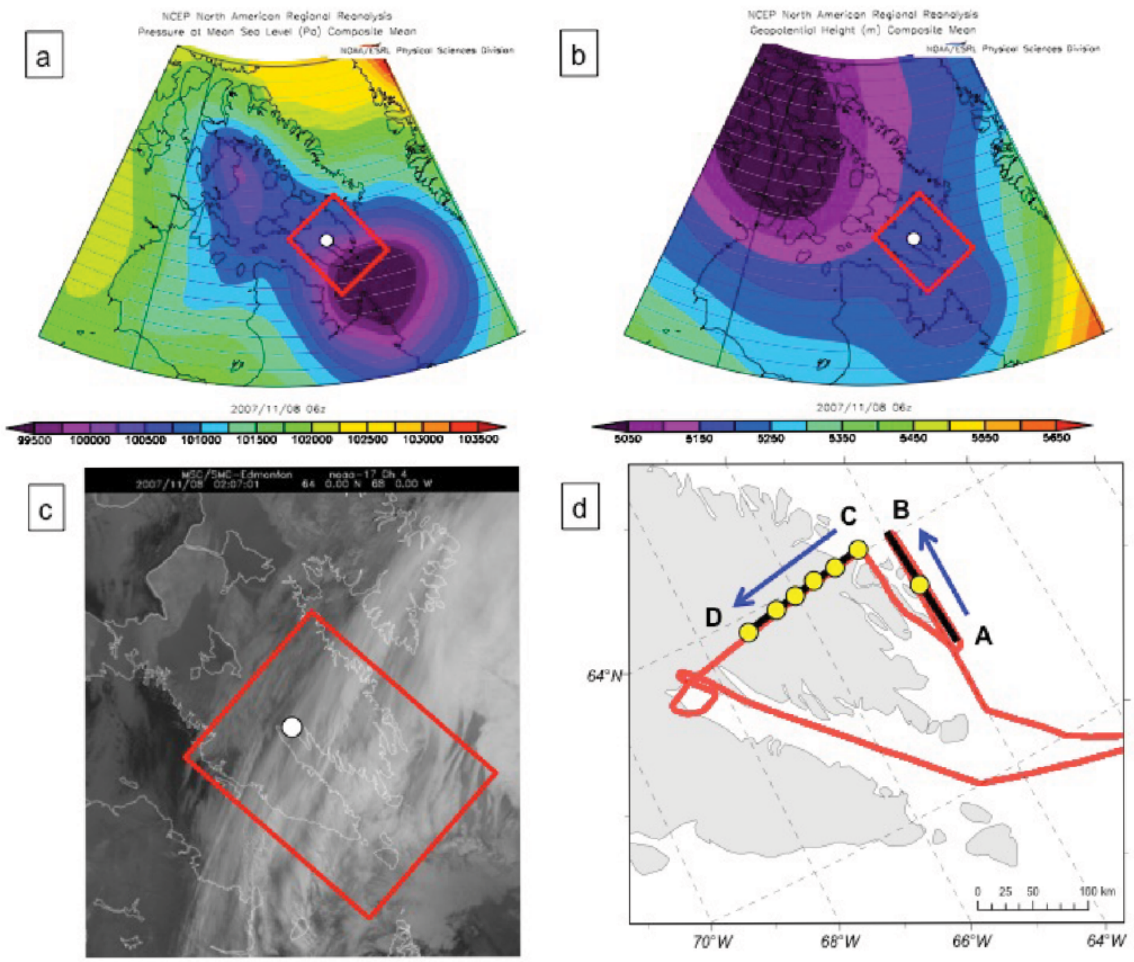

3.3.1.2 Upstream environment

3.3.1.2.1 Vertical atmospheric conditions

A time series of the in situ measurements from *F3* is presented in Figure 3.3. Temperature ranged from -29°C (5000 m) to -9°C (1000 m) (Figure 3.3), decreasing to -1°C at the surface (Figure 3.4a). The atmosphere was nearly saturated below 4500 m (Figure 3.3 and Figure 3.4a). Strong easterly winds were observed at all levels reaching maximum speeds between 20 and 22 m s^{-1} in a region between 300 and 700 m ASL (i.e. below the maximum height of the terrain), decreasing to approximately 12 m s^{-1} at the surface. Dropsonde data indicated a stable upstream environment in this case (Figure 3.4a).

The Froude number (*Fr*) was calculated for each case, where $Fr = U/(NH)$, and U is the upstream flow speed perpendicular to the terrain, N is the Brunt–Väisälä frequency and H is the height of the mountain barrier. The average height in the calculation of *Fr* was assumed to be the crest height parallel to the flight track over the terrain and the Brunt–Väisälä frequency was calculated from dropsonde data. The orography of Baffin Island is not an ideal 2-D barrier, however this calculation provides insight into the dynamics of the flow over the alpine barrier. The *Fr* was high (>1) in *F3*, the result of the strong cross-barrier flow and low mountain height, indicating flow was unrestricted at all levels.

TWC ranged from 0.6 g m^{-3} (1000 m) to 0.1 g m^{-3} (5000 m) (Figure 3.3). The highest value was measured at the lowest altitude (minute 151) and coincided with a period when the RID indicated supercooled liquid (LWC = 0.14 g m^{-3}).

Figure 3.3: Time series of flight data (10-second average) for case study 1 (F3– 8 November 2007). From top to bottom (a) aircraft altitude (m), (b) pressure (hPa), (c) temperature (black line) and dew-point temperature (red line) (^oC), (d) Rosemont Ice Detector (RID) (mV), (e) Total Water Content (black line), Liquid Water Content (dotted line) (g m^{-3}); (f) terrain height ASL (m).

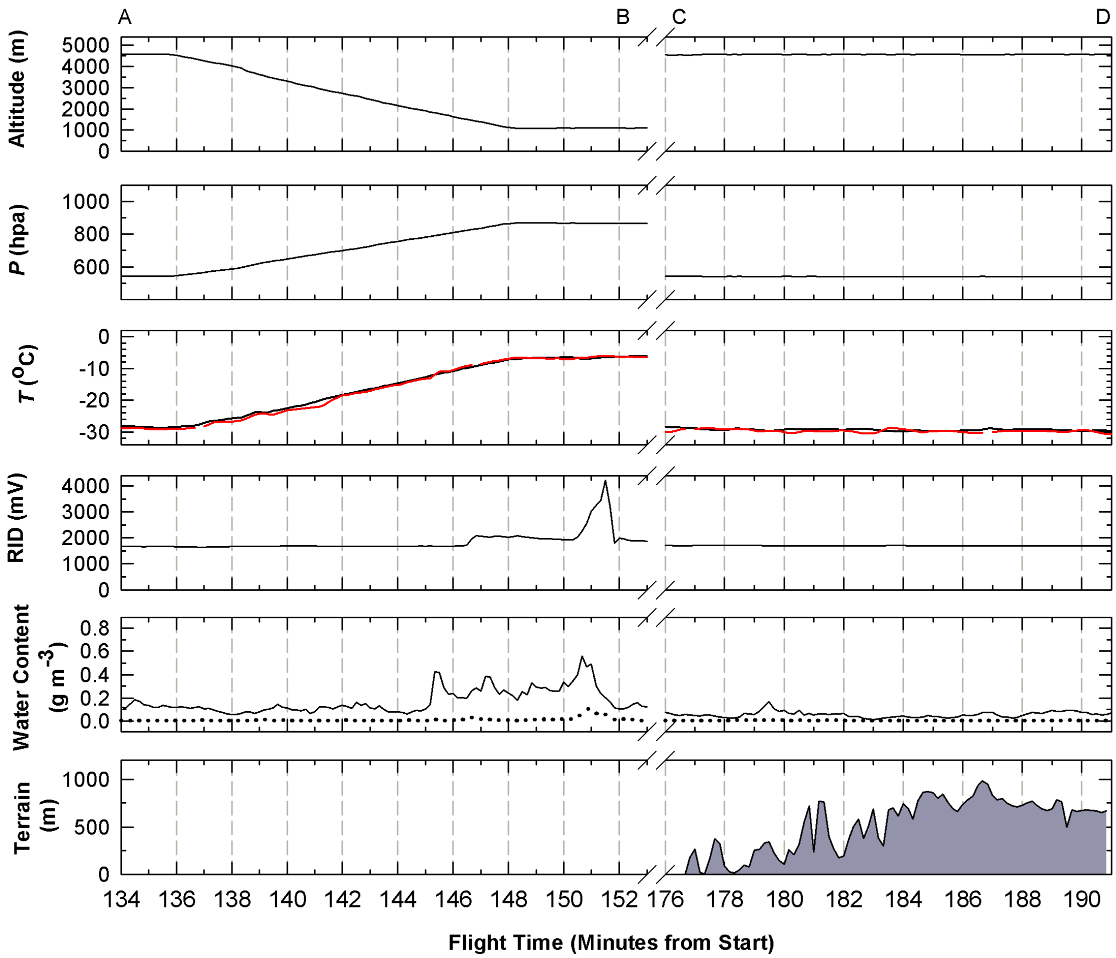

Figure 3.4: Dropsonde data for case study 1 (F3–8 November 2007). (a) Upstream vertical atmospheric profile (released at minute 136), (b) upslope vertical atmospheric profile (released at minute 185).

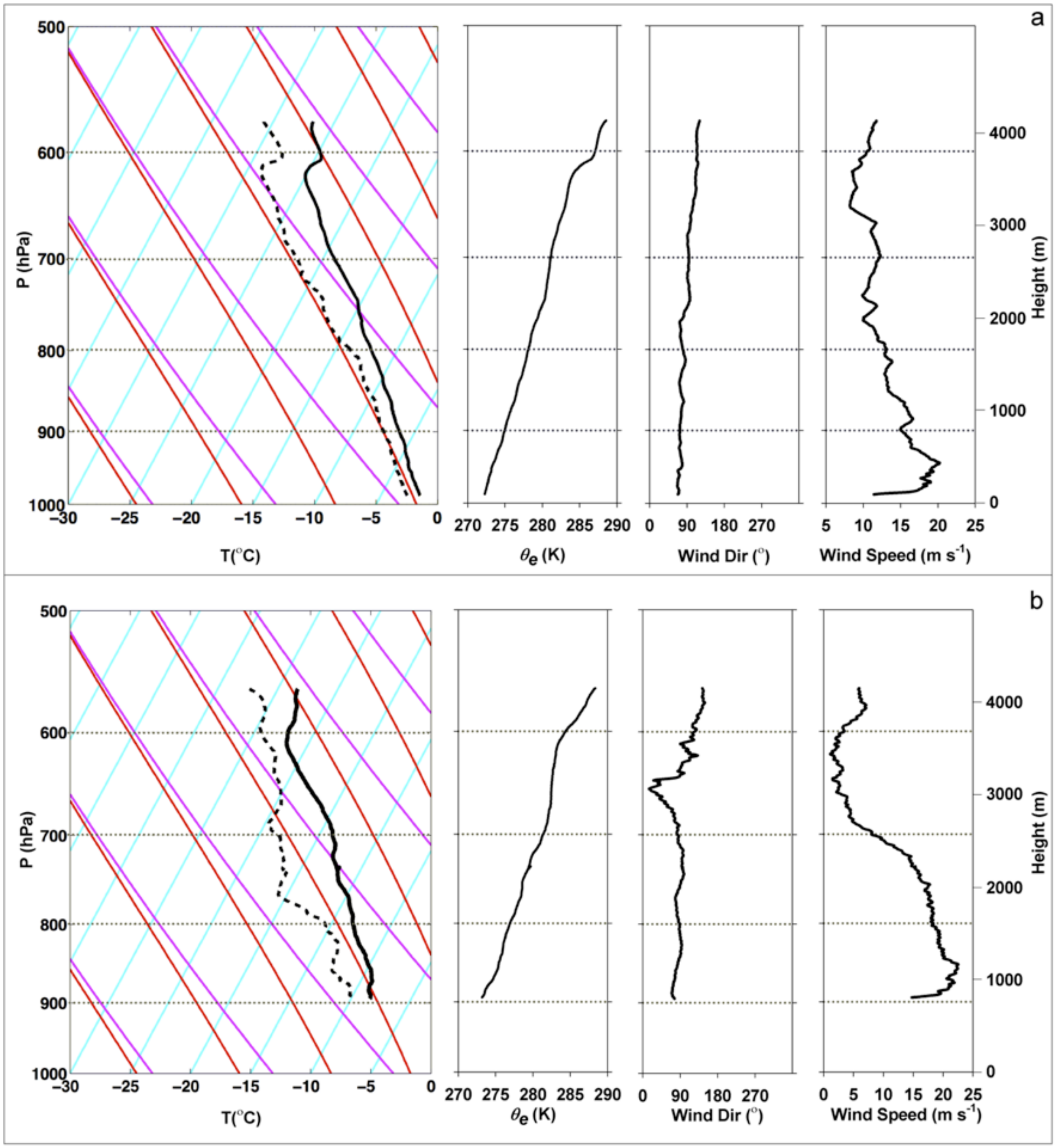

3.3.1.2.2 Cloud and precipitation features

Radar-derived cloud tops ranged from 6500 to 7000 m ASL with precipitation (dBZ > 0) throughout the cloud profile (Figure 3.5a). In general, reflectivity increased toward the surface. Typical surface values were 8 to 10 dBZ, and with a maximum of 14 dBZ (Figure 3.5a). Although not shown, nadir Doppler velocity measurements ~ 1 km upstream of the profile shown in Figure 3.5a, indicate fall speeds increased from 1 to 2 m s^{-1} towards the surface. Cloud-base height, estimated at the cloud condensation level, was 750 m ASL. Reflectivity returns near the surface prevented cloud-base height estimation using radar.

The particle spectra, determined by the PMS-2DC and PMS-2DP probes, shows that the highest concentrations of ice particles were observed in two of the smaller particle ranges (100 to 175 μm and 400 to 500 μm), with average concentrations of 9.5 m^{-3} μm^{-1} and 11.1 m^{-3} μm^{-1}, respectively (Figure 3.6a). This bi-modal distribution may be a reflection of the ice nucleation at different temperature regimes. Particle images show combinations of bullets and columns (rosettes), polycrystalline particles, plates, columns, and numerous particles irregular in shape in upper and mid cloud (3000 to 5000 m), transitioning to dendrites and stellar crystals between 2000 and 2500 m ASL (Figure 3.6b). Light to moderate accretion was observed on particles but the amounts were not consistent, suggesting particles passed through areas with variable liquid water. The increase in particle concentration and the appearance of dendrites is coincident with increased levels of TWC and LWC measured in the cloud (Figure 3.3). Below 2000 m ASL, particles consisted of plates, crystals and/or plates with secular branches, and double-capped columns (Figure 3.6b).

Figure 3.5: Doppler radar data for case study 1 (F3–8 November 2007). Left panels upstream profiles (a) reflectivity (dBZ) and (b) IWC (g m^{-3}). Right panels upslope profiles (c) reflectivity (dBZ) and (d) IWC (g m^{-3}); (e) Doppler velocity (m s^{-1}) - warm hues descent, cool hues ascent, (note the different x-axis scale from (c) and (d)). The terrain is outlined in black for reference, height ASL (m) from DEM. The white line throughout the figures represents the location of the aircraft. The black arrows indicate the direction of aircraft motion. Winds were from right to left in (c), (d), and (e) over the terrain.

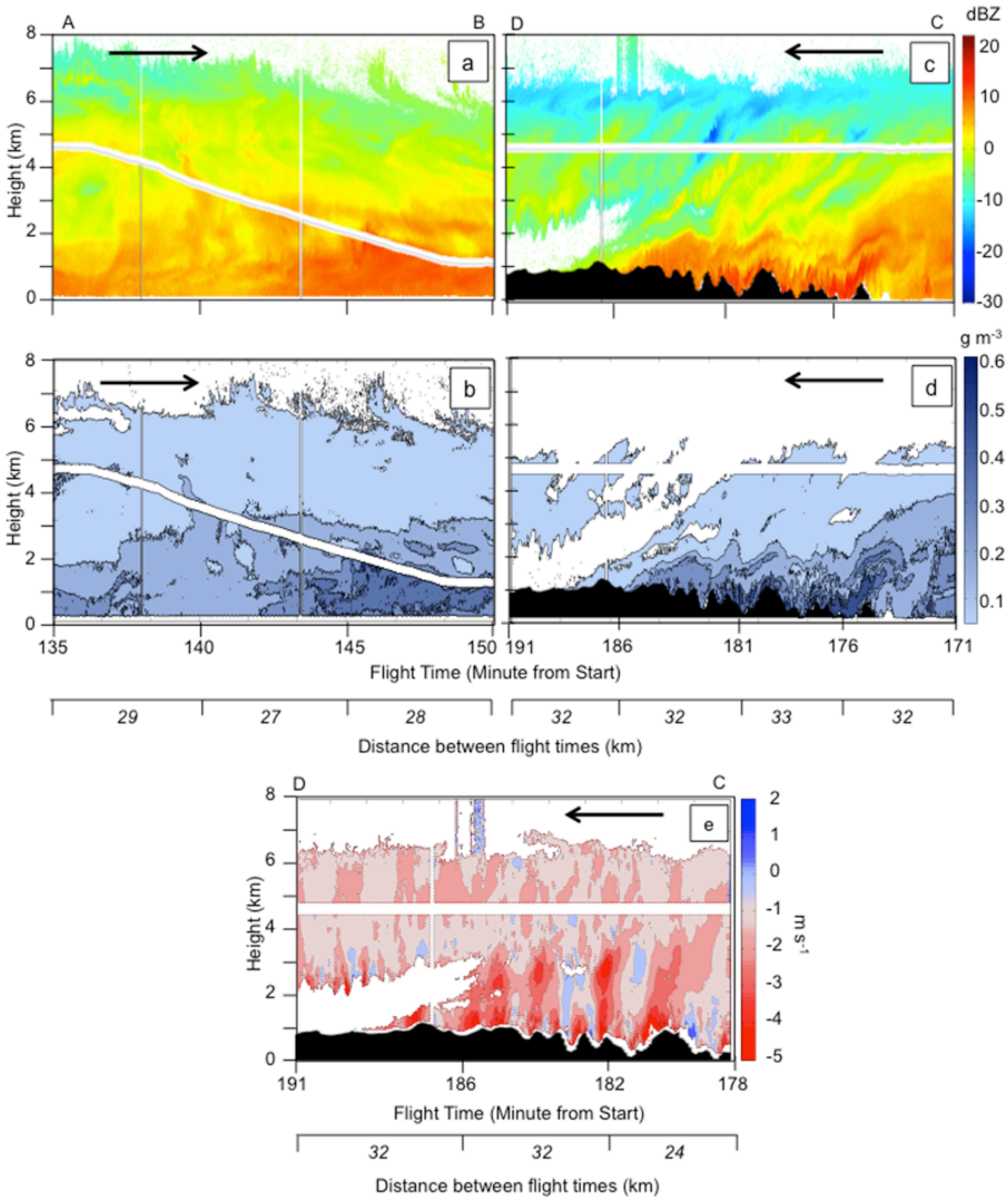

Figure 3.6: Hydrometeor characteristics for case study 1 (F3–8 November 2007). (a) Average particle spectrum (1000–4500 m ASL), (b) sample PMS-2DC images with height in cloud upstream of Hall Peninsula (1000–4500 m ASL), and (c) sample PMS-2DC images over terrain (4000 m ASL).

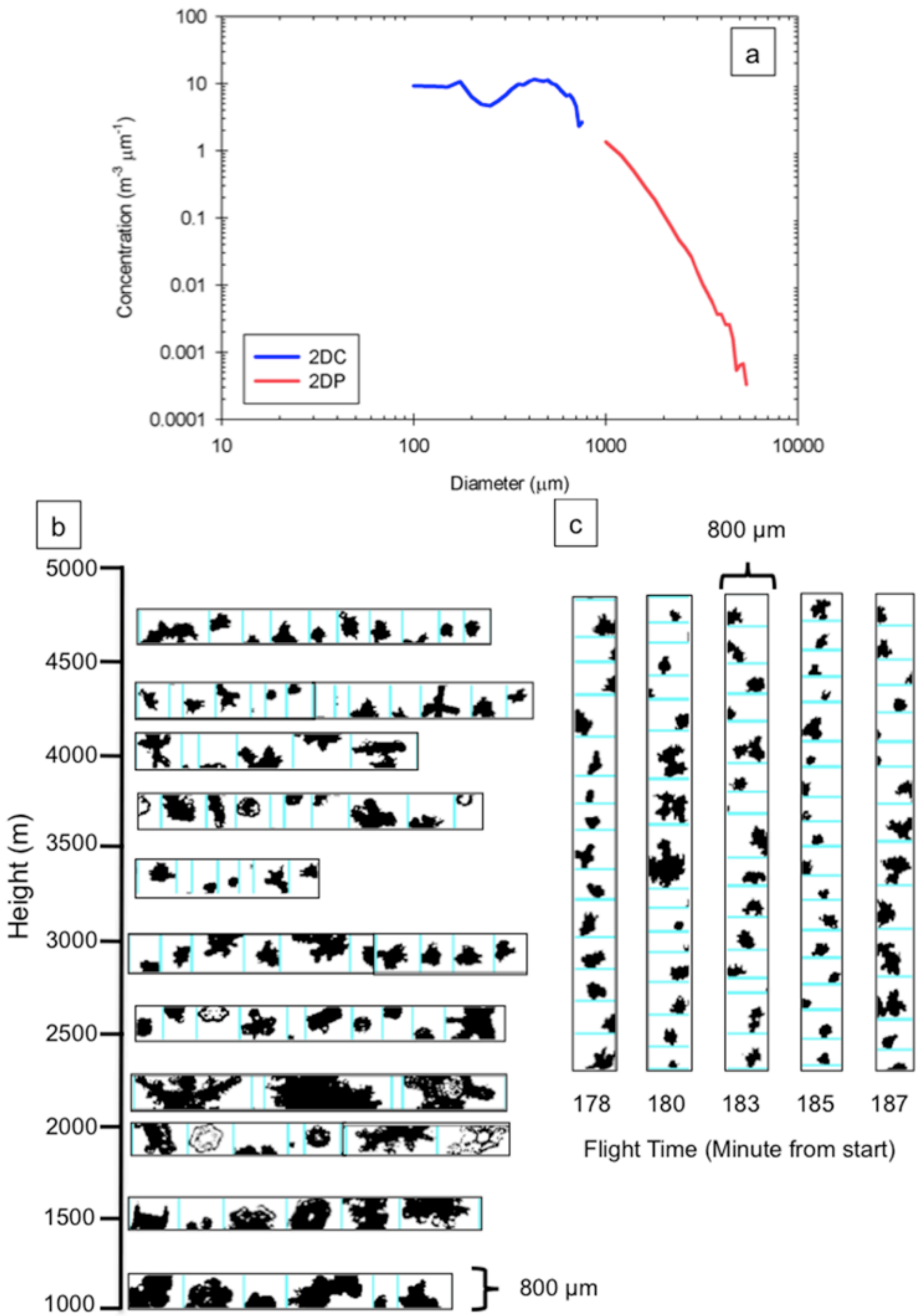

IWC was calculated for each cross section from the radar reflectivity data. The relationship between IWC and radar reflectivity was assumed to be IWC=0.097$Z^{0.59}$ where IWC is in grams per cubic metre as described by *Liu and Illingworth* [2000]. Upstream, IWC values were between 0.05 g m^{-3} (7000 m) and 0.2 g m^{-3} (3000 m), to a maximum of 0.4 g m^{-3} at the surface (Figure 3.5b). Total integrated IWC did not vary substantially along the upstream profile. It maintained values between 28 and 34 g m^{-2}.

3.3.1.3 Upslope cloud and precipitation observations

3.3.1.3.1 Vertical atmospheric conditions

Five dropsondes were released on the eastern (windward) side of the Hall Peninsula (Figure 3.7). The temperature profile showed little variability over the orography, compared to upstream (Figure 3.4a and Figure 3.4b) however, moisture varied significantly. Multiple dry layers between minutes 181 and 187, approximately 80 km inland were identified (Figure 3.7). For example, relative humidity was as low as 60% at 3000 m (minute 182) and 51% at 2500 m ASL (minute 188). At all levels winds were strong easterlies (no low-level blocking), to a maximum 22 m s^{-1} near the surface.

Figure 3.7: Cross section profiles of five dropsondes (minutes 176, 179, 182, 185, and 188) released over the Hall Peninsula. The contoured variables are relative humidity (%) colour shaded; potential temperature θ (K) (white dashed line), equivalent potential temperature θ_e (K) (black dashed line). The terrain from a DEM is overlaid in black.

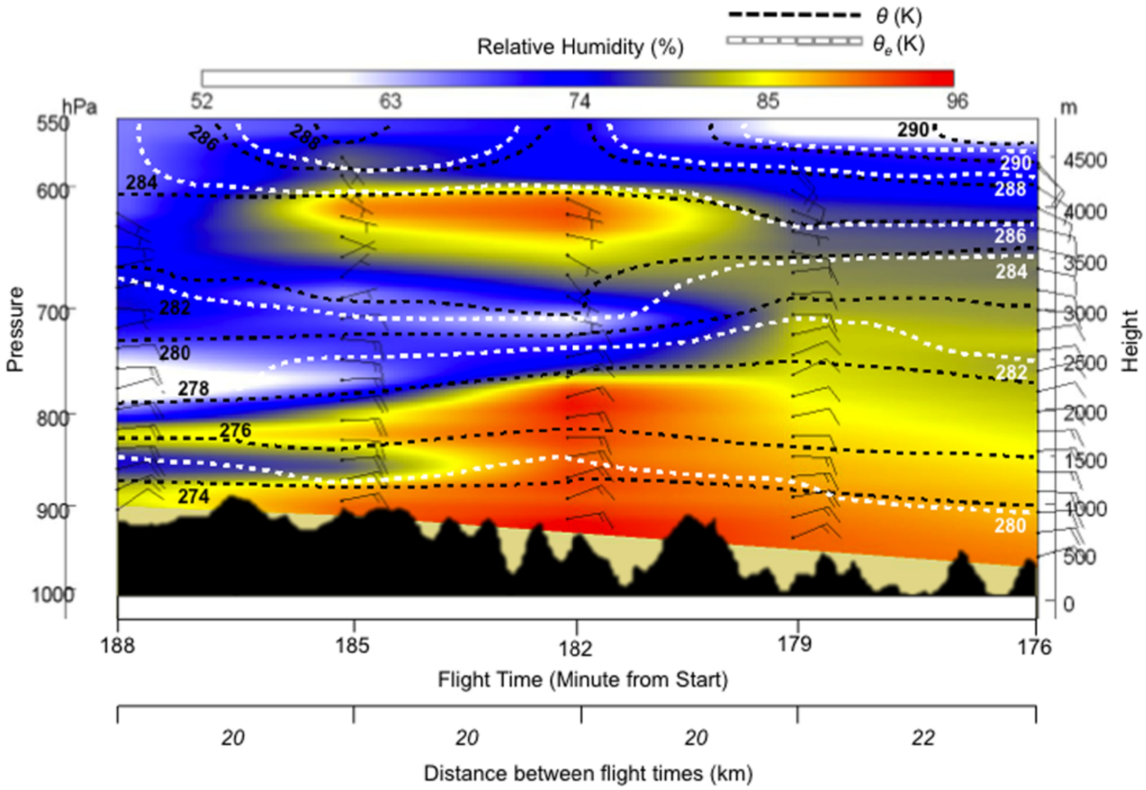

Instability was identified over the terrain. Theta-e (θ_e) and potential temperature (θ) isentropes show ascent in the moist levels when lifting over the terrain began (Figure 3.7). Results suggest there was additional mechanical lift that could supplement precipitation production beyond that of large-scale circulation alone. The θ_e and θ isentropes also show a slight descent in drier regions indicating an increase in stability < 2000 m, however, weaker stability aloft above the dry layers.

TWC was similar to measurements at the same height over adjacent ocean regions upstream, 0.1 to 0.2 g m^{-3} at 4500 m ASL (Figure 3.3). Data indicate the upper region of the cloud was saturated but no LWC near cloud-top.

3.3.1.3.2 Cloud and precipitation features

Radar-derived cloud-top height remained consistent over the orography indicating no additional vertical development over the terrain (Figure 3.5c). Cloud-base height, was 200 to 700 m ASL, increasing in altitude with increased distance inland. Reflectivity returns near the crest of the terrain, estimated at cloud-base height at 2000 m ASL. The reflectivity pattern suggests that sublimation was occurring below cloud-base at this point, so it is probable that cloud-base was higher than 2000 m.

The vertical structure of precipitation indicated fall streaks on the windward slopes of the Hall Peninsula. Reflectivity was higher over the orography than over adjacent ocean regions, reaching a maximum of 18 dBZ near the surface. Reflectivity near the surface remained above 10 dBZ to a distance of approximately 65 km inland (Figure 3.5c). In the lee of the Peninsula, no detectable reflectivity was identified below cloud-base. This suggests that precipitation did not reach the surface on the lee side of the terrain.

A notable cloud feature was identified in this case. A small wave-like pattern, consistent with the shape of the underlying terrain, existed in the reflectivity profile (Figure 3.5c). Doppler velocity measurements confirmed wave motion of the hydrometeors, with updrafts (1 and 2 m s^{-1}) on the windward side of slopes and downdrafts (1 and 2 m s^{-1}) on lee side of peaks (Figure 3.5e). Fall speeds maximum was

5 m s^{-1}, reflecting the influence that the downdraft regions had on falling particles rather than a precise measurement of particle speed. Wave frequency was estimated at 5 to 15 km.

IWC in the upslope profile was greater than those measured upstream of the terrain, reaching maximum values below 1000 m (0.6 to 0.8 g m^{-3}) (Figure 3.5d). Total integrated IWC decreased from 30 g m^{-2} at the coast, to 10 g m^{-2} over the crest of the Hall Peninsula.

Hydrometeor classification was limited to one height over the orography (4000 m). Columnar polycrystalline particles, numerous irregularly shaped accreted particles with some particle aggregation were identified (Figure 3.6c).

3.3.2 Case study 2: F5 – November 12, 2007

3.3.2.1 Synoptic situation and sea ice extent

At 1200 UTC on November 12, a vertically stacked (up to 500 hPa) weak barotropic low pressure system was situated west of Cumberland Sound in Foxe Basin with no distinguishable surface fronts (Figure 3.8). The system remained stationary for 24 hours prior to the CV-580 flight and produced a westerly to south-westerly wind regime perpendicular to the western slopes of the Cumberland Peninsula. A 24-hour snow accumulation of 12 cm was measured in Pangnirtung on November 12 [*Environment Canada*, 2013]. Cumberland Sound was ice-free except for a small 10/10 ice covered region at the head of the Sound. The satellite image suggests there may have been gravity wave motion upstream of Cumberland Sound, over the Meta Incognita and Hall Peninsulas (Figure 3.8c), but this was not confirmed by aircraft observations. Their presence would provide an additional growth mechanism for particles upstream of the *F5* study area and advection of these hydrometers may have contributed to the observed precipitation.

Figure 3.8: F5–12 November 2007 case overview. (a) SLP (3-hourly NCEP NARR composite) at 1200 UTC*, (b) 500 hPa geopotential height (3-hourly NCEP NARR composite) at 1200* UTC*, (c) NOAA-17 AVHRR channel 4 image at 1057* UTC*, (d) study region—flight track (red line) and data information (i.e., dropsonde (filled yellow circles), radar profile location (black line), and direction of aircraft (blue arrows)). The letters are used as reference locations in upcoming figures. The white dot in panels (a), (b), and (c) indicates the location of Iqaluit, Nunavut, and the red box indicates the case study region of interest (d).*

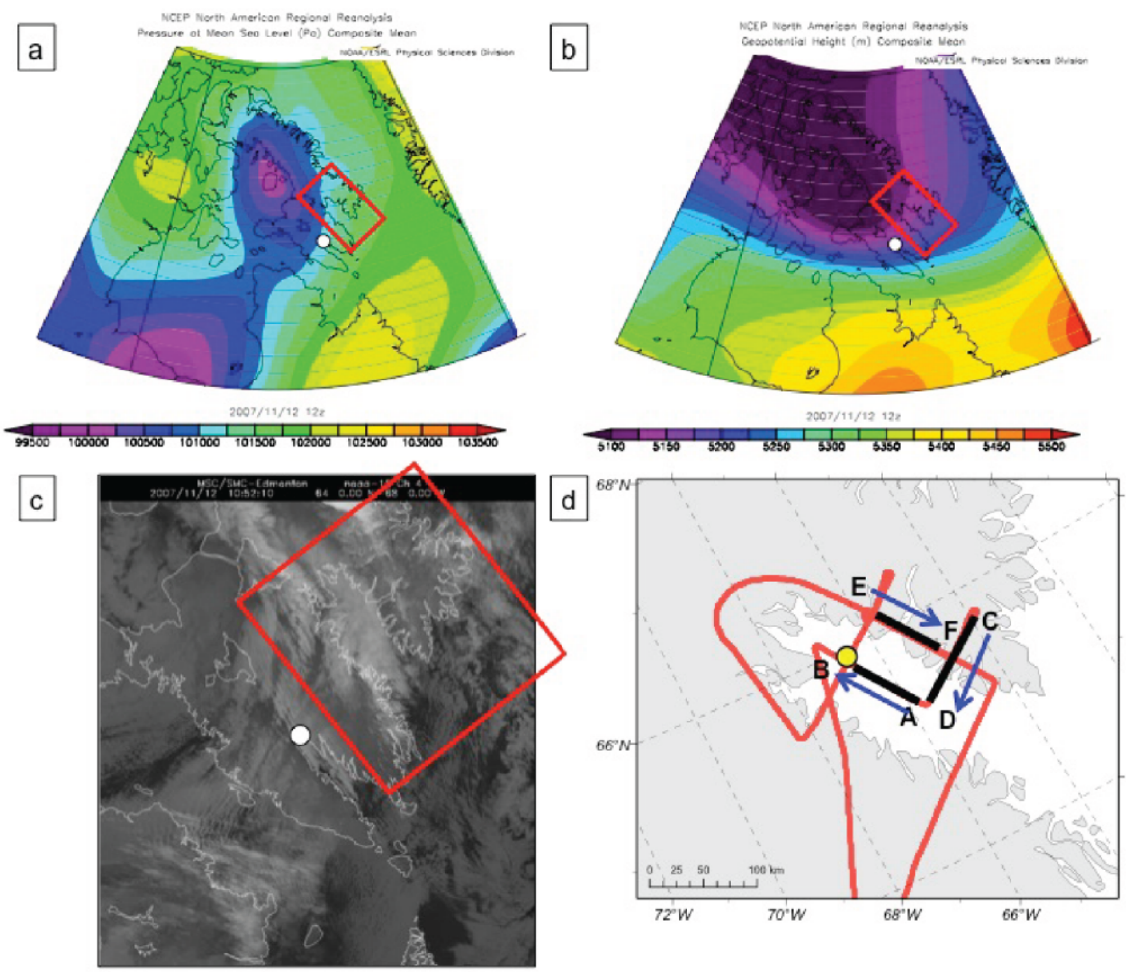

Three cross sections of atmospheric data are discussed in the case: (1) the upstream profile, collected in Cumberland Sound (minutes 204 to 219); (2) an upslope transect, parallel to the flow regime (minutes 185 to 196)); and (3) a second profile over the orography, parallel to topographical features, 15 km inland, perpendicular to the flow (minutes 54 to 65) (Figure 3.8d). Time series of the in situ atmospheric state parameters for the upstream and upslope profiles are presented in Figure 3.9.

<u>3.3.2.2 Upstream environment</u>

3.3.2.2.1 Vertical atmospheric conditions

Temperature ranged from -35°C (5000 m) to -10°C (600 m) (Figure 3.9), increasing to -6 °C at the surface (Figure 3.10). TWC was 0.1 to 0.2 g m^{-3} near cloud-top and rose to a maximum of 0.6 g m^{-3} at the lowest flight levels (600 m) (minute 219). The highest TWC measurements were associated with times when the aircraft was over open water. The RID indicated the presence of supercooled water, but values were lower than the sensitivity of the King Probe (Figure 3.9).

A dropsonde released in the middle of the Cumberland Sound, revealed the atmosphere was saturated and conditionally unstable in the lower boundary layer (< 1000 m ASL) with convective available potential energy (CAPE) being actively released upstream of the topography in Cumberland Sound (Figure 3.10). Winds below 1000 m were 12 m s^{-1} from the south-southeast, different from those inferred from the synoptic maps (south-westerly), showing the influence of the topography. The *Fr* was low (< 1), which suggests low-level blocking flow, and this may account for the apparent wind channelling evident in the dropsonde information in that the low level winds have the same orientation as the underlying terrain. The atmosphere was stable between 1000 and 2800 m ASL with cross-barrier winds from west-southwest at 8 m s^{-1}. Above 3000 m, there appears to be a jet, with winds increasing to 13 m s^{-1} within a conditionally unstable layer. Blocking in this case is likely the result of stronger stability aloft and the steep terrain of the Cumberland Peninsula.

Figure 3.9: Time series of flight data (10-second average) as in Figure 3.3 but for case study 2 (F5-12 November 2007).

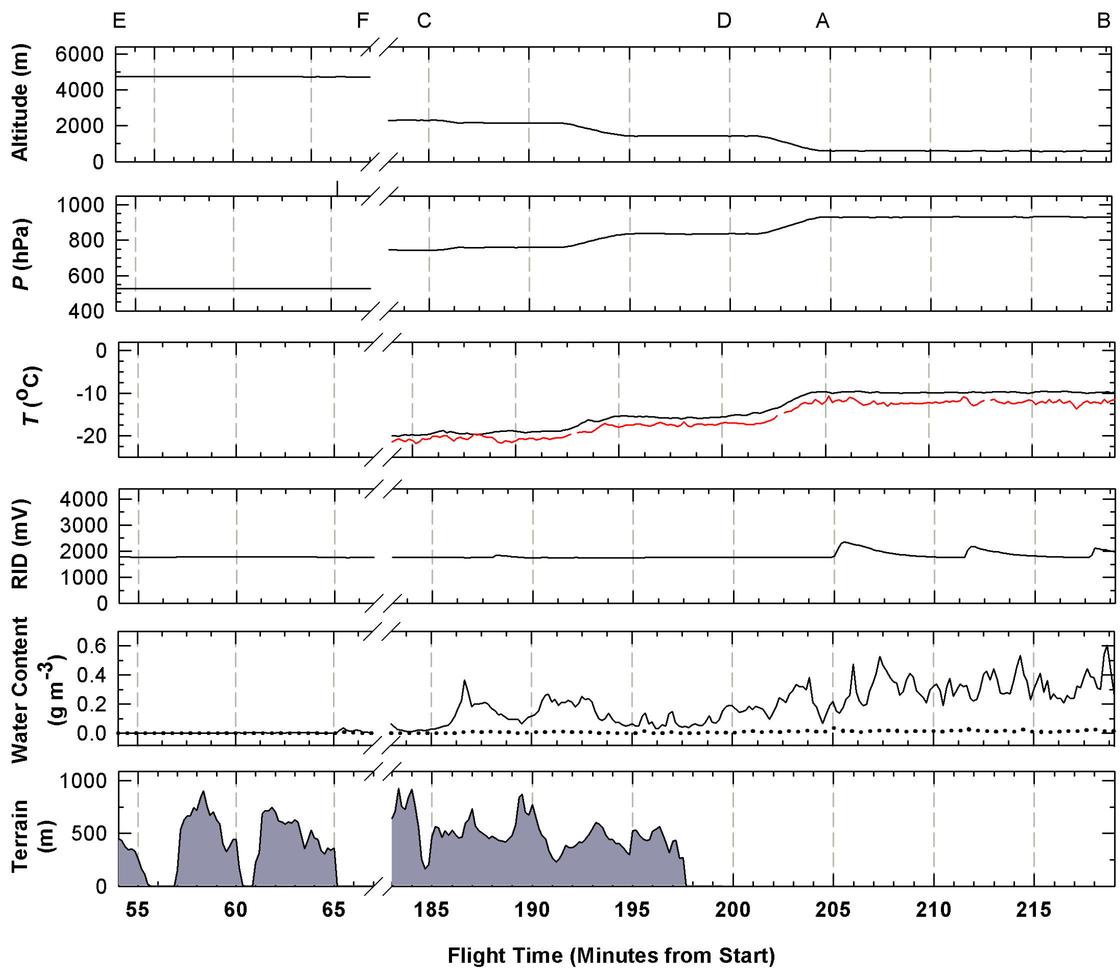

Figure 3.10: Vertical atmospheric profile characterizing the upstream environment in case study 2 (F5–12 November 2007). Dropsonde released at minute 149.

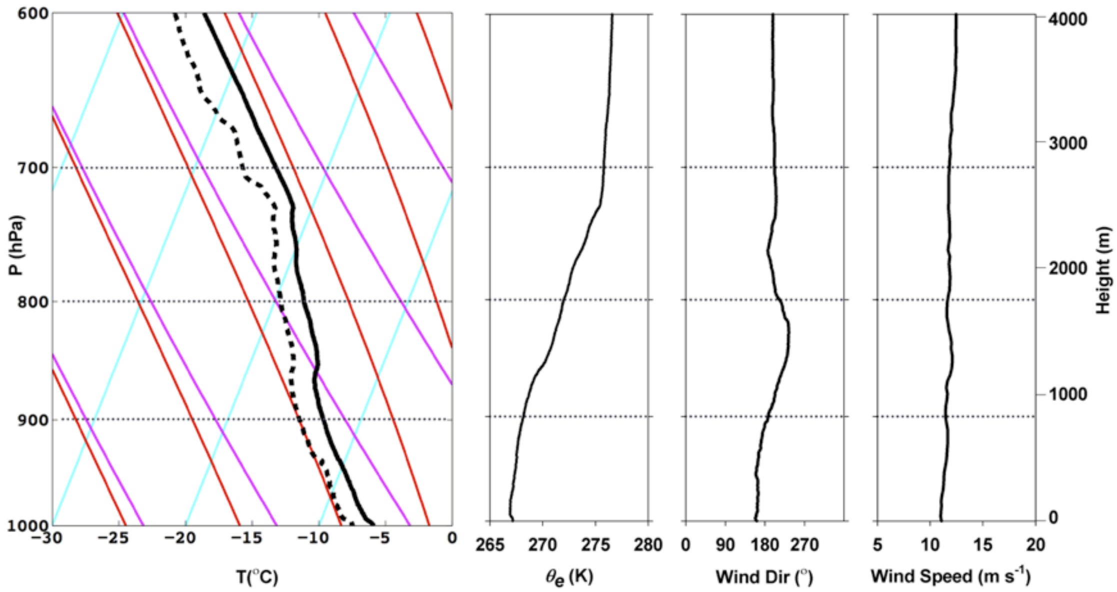

3.3.2.2.2 Cloud and precipitation features

Radar-derived cloud-tops were estimated between 2500 and 3500 m ASL (Figure 3.11a). Small-scale convective features are identifiable in cloud-tops, coincident with the instability layer. Reflectivity remained high below 2000 m up to a maximum of 14 dBZ (Figure 3.11a). Using the dropsonde data, cloud-base was estimated at 1000 m ASL. IWC increased towards the surface, to a maximum of 0.5 g m^{-3} (Figure 3.11b). Average total integrated IWC was 16 g m^{-2}, with a maximum of 20 g m^{-2}.

The average particle size spectrum between 500 and 2500 m indicated that the highest concentration of particles was in the size range of 200 to 425 µm (avg = 22.7 m^{-3} µm^{-1} per size bin) (Figure 3.12a). Although not shown, the variation of size spectrum with height indicated the concentration of larger particles (1000 to 5200 µm) increased towards the surface. The lower 1000 m of cloud was composed of dendrites and stellar crystals, needles, polycrystalline structures and circular particles that may be liquid water drops as indicated by the RID sensor (Figure 3.12b).

Figure 3.11: Doppler radar data for case study 2 (F5–12 November 2007). Left panels upstream profiles (a) reflectivity (dBZ) and (b) IWC (g m^{-3}). Right panels upslope profiles (c) reflectivity (dBZ) and (d) IWC (g m^{-3}). (e) Reflectivity (dBZ) profile over the terrain of Cumberland Peninsula. The terrain is outlined in black—height ASL (m) from DEM. The white line throughout the figures represents the location of the aircraft. The black arrows indicate the direction the aircraft travelled. Winds were from right to left in (c) and (d) over the terrain. Winds above 1000 m are perpendicular to the terrain in (e).

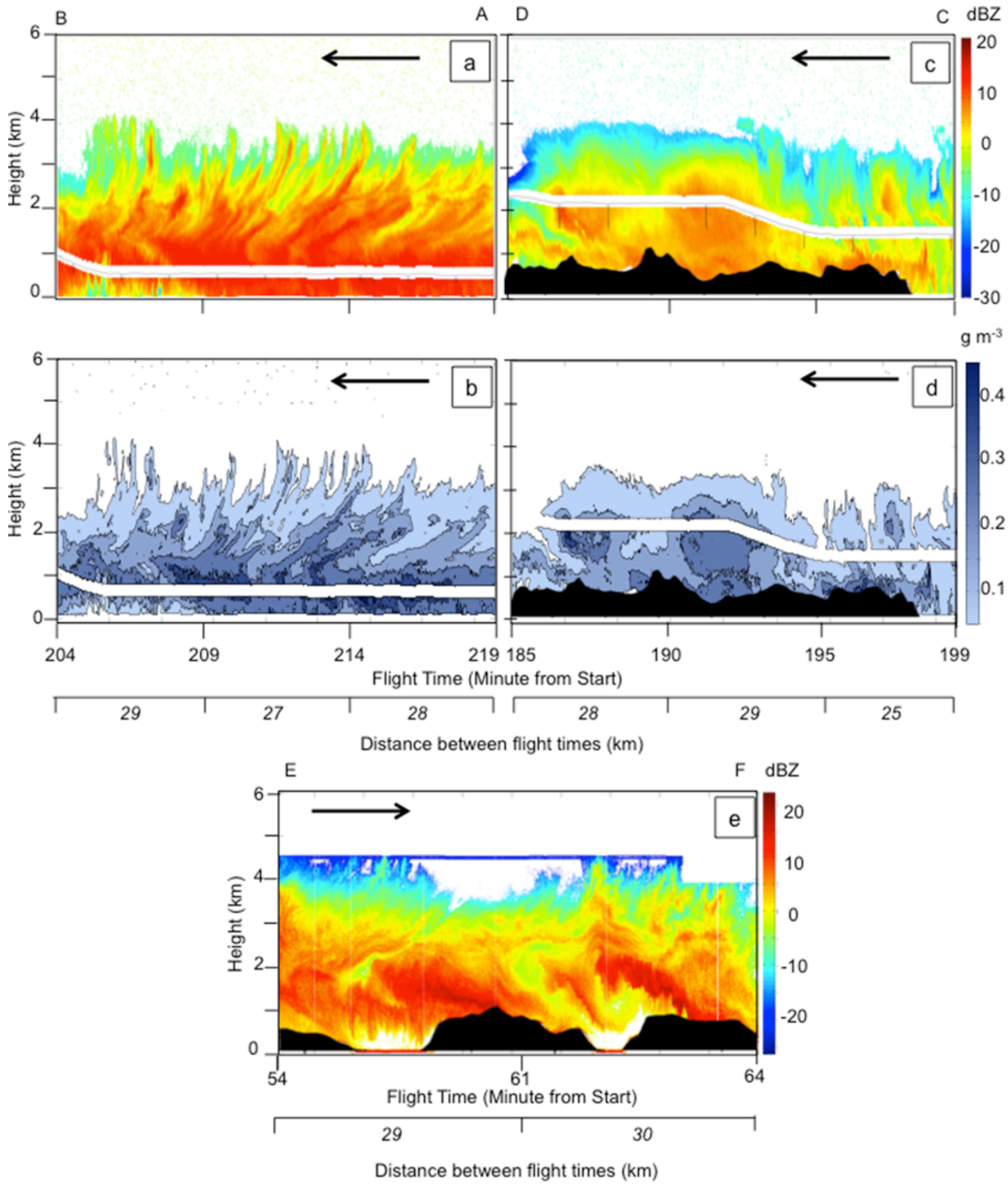

Figure 3.12: Hydrometeor characteristics for case study 2 (F5–12 November 2007). (a) Average particle concentration with height from upslope cloud (600 to 2500 m ASL); (b) sample PMS-2DC images from cloud upstream of Cumberland Peninsula from a height of 600 m, and (c) sample PMS-2DC images with height from upslope cloud (500 to 1500 m ASL).

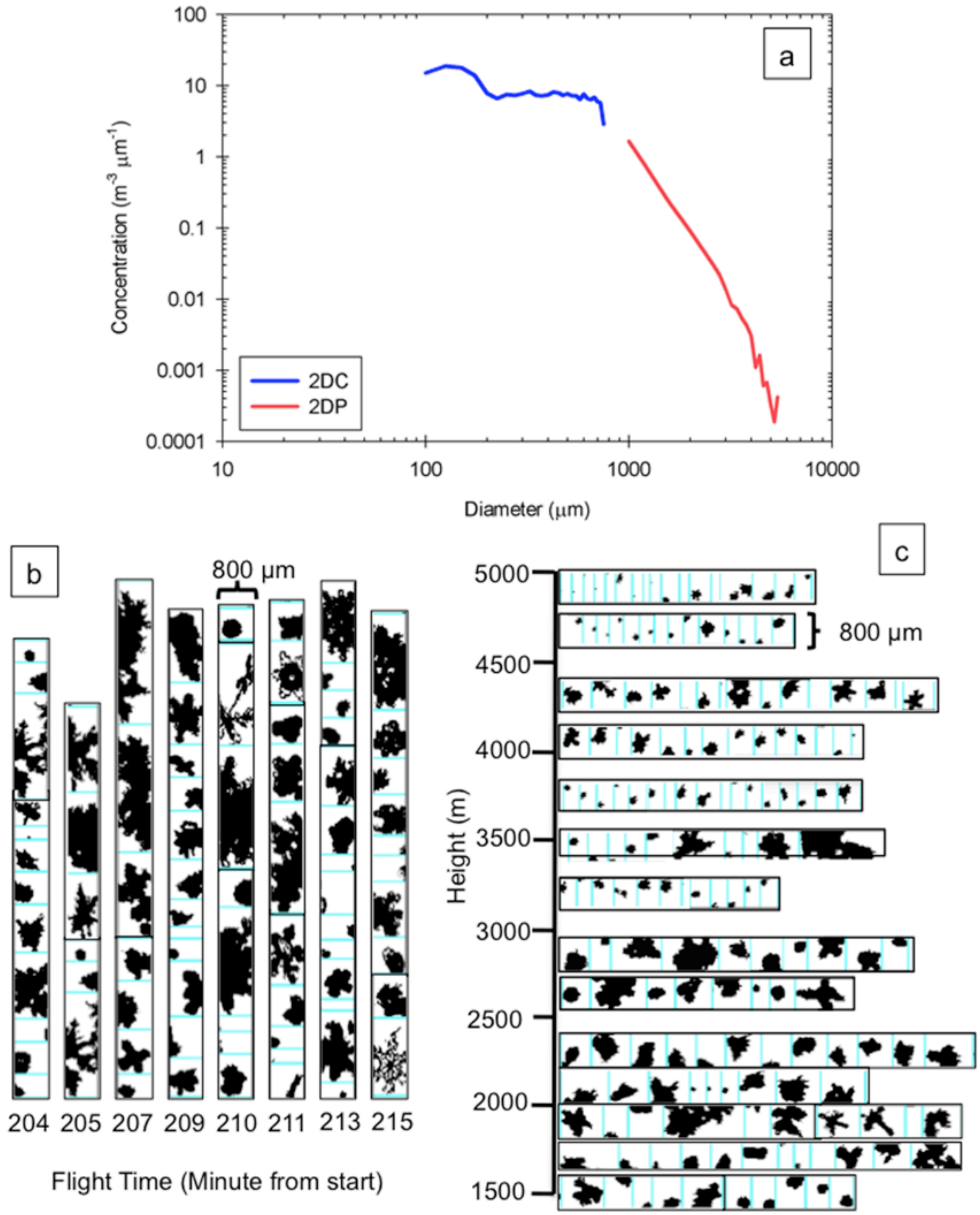

3.3.2.3 Upslope cloud and precipitation observations

3.3.2.3.1 Vertical atmospheric conditions

Temperatures near cloud-top and throughout the cloud profile were consistent with upstream observations (cloud-top T = -42°C) (Figure 3.9). However, the humidity was more spatially variable, from saturated to below saturation over short distances at similar altitudes (Figure 3.9). IWC also varied, ranging from 0.1 to 0.4 g m^{-3} (2100 m ASL) (Figure 3.9).

3.3.2.3.2 Cloud and precipitation features

The upslope reflectivity profile (parallel to flow regime) indicates that precipitation reached the surface on the windward side of the Cumberland Peninsula (8 to 10 dBZ), with pockets of enhanced reflectivity up to 14 dBZ to a distance of 60 km inland (Figure 3.11c). In most areas along the profile, reflectivity increased towards the surface.

Cloud-base height was identified at 500 to 750 m by the radar. The reflectivity structure indicates that cloud-base height is probably higher, but precipitation/sublimation below cloud-base prevents an accurate estimate.

The second radar profile reveals aspects of cloud and precipitation over the Cumberland Peninsula perpendicular to the flow regime (Figure 3.11e). Maximum reflectivity was 17 dBZ, where high reflectivity areas were linked to the shape of the underlying topographical features. The vertical reflectivity structure was variable, indicating a change in wind direction with height. Precipitation was inferred to reach the ground over elevated terrain, but not in the fiords. The strong winds aloft may have advected precipitation particles downstream and/or there may have been additional loss due to sublimation/evaporation in these areas.

Data collected over the Cumberland Peninsula provided the best characterization of particle habit over the terrain (Figure 3.12c). Near cloud-top (~5000 m ASL) particles were small (< 300 μm) and difficult to properly identify the shape from the 2D-C probe. Around 4000 to 4500 m, a combination of small irregularly shaped particles, polycrystalline particles, bullets and/or column rosettes and aggregates existed (Figure 3.12c). Circular particles, bullet rosettes and columns were observed between 300 and 1500 m.

IWC showed considerable variability over the terrain, regions of high IWC near the surface (0.4 g m^{-3}**)** and aloft in cellular pockets (0.3 g m^{-3}). Integrated IWC maximum (19.0 g m^{-2}) was identified approximately 30 km inland, thereafter, decreased with increasing distance from the coast to 5.0 g m^{-2} 60 km from Cumberland Sound (Figure 3.11d).

3.3.3 Case study 3: F13 – November 28, 2007

<u>3.3.3.1 Synoptic situation and sea ice extent</u>

Two circulations, a weak trough in Baffin Bay at 1200 UTC, coincidently with a stronger low pressure system (983 hPa) approaching Greenland, resulted in strong easterly wind upslope flow on the eastern side of the Cumberland Peninsula (Figure 3.13). The CV-580 flew northwest in Baffin Bay before traversing the eastern side of the Cumberland Peninsula parallel with the flow regime (Figure 3.13d). No Doppler velocity data are available in this case.

The CIS estimated $\geq 8/10$ ice concentrations around Cumberland Peninsula. Manual observations identified some open water regions present underneath the aircraft. Being mostly ice covered, the ocean offered very little moisture and/or heat in this case. Time series of the in situ atmospheric state parameters for the upstream and upslope profiles are presented in Figure 3.14.

Figure 3.13: F13–28 November 2007 case overview. (a) SLP (3-hourly NCEP NARR composite) at 1500 UTC, (b) 500 hPa geopotential height (3-hourly NCEP NARR composite) at 1500 UTC, (c) NOAA-17 AVHRR channel 4 image at 1630 UTC, and (d) study region—flight track (red line) and data information (i.e., dropsonde (filled yellow circles), radar profile location (black line), and direction of aircraft (blue arrows)). The letters are used as reference locations in upcoming figures. The white dot in panels (a), (b), and (c) indicates the location of Iqaluit, Nunavut, and the red box indicates the case study region of interest (d).

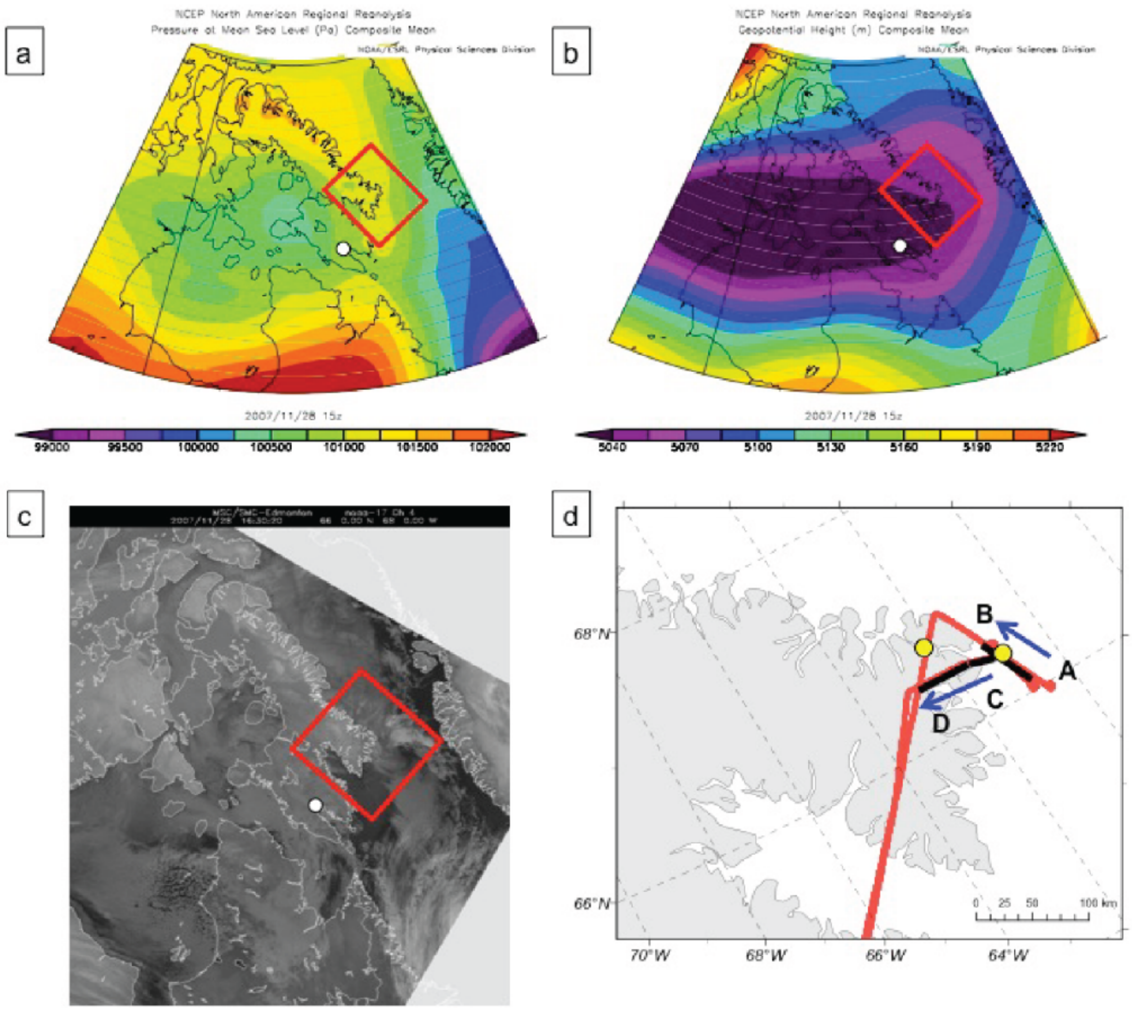

3.3.3.2 Upstream environment

3.3.3.2.1 Vertical atmospheric conditions

A thermal inversion between 250 and 1000 m was present, with the lower boundary layer unsaturated and stable (Figure 3.15a). Surface temperatures were -15°C, increasing to -4°C at the top of the inversion. Thereafter, temperature decreased to -35°C near cloud-top (~ 2000 m ASL). Cloud-top temperature was assessed at flight minute 67 (not shown), as the aircraft descended into the cloud prior to the A-B profile identified in Figure 3.14.Winds were strong (21 m s^{-1}) from the north below 500 m and parallel to the steeply sloped topography. The *Fr* was low (< 1), suggesting low-level blocking. Above the inversion, the atmosphere was conditionally unstable. In addition, the wind shifted to easterly (18 m s^{-1}) upslope flow, decreasing in speed with height (Figure 3.15a). Blocking in this case is likely the result of steep terrain and stronger stability linked to the high sea ice extent and thermal inversion.

TWC values were 0.1 g m^{-3} near cloud-top to a maximum of 0.2 g m^{-3} (600 m) (Figure 3.14). The RID identified supercooled water but values were low, at or below the sensitivity of the King probe, suggesting that supercooled liquid may or may not have been present at 1700 to 2000 m ASL in the upstream sector (Figure 3.14).

Figure 3.14: Time series of flight data (10-second average) as in Figures 3.3 and 3.9 but for case study 3 (F13–28 November 2007).

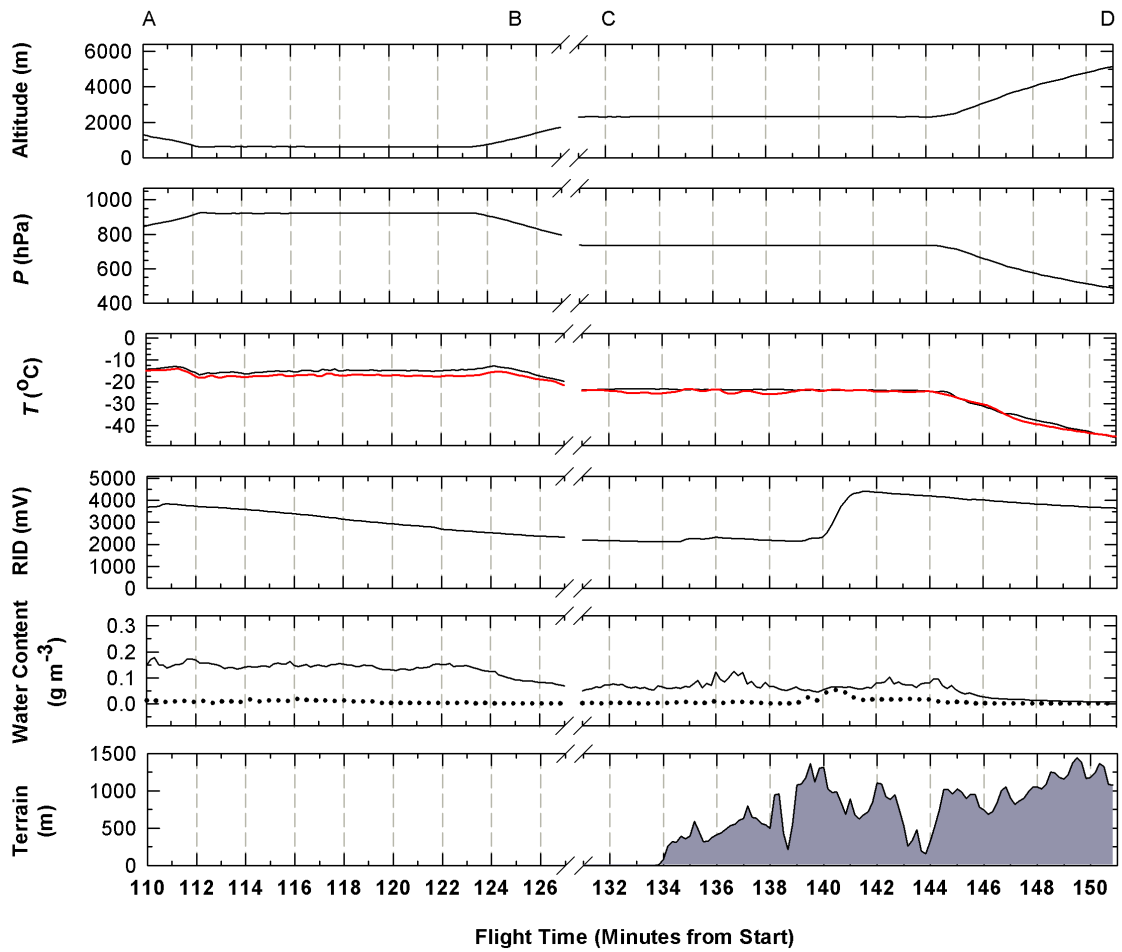

Figure 3.15: Dropsonde data for case study 3 – F13 – 28 November 2007: (a) upstream vertical atmospheric profile (released at minute 130): and (b) upslope vertical atmospheric profile (released at minute 47).

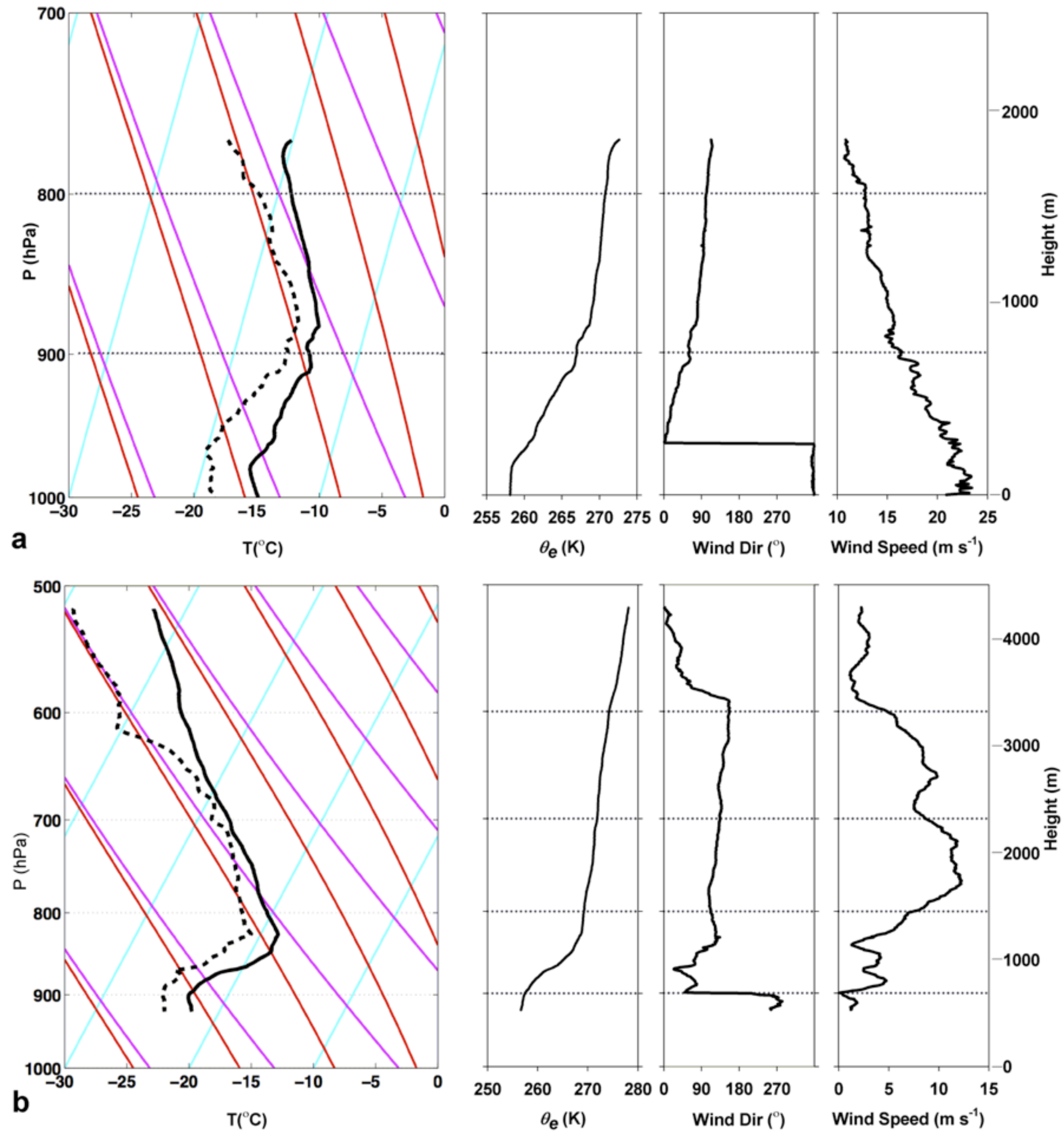

3.3.3.2.2 Cloud and precipitation features

Radar inferred cloud-top height was 2000 to 2500 m ASL (Figure 3.16a) with low reflectivity values. Most returns were < 1 dBZ and up to a maxima of 5 dBZ (1200 m), decreasing towards the surface in many areas along the profile. Light precipitation might have reached the surface in this case, but hydrometeor size/shape may have been modified as the particles fell through the unsaturated lower boundary layer. Cloud-base height was estimated at 500 m ASL from dropsonde data. Reflectivity returns below this height prevented a cloud-base measurement from the radar.

In-cloud IWC values were estimated at 0.01 g m^{-3} (2000 m ASL) to 0.2 g m^{-3} (surface). Total integrated IWC did not vary substantially with values of 2.0 to 4.0 g m^{-2} (Figure 3.16b).

High concentrations of small particles (100 to 400 μm) were present throughout the entire cloud profile (Figure 3.17a). Overall, the average concentration of ice particles was low (2.3 m^{-3} μm^{-1} per bin (100 to 800 μm); 0.22 m^{-3} μm^{-1} per bin (1000 to 4800 μm). Plates and irregularly shaped ice crystals, with some accretion were the most prominent habits near cloud-top (Figure 3.17b). Between 1200 and 1600 m, dendrites and stellar crystals sometimes with fernlike extensions near 1500 m existed. Particles in the lower cloud regions were pristine, plates and plates with sector-like, dendritic and broad branches (Figure 3.17b).

Figure 3.16: Doppler radar data for case study 3 (F13–28 November 2007). Left panels upstream profiles (a) reflectivity (dBZ) and (b) IWC (g m^{-3}). Right panels upslope profiles (c) reflectivity (dBZ) and (d) IWC (g m^{-3}). The white line throughout the figures represents the location of the aircraft. The black arrows indicate the direction of aircraft motion. Winds were from left to right in (c) and (d) over the terrain.

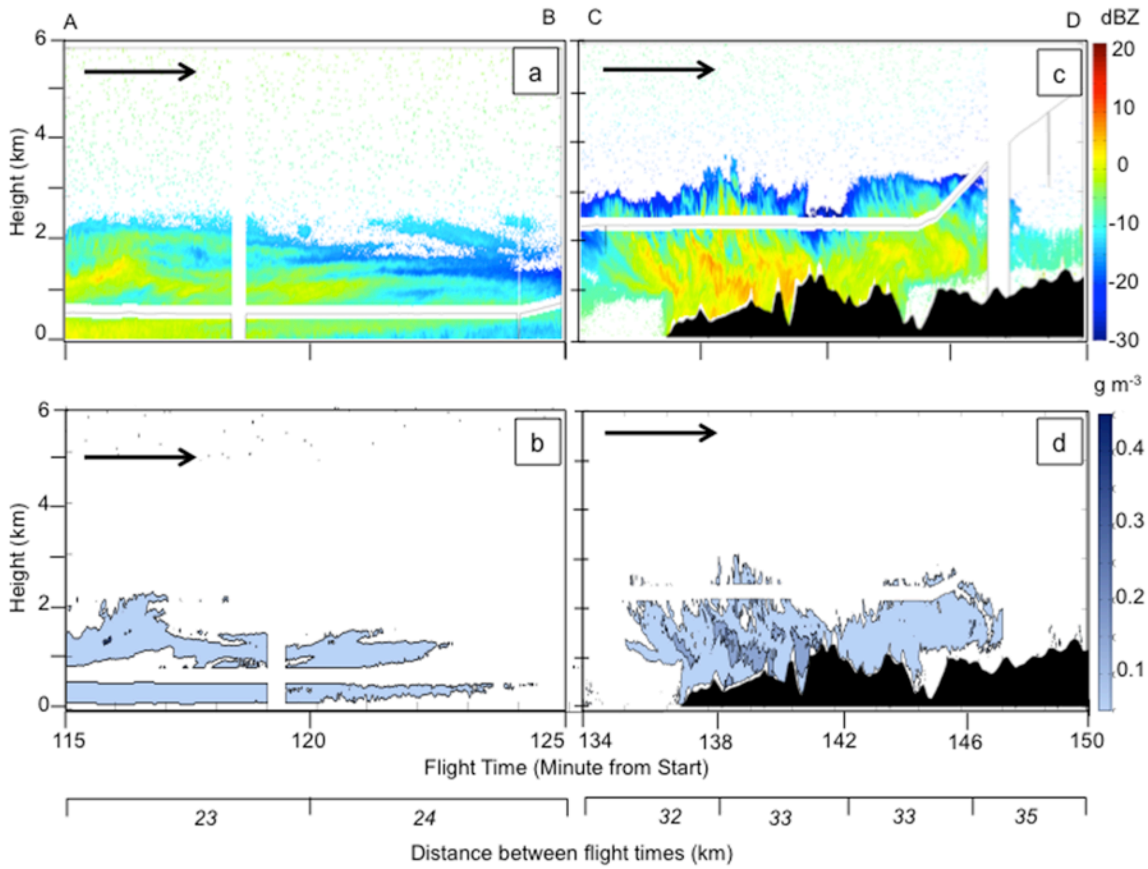

Figure 3.17: Hydrometeor characteristics for case study 3 (F13–28 November 2007). (a) Average particle concentration with height upstream environment (2200–600 m), (b) sample 2DC images with height upstream environment, and (c) sample 2DC images over the terrain at a height of 2100 m.

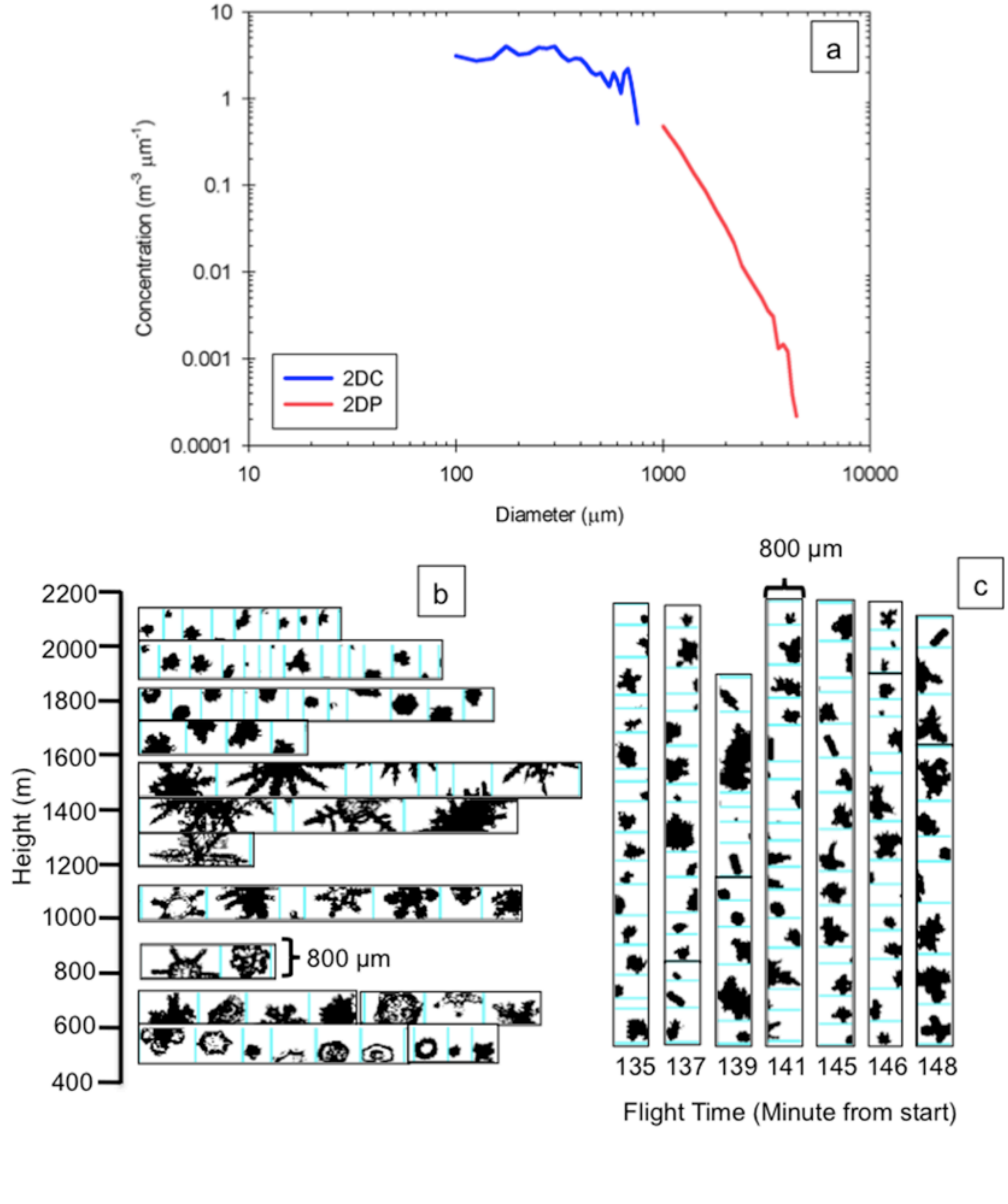

3.3.3.3 Upslope cloud and precipitation observations

3.3.3.3.1 Vertical atmospheric conditions

A dropsonde released north and prior to the radar profile shown in Figure 3.14 defined the vertical atmospheric conditions (minute 47) (Figure 3.15b). The atmosphere was saturated near cloud-top (2700 m) and conditionally unstable above 1000 m. Winds remained upslope from the east between 1000 and 2000 m ASL, shifting to south-easterly above 2000 m ASL. A maximum wind speed of 12 m s^{-1} was identified around 1700 m, decreasing to approximately 2 m s^{-1} at the surface (Figure 3.15b).

The aircraft remained near or above cloud-top over the terrain (Figure 3.14). Cloud-top temperatures were –30°C. The RID indicated the presence of LWC at cloud-top, with LWC < 0.1 g m^{-3} (minute 141) (Figure 3.14). TWC was low and consistent along the flight track up to a maximum of 0.1 g m^{-3} measured 15 km inland, decreasing thereafter (Figure 3.14).

3.3.3.3.2 Cloud and precipitation features

Cloud top was 500 m higher than the upstream profile (3000 m). Reflectivity maxima over the terrain increased to 8 dBZ. The radar and dropsonde data identified cloud-base height at 1000 m ASL. Fall streaks were identified in the radar profile up to a distance of 40 km inland (Figure 3.16c). Thereafter, the reflectivity profile indicated precipitation no longer reached the surface. In addition, small-scale convection was identified at cloud-top, characterized by pockets of vertically enhanced reflectivity. A feature that was not present in the upstream profile.

IWC was higher over the terrain than upstream, with in-cloud values ~0.1 g m^{-3} at most levels, up to a maximum of 0.5 g m^{-3} (Figure 3.16d). Total integrated IWC increased from 2.0 g m^{-2} to a maximum of 9.5 g m^{-2} approximately 20 km inland.

Small columnar and irregularly shaped ice crystals were common just below cloud-top (Figure 3.17c). Accretion was identified on some particles, but the amount was not consistent, indicating that particles travelled through variable amounts of liquid water when forming. Aggregates were also present.

3.4 Discussion

3.4.1 Precipitation over the orography of southern Baffin Island

Precipitation enhancement on the windward slopes of the terrain occurred in all case studies. Despite variability in the synoptic organization, precipitation over the orography exhibited similarities between events. For example, in all three case studies, maximum reflectivities were 3 to 4 dBZ higher than adjacent ocean regions upstream and reflectivities increased towards the surface up to distances of 30 to 60 km inland (Table 3.1).

Spatial variability in the reflectivity profile over the orography revealed that precipitation structure was more variable than over adjacent ocean regions in all three cases (Figure 3.5, Figure 3.11, Figure 3.16). Over the orography, fall streaks were common, compared to more uniform stratiform precipitation upstream. In addition, with increasing distance inland, higher reflectivities aloft became more common, decreasing towards the surface.

The three cases showed similarities, but nonetheless illustrated several differences based on synoptic organization. The two events driven by large-scale cyclonic circulations (*F3* and *F5*) were characterized by increased cloud depth, cloud height, TWC, particle concentrations and higher reflectivity values over the orography (Table 3.1). This result, although not surprising, does imply that organized large-scale circulations may result in greater precipitation enhancement over the terrain. However, this study also shows that weakly organized synoptic systems can also be important for precipitation production and/or enhancement over the orography.

Table 3.1: Summary characteristics of cloud and precipitation features identified during the three STAR case studies. Particle habit abbreviations: Combination bullet (CB); Combination columns (CC); Dendrites (Den); Stellar Crystals (StCry); Plates (Pl); Plates with secular extensions (Pl w sec); Double capped columns (dc C); Grapuel shaped (GS); Irregular (Irr); Columns (C). Note: '-' indicates no data was available or not applicable to specific upstream or upslope cases.

STAR case	*F3*		*F5*		*F13*	
	Upstream	*Upslope*	*Upstream*	*Upslope*	*Upstream*	*Upslope*
Cloud characteristics						
Cloud-top height (m)	7000	7000	4000	4000-4500	2000-2500	3000
Cloud-base height (m) DS – dropsonde, R – Radar	750	700-1200 (DS), 2000 (R)	1000 (DS)	500 – 750 (R)	500 (DS)	1000 (DS/R)
Cloud-top T (°C)	-40	-39	-35	-	-35	-42
Cloud-base T (°C)	-9	-10	-6	-6	-4	-22
Max dBZ (W-band)	14	18	14	17	5	8
Atmospheric variables						
Surface T (°C)	-1	-4	-6	-	-10	-20
Stability	Stable	Conditionally unstable (3000-4000 m)	Conditionally unstable (0 – 1000 m)	-	Stable (<1000 m)	Conditionally unstable (1700-2000 m)
Froude Number (*Fr*)	>1	-	< 1	-	< 1	-
Microphysical characteristics						
TWC (g m^{-3}) (height m)	0.07 (5000 m) - 0.7 (1000 m)	0.2 (4500 m)	0.1 (5000 m) - 0.6 (600 m)	0.4 (2000 m)	0.01 (2000 m) - 0.5 (surface)	0.2 (2000 m)
LWC (g m^{-3}) (RID height)	0.14 (1000 m)	-	0.02 (600 m)	-	0.03 (2250 m)	0.04 (2700 m)
IWC (g m^{-3}) (height m)	0.05 (5000 m) - 0.6 (1000 m)	0.05 (5000 m) - 0.8 (1000 m)	0.3 (2000 m) - 0.5 (1000 m)	0.4 (surface)	0.01 (2000 m) - 0.2 (surface)	0.01 (2000 m) - 0.2 (1000 m)
Max ∫IWC (g m^{-2})	34.0	32.0	20.0	19.0	4.0	9.5
Hydrometeor characteristics						
Types of ice particles (height)	Rosettes (CB &,CC), C, Pl (> 2500 m); Den, StCry (2500-2000 m); Pl, Pl w sec, dc C , Rosettes (CB & CC) (< 2000 m)	Rosettes (CB), C, GS (4500 m)	Den, StCry, Rosettes (CB), Liquid Drops (600-1000 m)	Irr, C, Pl, Rosettes (CB) (1500 - 5000 m)	Pl, StCry, Den (500-2000 m	Irr, C, Pl (2100 m)
Accretion level	Light to moderate	Light to moderate	Moderate to heavy	Moderate	Light	Light to moderate
Fall speeds	1-2 m s^{-1}; updrafts 0.5-1 m s^{-1} (surface and within 250 m of cloud-top)	1-5 m s^{-1}; updrafts 1-2 m s^{-1} (mid-cloud 2000 - 4000 m)	1-2 m s^{-1}; updrafts 1-2 m s^{-1} (4000 m)	1-2 m s^{-1}; updrafts 1-2 m s^{-1} (near surface)	-	-
Max diameter (μm) (height)	5200 (1000 m)	2000 (4500 m)	3200 (600 m)	2400 (2100 m)	4800 (1000 m)	2600 (2200 m)
Median size (average concentration) per bin	100-175 (9.5 m^{-3} μm^{-1}); 400-500 (11.1 m^{-3} μm^{-1})		100-200 (16.4 m^{-3} μm^{-1}; 225-425 (22.7 m^{-3} μm^{-1})		175 (4.0 m^{-3} μm^{-1}; 275-325 (3.8 m^{-3} μm^{-1})	

3.4.2 Factors associated with precipitation enhancement over orography

Precipitation enhancement over the orography was not a surprising result. However the number of different factors that influence cloud and precipitation over the orography, beyond lifting air over an orographic barrier was. This included variable dynamic flow regimes, terrain shape, atmospheric stability and atmosphere-ocean exchanges.

The most dramatic precipitation enhancement of the three cases occurred in the *F3*. Reflectivity values were higher than the other cases, and increased towards the surface on the entire windward slope of the Hall Peninsula. Gravity waves and upslope flow at all levels of the atmosphere (no low-level blocking) were the main factors associated with precipitation enhancement.

Gravity waves were present over horizontal distances of 5 to 15 km with updrafts/downdrafts of 1 to 2 m s^{-1} and 1 to 5 m s^{-1} respectively (Figure 3.5). The wave structure showed evidence of terrain-induced variations in the reflectivity profile. In mid-latitude cases, gravity waves have been found to significantly enhance precipitation over subsequent ridges by directly increasing condensation rates and enhancing precipitation generation aloft independent of large-scale baroclinic systems [*Reinking, Snider, & Coen,* 2000; *Garverts, Smull, & Mass,* 2007]. Gravity waves in *F3* occurred at a slightly higher frequency compared to a mid-latitude case from IMPROVE-II [*Garverts et al.,* 2007] despite both cases being associated with cold season pre-frontal flow. The lower frequency wavelength in the IMPROVE-II case (~18 km) may be the result of differences in wind fields. The storm event in *Garverts et al.* [2007] was characteristic of a strongly sheared wind environment at low levels, which *Smith* [1980] demonstrated would limit the upward penetration of topographically generated waves. In the *Garverts et al.* [2007] case, prevailing winds veered aloft, damping vertical wave penetration. *F3* wind fields remained strong easterly (upslope) at all levels and in phase with wave motion in this case, which would favour higher amplitude gravity waves over the terrain (Figure 3.4).

The shape of the terrain on the Hall Peninsula also contributed to precipitation enhancement in *F3*. Compared to the steep terrain of the Cumberland Peninsula, the Hall Peninsula has a more gradual slope from the coast to the crest (Figure 3.1). As a result, no low-level blocking occurred resulting in all lower levels of moist air to be lifted over the terrain, increasing potential for precipitation generation aloft. In contrast, low-level blocking occurred in the other two case studies associated with the Cumberland Peninsula (*F5* and *F13*), reducing lifting over the terrain in those cases (Table 3.1).

The upstream surface environment in *F5* was an important factor enhancing precipitation on the Cumberland Peninsula. Low sea ice extent (< 3/10s), in conjunction with a strong temperature gradient between the atmosphere and ocean, resulted in upward exchanges of heat and moisture and the initiation of convection (Table 3.1, Figure 3.10). This provided an enhanced growth environment for particles before air was lifted. In addition, it is probable that the mechanical lifting of the unstable air over the terrain further destabilized it and resulted in embedded convection in the cloud. These enhancements were beyond that resulting from synoptic circulations and air lifting over the terrain alone.

Similarly, in *F13*, precipitation enhancement and vertical cloud development over the terrain were linked in part to instability (Table 3.1, Figure 3.15). Above the thermal inversion, the atmosphere was conditionally unstable and moist, which suggests that strong upslope flow over the terrain may result in embedded convection and aid in particle growth on windward slopes.

3.4.3 Factors associated with decreasing precipitation over orography

Several factors acted to reduce precipitation over the orography, including sublimation, high sea ice extent and low-level blocking in the upstream environment. A discussion of microphysical features and their influence on cloud and precipitation over the terrain will follow in section 3.4.4.

Sublimation below cloud-base and between dry layers reduced or eliminated precipitation reaching the surface in all cases (Figure 3.5, Figure 3.11, Figure 3.16). With increasing distance inland, it became more common in the cloud profile to have higher reflectivities aloft decreasing towards the surface. These regions often coincided with dry layers such that hydrometeors passing through these regions may have been altered in size and/or shape through sublimation and/or were horizontally advected before reaching the surface (Figure 3.7). Reflectivity remained > 0 dBZ towards the surface in some regions, suggesting that precipitation still reached the ground but at a reduced amount. Results indicate that with increasing distance from the coast, particles were more susceptible to sublimation than over adjacent ocean regions.

The presence of sea ice also influenced precipitation over orography. In *F13*, high sea ice extent (>8/10s) contributed in part to low TWC and LWC throughout the cloud profile by limiting upward exchanges of heat and moisture (Table 3.1). The presence of sea ice also aided in development of a thermal inversion, which resulted in low-level blocking and reduced lift of surface winds over the terrain. Consequently, there was less chance for enhanced condensation and precipitation by reducing upslope flow.

3.4.4 Microphysical features over orography

High-resolution measurements allowed for an examination of microphysical features over the terrain. Characteristics were linked to the multiple factors previously identified to play active roles in enhancing (section 3.4.2) and/or reducing (section 3.4.3) cloud and precipitation over the orography.

Clouds were mainly glaciated, but low amounts of liquid water (0.04 to 0.14 g m^{-3}) were detected in all cases (Table 3.1). The vertical structure of TWC and IWC was similar between cases, with values increasing from cloud-top to the surface (Figure 3.3, Figure 3.9, Figure 3.14). However, this was not the case over the orography in dry layers (Figure 3.3 and Figure 3.7). Differences in microphysical characteristics were associated with synoptic organization. The two events driven by large-scale cyclonic circulations (*F3* and *F5*) had similar, but higher total and ice water contents and increased particle concentrations in the clouds over the orography compared to *F13* (Table 3.1). This result is not surprising, but interesting to note that similarities were present between storms of different origins.

The vertical structure of IWC with height showed similarities and differences with other studies. Peak values for cases associated with organized cyclonic circulations (*F3* and *F5*) were not substantially different from values found by *Henson et al.* [2011] over Iqaluit and *Boudala, Issac, Fu and Cober* [2002] who used data from multiple research projects all north of 45°N latitude. However, total and ice water contents for *F13* associated with a weakly organized synoptic system were an order of magnitude lower.

Combinations of irregularly shaped particles, polycrystalline particles, bullets and/or column rosettes were present in the mid-to-upper cloud profile over the orography (Table 3.1). Fragmented particles were also present, suggesting that cloud particles were additionally formed through secondary processes not involving nucleation. Particles with light to moderate accretion were present and more frequent particle aggregation occurred than over adjacent ocean regions (Table 3.1, Figure 3.12, Figure 3.17). As a result, higher concentrations of larger particles (1000 to 2600 μm) over the orography existed in two cases (*F3* and *F13*) compared to similar heights upstream (Figure 3.18). Dynamic and thermodynamic factors, such as gravity waves and embedded convection over the orography would contribute to increased deposition and precipitation generation aloft, in addition to increasing potential for particles collisions, which may be why accretion and aggregation were more common over the orography than over adjacent ocean regions upstream.

Figure 3.18: Comparison of average particle concentration (PMS-2DC and PMS-2DP) between the upstream and upslope environment in the three case studies. (a) F3–8 November 2007 at 4000 m, (b) F5–12 November 2007 at 1500 m, and (c) F13–28 November 2007 at a height of 2100 m.

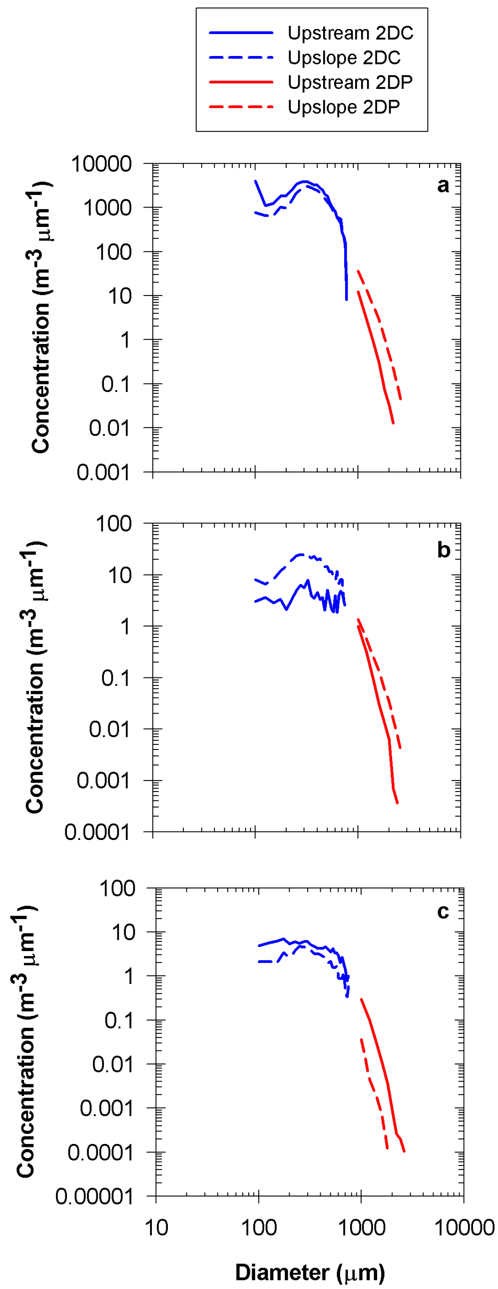

As a result, accretion and aggregation appear to be important determinants of whether precipitation will reach the surface over the orography. Sublimation was previously identified as a factor that reduced precipitation. In contrast, enhanced particle growth through accretion and aggregation increases particle density and may increase fall velocities, thereby increasing the probability of ice particles reaching the ground before they completely sublimate. Lower concentrations of small (100 to 800 μm) particles existed over the orography compared to upstream, suggesting that smaller particles over the orography may be sublimating before reaching the ground due to their low density and low fall velocities. It is also possible that the lower concentration of small particles over the orography is the result of particle aggregation. Without aggregation or accretion, it is probable that more ice particles would have sublimated before reaching the ground.

Previous ground-based studies have noted the occurrence of accretion and aggregation at the surface in Iqaluit [*Roberts et al.,* 2008; *Henson et al.,* 2011]. The present work provides a more comprehensive explanation into why there is enhanced particle growth over orography, which increases the probability of precipitation reaching the ground. Despite environmental differences between mid-latitude regions and the Arctic such as low moisture content and varied stability in the planetary boundary layer as a result of sea ice cover and reduced solar input, hydrometeors observed over Baffin Island and surrounding area were not substantially different from observations during field projects in mid-latitude regions [*Stoelinga et al.,* 2001; *Rotunno & Houze,* 2005; *Isaac et al.,* 2012; among others].

3.5 Concluding Remarks

This study identified characteristics of cloud and precipitation over the orography on southern Baffin Island during STAR. Three case studies provided a number of key observations of how cloud and precipitation features are modified over the orography and also vary with synoptic and sea ice conditions.

A number of factors acted to enhance or reduce precipitation over the orography. Variable dynamic flow regimes, terrain shape, atmospheric stability and atmosphere-ocean exchanges were attributed to precipitation enhancement. In contrast, several factors acted to reduce precipitation, including sublimation, high sea ice extent and low-level blocking in the upstream environment. Accretion and aggregation were additionally identified as important particle growth mechanisms since, by increasing particle density and may increase fall velocities, they increased the probability of ice particles reaching the surface.

The limited number of case studies, over a short period (one-month), means generalizations are not possible. However, this study is an important step to improved understanding of factors that influence clouds and precipitation in high latitude regions. Future research can expand on the analysis here, but high-resolution data of similar nature are required. Given the scarcity of surface-based precipitation monitoring instrumentation in high latitude and mountain regions, there may be an increased reliance on satellite precipitation retrievals in the future. However, low reflectivity values identified in this study indicate that much of the precipitation over southern Baffin Island will remain undetected by upcoming satellite-precipitation systems such as the Global Precipitation Measurement (GPM) satellite, based on its minimum threshold (12 dBZ)

[*Hou et al.,* 2013]. Satellite precipitation retrievals in high latitude regions may have limitations.

Anticipated climatic changes such as increased atmospheric temperature, increased moisture content and delayed onset of sea ice in the autumn, may lead to enhanced orographic precipitation over southern Baffin Island but this must be confirmed and quantified. To address this issue as well as those linked with weather forecasting, high-resolution model studies are first needed to examine terrain and associated dynamics and microphysics as well as key processes in the upstream environment.

In summary, this study has documented clouds and precipitation features over orography for three cases over southern Baffin Island. These results indicate that the complexity of these critical features over terrain in high latitude regions poses considerable challenges for modelling.

3.6 References

Asuma, Y., Inoune, Y., Kikuchi, Y.K., Kajiokawa, M., Sata, N., and, Hayaska, T. (2000). Wintertime precipitation behavior in the western Canadian Arctic region. *Journal of Geophysical Research, 105, D11,* doi:10.1029/1999JD901124.

Barstad, I. and Smith, R.B. (2005). Evaluation of an orographic precipitation model. *Journal of Hydrometeorology, 6,* 85-99.

Bond, N.A., Mass, C.F., Smull, B.F., Houze, R.A., Yang, M.-J., Colle, B.A., Braun, S.A., Shapiro, M.A., Colman, B.R., Neiman, P.J., Overland, J.E., Neff, W.D., and Dolye, J.D. (1997). The coastal observation and simulation with topography (COAST) experiment. *Bulletin of the American Meteorological Society*, 1941-1955.

Boudala, F. S., Isaac, G.A., Fu, Q., and Cober, S.G. (2002). Parameterization of effective ice particle size for high-latitude clouds. *International Journal of Climatology, 22***,** 1267-1284.

Burford, J.E. and Stewart, R.E. (1998). The sublimation of falling snow over the Mackenzie River Basin. *Atmospheric Research, 49*, 289-314.

Cober, S.G, Isaac. G.A., and Strapp, J.W. (2001). Characterization of aircraft icing events that include supercooled large drops. *Journal of Applied Meteorology, 40,* 1984-2001.

Colle, B.A. (2004). Sensitivity of orographic precipitation to changing ambient conditions and terrain geometrics: An idealized modelling perspective. *Journal of Atmospheric Sciences, 61,* 588-608.

Curry, J.A. Hobbs, P.V., King, M.D., Randall, D.A., Minnis, P., Isacc, G.A., Pinto, J.O., Uttal, T., Bucholtz, A., Cripe, D.G., Gerber, H., Fairall, C.W., Garrett, T.J., Hudson, J., IntrierI, J.M., Jakob, C., Jensen, T., Lawson, P., Marcotte, D., Nguyen, L., Pilewskie, P., Rangno, A., Rogers, D.C., Strawbridge, K.B., Valero, F.P.J., Williams, A.G., and Wylie, D. (2000). FIRE Arctic Clouds Experiment. *Bulletin of the American Meteorological Society, 81*, 5–29.

Curry, J.A., Rossow, W.B., Randall, D.A., and Schramm, J.L. (1996). Overview of Arctic cloud and radiation characteristics. *Journal of Climate, 9,* 1731–1764.

Deacu, D., Zandra. A., and Hanesiak, J. (2010). Simulating wind channelling over Frobisher Bay and its interaction with downslope winds during the 7-8 November 2006 Wind Event. *Atmosphere-Ocean. 48*, 101-121. doi:10.3137/AO1109.2010.

Environment Canada (2013). Daily precipitation data at Pangnirtung, Nunavut. National climate data and information archive. Retrieved from: http://climate.weather.gc.ca/climateData/hourlydata_e.html Last accessed: November 2012.

Garvert, M.F., Smull, B., and Mass, C. (2007). Multiscale mountain waves influencing a major orographic precipitation event. *Journal of Atmospheric Sciences, 64,* 711-737.

Hanesiak, J., Stewart, R.E., Szeto, K., Hudak, D., and Leighton, H. (1997). The structure, water budget, and radiational features of a high-latitude warm front. *Journal of Atmospheric Sciences*. 12**,** 1553–1573.

Hanesiak, J., Stewart, R.E., Taylor, P., Moore, K., Barber, D., McBean, G., Strapp, J.W. Wolde, M., Goodson, R., Hudson, E., Hudak, D., Scott, J., Liu, G., Gilligan, J., Biswas, S., Desjardins, D., Dyck, R., Fargey, S., Field, R., Gascon, G., Gordon, M., Greene, H., Hay, C., Henson, W., Hochheim, K., Laplante, A., Martin, R., Melzer, M.A., and Zhang, S. (2010). Storm Studies in the Arctic: The meteorological field project. *Bulletin of the American Meteorological Society, 91,* 47-68. doi:10.1175/2009BAMS2693.1

Henson, W., Stewart, R., and Hudak, D. (2011). Vertical reflectivity profiles of precipitation over Iqaluit, Nunavut during Autumn 2007. *Atmospheric Research*, *99*, 217-229. doi: 10.1016/j.atmosres.2010.10.009.

Hobbs, P.V. (1975). The nature of winter clouds and precipitation in the Cascade Mountains and their artificial seeding. Part 1: natural conditions. *Journal of Applied Meteorology, 14***,** 783-804.

Hobbs, P.V. and Rango, A.L. (1998). Microstructures of low and middle-level clouds over the Beaufort Sea, *Quarterly Journal of the Royal Meteorological Society* 124, 2035-2071.

Hock, T. and Franklin, J.L. (1999). The NCAR GPS dropwindsonde. *Bulletin of the American Meteorological Society, 80,* 407-420.

Hou, A.Y., Kakar, R.K., Neeck, S., Azibarizin, A.A., Kummerow, C.D., Kojima, M., Oki, R., Nakamura, K., and Iguchi, T. (2013). The Global Precipitation Measurement (GPM) mission. *Bulletin of the American Meteorological Society,* Advance online publication. doi: 10.1175/BAMS-D-13-00164.1

Houze, R.A. (1993). Cloud Dynamics. International Geophysics Series, Volume 53. Academic Press, Inc. San Diego, CA, USA. 573 pages.

Houze, R.A, James, C.N., and Medina, S. (2001). Radar observations of precipitation and airflow on the Mediterranean side of the Alps: Autumn 1998 and 1999. *Quarterly Journal of the Royal Meteorological Society, 127***,** 2537-2558.

Houze, R.A. and Medina, S. (2005). Turbulence as a mechanism for orographic enhancement. *Journal of Atmospheric Sciences, 62,* 3599-3623.

Howell, S. Tivy, A., Yackel. J., and McCourt, S. (2008). Multi-year sea-ice conditions in the western Canadian Arctic Archipelago region of the northwest passage: 1968:2006. *Atmosphere-Ocean, 46,* 229-242.

Hudak, D.R. and Young, M.C. (2002). Storm climatology of the southern Beaufort Sea. *Atmosphere-Ocean, 40,* 145-158.

IPCC. (2013). Climate Change 2013: The Physical Science Basis. Contribution of Working Group I to the Fifth Assessment Report of the IntergovernmentalPanel on Climate Change [Stocker, T.F., D. Qin, G.-K. Plattner, M. Tignor, S.K. Allen, J. Boschung, A. Nauels, Y. Xia, V. Bex and P.M. Midgley (eds.)]. Cambridge University Press, Cambridge, United Kingdom and New York, NY, USA, 1535 pp.

Isaac G.A., Joe, P. Mailhot, J., Bailey, M., Belair, S., Boudala, F., Brugman, M., Campos, E., Carpenter, R., Crawford, R.W., Cober, S., Denis, B., Doyle, C., Reeves, H., Gultepe, I., Heiden, T., Heckman, I., Huang, L., Milbrandt, J.A., Mo, R., Rasmussen, R., Smith, T., Stewart. R.E., and Wang, D. (2012). Science of nowcasting Olympic weather for Vancouver 2010 (SNOW-V10): A world weather research programme project**.** *Pure and Applied Geophysics, 169*, doi:10.1007/s00024-012-0579-0

Jiang, Q. and Smith, R. (2003). Cloud timescales and orographic precipitation*. Journal of Atmospheric Sciences,* 60, 1543-1559.

Korolev, A.L., Issac, G.A., and Hallett, J. (1999). Ice Particle habits in Arctic Clouds. *Geophsyical Research Letters, 26*, 1299-1302.

Korolev, A.L, Issac, G.A., Cober, S., Strapp. J.W., and Hallett, J. (2003). Microphysical characterization of mixed-phase clouds. *Quarterly Journal of the Royal Meteorological Society*, *129*, 39–65.

Korolev, A., Emery, E.F., Strapp, J.W., Cober, S.C., Isaac, G.A., Wasey. M., and Marcotte, D. (2011). Small ice particles in tropospheric clouds: fact or artifact? Airborne Icing Instrumentation Evaluation Experiment. *Bulletin of the American Meteorological Society, 92,* 967-973.

Laplante, A., Stewart, R., and Henson, W. (2012). Characterization of cloud and precipitation features over southern Baffin Island and adjacent areas during STAR. *Atmosphere-Ocean, 50,* 54-69. doi:10.1080/07055900.2011.646535.

Liu, C. and Illingworth, A.J. (2000). Toward more accurate retrievals of ice water content from radar measurements of clouds. *Journal of Applied Meteorology, 39,* 1130–1146.

McFarquhar, G.M., Zhang, G., Poellot, M.R., Kok, G.L., McCoy, R., Tooman, T., Fridlind. A., and Heymsfield, A. J. (2007). Ice properties of single-layer stratocumulus during the Mixed-Phase Arctic Cloud Experiment: 1. Observations. *Journal of Geophysical Research., 112,* D24201, doi:10.1029/2007JD008633.

Medina, S. and Houze, R.A. (2003). Air motions and precipitation growth in Alpine Storms. *Quarterly Journal of the Royal Meteorological Society, 129*, 345-371.

Mesinger F., Dimego, G., Kalnay, E., Mitchell, K., Shafran, P.C., Ebisuzaki, W., Jović, D., Woollen, J., Rogers, E., Berbery, E.H., Ek, M.B., Fan, Y., Grumbine, R., Higgins, W., Li, H., Lin, Y., Manikin, G., Parrish, G., and Shi, W. (2006). North American Regional Reanalysis. *Bulletin of the American Meteorological Society, 87,* 343-360.

Morrison, H., Zuidema, P., McFarquhar, G.M., Bansemer. A., and Heymsfield, A.J. (2011). Snow microphysical observations in shallow mixed-phase and deep frontal Arctic cloud systems. *Quarterly Journal of the Royal Meteorological Society, 137*, 1589–1601.

Neiman, P.J., Ralph, F.M., White, A.B., Kingsmill, D.E., and Persson, P.O.G. (2002). The statistical relationship between upslope flow and rainfall in California's coastal mountains: Observations during CALJET. *Monthly Weather Review*, *130,* 1468-1492.

Rasmussen, R., Poliovich, M., Sand, W., Stossmeister, G., Bernstein, B., Elmore, K., Marwitz, J., McGinley, J., Smart, J., Westwater, E., Standkov, B.B., Pielke, R., Rutledge, Wesley, S.D., Powell, N., and Burrows, B. (1992). Winter Icing and Storms Project (WISP). *Bulletin of the American Meteorological Society, 73,* 951–974.

Reinking, R.F.; Snider, J.B., and Coen, J.L. (2000). Influences of Storm-Embedded Orographic Gravity Waves on Cloud Liquid Water and Precipitation. *Journal of Applied Meteorology,* 39, 733-759.

Reynolds, D.W. and Dennis, A.S. (1986). A review of the Sierra Cooperative Pilot Project. *Bulletin of the American Meteorological Society*, *67,* 513-523.

Roberts, E., Nawri. N., and Stewart, R.E. (2008). On the storms passing over southern Baffin Island during Autumn 2005. *Arctic,* 61, 309-321.

Rotunno, R. and Houze, R.A. (2007). Lessons on orographic precipitation from the Mesoscale Alpine Programme. *Quarterly Journal of the Royal Meteorological Society*, *133,* 811–830.

Shupe, M.D., Matrosov, S.Y., and Uttal, T. (2006). Arctic mixed-phase cloud properties derived from surface-based sensors at SHEBA. *Journal of Atmospheric Sciences, 63*, 697-711.

Smith, R.B. (1979). The influence of mountains on the atmosphere. *Advanced Geophysics, 21***,** 187-230.

Smith, R.B., Jiang, Q., Fearson, M.G., Tabary, P., Dororninger, M., Doyle, J.D., and Benoit, R. (2003). Orographic precipitation and air mass transformation: an alpine example. *Quarterly Journal of the Royal Meteorological Society, 129***,** 433-454.

Stewart, R.E., Szeto, K.K., Reinking, R.F., Clough, S.A., and Ballard, S.P. (1998). Midlatitude cyclone cloud systems and their features affecting large scales and climate, *Reviews of Geophysics, 36,* 245-273.

Stewart, R.E., Burford, J.E., Hudak, D.R., Currie, B., Kochtubajda, B., Rodriguez, P., and Liu, J. (2004). Weather systems occurring over Fort Simpson, Northwest Territories, Canada, during three seasons of 1998–1999: Part 2. Precipitation features. *Journal of Geophysical Research, 189,* 1984-2012.

Stoelinga, M.T. Hobbs, P.V., Mass, C.V., Locatelli, J.D., Colle, B.A. Houze, R.A., Rangno, A.L., Bond, N.A., Smull, B.F., Rasmussen, R.M., Thompson, G., and Colman, B.R. (2003). Improvement of microphysical parameterization through observational verification experiment (IMPROVE). *Bulletin of the American Meteorological Society, 84,* 1807–1826.

Strapp, J.W, Albers, F., Reuter, A., Korolev, A.V., Maixer, U., Rashke., E. and Z. Vukovic. (2001). Laboratory measurements of the response of the PMS OAP-2DC. *Journal of Atmospheric and Oceanic Technology, 18,* 1150-1170.

Uttal, T.U., Curry, J.A., McPhee, M.G., Perovich, D., Moritz, R.E., Maslanik, J.A., Guest, P.S., Stern, H.L., Moore, J.A., Turenne, R., Hieberg, A., Serreze, M.C., Wylie, D.P., Persson, O.G., Paulson, C.A., Halle, C., Morison, J.A., Wheeler, P.E., Makshtas, A., Welch, A., Shupe, M.D., Intrieri, J.M., Stamnes, K., Lindsey, R.W., Pinkel, R., Pegau, W.S., Stanton, T.P., and Grenfeld, T.C. (2002). Surface heat budget of the Arctic Ocean *Bulletin of the American Meteorological Society, 82,* 255-275.

Verlinde, J., Harrington, J.Y., McFarquhar, G.M., Yannuzzi, V.T., Avramov, A., Greenberg, S., Johnson, N., Zhang, G., Poellot, M.R., Mather, J.H., Turner, D.D., Eloranta, E.W., Zak, B.D., Prenni, A. J., Daniel, J.S., Kok, G.L., Tobin, D.C., Holz, R., Sassen, K., Spangenberg, D., Minnis, P., Tooman, T. P., Ivey, M.D., Richardson, S.J., Bahrmann, C P., Shupe, M., Demott, P. J., Heymsfield, A.J., and Schofield, R. (2007). The mixed-phase Arctic cloud experiment. *Bulletin of the American Meteorological Society*, *88,* 205-222.

Woods, C.P., Stoelinga, M.T., Locatelli, J.D., and Hobbs, P.V. (2005). Microphysical processes and synergistic interactions between front and orographic forcing of precipitation during the 13 December 2001 IMPROVE-2 event over the Oregon Cascades. *Journal of Atmospheric Sciences, 62,* 3492-3519.

Yuter, S.E. and Houze, R.A. (2003). Microphysical modes of precipitation growth determined by S-band vertically pointing radar in orographic precipitation during MAP. *Quarterly Journal of the Royal Meteorological Society, 129*, 455–476.

CHAPTER 4: CHARACTERIZATION OF AN UNEXPECTED SNOWFALL EVENT IN IQALUIT, NUNAVUT AND SURROUNDING AREA DURING THE STORM STUDIES IN THE ARCTIC FIELD PROJECT

Shannon Fargey[1], William Henson[2], John Hanesiak[1] and Ron Goodson[3]

[1] Centre for Earth Observation Science, Department of Environment and Geography, University of Manitoba, Winnipeg, Manitoba, Canada

[2]AMEC Environment & Infrastructure, Ottawa, Ontario, Canada

[3]Hydrometeorology and Arctic Laboratory, Environment Canada, Edmonton, Alberta, Canada

Journal of Geophysical Research – Atmospheres, 119 (9), *5492-5511*

doi: 10.1002/2013JD021176

This chapter examines the mechanisms that led to the event an unexpected high latitude snowfall event over Iqaluit, Nunavut and the surrounding area. Analysis of the Canadian operational Global Environmental Multi-scale Limited Area model provides some insight into why it was not well forecast.

Abstract

Small accumulation precipitation events contribute to more than 50% of total accumulation in the area, and occur at a greater frequency than high accumulation events. Despite their importance, the processes controlling them have not been investigated in sufficient detail. This study characterizes an unexpected high latitude snowfall event at Iqaluit, Nunavut and surrounding area during the Storm Studies in the Arctic (STAR) field project. High-resolution data collected, from both ground based and airborne Doppler radar, along with upper air and surface observations, provided the basis for analysis of the conditions that led to the event and offer some insight as to why it was not well forecast by the Canadian operational model.

Several factors worked in concert to produce this event. Low-level convection and upslope processes were important in cloud and precipitation generation over the orography upstream. When combined with additional lift from the passing of a weak trough, cloud and precipitation production were enhanced, allowing these features to penetrate over the terrain, and resulted in precipitation at Iqaluit. Analysis of the Global Environmental Multi-scale Limited Area Model (2.5 km resolution output), suggests that upstream convection and upslope processes were affected by model errors. As a consequence, precipitation onset was delayed and total accumulation was 50% lower than observations. Results indicate that the complexity of precipitation events in the region represents a significant challenge for predicting and modelling and to understanding their role in the hydrological cycle.

4.1. Introduction

An improved understanding of precipitation in the Arctic is required to assess the impact of a changing climate on the hydrologic cycle [*AMAP*, 2011]. However, precipitation forecasting and modelling in the Arctic continues to be a problem, primarily due to a lack of field data and limited observational studies required to effectively characterize the many mechanisms responsible for precipitation production in high latitude environments. This translates to variable agreement between modelling studies and weather station data [*Sinclair & Watterson*, 1999; *McCabe, Clark, & Serreze,* 2001; *Yin,* 2005; *Serreze, Barrett, & Lo,* 2005; *Lambert & Fyfe*, 2006; *Finnis, Holland, Serreze, & Cassano* 2007; *Higgins & Cassano,* 2009; *Stroeve, Serreze, Barrett, & Kindi* 2011], with discrepancies partially attributed to the observational scale used in comparisons (station versus grid point), low precipitation amounts, and the fact that stations are limited to typically coastal, low elevation topographies. To improve these differences, and provide a more accurate representation of precipitation in models, additional observational data are required.

A number of major field programs have been conducted in the Canadian Arctic. Datasets collected during the Beaufort and Arctic Storms Experiment [BASE; *Hanesiak. Stewart, Szeto, Hudak, & Leighton,* 1997; *Stewart et al*., 2004; *Hudak et al*. 2004] and the Mackenzie Global Energy and Water Cycle Experiment (GEWEX) Study [MAGS; *Stewart, Szeto, Reinking, Clough, & Ballard,* 1998; *Asuma et al.,* 2000] and the Storm Studies in the Arctic [STAR; *Gascon, Stewart, & Henson,* 2010; *Henson, Stewart, & Hudak,* 2011; *Laplante, Stewart, & Henson,* 2012; *Fargey, Hanesiak, Stewart, & Wolde,* 2014], among others, have been analyzed with the purpose of characterizing Arctic clouds, precipitation and storm systems. Unique features included the prevalence of multilayered systems, the cold temperatures of low clouds and significant sublimation effects in the initial stages of storm events and between cloud layers [*Stewart et al.,* 2004; *Henson et al.*, 2011; *Laplante et al*, 2012]. In addition, during the cold season (October to April) precipitation events were often associated with low to trace amounts and more likely to fall exclusively as snow because of the sub-freezing temperature profile [*Hanesiak et al.*, 1997; *Stewart et al.*, 2004]. *Laplante et al*. [2012] also showed that precipitating clouds were generally higher than mean values and were colder and thicker than non-precipitating clouds.

The formation of precipitation in the Arctic arises through a variety of mechanisms during the cold season. Synoptic-scale extratropical cyclones are fairly common in the Arctic, and important for precipitation production, with a frequency of about one per week [*Hanesiak et al.,* 1997; *Hanesiak et al*., 2010]. These types of storms arrive from numerous source regions, which include but are not limited to, the Beaufort Sea, the Canadian Prairies, the Atlantic Ocean or Baffin Bay regions [*Stewart et al.*, 1995; *Hudson, Aihoshi, Gaines, Simard, & Mulluck,* 2001; *Intihar & Stewart*, 2005]. Due to their potential association with severe and hazardous weather, a number of studies have examined their general character [*Hudak et al*. 2004; *Stewart et al*., 2004; *Intihar & Stewart*, 2005; *Roberts, Nawri, & Stewart,* 2008; *Gascon et al.,* 2010; *Henson et al.,* 2011].

Orographic forcing and convection over open-ocean also influence precipitation production, particularly in the eastern Canadian Arctic [*Intihar & Stewart*, 2005; *Hanesiak et al.,* 2010; *Fargey et al.,* 2014]. Significant topography provides multiple lifting areas for advancing flows, and the adjacent ocean provides a moisture source along dominant storm tracks [*Stewart et al.,* 1995; *Intihar & Stewart,* 2005]. Previous studies have shown that precipitation results from orographic lift alone, or is enhanced by the interaction of large-scale baroclinic systems with orography [*Intihar & Stewart*, 2005; *Gascon et al.,* 2010; *Fargey et al.,* 2014]. Recently, results from the STAR field experiment showed that multiple factors, including variable dynamic flow regimes such as gravity waves and upslope flow at all levels (high Froude number) contributed to enhanced precipitation generation aloft, over the orography of Baffin Island, located in the south-east Canadian Arctic [*Fargey et al.,* 2014].

In addition, sea ice extent influences atmospheric moisture availability, cloud formation [*Curry, Rossow, Randall, & Scharamm,* 1996] and atmospheric stability [*Deacu, Zandra, & Hanesiak,* 2010], influencing the environment under which precipitation forms in the region. Seasonally, low-level convection is fairly common in the fall and early winter in many parts of the Arctic, including the eastern Canadian Arctic [*Renfrew & Moore,* 1999; *Serreze & Hurst,* 2000*; Liu, Moore, Tsuboki, & Renfrew,* 2006; *Hanesiak et al.,* 2010]. The comparatively warm ocean surface underling a cold atmosphere will foster low-level instability, and may give rise to shallow convection and sometimes precipitating clouds [*Wacker, Potty, Luples, Hartman, & Raschdorfer,* 2005]. *Fargey et al.* [2014] showed that instability upstream of the orography of Baffin Island led to enhanced precipitation on windward slopes when combined with upslope flow.

During the cold season, a significant portion (up to 36%) of monthly precipitation is the consequence of one or more extreme cyclonic events [*Intihar & Stewart*, 2005].

However, small accumulation events (≤ 2 mm liquid equivalent) occur at a greater frequency than high accumulation events and contribute to more than 50% of total accumulation in the area [*Gascon et al.* 2010]. Despite their importance, small accumulation events have received little attention to date and the processes controlling them have not been investigated in sufficient detail.

The main objective of this paper is to characterize an unexpected small accumulation high latitude snowfall event over Iqaluit, Nunavut and the surrounding area, and gain some insight as to why it was not well forecast by the Canadian operational model. This case was selected from a sub-set of data collected during the STAR field campaign as it was identified as a relevant opportunity to examine the influence of upslope processes and low-level convection on small precipitation events in the region.

This chapter is organized as follows. In section 4.2, the study area and data are described. The precipitation event is characterized in section 4.3, and includes an examination of conditions over Iqaluit, the adjacent ocean region, and the orography upstream. This is followed by a comparison with output from a high resolution, limited area model. In section 4.4, a discussion of the results is made, and concluding remarks follow in section 4.5.

4.2. Study Area and Data

4.2.1 Location

The STAR project focused on southern Baffin Island, in the south-east Canadian Arctic, and was based out of Iqaluit (Figure 4.1). The community is located at the head of

Frobisher Bay and the beginning of the Sylvia Grinnell river valley, surrounded by two quasi-parallel mountain ranges of northwest-southeast orientation. Within 50 km of Iqaluit, the terrain of the Meta Incognita and Hall Peninsulas rise to 600 m and 750 m above mean sea level, respectively.

During the STAR observation period (October to November 2007), there were several precipitation events including both high and low accumulations [*Henson et al.,* 2011]. Low accumulations occurred at a greater frequency (68%) and comprised 35% of the total precipitation (36 mm) recorded during the project. At Iqaluit, a climatological study suggests that during the cold season, precipitation events are typically small in accumulation (average daily accumulation is 1.5 mm liquid equivalent) and are more frequent [*Gascon et al.,* 2010]. Over 90% of precipitation events were < 5 mm (liquid equivalent) comprising 56% of total precipitation, while events with ≤ 2 mm (liquid equivalent) comprise 51% of total precipitation.

Sea ice concentration in both Hudson Strait and Davis Strait were below average during STAR, while Frobisher Bay experienced normal ice conditions [*Hanesiak et al.,* 2010]. *Cavalieri, Parkinson, Gloersen and Zwally* [1996] identified a significant declining sea ice concentration trend of -27% per decade between late October and early November in Hudson Strait, with evidence that this rate has accelerated in the last decade [*Kattsov et al.,* 2011]. As will be shown, open water (lack of ice) upstream of the orography, was an important contribution to precipitation production for this case.

Figure 4.1: Topographic map of southern Baffin Island in Nunavut (1 km Digital Elevation Model (DEM) resolution) with the locations of data collection areas. Inset map indicates location of study area (red box) within Canada. The letters are used as reference locations in an upcoming figure.

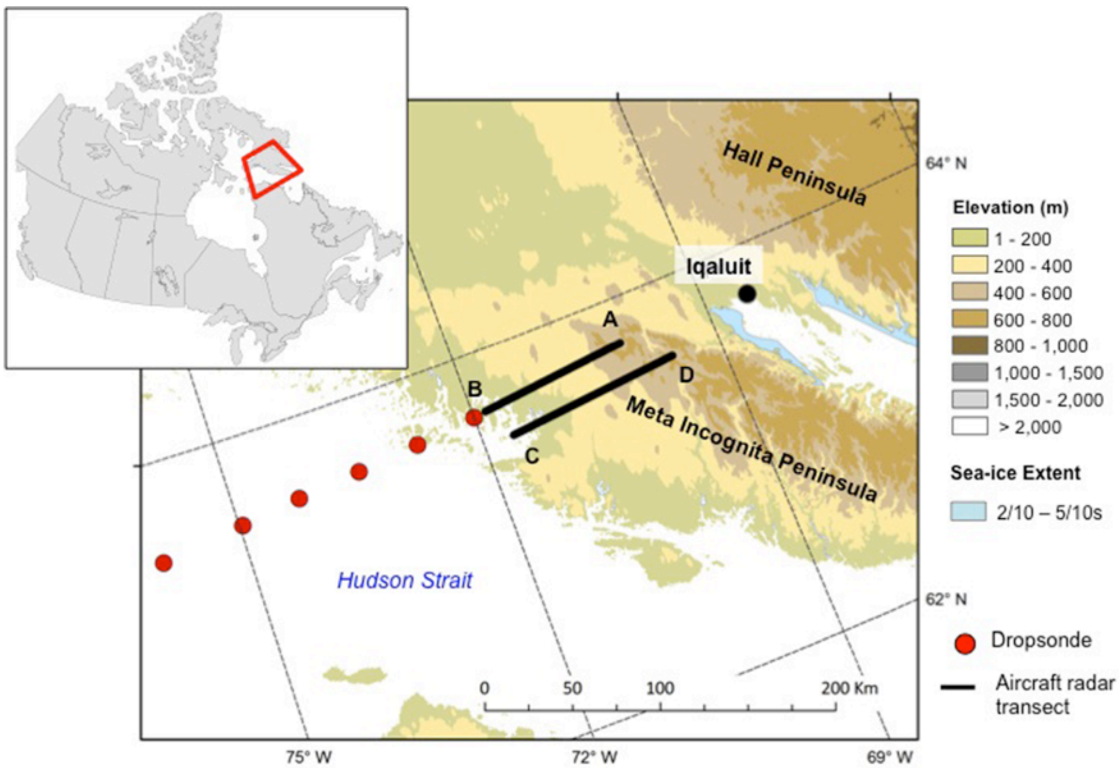

4.2.2 Instrumentation

<u>4.2.2.1 Research aircraft</u>

The National Research Council of Canada's Convair-580 research aircraft uses the Airborne W-band (3.2 mm wavelength) and X-band (3.2 cm wavelength) NAWX polarimetric Doppler cloud radar system. The radar system operates with a 0.4 to 0.7° beam width and at 30 to 60 m vertical resolution [*Hanesiak et al.,* 2010]. The aircraft was equipped with an Airborne Vertical Atmospheric Profiling System (AVAPS; GPS dropsonde system), and used modified RD-93 type dropsonde units, providing remote temperature, humidity, and wind profiles below the aircraft [*Hock & Franklin,* 1999]. The presence of supercooled water in cloud was assessed with the PMS King LWC probe (0.05 g m^{-3} sensitivity), and Rosemont Icing Detector (RID). A complete list of aircraft instrumentation operated during STAR can be found in *Hanesiak et al.* [2010].

4.2.2.2 X-band Doppler radar

A ground-based X-band Doppler radar, owned and operated by Environment Canada (EC), was deployed in Iqaluit (Figure 4.1). The radar has a peak power of 25 kW and a beam width of 2.5°, with an operational radius of approximately 50 km. Its normal operating procedure repeated every 15 minutes, involved volume scans, Range Height Indicators (RHIs), Doppler Plan Position Indicator (PPI) scans on selected azimuths and was operated in vertical stare mode. For the STAR campaign it was configured for a pulse duration during was 0.4 μs, and pulse repetition frequency of 2000 s^{-1}. The range resolution was 50 m and the minimum detectable signal of the radar is 17 dBZ at 1 km. Additional information on the X-band radar system can be found in *Henson et al.* [2011].

4.2.2.3 Precipitation and upper air measurements

A Geonor 200B all-weather gauge (0.1 mm resolution) situated inside an octagonal Double Fence Intercomparison Reference (DFIR) shield, minimizing wind effects [*Sevruk et al.,* 2009], recorded accumulation during the event. In conjunction with gauge measurements, a Thies Clima Laser Precipitation Monitor (LPM) provided information about precipitating hydrometeors. The LPM detailed concentration and particle size distributions (averaged over 1-minute), for intervals from 125 to 8000 μm during the event [*Fargey et al.,* 2008]. LPM data for this case were investigated at 1-minute, 10-minute, 30-minute and 1-hour averaged intervals. Results show that similarities were present in distribution and concentration patterns for all time intervals in this case. As a result, hourly averaged data were deemed to provide sufficient information on how these features varied over the case study period. High-resolution photographs of the precipitation hydrometeors were also taken using a Nikon D1x digital camera equipped with a macro lens, following the procedure of *Roberts et al*. [2008].

Standard upper air measurements were made by EC, who conduct regular rawinsonde launches at 12-hour intervals using Vaisala RS92-SGP units as part of their upper air observational network, the only location on Baffin Island to do so. During STAR, standard upper air releases were supplemented with additional rawinsondes during intensive observation periods, released by STAR personnel. Sounding temperature, relative humidity, pressure and wind data were recorded at 10-second intervals, with accuracies of ±1.0 hPa for pressure, ±0.1°C for temperature, < 5% for relative humidity, 10 m horizontal position uncertainty, 0.1 m s^{-1} vertical measurement uncertainty, and 2° directional measurement uncertainty.

4.2.2.4 Ancillary data

Hourly surface meteorological observations were performed at the Iqaluit airport, adjacent to the EC Iqaluit site where the X-band radar was located. Digital records were obtained from the EC online archive [*Environment Canada,* 2013]. Data on sea ice cover were available from the Canadian Ice Service Digital Archive (CISDA). Weekly ice charts were created from an integration of all available real-time sea ice information from various remote sensing satellite sensors, aerial reconnaissance, ship reports, and operational model results, described in depth by *Howell, Tivy, Yackel and McCourt* [2008]. National Centers for Environmental Prediction (NCEP) North American Regional Reanalysis (NARR) composites were obtained from the National Oceanic and Atmospheric Administration (NOAA). Information on resolution and accuracy can be found in *Mesinger et al.* [2006].

4.2.2.3 Model description

For this analysis, the Global Environmental Multi-scale Limited Area Model with a 2.5 km resolution (GEM-LAM 2.5) was run in experimental operational mode [*Erfani et al*., 2006]. The initial and boundary conditions were extracted for the hourly output of the GEM regional model (15 km resolution), with initial conditions from the global forecasting system of the CMC and integrated for 48-hours [*Mailhot et al.* 2006]. For this case study, the model was run for an eighteen-hour period, between 1200 UTC November 9 and 0600 UTC November 10, which captured the development and cessation of the event.

GEM-LAM 2.5 is non-hydrostatic and uses semi-implicit semi-Lagrangian time integration. There are 58 vertical sigma-pressure levels up to 10 hPa. The physical parameterizations used include a unified cloudiness-turbulence scheme for the planetary boundary layer [*Belair et al.,* 2005], a radiation scheme [*Garand & Mailhot,* 1990], and a shallow convection scheme [*Belair, Mailhot, Girard, & Vaillancourt,* 2005]. Cloud microphysical processes and precipitation were parameterized using the Kong-Yau microphysical scheme [*Kong & Yau,* 1997]. This scheme has two ice-phase categories, a hybrid pristine ice-snow (referred to in this paper as snow) and a graupel category (which behaves as hail for large mixing ratios). Snow is represented as a spherical particle with a prescribed constant density [*Kong & Yau,* 1997]. The model's surface component set a mosaic approach with four surface types: land (snow), open water, sea ice and glaciers. More details about the model can be found in *Erfani et al.* [2006].

4.3 Characterization of the snowfall event

4.3.1 Synoptic overview

At 0000 UTC on November 8 2007, a vertically stacked barotropic low pressure system, with a central pressure of 1001 hPa, was located north-west of Iqaluit (Figure 4.2). The system remained quasi-stationary over northern Baffin Island for the majority of its existence, until 1200 UTC on November 10. The position of the low centre resulted in cold, west to south-west winds, blowing over Hudson Strait and the Meta Incognita Peninsula. In conjunction with this large-scale circulation, a small trough developed over Hudson Bay at 0500 UTC November 9 and tracked north-east towards southern Baffin Island (Figure 4.2). Surface analysis indicates the trough was positioned south-west of the Meta Incognita Peninsula at approximately 1800 UTC, and by 0000 UTC November 10, it had moved north-east of Iqaluit. The estimated time of the trough's passage over Iqaluit is examined in more detail using surface and radar data in section 4.3.2 as it was found to assist in precipitation production for this case.

Low-level convective towers and roll vortices were present over Hudson Strait upstream from Baffin Island due to cold air advection behind the low pressure system, with cloud tops up to 2200 m [*Hanesiak et al.,* 2010]. These features were visible in IR satellite images (not shown) for the duration of the precipitation event at Iqaluit and persisted for six hours thereafter.

Figure 4.2: Synoptic overview: sea level pressure (SLP) (NCEP NARR composite mean) at: 1200 November 9 (top), 1800 November 9 (middle) and 0000 November 10, 2007 (bottom). The black dot indicates location of Iqaluit, NU.

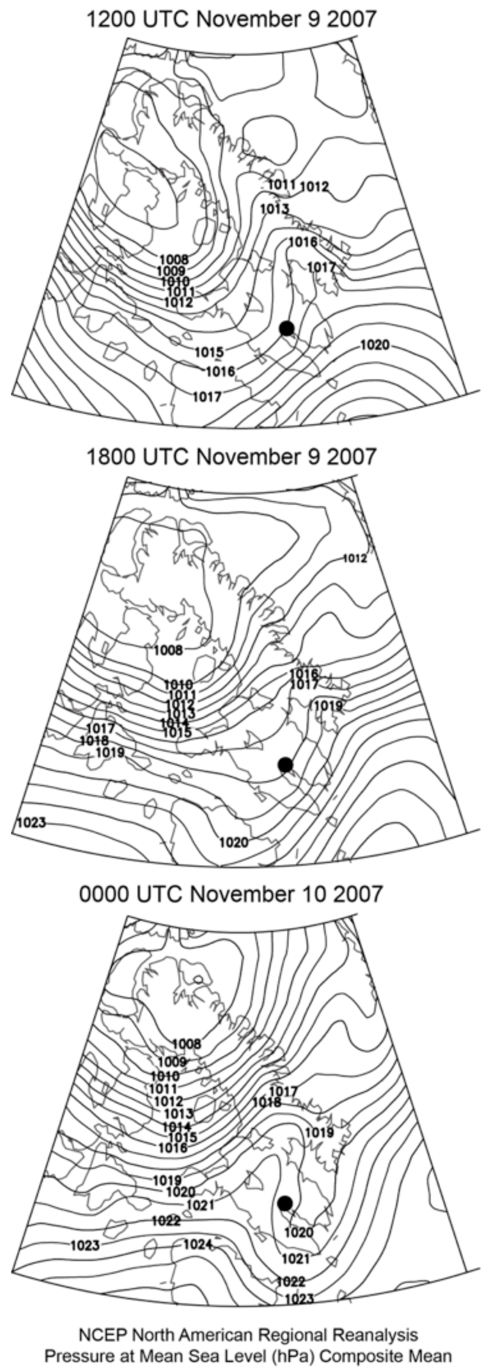

4.3.2 Conditions at Iqaluit

4.3.2.1 Precipitation at the surface

Unexpected precipitation fell for a period of 4-hours in Iqaluit, from 1800 to 2200 UTC November 9, resulting in 2.2 mm liquid equivalent accumulation and reduced visibility to 300 m (Figure 4.3). At the beginning of the event (1800 to 1900 UTC) almost all hydrometeors were smaller than 1250 μm (Figure 4.4). Between 1900 to 2100 UTC the number of precipitating hydrometeors increased substantially and approximately 20% were large hydrometeors (3000 and 6000 μm). Over the duration of the event, precipitating hydrometeors sized between 1000 and 1250 μm were most common, but hydrometeors up to 7500 μm were present at times (Figure 4.4).

Hydrometeor characteristics from the period of heaviest precipitation, 2000 to 2050 UTC, indicate snow fell mainly as accreted particles, which were irregular in shape (Figure 4.5). Some of the rimed hydrometeors had unrimed facets, which indicate the occurrence of depositional growth after rime was deposited. This likely occurred when the hydrometeor transitioned into a different region of the cloud. Fragmented dendrites, columnar, sector-like crystals and aggregates were present. Small hydrometeor fragments (< 100 μm) imply collisions occurred aloft.

These results, along with others from recent studies in the region, show that accretion and aggregation are important determinants of whether precipitation will reach the surface over Baffin Island [*Roberts et al.,* 2008; *Henson et al.,* 2011; *Fargey et al.,* 2014]. Enhanced growth through these mechanisms would increase density and may increase fall velocities, increasing the probability of hydrometeors reaching the ground before they completely sublimate.

Figure 4.3: Time series of surface observations (Obs) and GEM-LAM 2.5 model output at Iqaluit, NU during event. Snowfall is shown as cumulative precipitation (water equivalent) over time. The start and end of precipitation in the observations (black) and model (grey) is identified with arrows.

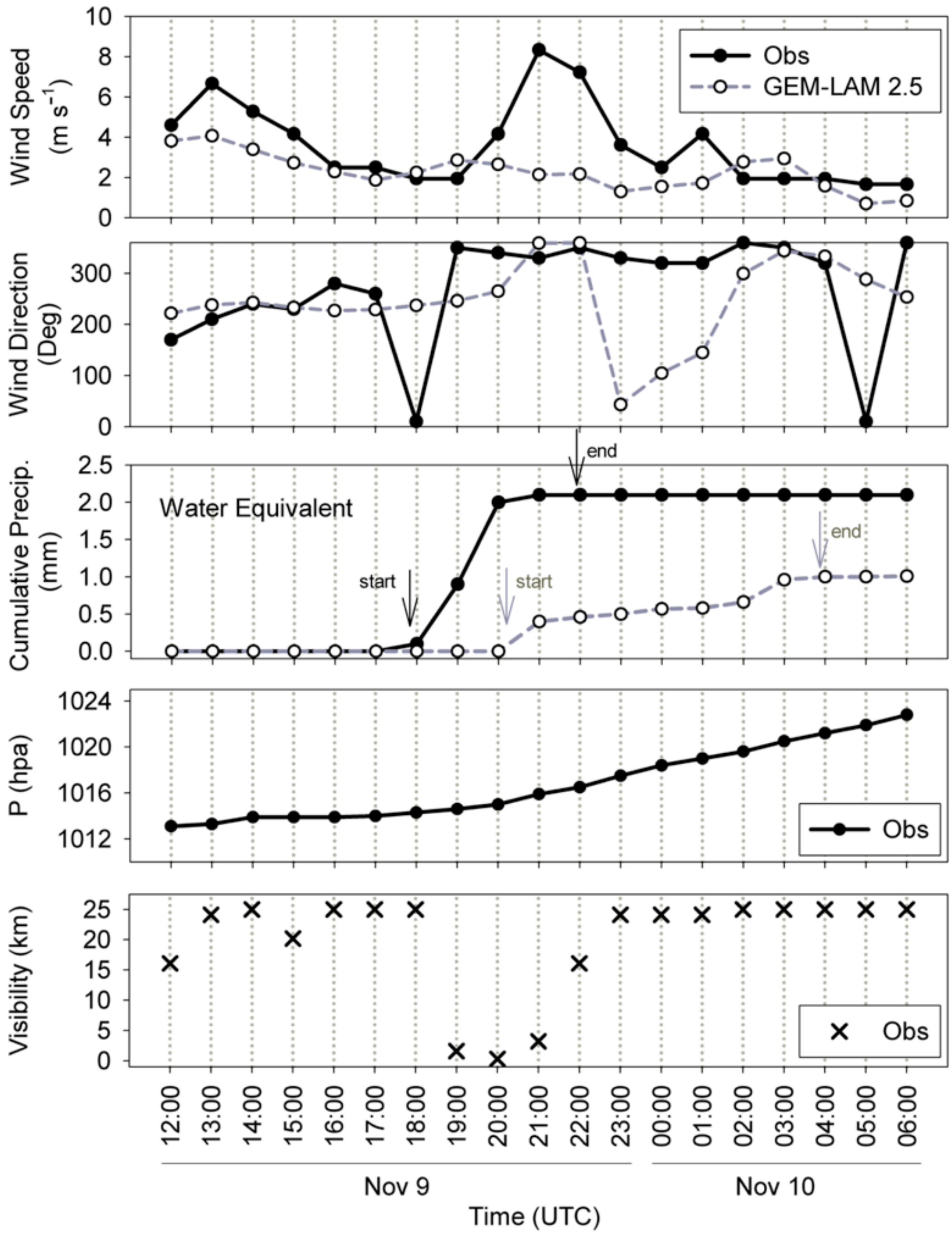

Figure 4.4: Hourly averaged particle size distribution of precipitating hydrometeors at Iqaluit, NU during event.

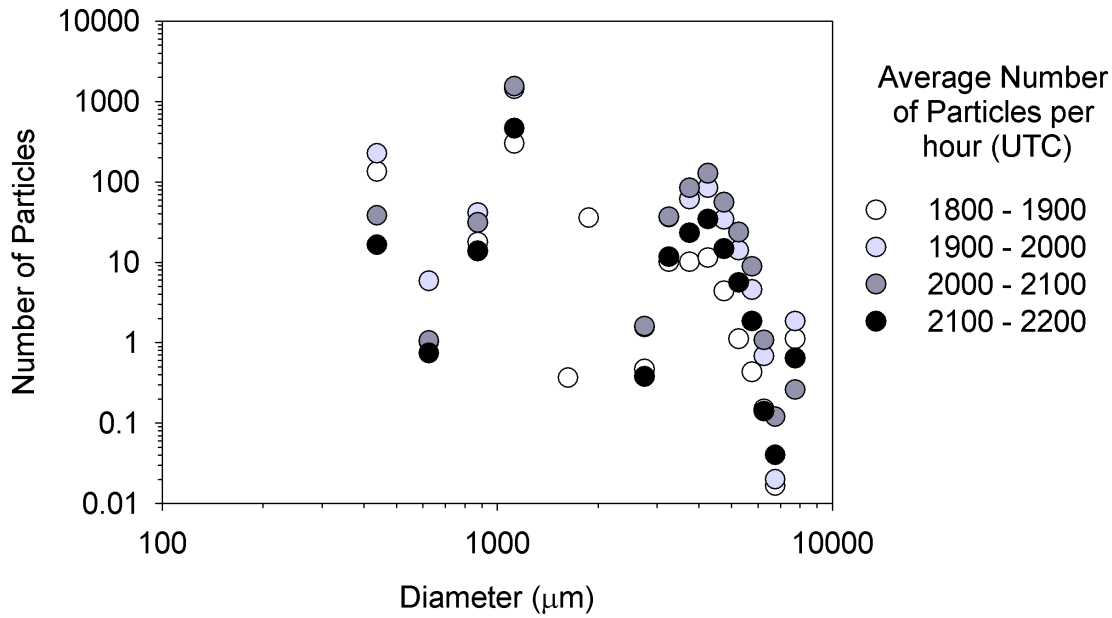

Figure 4.5: Composite image of photographs taken between the times of 20:00 and 20:50 UTC November 9 of precipitating hydrometeors at Iqaluit, NU.

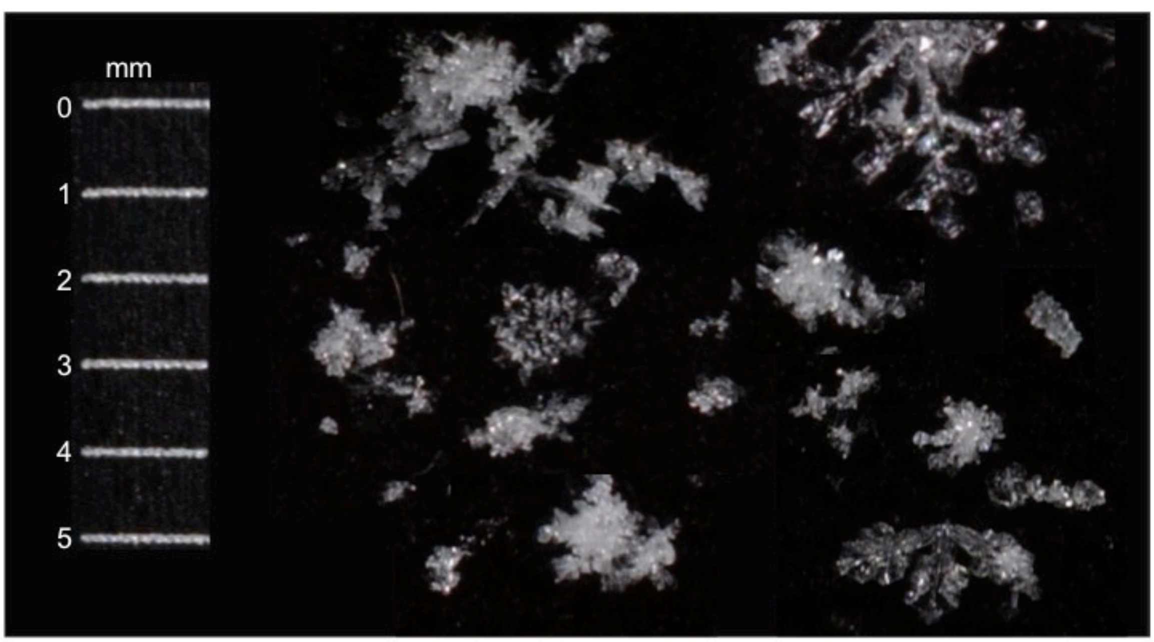

4.3.2.2 Upper air and surface measurements

The evolution of atmospheric conditions at Iqaluit during the storm was examined using a combination of surface observations and a series of three rawinsondes (Figure 4.6). Between 1200 UTC November 9 to 0000 UTC November 10, the temperature profile displayed little variability. Surface temperatures ranged from -7 to -9°C over the cross section, decreasing to -35°C at 5000 m. However, after 2100 UTC, a slight descent in temperature isotherms below 1200 m is present in Figure 4.6. Surface pressure remained constant from 1200 to 1900 UTC, after which a steady increase occurred suggesting the relatively weak trough moved away from Iqaluit at this time (Figure 4.3). The influence of the trough was also evidenced by a wind shift from south-west to north-westerly at the surface (shown in both sounding (Figure 4.6) and surface data (Figure 4.3)), with a coincident decrease in surface winds to 2 m s^{-1} (Figure 4.3). Channelling of surface winds along the surrounding orography at Iqaluit is not uncommon after the passing of a weather system [*Nawri & Stewart*, 2006; *Nawri & Stewart*, 2008]. *Nawri and Stewart* [2008] showed a connection with eastward moving cyclones near the Iqaluit site and a shift to either northwest or southeast directions. Winds above 1200 m, showed little variability, south-westerly increasing from 15 to 30 m s^{-1}, between 1200 and 5000 m, respectively (Figure 4.6).

Moist layers were present from 1000 to 2500 m and 5000 to 7000 m, and separated by a 30% relative humidity dry layer, as detected by the 1200 UTC November 9 sounding. By 2100 UTC, the atmosphere below 5000 m was near saturation with respect to water, which suggests loss from sublimation may have been minimal. This is confirmed by the presence of small hydrometeors in both the LPM data (Figure 4.4) and high-resolution photographs (Figure 4.5). Three-hours later, precipitation had concluded, coinciding with the development of multiple dry layers (Figure 4.6). Although not shown, RHI velocity scans show downslope flow, from the west behind the trough, contributing to the development of the dry layers detected in the 0000 November 10 sounding. A coincident decrease in temperatures below 1200 m (Figure 4.6), and decrease in number of hydrometeors smaller than 1000 μm (Figure 4.4) suggests that sublimational cooling was occurring. The decrease in temperature may also be the result of cold air advection behind the trough.

Figure 4.6: Time height cross section of three rawinsondes released at Iqaluit, NU. Contoured variables: relative humidity (%) colour shading, temperature (°C) dashed line. The black line on the bottom of the figure indicates when precipitation was observed at Iqaluit, NU.

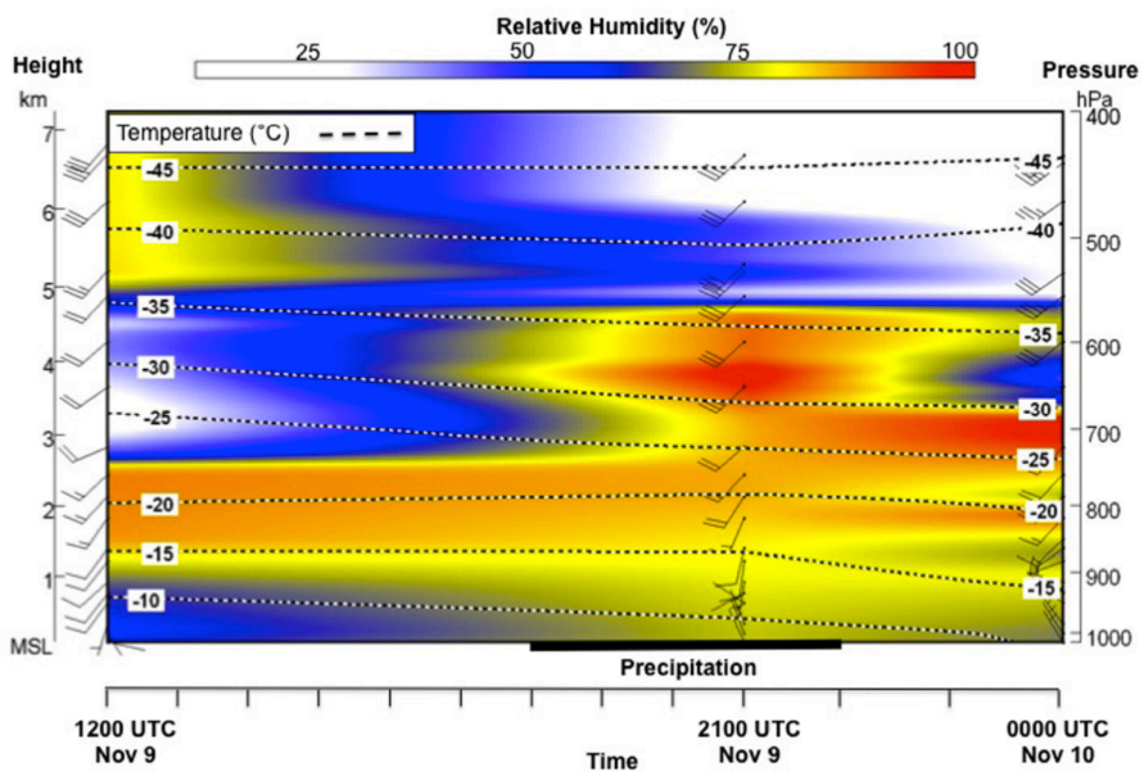

The three soundings profiles at Iqaluit were stable, indicating the trough did not result in significant destabilization in the layers aloft. As such, horizontal advection of hydrometeors from upstream of Iqaluit and convergence aloft from the passing of the trough, were likely the primary causes of precipitation. This will be examined in more detail in section 4.3.3 when the upstream environment is discussed.

<u>4.3.2.3 RHI vertical cross sections</u>

Cloud and precipitation features over Iqaluit were assessed using X-band radar data while operating in RHI mode at azimuths of 45°, 135°, 225°, and 315°. Vertical cross sections were created by combining radar scans at 225° and 45° azimuths for a south-west to north-east direction, which represents a profile parallel to wind above 1000 m and perpendicular to the orography.

The vertical structure of precipitation was associated with fall streaks, which were tilted above 2000 m, consistent with the wind regime (Figure 4.7). At 1839 UTC high reflectivities (20 to 24 dBZ) are present aloft but do not extend to the surface. After 1900 UTC precipitation is inferred at Iqaluit and over surrounding topography. The heaviest precipitation occurred after the passing of the trough, between 2000 to 2100 UTC, as indicated by the enhanced near surface reflectivity (Figure 4.7). After this time there were several occasions where reflectivities were present aloft but not near the surface, indicating precipitation was no longer reaching the ground. Maximum reflectivity was lower than observed during major precipitation events during STAR associated with mid-latitude cyclones [> 28 dBZ; *Henson et al.*, 2011].

Figure 4.7: South-west to north-east radar reflectivity vertical cross sections during event at Iqaluit, NU. Data shown at times of 18:39, 19:39, 20:39, 21:39 and 22:39 UTC November 9, 2007. The vertical axis is the height above the radar (km) and the horizontal axis is the horizontal distance (km) away from the radar.

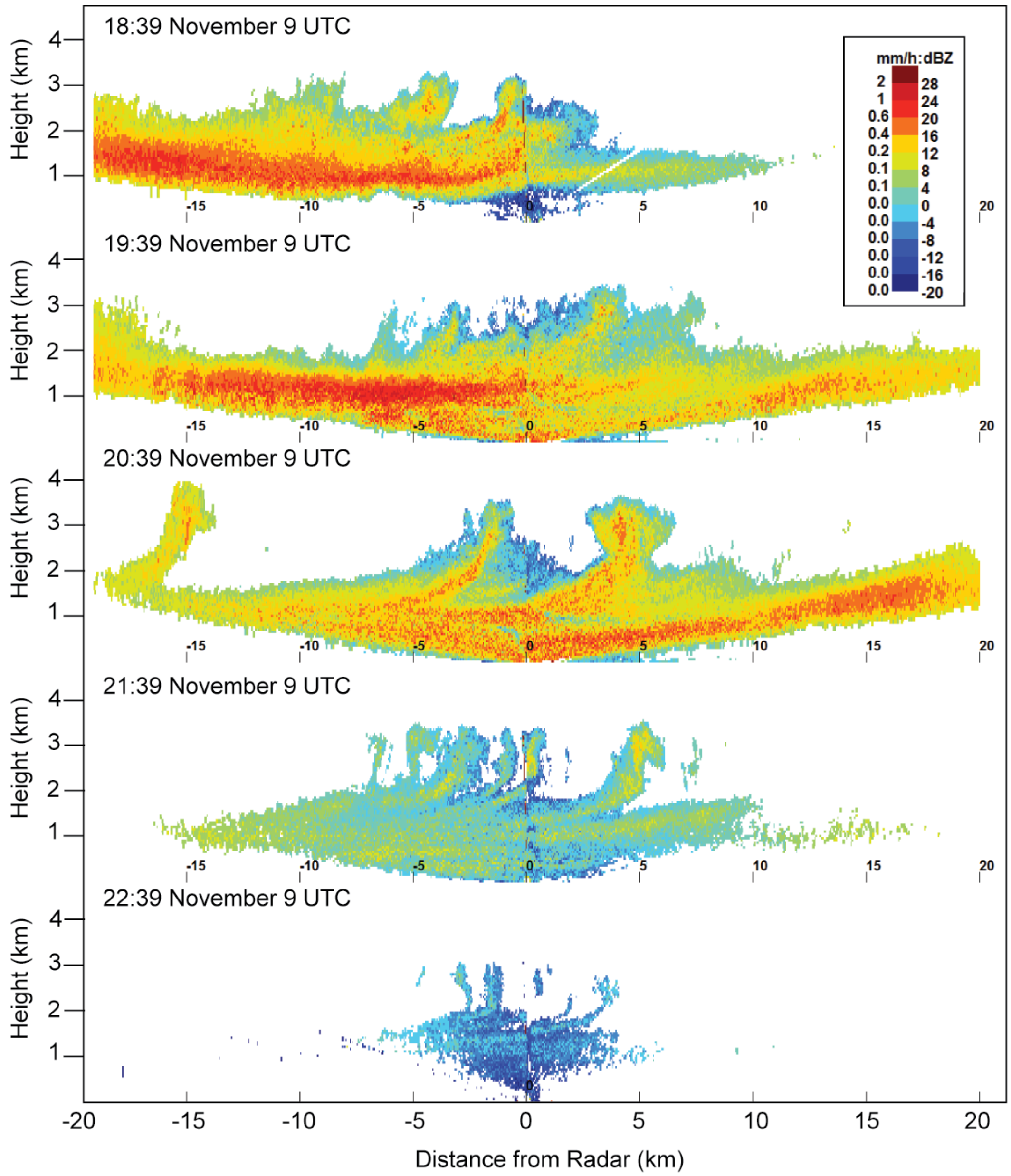

4.3.2.4 Velocity azimuth display

The wind speed and direction was determined from the 15° elevation Doppler PPI scan. For analysis purposes, at any particular range, a minimum of 75% of data were required before a sine wave was fitted to the data.

A depression in the wind speed with height profile, coupled with coincident low speeds near the surface, suggests that the trough was positioned over Iqaluit around 1921 UTC (Figure 4.8). This was confirmed by RHI velocity scans (not shown) that showed minimum winds between 1909 and 1924 UTC, thereafter, wind speeds steadily increased near the surface (Figure 4.8).

Figure 4.8: Velocity azimuth display of wind speed as a function of time during event at Iqaluit, NU.

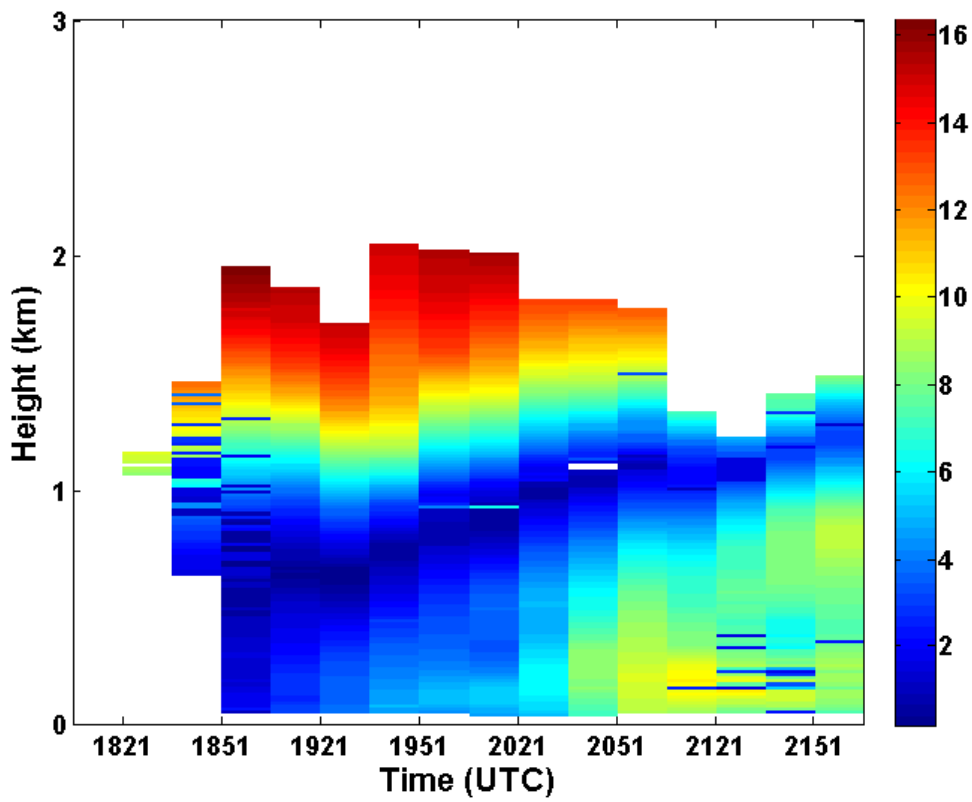

4.3.2.5 Vertical radar reflectivity and velocity with height

Contoured Frequency Altitude Diagrams (CFAD) were created using vertical pointing mode radar scans for the snowfall event (1800 to 2200 UTC). Following the technique of *Stewart et al.* [2004], CFAD were normalized with respect to the maximum occurrence based on results of *Hitchfeld & Bordan* [1954] and using the Z-S relationship from *Imai* [1960] to limit the attenuation to < 6% for the event.

The majority of radar reflectivity values occurred in three ranges, between 18 to 20 dBZ, 0 to 5 dBZ and -10 to 0 dBZ, respectively (Figure 4.9). A slight increase in reflectivity towards the surface indicates that hydrometeors grew as they fell. Growth was also evident in the vertical velocity CFAD, where fall speeds increased from 0.5 to 1 m s^{-1} towards the ground (Figure 4.9). A coincident increase in vertical velocity and high reflectivities (18 to 20 dBZ) began at 1200 m, although larger particles do not necessarily mean faster fall speeds. Depending on particle shape, an increase in size may increase frictional resistance and may reduce fall speeds.

Proportionally there were a greater number of reflectivities between the heights of 750 and 1800 m, compared to the number occurring just above the surface. This implies the partial removal, and/or a reduction in size, of hydrometeors as they fell. Results from this particular event show that a combination of sublimation and advection influenced hydrometeors reaching the surface. The development of dry layers aloft after 2100 UTC (Figure 4.6) indicates hydrometeors were subjected to some mass loss towards the end of the precipitation event. However, had sublimation been the only variable influencing the falling precipitation, there would have been a tilt towards lower reflectivities in the CFAD diagrams [*Stewart et al.,* 2004], which is not present in Figure 4.9. The RHI cross sections show enhanced reflectivities downstream of Iqaluit, which may be representative of some hydrometeor advection along with upslope processes, also influencing precipitation reaching the surface in Iqaluit. These reflectivity ranges and dry layers can also be seen in Figure 4.7.

Figure 4.9: Normalized Contour Frequency Altitude Diagrams (CFAD) during event. (top) Percentage for radar reflectivity (dBZ) as a function of height; (bottom) Percentage for vertical velocities (m s^{-1}) as a function of height at Iqaluit, NU.

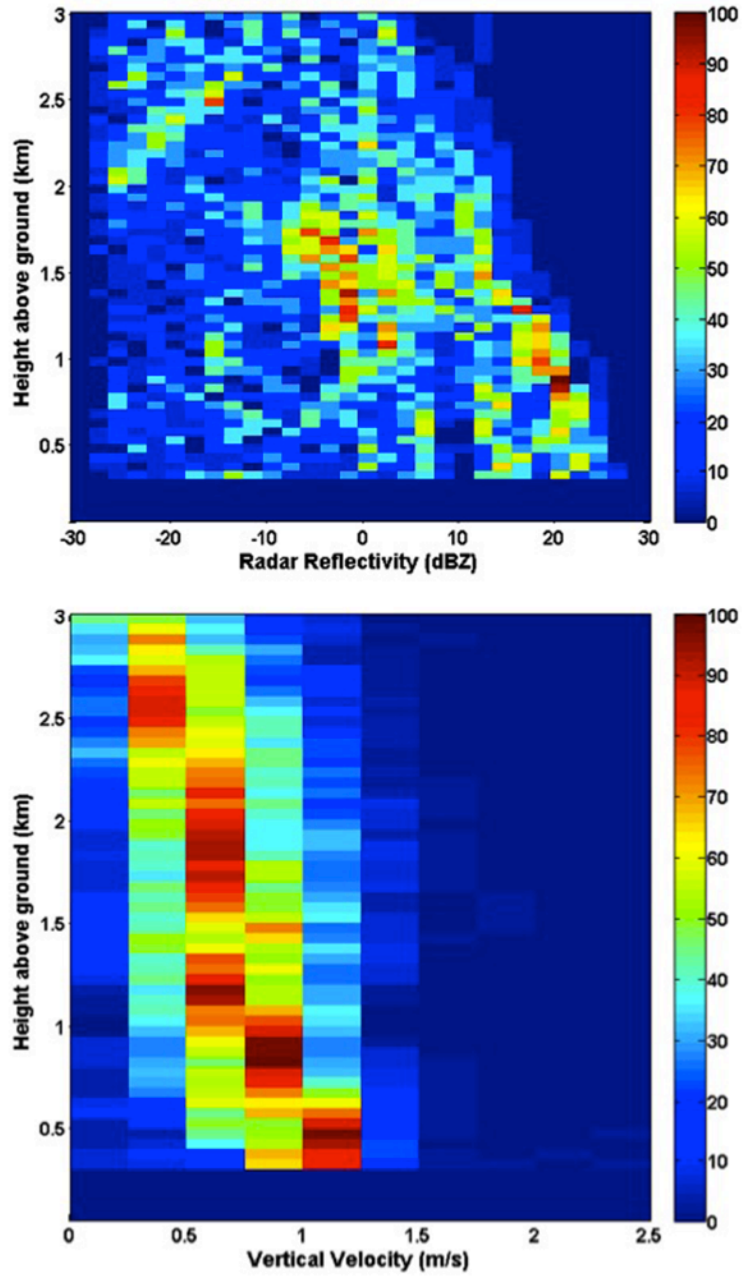

4.3.2.6 Ice water content

Using the relationship between ice water content (IWC) and radar reflectivity, ice water content was calculated, where IWC = $0.0137Z^{0.643}$ in grams per cubic meter as described by *Liu and Illingsworth* [2000]. The lower 250 m was not included in the calculations due to ground clutter.

Integrated IWC increased rapidly to a maximum of 4.8 kg m^{-2} around 2030 UTC, in the lee of the passage of the trough. Around the same time, the greatest observed reflectivity value and highest echo top occurred (Figure 4.10). IWC decreased rapidly after this time. Temporal variably in the IWC profile suggests there were times of very little ice water aloft interspersed with more intense periods. The peak IWC value for this case study was lower than previous studies in the Canadian Arctic, which characterized precipitation events associated with mid-latitude cyclones [*Hudak et al.,* 2004; *Henson et al.,* 2011]. This event appears to be the result of local conditions, with some large-scale forcing, which may contribute to differences.

Figure 4.10: Vertically integrated ice water content (kg m^{-2}) as a function of time based on radar reflectivity measurements at Iqaluit, NU, during event. The triangle at the top of the figure indicates the time when the greatest reflectivity as observed and the cross indicates the time when the highest echo top was observed.

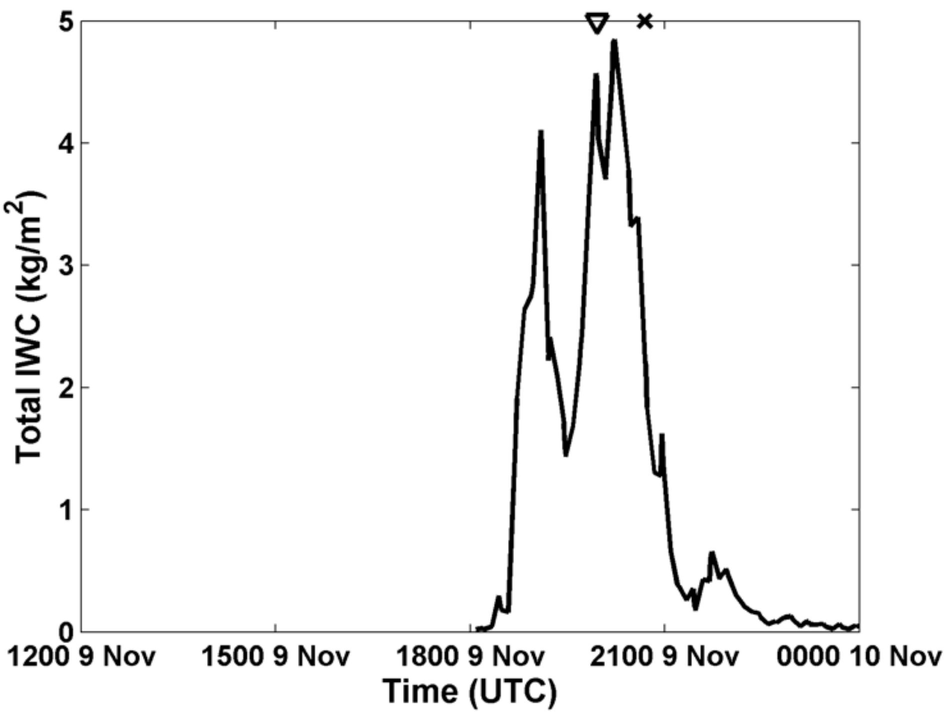

4.3.3 Upstream environment

Upstream of Iqaluit, the evolution of atmospheric conditions during the event was evaluated with data from the research aircraft. A series of six dropsondes released over Hudson Strait provide a cross section of the atmosphere over the adjacent ocean region, while cloud and precipitation features over the orography (windward side of the Meta Incognita Peninsula) was examined with two W-band radar profiles (Figure 4.1). The A-B profile corresponds to the outbound flight from Iqaluit and the C-D profile the return inbound flight approximately 3-hours later (Figure 4.1). Unfortunately, no W-band radar data from the aircraft were available over Iqaluit and no X-band radar data from the aircraft was available in this case.

4.3.3.1 Conditions over adjacent ocean region

Soundings from Coral Harbour (located upstream of Baffin Island) prior the event suggest that surface-based convective available potential energy (SCAPE) was from 110 to 170 J kg^{-1} when the surface conditions were modified to above ocean temperatures. Over Hudson Strait, the near surface air temperature was -10°C, decreasing to -37°C at 4000 m (Figure 4.11). This resulted in low-level convection over the open water, where convective available potential energy (CAPE) was actively being released. Potential temperature (θ) isentropes show ascent in the moist levels below 2000 m, with increasing stability in dry areas aloft (Figure 4.11). Winds were westerly at all levels, 8 m s^{-1} near the surface, increasing to 15 m s^{-1} at 4000 m (Figure 4.11).

To investigate the potential for elevated convection as the air flowed into the terrain, parcels were lifted from 900 hPa using the dropsonde data. The upstream vertical dropsonde profile showed conditional instability where lifted parcels (due to terrain) were located. This likely enhanced cloud and precipitation production over the topography, but assessing how much is difficult to provide. Small-scale convective features are present near cloud-top in the aircraft radar profiles (shown in section 3.3.2).

Cloud-bases inferred from dropsondes were between 750 to 1000 m. The W-band radar indicated a cloud layer between 1000 to 2000 m was present near the coast, but no precipitation. Due to possible W-band attenuation, cloud-base radar estimates may be higher than recorded values.

Figure 4.11: Cross section of atmosphere over adjacent ocean region created from a series of six dropsondes released over Hudson Strait. Dropsondes were released in succession at ~2100 UTC November 9. Contoured variables: relative humidity (%) coloured background, potential temperature θ (K) (dashed line).

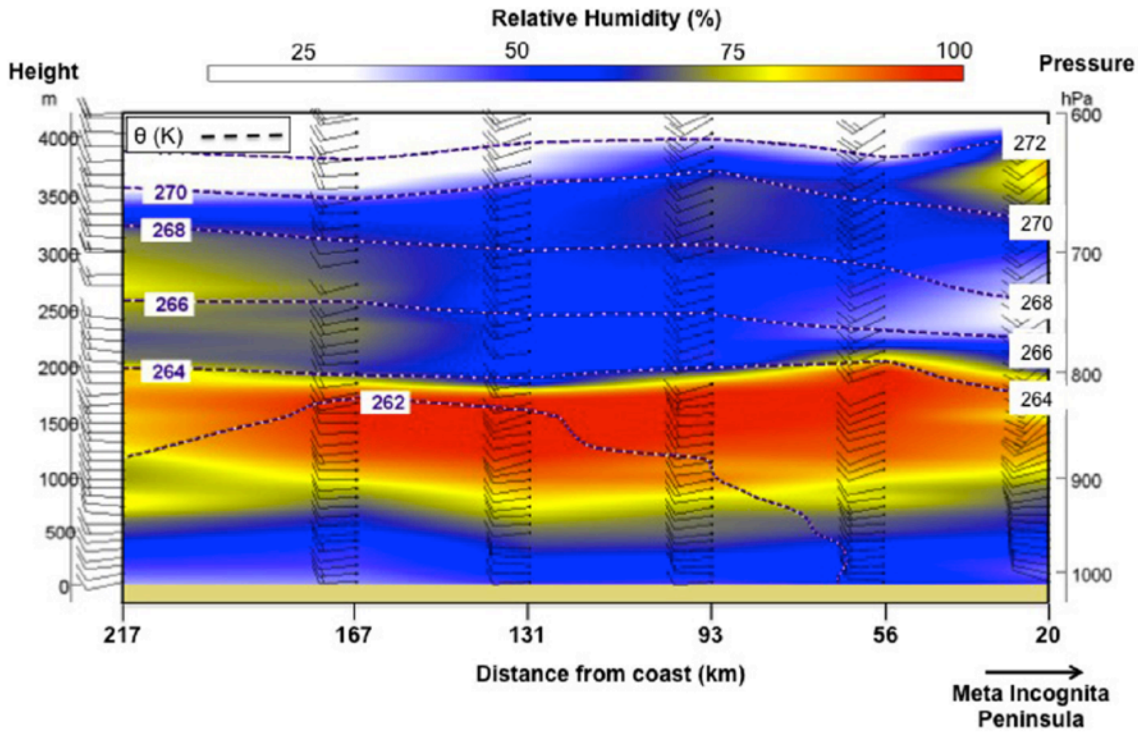

There were both similarities and differences between Iqaluit and the upstream environment. A moist layer between 1000 and 2000 m, with dry air below was present in both the upstream environment and in the 1200 UTC Iqaluit sounding (Figure 4.6). Winds aloft remained similar at the two locations through the event, but differences near the surface were present. Differences can be explained by the influence of the surrounding topography at Iqaluit. Prior to the passing of the trough, channelled flow along the Sylvia Grinnell river valley resulted in a south-easterly surface wind, shifting to south-westerly winds aloft. The passage of the trough resulted in a wind shift to north-westerly between the surface and 600 m at Iqaluit.

4.3.3.2 Cloud and precipitation features over the orography

Over the orography of the Meta Incognita Peninsula, radar derived cloud height was 2500 to 2900 m during the outbound flight ~ 2100 UTC (A-B profile) (Figure 4.12a). Cloud height and reflectivity values were enhanced compared to features over Hudson Strait. In general, reflectivity increased toward the surface, with precipitation (dBZ > 0) inferred on the windward slope extending to the crest of the terrain. Typical surface values were 3 to 5 dBZ, to a maximum of 10 dBZ. Nadir Doppler velocity measurements estimate fall speeds between 1 to 2 m s^{-1} in most areas, with updrafts of 0.5 to 1 m s^{-1} in the upper 250 m of the cloud (Figure 4.12b). The updraft regions coincided with enhanced reflectivity pockets and supercooled water at cloud-top ~ 0.1 g m^{-3}, suggesting an environment for additional growth.

Radar derived cloud features during the inbound (C-D) cross section showed some differences (Figure 4.12c). Cloud-top height was lower, 2000 to 2200 m and stronger reflectivity returns within 40 km of the coast, up to a maximum of 15 dBZ, were present. With increasing distance inland, reflectivity decreased, with a coincident decrease in hydrometeor fall speeds towards the surface, from 2 to 0.5 m s^{-1} (Figure 4.12d), indicating hydrometeors were losing mass as they fell.

Figure 4.12: W-band Doppler radar data over the Meta Incognita Peninsula. Outbound flight ~ 2100 UTC November 9 (a) reflectivity (dBZ) (b) Doppler velocity (m s^{-1}). Inbound flight ~ 00:00 UTC November 10 (c) reflectivity (dBZ) (d) Doppler velocity (m s^{-1}) - warm hues descent, cool hues ascent. Terrain outlined in black for reference - height in meters (m) above mean sea level from DEM. The black arrow indicates direction of aircraft motion. Winds were from left to right in each image.

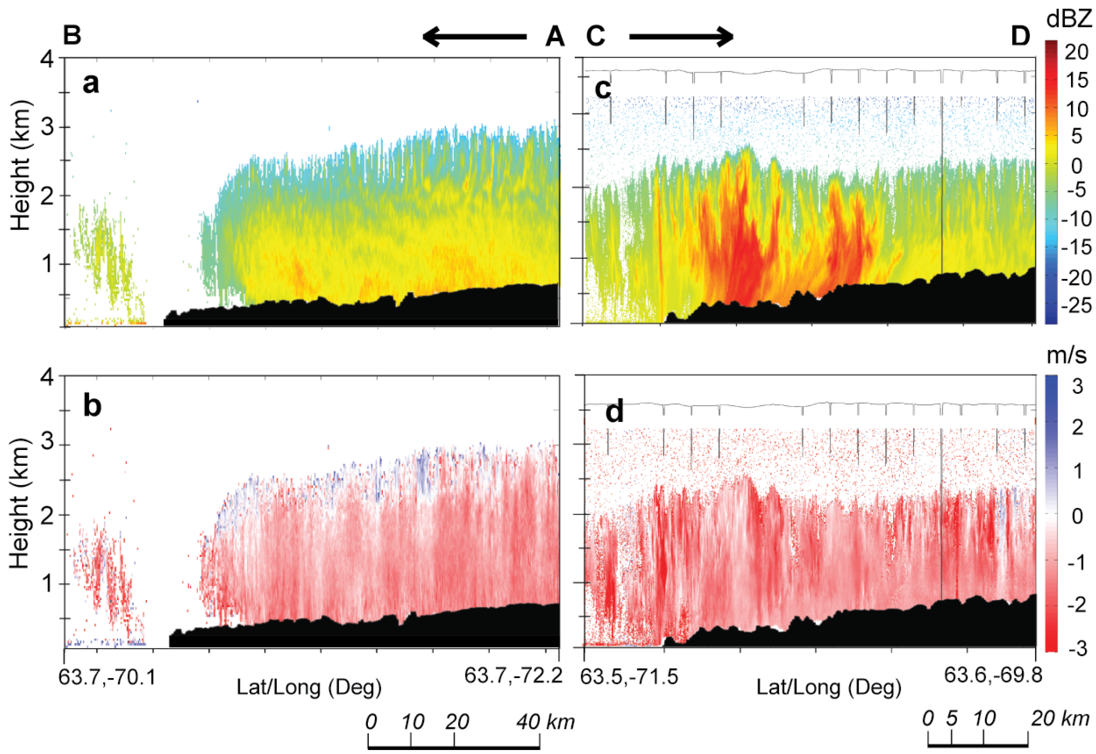

These key differences between the two radar profiles can in part be explained by the influence of the trough on the environment. The trough provided additional lift over the terrain and created an environment conducive to particle growth over the orography. This is evidenced by vertical cloud development (up to 900 m higher) and the increase in reflectivity and fall speeds towards the surface on the entire windward slope of the Meta Incognita Peninsula, shown in the A-B profile (Figure 4.12a and Figure 4.12b). In contrast, without the additional lift from the trough, cloud heights were lower, and with increasing distance inland, reflectivity and vertical velocities decreased towards the surfaces, shown in the C-D profile (Figure 4.12c and Figure 4.12d). This environment indicates mass loss over the orography, decreasing the probability of snow reaching Iqaluit. Even though low-level convection was ongoing over Hudson Strait, and upslope flow of conditionally unstable air did result in some orographic precipitation enhancement over a short distance (~40 km), these contributing mechanisms were unable to foster cloud development and hydrometeor growth to the altitudes required for precipitation to penetrate over the terrain to Iqaluit. As a result, the passing of the trough appears to have been necessary to bring precipitation to Iqaluit in this case.

4.3.4 Data comparisons with GEM-LAM 2.5

To provide some insight into how the Canadian operational model represented the environment in this case, verification of GEM-LAM 2.5 output was performed. Objective error statistics of temperature, dew-point temperature, wind speed and direction were computed using dropsonde data. A linear interpolation of model outputs to dropsonde locations in the vertical profile was used, with consideration for dropsonde drift. Model performance was evaluated using simple scores, bias and standard error, following a similar procedure to *Mailhot et al.* [2012]. The Bias is defined as equation 4.1:

$$Bias = \frac{1}{N}\sum_{i=1}^{N} \hat{y}_i - y_i \qquad (4.1)$$

while standard error (se) is defined as equation 4.2:

$$s_e = \sqrt{\frac{\sum_{i=1}^{n}(\hat{y}_i - y_i)^2}{n-2}} \qquad (4.2)$$

where $\hat{y}_i$ is the model-predicted value and y_i is the observed value for each i of n observations. Individual dropsonde residuals (e_i) were also used to assess model performance, defined as equation 4.3:

$$e_i = \hat{y}_i - y_i \tag{4.3}$$

At Iqaluit, model output was extracted to the EC Iqaluit site location, where precipitation and meteorological station data were collected. For the purpose of evaluating the model's ability to identify the passing of the trough and accumulation for this particular event, surface variables including precipitation, wind speed and direction were examined in conjunction with a time series of velocity with height over Iqaluit.

4.3.4.1 Validation of upstream environment using dropsondes

In the upstream environment, standard error throughout the entire vertical profile, for temperature and dew-point temperature was between 1.0 and 1.7 °C, and 3.0 and 5.4°C, respectively (Figure 4.13). Temperature error improved with increasing distance from land, whereas dew-point temperature did not. Error associated with wind speed, decreased from 4 to 1.8 m s^{-1}, with increasing distance from terrain. Wind direction error was between 9° to 16° but are represented well overall (Figure 4.13).

Figure 4.13: Standard error for GEM-LAM 2.5 vertical profiles, based on comparison to dropsonde data: temperature (T), dew-point temperature (Td), wind speed (WS) and wind direction (WD).

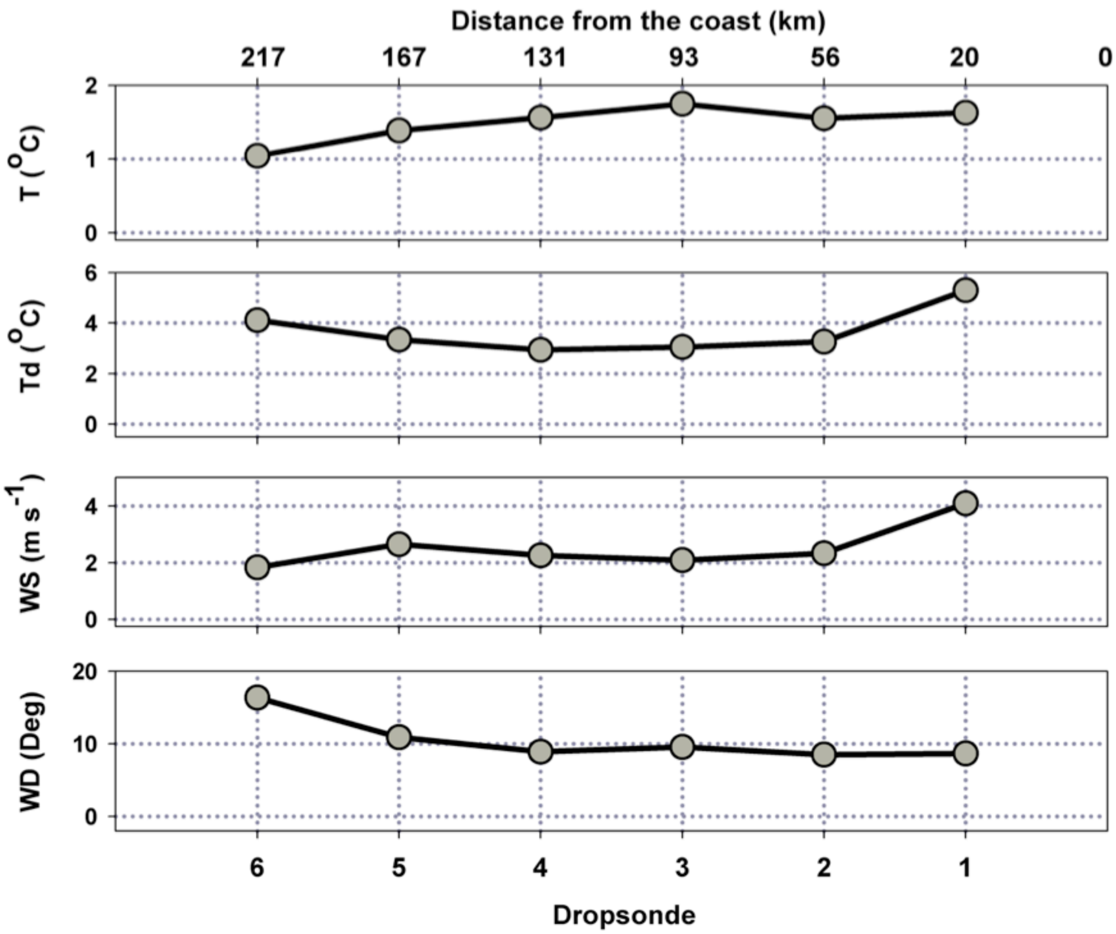

The comparison of dropsondes and modeled sounding profiles shows that at lower altitudes, the model consistently overestimated temperature (~ 2 °C) and moisture (Td between 0.5 and 3 °C higher than observations) (Figure 3.14). The temperature-dew-point spread indicates the model lifting condensation level (LCL) was between 100 and 500 m above actual LCL. Consequently, clouds were formed in different locations. In addition, some model sounding profiles (Dropsonde 5 and 6) show the presence of a dry layer, a feature not prominent in the observations. The upstream environment was conditionally unstable, similar to observations, but errors in temperature and moisture imply reduced exchange between the atmosphere and ocean, limiting convection compared to observations.

The evaluation of model bias in the vertical profile is shown in Figure 3.15. As noted in the sounding profile comparison, at altitudes lower than 800 hPa, temperature and humidity was positively biased (model was too warm and moist). Error was fairly consistent for all sounding profiles below 800 hPa altitude, but inter-sounding variability increased with increasing altitude. For example, error for dew-point temperature at 850 hPa, was large (10 °C) for Dropsonde 1, whereas at the same height, Dropsonde 6 (furthest from the terrain) was < 1 °C. In addition, both positive and negative errors at similar altitudes were common.

Considerable inter-dropsonde variability was also present in the wind speed residuals (Figure 3.15). Near-surface wind speeds were generally negative (too weak), but with increasing altitude, wind speed error was inconsistent. Above 900 hPa both positive and negative error occurred at similar altitudes. Overall wind direction was well represented in this case. Bias was generally within 10° of the observations at altitudes lower than 800 hPa. Despite errors, direction still designated upslope flow in the model environment, which is important for this case.

Figure 4.14: Comparison of dropsonde data (black) and extracted GEM-LAM 2.5 sounding profiles (red). Temperature (solid line) and dew-point temperature (dashed line).

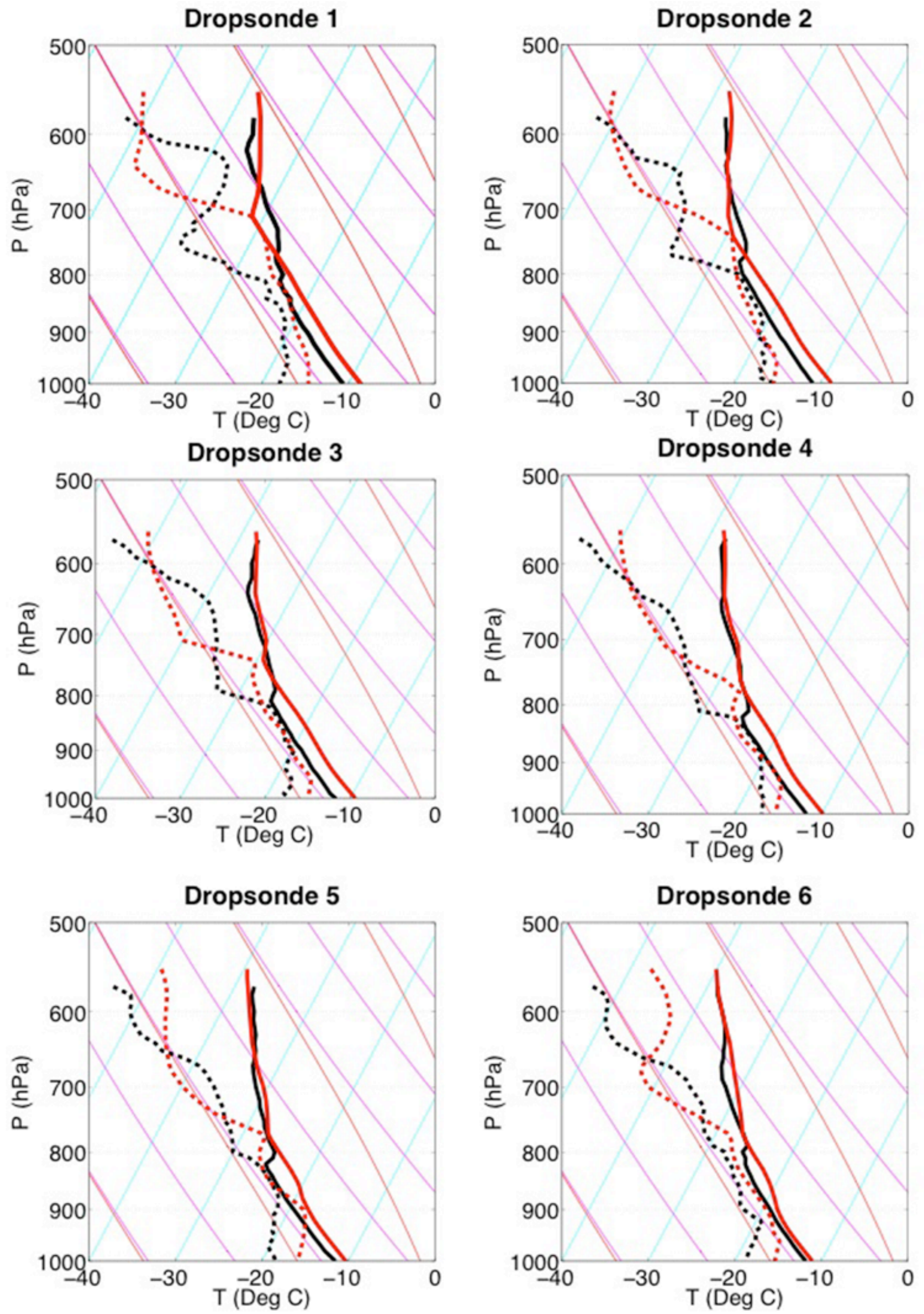

Figure 4.15: Bias (black line) and GEM-LAM 2.5 model residuals (coloured lines), from the comparison of extracted GEM-LAM 2.5 sounding profiles to dropsonde data: temperature (T), dew-point temperature (Td), wind speed (WS) and wind direction (WD). Dropsondes were given an abbreviated name in figure. For example, dropsonde 1 = Drop 1.

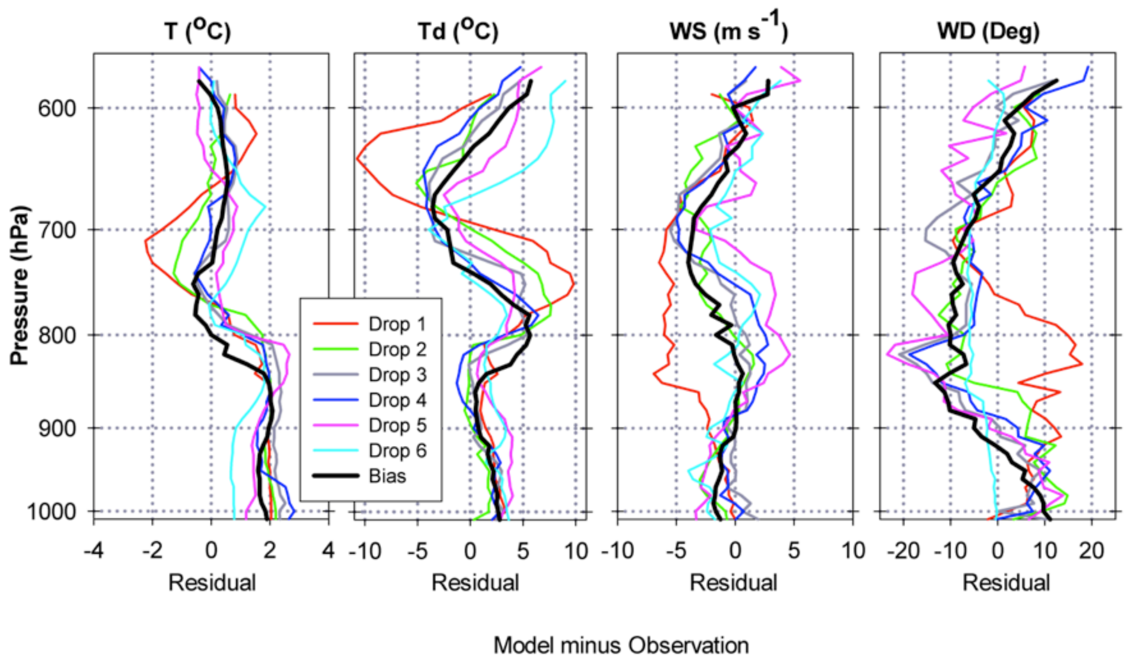

To evaluate the behaviour of the atmospheric flow impinging on the topography of the Meta Incognita Peninsula, the Froude (*Fr*) number was calculated using the model soundings and the dropsondes following a similar procedure to *Medina & Houze* [2005]. The *Fr* for both the model and observations were high (> 1), which confirms a strong upslope component existed for both. However, the *Fr* in the model was smaller (2.4), compared to observations (3.1). Differences can be attributed to weaker flow strength at low-altitudes in the model and slightly greater instability in the observations. Consequently, modeled upslope precipitation processes were not as strong as observations.

4.3.4.2 Validation of precipitation at Iqaluit

GEM-LAM 2.5 output shows that in the model environment, precipitation fell between 2100 UTC November 9 and 0400 UTC November 10, indicating a 3-hour delayed onset and an event duration four hours longer than observations (Figure 4.3). Total accumulation in the model was 50% lower, 1.1 mm liquid water equivalent, at the Iqaluit site (Figure 4.3).

The inaccurate timing of precipitation in the model can be attributed to its representation of the trough. Figure 4.16 shows a time series of hourly velocity profiles with height over Iqaluit. The trough's passage in the model can be identified by the depression in the wind speed with height between 2100 and 2300 UTC, with the coincident directional shift and reduction in speed near the surface. Thereafter, wind speeds steadily increased, suggesting the trough transitioned away from the region at this time. As seen in the observations, the onset of precipitation coincides with the presence of the trough in the model. However, the timing was approximately 3-hours later.

A lack of snow in the model can be attributed in part to its representation of the upstream environment. Errors in temperature and moisture were shown to limit convection and influenced the models temperature dew-point spread. As a result, cloud bases were too high and dry layers were present in some profiles. The combination of these factors reduced the potential for hydrometeor growth and consequently the amount of precipitation that reached Iqaluit. Wind speed errors were also a factor. At altitudes lower than 900 hPa, the model winds were too weak (by 1 to 4 m s^{-1}), which reduced upslope processes (lower *Fr* number). It is also possible, that due to a general positive wind speed bias at altitudes above 900 hPa (up to 5 m s^{-1}), smaller hydrometeors would have been advected further downstream, reducing accumulation at the Iqaluit site.

Figure 4.16: GEM-LAM 2.5 time height cross section of winds above Iqaluit, NU. Wind barbs and color shading in knots.

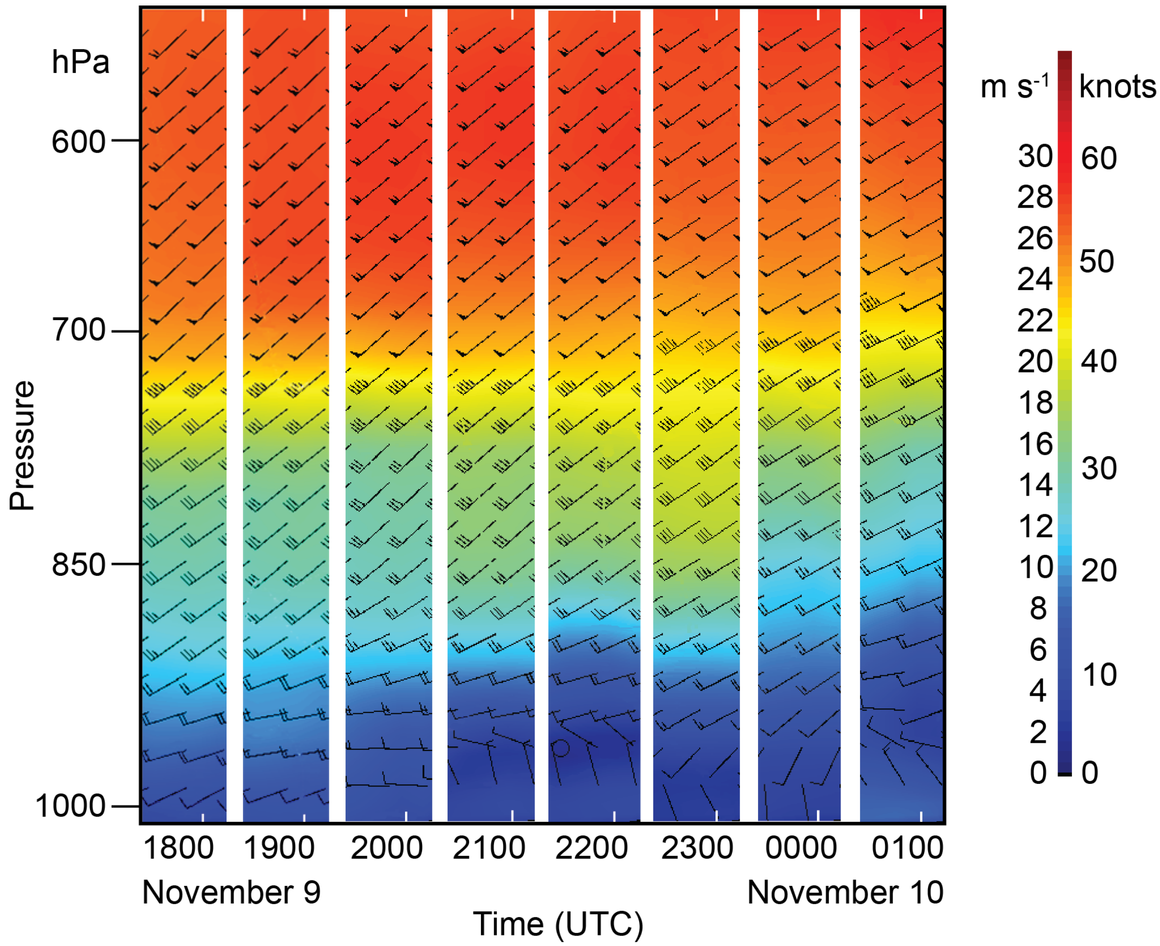

4.4 Discussion

4.4.1 Conditions that led to the snowfall event

Several factors were shown to produce this event. Working in concert, instability over Hudson Strait, upslope lifting of air over the orography of Meta Incognita Peninsula and the passing of a small trough, led to an unexpected small accumulation event at Iqaluit and surrounding area.

The arrangement of cold atmospheric temperatures, over a relatively warmer ocean (near 0°C), generated low-level convective instability (SCAPE from 110 to 170 J kg^{-1}), where energy was actively being released in the atmosphere (Figure 4.14). The W-band radar showed that near the terrain, convection produced a cloud layer between 1000 and 2000 m, but no precipitation (Figure 4.12a). Strong upslope flow (8 to 15 m s^{-1}) of the unstable air promoted cloud and precipitation production over the terrain. Maximum reflectivity was enhanced by 10 dBZ, and small-scale convective features at cloud-top were present (Figure 4.12c). The passing of the trough was shown to provide additional convergence aloft, that when combined with orographic forcing, resulted in an environment conducive to thicker cloud (up to 900 m higher) and enhanced hydrometeor growth, evidenced by reflectivities and fall velocities (from 0.5 to 1.5 m s^{-1}) that increased towards the surface on the entire windward slope of the Meta Incognita Peninsula (Figure 4.12a). The trough enhanced cloud and precipitation production to greater altitudes aloft, and brought snowfall over the terrain into the Iqaluit region.

At Iqaluit, the passing of the trough was also shown to redistribute moisture near the surface, and influence precipitation (Figure 4.6). In this environment, the average hydrometeor increased in mass as they fell, evidenced by an increase in reflectivity and fall speeds (from 0.5 to 1 m s^{-1}) towards the ground (Figure 4.10), where accretion and aggregation were found to be active growth mechanisms (Figure 4.5). Precipitating hydrometeors sized between 1000 and 1250 μm were most common during the event, but hydrometeors up to 7500 μm were present. Loss from sublimation was minimal while precipitation was falling in Iqaluit, confirmed by the presence of both small and large hydrometeors at the surface (Figure 4.4 and Figure 4.5).

After the trough moved away from the area, there was still some orographic precipitation enhancement on the windward slope of the Meta Incognita Peninsula, evidenced by high reflectivities near the surface (maximum 15 dBZ) and vertical cloud development (~200 m higher) within 40 km of the coast. However, with increasing distance from the coast, it became more common for higher reflectivities aloft, decreasing towards the surface (Figure 4.12b). Under these conditions, hydrometeors were likely smaller and more susceptible to sublimation before reaching the ground, due to their low density and fall velocities. In addition, downslope flow behind the trough contributed to the development of dry layers aloft at Iqaluit (Figure 4.5). Consequently, any hydrometeors that were advected towards the community, as a result of orographic processes, would likely be subjected to further mass loss.

At Iqaluit, downslope flow behind the trough contributed to the development of dry layers aloft (Figure 4.5). Consequently, any hydrometeors that were advected towards the community, as a result of orographic processes upstream, were subjected to further mass loss. Near the end of the event, sublimation was confirmed over Iqaluit, evidenced by the decrease in the number of small hydrometeors and a coincident decrease in temperature below cloud-base (Figure 4.4 and Figure 4.6).

These results show that low-level convection and upslope processes were important in cloud and precipitation production over the orography upstream, but were not able to force cloud development and precipitation generation to the altitudes required for precipitation to get over the terrain to Iqaluit. When combined with additional lift from the trough, cloud and precipitation production were enhanced over the orography, allowing these features to penetrate over the terrain, and resulted in precipitation at Iqaluit.

4.4.2 Validation of GEM-LAM 2.5

The STAR data set provided a rare opportunity for a model comparison in a region where field data are scarce. The GEM-LAM 2.5 output was examined to offer some insight into why precipitation onset at Iqaluit was delayed and total accumulation was 50% lower than observations (Figure 4.3). From this limited work, model errors where shown to have implications for cloud and precipitation production and their forecast.

The model was skilful in its ability to pick up the passage of the trough over Iqaluit, but 3-hours later than observations (Figure 4.3 and Figure 4.16). This delayed the onset of precipitation in the model environment. Similar to observations, its presence coincided with the beginning of the snowfall at Iqaluit.

Appreciable errors were noted for temperature and moisture near the surface in the upstream environment (Figure 4.13, Figure 4.14, Figure 4.15). At lower altitudes, the model environment was consistently too warm (commonly 2 °C) and moist (*Td* between 0.5 and 3 °C higher than observations), which indicates reduced exchange between ocean and atmosphere, limiting convection. Further errors were shown in the dew-point depression profiles. As a result, cloud-bases were too high (100 to 500 m) and dry layers were present, reducing the potential for hydrometeor growth before air was lifted over the terrain (Figure 4.14). Wind speeds were underestimated by 4 m s^{-1} at times, weakening upslope processes, confirmed by a lower *Fr* number (Figure 4.15). Combined, these errors contributed to less precipitation production in the model.

The accuracy of the forecast for precipitation (occurrence and amount) is highly dependent on the microphysical scheme. The nature of snowfall for this event was variable. At the surface, different habits and size spectra were observed, along with varying degrees of rime, aggregation and the presence of particle fragments. Sublimational processes also altered hydrometeor shape and mass at times. Results suggest that the use of the Kong-Yau scheme's spherical representation of snow, with prescribed fall velocities for particles of different sizes in a hydrometeor category, cannot be assumed in this case. Microphysical schemes and conversion processes need to be adjusted or further generalized for the cold season processes.

The limited number of comparisons between model and observations in this study mean generalizations are not possible; however, we recommend that model developers investigate errors pertaining to low-level convection in the Arctic and upslope flow, which have been shown to contribute to the generation of small-accumulation events in the region. Without extensive model sensitivity tests, we are unable to determine whether the warm, moist bias and weakened dynamic forcing originated within the model, or whether other errors were responsible. It is possible that they could have propagated northward from the mid-latitudes through the regional model, or from the initial starting conditions. The objective of this study was not to identify the origin of simulation errors in this environment, but there is a certainly a need for this work in the future.

4.5 Concluding remarks

This study characterizes an unexpected snowfall event at Iqaluit, Nunavut and surrounding area. Both aircraft and ground-based radar were used, providing a number of key observations of this small accumulation event. Results show that the combined influence of low-level convection, upslope processes and the passage of a weak trough led to this event. This was one case study, so generalizations are not possible, however, results from the GEM-LAM 2.5 comparison suggest that upstream convection and upslope processes were affected by model errors, and could account for variability in precipitation between model and observations in some cases.

Based on factors found to influence this event, such as convection over open ocean, anticipated consequences of climate changes such as, delayed onset of sea ice in the autumn and increased atmospheric temperature, create an environment where these types of events may increase in frequency, but this must be confirmed and quantified. To address this issue and those linked with weather forecasting, high-resolution model studies are needed.

Future research can expand on the analysis here, but high-resolution data of similar nature are required. Given the scarcity of surface-based precipitation monitoring instrumentation in high latitude regions, reliance on satellite precipitation retrievals may increase. However, low reflectivity values identified in this study and others [*Henson et al.,* 2011; *Fargey et al.,* 2014] have shown that much of the precipitation over southern

Baffin Island will remain undetected by new satellite-precipitation systems such as Global Precipitation Measurement (GPM) satellite, based on its minimum detection threshold [12 dBZ; *Hou et al.,* 2013]. Satellite precipitation retrievals may have limitations in high latitude regions, particularly for hydrological cycle assessments.

In summary, high-resolution data collected during STAR provided the basis for analysis of the conditions that led to a snowfall event in the eastern Canadian Arctic and provided some insight as to why it was not well forecast by the Canadian operational model. Future research can expand on the analysis presented here with respect to GEM-LAM 2.5 model validation in the Arctic, but nonetheless this study has provided some initial results on its ability to characterize and predict a small accumulation event in the region. The complexity of these events represents a significant challenge for predicting and modeling and to understanding their role in the hydrological cycle and on the regions climate.

4.6 References

Arctic Monitoring and Assessment Programme (AMAP). (2011). Snow, Water, Ice and Permafrost in the Arctic (SWIPA): Climate Change and the Cryosphere. Oslo, Norway. 538 pages.

Asuma, Y., Inoune, Y., Kikuchi, Y.K., Kajiokawa, M., Sata, N., and, Hayaska, T. (2000). Wintertime precipitation behavior in the western Canadian Arctic region. *Journal of Geophysical Research, 105, D11,* doi:10.1029/1999JD901124.

Belair, S., Mailhot, J., Girard, J., and Vaillancourt, P. (2005). Boundary layer and shallow cumulus clouds in a medium-range forecast of a largescale weather system. *Monthly Weather Review, 133,* 1938–1960. doi:10.1175/MWR2958.1.

Cavalieri, D., Parkinson, C., Gloersen, P., and Zwally, H.J. (1996). Sea ice concentrations from Nimbus-7 SMMR and DMSP SSM/I passive microwave data, 1980-2005. Updated 2008. Boulder, Colorado USA: National Snow and Ice Data Center. Digital media.

Curry, J.A., Rossow, W.B., Randall, D.A., and Schramm, J.L. (1996). Overview of Arctic cloud and radiation characteristics. *Journal of Climate, 9,* 1731–1764.

Deacu, D., Zandra. A., and Hanesiak, J. (2010). Simulating wind channelling over Frobisher Bay and its interaction with downslope winds during the 7-8 November 2006 Wind Event. *Atmosphere-Ocean. 48*, 101-121. doi:10.3137/AO1109.2010.

Environment Canada (2013). Hourly surface observations at Iqaluit, Nunavut. National climate data and information archive. Retrieved from: http://climate.weather.gc.ca/climateData/hourlydata_e.html?timeframe=1&Prov=NU&StationID=1758&hlyRange=1953-01-01%7C2013-11-10&Year=2007&Month=11&Day=9. Last accessed: November 2013.

Erfani, A., Mailhot, J., Methot, A., Gravel, S., Desgagne, M., Plante, A., Sills, D., King, P., and Ashton, A. (2006). The 2.5 km horizontal resolution limited area version of the Global Environmental Multiscale model over southern Ontario and Quebec. *In: Abstracts of 15th International Great Lakes Operational Meteorology Workshop, 25–27 October 2006*, Niagara Falls, Ontario, Canada.

Fargey, S., Hanesiak, J., Liu, G., Gilligan, J., and Stewart, R. (editors) (2008). Storm Studies in the Arctic (STAR) Data Report. Centre for Earth Observation Science, 440 Wallace Building, University of Manitoba, Winnipeg, Manitoba, Canada, 75 pages.

Fargey, S., Hanesiak, J., Stewart, R., and Wolde, M. (2014). Aircraft observations of orographic cloud and precipitation features over southern Baffin Island, Nunavut, Canada. *Atmosphere-Ocean*. *52,* 54-76. doi:10.1080/07055900.2013.855624.

Finnis, J., Holland, M.M., Serreze, M.C., and Cassano, J.J. (2007). Response of Northern Hemisphere extratropical cyclone activity and associated precipitation to climate change, as represented by the Community Climate System Model. *Journal of Geophysical Research - Biogeosciences*. *112*, 2005–2012. doi:10.1029/2006JG000286.

Garand, L. and Mailhot, J. (1990). The influence of infrared radiation on numerical weather forecasts. *In: Proceedings of the seventh Conference on Atmospheric Radiation, 23–27 July 1990*, San Francisco, USA.

Gascon, G., Stewart, R.E., and Henson, W. (2010). Major cold-season precipitation events at Iqaluit, Nunavut. *Arctic.* 63, 327–337.

Hanesiak, J., Stewart, R.E., Szeto, K., Hudak, D., and Leighton, H. (1997). The structure, water budget, and radiational features of a high-latitude warm front. *Journal of Atmospheric Sciences, 12*, 1553–1573.

Hanesiak, J., Stewart, R.E., Taylor, P., Moore, K., Barber, D., McBean, G., Strapp, J.W. Wolde, M., Goodson, R., Hudson, E., Hudak, D., Scott, J., Liu, G., Gilligan, J., Biswas, S., Desjardins, D., Dyck, R., Fargey, S., Field, R., Gascon, G., Gordon, M., Greene, H., Hay, C., Henson, W., Hochheim, K., Laplante, A., Martin, R., Melzer, M.A., and Zhang, S. (2010). Storm Studies in the Arctic: The meteorological field project. *Bulletin of the American Meteorological Society, 91,* 47-68. doi:10.1175/2009BAMS2693.1

Henson, W., Stewart, R., and Hudak, D. (2011). Vertical reflectivity profiles of precipitation over Iqaluit, Nunavut during Autumn 2007. *Atmospheric Research*, *99*, 217-229. doi: 10.1016/j.atmosres.2010.10.009.

Higgins, M.E. and Cassano, J.J. (2009). Impacts of reduced sea-ice on winter Artic atmospheric circulation, precipitation and temperature. *Journal of Geophysical Research,* 114, D16107, doi:10.1029/2009JD011884.

Hitchfeld, W. and Bordan, J. (1954). Errors inherent in the radar measurement of rainfall at attenuating wavelengths. *Journal of Meteorology, 11*, 56-67.

Hock, T. and Franklin, J.L. (1999). The NCAR GPS dropwindsonde. *Bulletin of the American Meteorological Society, 80,* 407-420.

Hou, A.Y., Kakar, R.K., Neeck, S., Azibarizin, A.A., Kummerow, C.D., Kojima, M., Oki, R., Nakamura, K., and Iguchi, T. (2013). The Global Precipitation Measurement (GPM) mission. *Bulletin of the American Meteorological Society,* Advance online publication. doi: 10.1175/BAMS-D-13-00164.1

Howell, S. Tivy, A., Yackel. J., and McCourt, S. (2008). Multi-year sea-ice conditions in the western Canadian Arctic Archipelago region of the northwest passage: 1968:2006. *Atmosphere-Ocean, 46,* 229-242.

Hudak, D., Currie, D., Stewart, R. Rodriguez, P., Burford, J., Bussieres, N., and Kochtubajda, B. (2004). Weather systems occurring over Fort Simpson, Northwest Territories, Canada, during three seasons of 1998-1999: 1. Cloud features. *Journal of Geophysical Research, 109,* D22108. doi:10.1029/2004JD004876.

Hudson, E., Aihoshi, D., Gaines, T., Simard, G., and Mulluck, J. (2001). The weather of Nunavut and the Arctic. Nav. Canada. 230 pages.

Imai, J. (1960). Raindrop size distributions and the Z-R relationship. *In Proc. Eighth Weather Radar Conference Boston, MA, American Meteorological Society*, pp 321-326.

Intihar, M.R. and Stewart, R.E. (2005). Extratropical cyclones and precipitation within the Canadian archipelago during the cold season. *Arctic*. 58, 162-174.

Kattsov, V.M. Ryabinin, V.E., Overland, J.E., Serreze, M.C., Visbeck, M., Walsh, J.E., Meier, W., and Zhang, X. (2011). Arctic sea-ice change: a grand challenge of climate science. *Journal of Glaciology, 56,* 1115-1121. doi: 10.3189/002214311796406176.

Kong, F., and Yau, M.K. (1997). An explicit approach to microphysics in MC2. *Atmosphere-Ocean, 35,* 257–291.

Lambert, S.J. and Fyfe, J.C. (2006). Changes in winter cyclone frequencies and strengths simulated in enhanced greenhouse warming experiments: results from the models participating in the IPCC diagnostic exercise*.* *Climate Dynamics*, *26,* 713-728. doi: 10.1007/s00382-006-0110-3.

Laplante, A., Stewart, R., and Henson, W. (2012). Characterization of cloud and precipitation features over southern Baffin Island and adjacent areas during STAR. *Atmosphere-Ocean*, *50*, 54-69. doi:10.1080/07055900.2011.646535.

Liu, A. Q., Moore, G.W.K., Tsuboki, K., and Renfrew, I. (2006). The effect of the sea-ice zone on the development of boundary-layer roll clouds during cold air outbreaks. *Boundary-Layer Meteorology, 118*, 557–581. doi: 10.1007/s10546-005-6434-4.

Liu, C. and Illingworth, A.J. (2000). Toward more accurate retrievals of ice water content from radar measurements of clouds. *Journal of Applied Meteorology, 39,* 1130–1146.

Mailhot, J., Milbrandt, J.A., Ciguere, A., McTaggart-Cowan, R., Erfani, A., Denis, B., Glazer, A., and Vallee, M. (2012). An experimental high-resolution forecast system during the Vancouver 2010 Winter Olympic and Paraolympic Games. *Pure and Applied Geophysics*. doi10.1007/s00024-012-0520-6.

Mailhot, J., Bélair, S., Lefaivre, L., Bilodeau, B., Desgagné, M., Girard, C., Glazer, A., Leduc, A-M., Methot, A-M., Patoine, A., Plante, A., Rahil, A., Talbot, D., Tremblay, A., Vaillancourt, P., Zadra, A., and Qaddouri, A. (2006). The 15-km version of the Canadian regional forecast system. *Atmosphere-Ocean*, 44, 133-149. doi: 10.3137/ao.440202.

Medina, S. and Houze, R.A. (2003). Air motions and precipitation growth in Alpine Storms. *Quarterly Journal of the Royal Meteorological Society, 129*, 345-371.

McCabe, G.J., Clark, M.P., and Serreze, M.C. (2001). Trends in Northern Hemisphere surface cyclone frequency and intensity. *Journal of Climate, 14,* 2763-2768.

Nawri, N., and Stewart, R.E. (2006). Climatological features of orographic low-level jets over Frobisher Bay. *Atmosphere-Ocean*, 44, 397-413

Nawri, N., and Stewart, R. E. (2008). Channelling of high-latitude boundary-layer flow. *Nonlinear Processes in Geophysics, 15*, 33-52.

Renfrew, L.A., and Moore, G.W.K. (1999). An example cold-air outbreak over the Labrador Sea: roll vortices and air-sea interaction. *Monthly Weather Review, 127,* 2379-2394.

Roberts, E., Nawri. N., and Stewart, R.E. (2008). On the storms passing over southern Baffin Island during Autumn 2005. *Arctic,* 61, 309-321.

Serreze, M.C. and Hurst, C.M. (2000). Representation of mean Arctic precipitation from NCEP-NCAR and ERA Reanalysis. *Journal of Climate, 13,* 182-201.

Serreze, M.C., Barrett, A.P. and Lo, F. (2005). Northern high-latitude precipitation as depicted by atmospheric reanalyses and satellite retrievals. *Monthly Weather Review*, *133*, 3407-3430. doi:10.1175/MWR3047.1.

Sevruk, B., Ondrás, M., and Chvíla, B. (2009). The WMO precipitation measurement intercomparisons. *Atmospheric Research*, 92, 376-380.

Sinclair, M.R. and Watterson, I.G. (1999). Objective assessment of extratropical weather systems in simulated climates. *Journal of Climate. 12,* 3467-3485.

Stewart, R.E., Bachand, D., Dunkley, R.R., Giles, C., Lawson, B., Legal, L., Miller, S.T., Murphy, B.P., Parker, M.N., Paruk, B.J., and Yau, M.K. (1995). On winter storms over Canada. *Atmosphere-Ocean, 33*, 223-248.

Stewart, R.E., Szeto, K.K., Reinking, R.F., Clough, S.A., and Ballard, S.P. (1998). Midlatitude cyclone cloud systems and their features affecting large scales and climate, *Reviews of Geophysics, 36,* 245-273.

Stewart, R.E., Burford, J.E., Hudak, D.R., Currie, B., Kochtubajda, B., Rodriguez, P., and Liu, J. (2004). Weather systems occurring over Fort Simpson, Northwest Territories, Canada, during three seasons of 1998–1999: Part 2. Precipitation features. *Journal of Geophysical Research, 189,* 1984-2012.

Stroeve, J.C., Serreze, M.C, Barrett, A., and Kindig, D.N. (2011). Attribution of recent changes in autumn cyclone associated precipitation in the Arctic. *Tellus A*, 63, 653-663. doi 10.1111/j.1600 0870.2011.00515.x.

Wacker, U., Potty, K.V.J., Lupkes, C., Hartman, J., and Raschdorfer, M. (2005). A case study on a polar cold air outbreak over Fram Strait using a mesoscale weather prediction model. *Boundary-Layer Meteo*rology, 117, 301-336. doi: 10.1007/s10546-005-2189-1.

Yin, J.H. (2005). A consistent poleward shift of the storm tracks in simulations of 21st century climate. *Geophysical Research Letters, 32,* doi:10.1029/2005GL023684.

CHAPTER 5: AN EVALUATION OF VERTICAL PROFILES USING A LIMITED AREA NUMERICAL WEATHER PREDICTION MODEL OVER BAFFIN ISLAND AND SURROUNDING AREA DURING AUTUMN 2007

Shannon Fargey[1], John Hanesiak[1] and Ron Goodson[2]

[1] Centre for Earth Observation Science, Department of Environment and Geography, University of Manitoba, Winnipeg, Manitoba, Canada

[2]Hydrometeorology and Arctic Laboratory, Environment Canada, Edmonton, Alberta, Canada

Prepared for submission to Arctic.

This chapter evaluates the accuracy of the Canadian operational limited area model over Baffin Island and surrounding area, autumn 2007. Descriptions of model errors and proficiencies during four STAR case studies are examined for different synoptic forcing and surface environments, including orography, open water and sea ice. The skill of the model is also discussed in the context of its ability to accurately represent clouds and forecast precipitation.

Abstract

Models provide detailed analyses of short-term weather phenomena and long-term climate issues such as global change. It follows that assessments of model accuracy are of importance. In this study the Global Environmental Multi-Scale model at 2.5 km grid resolution (GEM-LAM 2.5), was evaluated using vertical profiles from dropsondes collected in proximity to southern Baffin Island, Nunavut during the 2007 Storm Studies in the Arctic (STAR) field project. Descriptions of model errors and proficiencies for different synoptic conditions and surface environments, including orography, open water and sea ice are combined with a general assessment of model performance. Overall the model overestimated temperature (~1 to 2°C), with the exception of profiles over sea ice where difficulties representing temperature inversions resulted in both positive and negative bias in the vertical profile. The model generally over-predicted moisture (~0.1 to 0.3 g kg^{-1}), but this was not consistent. Over open water, standard errors for moisture were much larger for cyclonically driven events compared to weakly forced events, and in a high sea ice cover environment the model showed a greater tendency to underestimate moisture content (-0.2 g kg^{-1}). Wind speed was usually underestimated, resulting in model predictions of weaker upslope processes compared to observations. Errors in wind direction were large (> 90°) at times, but in most cases were ≤ 20°. In cases where multiple cloud layers were present, GEM-LAM 2.5 was usually able to capture this feature but the dry layer depth was inaccurate. In addition cloud-tops were usually overestimated (200 to 300 m) and cloud-bases were too low (-50 to -500 m). Large errors commonly occurred above or in proximity to an ice-covered surface and it is important to learn if these errors are a common in the model.

5.1 Introduction

During this century a large warming trend is expected to occur in the Arctic during the cold season (autumn and winter) due to loss of summer sea ice, enhanced absorption of solar radiation into the upper-ocean, and subsequent autumnal release of heat to the atmosphere [*AMAP*, 2011]. The Arctic is also projected to see pronounced seasonal changes in precipitation, with the largest relative increases also during the cold season [*Kirtman et al.*, 2013]. For meaningful and practical model simulations, leading to detailed analyses of changing weather and climate phenomena, model accuracy assessments are essential.

Global climate models (GCMs) enable simulations of the response of the global climate system. However, the relatively coarse resolution of GCMs prevents accurate simulations of temperature, precipitation and dynamic processes in complex topographical areas such as along boundaries between sea ice and open water [*Simjanovski, Girard, & Du,* 2011]. Consequently, large surface air temperature biases have been shown to occur [*Chapman & Walsh*, 2007], along with inadequate representations of precipitation and cloud cover [*Curry, Rossow, Randall, & Scharamm,* 1996; *Meehl, Boer, Covey, Latif, & Stouffer,* 2000] in model simulations. The *IPCC* [2013] also identified that the smoothed representation of topography in GCMs results in large uncertainties in modelled snowfall and cloud cover in regions where orographic lifting occurs.

Regional climate models (RCMs) use higher-resolution grids to provide better reproductions of atmospheric characteristics and processes compared to GCMs [*Cassano, Box, Bromwich, Li, & Steffen,* 2001; *Morrison, Shupe, & Curry,* 2003; *Tjernstrom et al.*

2004; *Wyser et al.,* 2008]. Recently, the performance of an ensemble of RCMs was investigated in the western Arctic over one year over a domain that encompassed the Surface Heat Budget of the Arctic Ocean (SHEBA; *Uttal et al.,* 2002) experiment. For most models, mean temperature bias was usually < 1°C, with root-mean-square error around 3°C. In addition, the model environments were usually too dry, mean bias ~ -0.2 g kg^{-1}. Wind speed errors were shown to be variable depending on the model used. Bias could be too high (1.5 m s^{-1}) or too low (1 m s^{-1}), and showed a systematic increase for higher wind speeds (> 10 m s^{-1}) [*Tjernstrom et al*., 2004]. Other research has shown that large errors in the simulation of clouds, their properties and distribution continue to be a problem in RCMs [*Zhang, Gong, Leaitch, & Strapp*, 2007; *Wyser et al.,* 2008].

Numerical weather prediction (NWP) models have been notably improved in recent years though challenges in predicting clouds, precipitation, and circulation dynamics remain. The lack of input data for the Arctic region, compared to lower latitudes, has been shown to hamper the initialization of NWP models [*Curry et al*., 1996; *Uttal et al.,* 2002]. In addition, the sparse network of observations is inadequate for verification over all areas of the Arctic, particularly regions with complex terrain [*Serreze, Barrett, & Lo,* 2005]. A further concern is the lack of model parameterizations developed specifically for high latitudes. Current parameterizations of clouds, precipitation, boundary layer and thermodynamic processes have been developed for lower latitude environments and may not adequately represent Arctic conditions [*Curry et al*., 1996; *Wyser et al*., 2005; *Lachlan-Cope*, 2010].

The Canadian Global Environmental Multi-Scale limited area model (GEM-LAM 2.5), which operates at a 2.5 km grid cell resolution, has demonstrated improved representations of local conditions (orography and surface type), physical processes (cloud microphysical parameterizations, radiation, and others), and dynamical organization of weather systems at both the synoptic and local scales [*Erfani et al.* 2006; *Yang et al.,* 2010; *Mailhot et al.*, 2012]. However, our current understanding of its accuracy has largely come from research focused on mid-latitude regions [*Yang et al.,* 2010; *Taylor et al.,* 2011; *Isaac et al.,* 2012; *Mailhot et al.,* 2012]. Although, recent evaluations of GEM-LAM 2.5 performance have included the Arctic [*Deacu, Zadra, & Hanesiak,* 2010; *Paquin-Ricard, Jones, & Vaillancourt*, 2010; *Simjanovski et al.,* 2011; *Hanesiak, Brimelow, Zadra, Goodson, & Liu,* 2013; *Fargey, Henson, Hanesiak, & Goodson,* 2014a], a comprehensive assessment of model performance is lacking.

For a region west of the Canadian Arctic Archipelago, the model overestimated air temperature between the surface and 900 hPa, leading to a coincident positive bias in specific humidity during winter. However, between 900 and 600 hPa the model environment remained too warm, but moisture was underestimated (too dry) showing that the characterization of moisture can be variable [*Paquin-Ricard, et al.*, 2010; *Simjanovski et al.,* 2011]. Precipitation was underestimated early in the cold season (September to November) and overestimated in spring and summer, with the former linked to a dry bias in the model [*Simjanovski et al.,* 2011] and the latter mainly confined to light precipitation events [*Paquin-Ricard, et al.*, 2010; *Simjanovski et al.,* 2011]. Generally, results point to better model representation of high-accumulation events in the Arctic.

Examination of the skill of the GEM-LAM 2.5 to simulate strong wind events at Iqaluit, Nunavut has shown that large-scale and mesoscale flows are adequately described, but complex terrain results in poor performance at the local scale [*Deacu et* *al*., 2010; *Hanesiak et al.*, 2013]. The timing of these events was well predicted by the model (to within ~3-hours), though there was a tendency to underestimate the peak wind speed [*Hanesiak et al.,* 2013]. *Goodson* [2008] also showed that GEM-LAM 2.5 was able to represent the complex surface flows around the community of Pangnirtung on Baffin Island for a strong wind event. In that study, the ability of GEM-LAM 2.5 to resolve the width of the fjord and the height of the regional orography improved the accuracy of low-level winds (below 600 m) and the general character of the air temperature and humidity during the event.

Analysis of a small accumulation event over Iqaluit, Nunavut and surrounding area showed that GEM-LAM 2.5 errors had implications for cloud and precipitation production and their forecast [*Fargey et a*l., 2014b]. The model represented the multiple factors shown to produce the event but contained errors. This resulted in the delayed onset of snow and total accumulation in the model 50% lower than observed. Model errors included: a warm (~ 2 °C) and moist (dew-point temperature between 0.5 and 3 °C higher than observations) bias upstream, limiting low-level convection; dew-point depression profiles which resulted in cloud-bases that were too high (100 to 500 m) and the presence of dry layers not in the observations, reducing the potential for hydrometeor growth before air was lifted over the terrain; and an underestimation of wind speeds by ~4 m s^{-1}, resulting in weakened upslope processes. When combined, the errors were shown to contribute to less precipitation production than observed.

During the autumn of 2007 the Storm Studies in the Arctic (STAR) field project was conducted to better understand the physical features of Arctic storms, their hazards, and the processes controlling them to facilitate improved predictions [*Hanesiak et al.*

2010]. STAR focused on weather phenomena around southern Baffin Island in Nunavut, a region that contains some of the most significant topography and highest precipitation in the Canadian Arctic. In this study, data from STAR are used to investigate the skill of the GEM-LAM 2.5 model. Emphasis is placed on four specific cases derived from several vertical profiles from dropsondes (n = 28) released from a research aircraft. These data comprise variable synoptic conditions and different surface types, including terrain, open water and sea ice.

In section 5.2 the study area and case studies are described, along with a description of the methodology. Section 5.3 presents the GEM-LAM 2.5 comparison, followed by section 5.4, which synthesizes and discusses key aspects of the findings. Concluding remarks are made in section 5.5.

5.2 Data and Methodology

5.2.1 Study area and case studies

The topography surrounding southern Baffin Island, Nunavut is complex (Figure 5.1). Three quasi-parallel mountain ranges on individual peninsulas, with northwest-southeast orientation, create multiple lifting regions for advancing flow combined with variable surfaces that influence moisture. The western-most peninsula is Meta Incognita, which has the smallest and most gradually inclined topography, between 600 and 700 m above mean sea level (ASL). The Hall Peninsula reaches a maximum elevation near 1000 m, with a steeply sloped transition from ocean to land on its eastern margin. The highest topography, near 2000 m, is found on the Cumberland Peninsula. Peninsula width varies, with the narrowest being the Meta Incognita (approximately 125 km), followed by the Hall and Cumberland Peninsulas (each approximately 200 km).

Of the 14 Intensive Observation Periods (IOPs) during STAR, only four correspond to events (case studies) where GEM-LAM 2.5 data are available for comparison. Case studies are identified by the corresponding aircraft flight number and calendar date in 2007: *F3* – November 8, *F4* - November 9, *F5* - November 12, *F13* – November 28 (Table 5.1). They provide an opportunity to investigate the model performance associated with both major cyclonic systems (*F3* and *F5*), and weak troughs (*F4* and *F13*), all of which resulted in cloud cover and orographic precipitation (Table 5.1). A comprehensive description of the synoptic conditions for *F3*, *F5*, and *F13* can be found in sections 3.3.1.1, 3.3.2.1 and 3.3.3.1, respectively [*Fargey et al.,* 2014]. Synoptic conditions for the *F4* case study can be found in section 4.3.1 [*Fargey et al.*, 2014b]. The six dropsonde profiles used in *Fargey et al.*, [2014b] are included in this study in order to improve the overall statistical analysis and enable as assessment of model performance in that work compared to other cases.

Figure 5.1: Topographic map of southern Baffin Island in Nunavut (1 km Digital Elevation Model resolution). Location of dropsonde data collection - colour filled circles – for the difference STAR case studies. The inset map indicates the location of the study area (red box) within Canada.

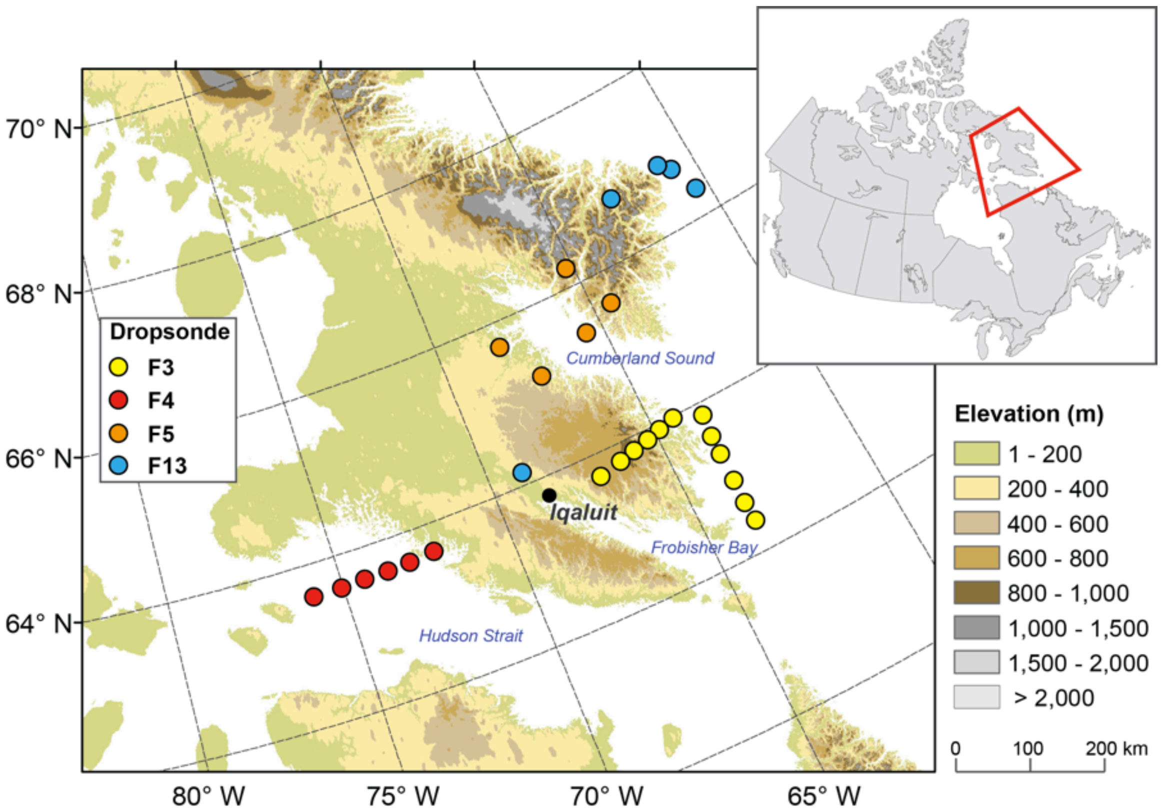

Each case study corresponds to variable surface environments as defined by the general character over which the dropsonde landed (Table 5.1). Dropsondes released over the ocean were categorized as open water (OW), over terrain with open water upstream as land (LD), and over sea ice with concentration greater than or equal to 8/10 (from Canadian Ice Service charts) as ice-covered (ICE). Dropsondes released over land but with an ice concentration of greater than or equal to 8/10 upstream were defined as land with ice upstream (LD-ICE). During the autumn of 2007, sea ice concentration in both

Hudson Strait and Davis Strait were below average, while Frobisher Bay and Baffin Bay experienced normal ice conditions [*Hanesiak et al.,* 2010]. At the time of *F3*, the estimated ice concentration around the Hall Peninsula was less than 3/10, thereby not significantly reducing local moisture sources and/or energy exchange between the atmosphere and ocean. Similarly, during *F4* and *F5*, both Hudson Strait and Cumberland Sound were ice free, except for a small (< 1 km) 10/10 ice-covered area along the coastline. Ice concentration during *F13* was greater than or equal to 8/10. Some open water regions were visually observed below the aircraft, though the predominantly ice covered ocean was generally assumed to impede moisture and heat transport to the atmosphere in this case.

Table 5.1: Description of case studies and characterization of dropsondes.

STAR Case ID	Date 2007	Event Forcing	Surface Environment (number of dropsondes released)			
			Ocean (open water)	Land	Ice (>8/10s)	Land with ice upstream (>8/10s)
F3	Nov. 8	Cyclone	6	6	-	-
F4	Nov. 9	Weak trough	6	-	-	-
F5	Nov. 12	Cyclone	2	3	-	-
F13	Nov. 28	Weak trough	-		3	2

5.2.2 GEM-LAM 2.5 and observations

5.2.2.1 Model configuration

The 2.5 km limited area configuration of the GEM- LAM 2.5 is non-hydrostatic and uses semi-implicit semi-Lagrangian time integration. There are 58 vertical sigma-pressure levels up to 10 hPa. For this analysis, the model was run in experimental operational mode [*Erfani et al*., 2006]. The initial and boundary conditions were extracted for the hourly output of the GEM regional model (15 km resolution), with initial conditions derived from the global forecasting system of the CMC and integrated for 48-hours [*Côté, Gravel, Méthot, Patoine, Roch, & Staniforth*, 1998; *Mailhot et al*. 2006]. The model was run for a minimum of 8-hours for each case and data coincident to aircraft flight times were provided. The GEM-LAM 2.5 Arctic domain at the time of the simulation is shown in Figure 5.2a.

Physical parameterizations include a unified cloudiness-turbulence scheme for the planetary boundary layer [*Belair, Mailhot, Girard, & Vaillancourt,* 2005]; a radiation scheme [*Garand & Mailhot*, 1990]; and a shallow convection scheme [*Belair et al*., 2005]. Cloud microphysical processes and precipitation were parameterized using the Kong-Yau microphysical scheme [*Kong & Yau*, 1997], which represents solid precipitation as spherical particles with a prescribed constant density, with two ice-phases: a hybrid pristine ice-snow and a graupel category. The explicit moisture scheme uses cloud ice as a prognostic resolvable variable assuming that the grid cell is completely filled with hydrometeors. Cloud ice sublimates when the air is sub-saturated with respect to ice and growth by deposition occurs when relative humidity is greater than 100% [*Mailhot*, 1994].

The model surface component set a mosaic approach with four surface types: land, open water, sea ice and glaciers [*Erfani et al*., 2006]. The sea ice fraction in the regional model is updated with weekly Canadian Ice Service data, which is interpolated to model resolution. Despite losing resolution, concentration and coverage in the model were very well matched to the observations based on inspection of the ice charts.

However the generalization to model resolution means small-scale features such as leads are not considered. Ice fraction included in the model on November 28 is shown in Figure 5.2b. This represents the ice extent environment during the *F13* case study.

Figure 5.2: (a) GEM-LAM 2.5 Arctic domain (white box), model elevation shaded; (b) Sea ice fraction included in the model on November 28, 2007 run, ice extent observations updated November 26, 2007. Land masked in white.

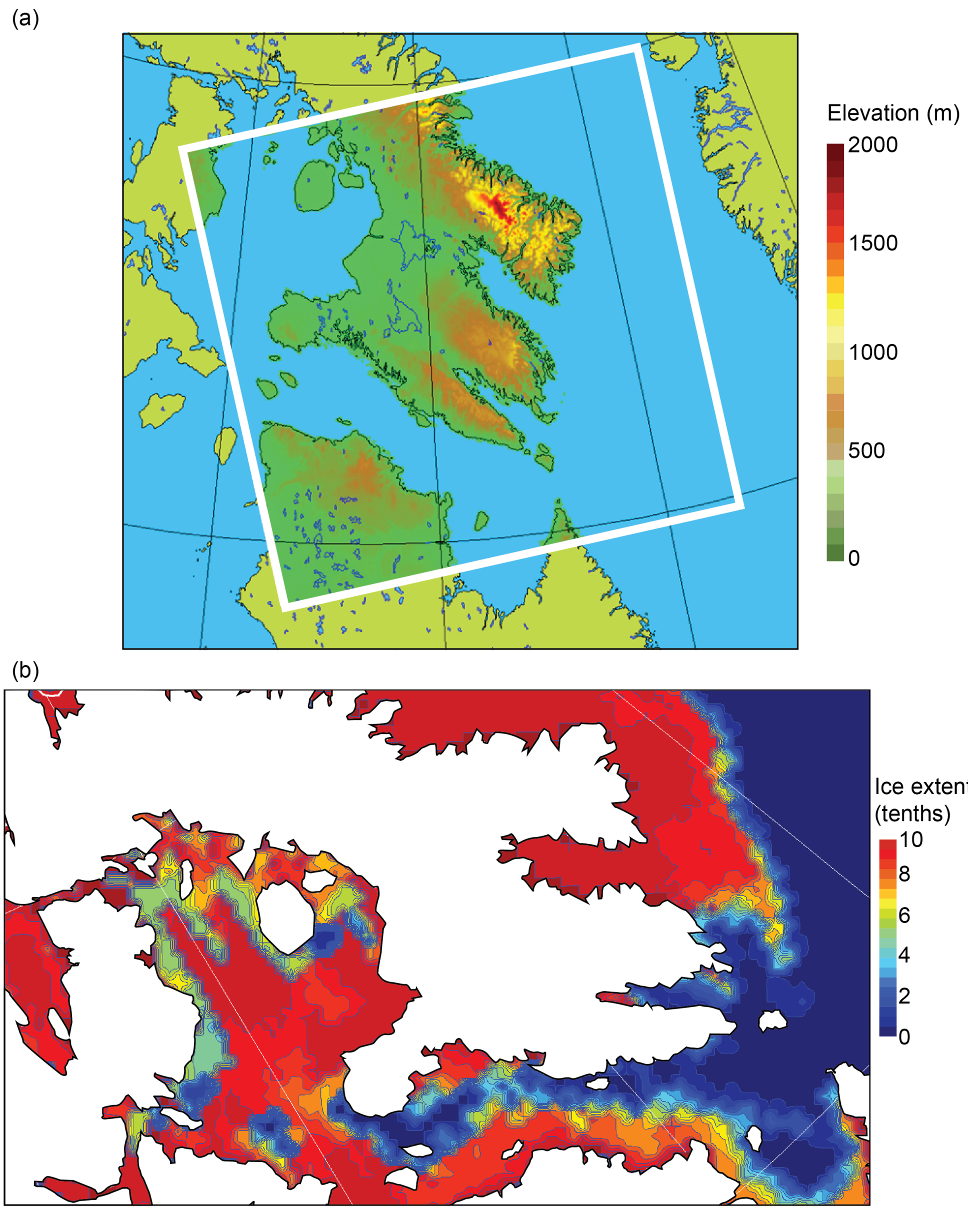

5.2.2.2 Dropsonde and radar data

The Convair-580 research aircraft, instrumented by Environment Canada and the National Research Council of Canada, was equipped with an Airborne Vertical

Atmospheric Profiling System (AVAPS; GPS dropsonde system). The AVAPS provided remote temperature, humidity, and wind profiles below the aircraft. The dropsonde units were the modified RD-93 type, providing thermodynamic and wind data at 0.5 s intervals (vertical resolutions of approximately 5 m), with accuracies of: 1.0 hPa for pressure, 0.2°C for temperature, < 0.5 m s^{-1} for wind components and < 5% for relative humidity [*Hock & Franklin*, 1999]. The aircraft also used an onboard 95 GHz (3.2 mm wavelength) cloud profiling radar system (W-band), with 0.7 beam width and 30 to 60 m vertical resolution, providing continuous reflectivity cross sections above and below the aircraft from upward- and downward-pointing fixed antennae [*Hanesiak et al.,* 2010].

Given the dropsonde information, it is possible to estimate the presence of clouds. This was carried out based on an algorithm in Air Weather Service [1979], which bases the presence of clouds on dew-point spread at a given air temperature. Cloud-base height was estimated at the cloud condensation level, while cloud-top was estimated at the equilibrium level. In an instance where multiple cloud layers were present, cloud-top refers to maximum height of the highest layer and cloud-base refers to the base height of the lowest layer.

5.2.3 Validation of GEM-LAM 2.5 profiles

Model output was extracted coincident to dropsonde locations in the vertical profile, using a linear interpolation of the data with consideration for dropsonde drift. Model performance was evaluated using standard error (s_e), calculated throughout the entire vertical profile, and bias statistics for temperature (T), dew-point temperature (Td), specific humidity (q), wind speed (WS) and wind direction (WD) following a similar procedure to *Mailhot et al.* [2012]. Bias is defined as:

$$Bias = \frac{1}{N}\sum_{i=1}^{N} \hat{y}_i - y_i \quad (5.1)$$

and standard error (s_e) is defined as:

$$s_e = \sqrt{\frac{\sum_{i=1}^{n}(\hat{y}_i - y_i)^2}{n-2}} \quad (5.2)$$

where $\hat{y}_i$ is the model-predicted value and y_i is the observed value for each i of n observations. Individual dropsonde residuals (e_i):

$$e_i = \hat{y}_i - y_i \quad (5.3)$$

were used to assess model performance.

The Spearman's rank ρ correlation coefficient was used to investigate the relationship with model error and distance from the land and distance inland (section 5.3.2). Spearman's ρ correlation coefficient (r_s) is defined as,

$$r_s = 1 - \frac{6\sum_{i=1}^{n} d_i^2}{n^3 - n} \quad (5.4)$$

where d_i, is the squared difference between the ranks for observations i, and n is the sample size [*Rogerson*, 2006]. This non-parametric statistic was used because the assumption of normality was not satisfied, in addition to the small sample size of data used in this study.

5.3 Results

5.3.1 Standard error of meteorological variables

Se values, calculated throughout the entire vertical profile, revealed differences based on surface type and synoptic forcing (Table 5.2). The *Se* of temperature over OW and LD were low (1.3˚C and 1.5˚C respectively). The *Se* of temperature over ICE was the largest of all surface types (3.1˚C). The *Se* of dew-point temperature was consistently high for all cases (~4.0 to 5.0˚C). The largest *Se* of specific humidity was seen over OW and LD (0.30 and 0.31 g kg^{-1} respectively) while the lowest was over ICE (0.18 g kg^{-1}). Proportionally, these errors are quite large considering observations rarely exceeded 2.0 g kg^{-1}.

Table 5.2: Average standard error for different surface environments and event forcing. Standard deviation of error presented in parentheses.

	N	*T (°C)*	*Td (°C)*	*q (g kg^{-1})*	*WS (m s^{-1})*	*WD (°)*
Different Surface Environments						
Open water	*14*	1.3 (± 0.3)	4.1 (± 1.4)	0.31 (± 0.18)	1.7 (± 1.9)	13.5 (± 6.8)
Land	*9*	1.5 (± 1.5)	4.2 (± 1.3)	0.30 (± 0.06)	3.0 (± 1.4)	19.8 (± 8.3)
Ice	*3*	3.1 (± 0.8)	4.2 (± 1.4)	0.18 (± 0.11)	10.4 (± 3.5)	121.0 (± 28.0)
Land with ice upstream	2	2.1 (± 0.1)	5.3 (± 1.8)	0.25 (± 0.13)	3.9 (± 2.2)	97.1 (± 36.8)
Synoptic Forcing						
Cyclone	*17*	1.3 (± 1.1)	4.4 (± 1.4)	0.34 (± 0.11)	3.8 (± 1.8)	17.8 (± 8.2)
Weak trough	*11*	2.1 (± 0.8)	4.1 (± 1.1)	0.21 (± 0.08)	4.9 (± 4.0)	56.4 (± 56.0)

The model best represented wind speed over OW (*Se* = 1.7 m s^{-1}). Over ICE, wind speed *Se* was much larger and highly variable (10.4 ± 3.5 m s^{-1}). Wind direction was poorly represented over ICE and LD-ICE (*Se* > 90°), indicating considerable error in the dynamical flow regime over these surfaces. It is important to note that these errors are case specific (*F13*), but nonetheless suggest the GEM-LAM 2.5 at times can contain considerable error. Wind direction *Se* values were relatively constant and lower (≤ 20°) for other surfaces.

Model standard error was also shown to vary based on synoptic forcing. Temperature and wind variables were generally well represented in cyclonically driven events, while humidity was better represented during events driven by weakly organised synoptic systems. The *Se* statistic for wind direction error was strongly influenced by results from *F13*, and do not appear to reflect error for all cases with weak synoptic forcing. When examined as an individual case, wind direction error in *F4* was more comparable with cyclonic cases [*Fargey et al*., 2014b]. These results show that similarities are present for different meteorological forcings, but considerable variability on a case-by-case basis can occur.

5.3.2 Performance based on proximity to land

In general, *Se* of most variables was not correlated with location (Table 5.3). The *Se* of specific humidity was the only variable with a significant correlation (although weak), as *Se* increased with distance inland from the coast (Table 5.3).

Table 5.3: Correlation (Spearman's ρ correlation coefficient) between standard error and proximity to land. Significant variables shaded grey, with bold font.

	T (°C)	*Td (°C)*	*q (g kg^{-1})*	*WS (m s^{-1})*	*WD (°)*
Distance inland					
Correlation Coefficient	-0.31	0.07	**0.57**	0.23	0.46
Sig. (2-tailed)	0.247	0.787	**0.021**	0.383	0.073
n	*16*	*16*	*16*	*16*	*16*
Distance away from land					
Correlation Coefficient	-0.11	-0.38	-0.12	-0.32	0.54
Sig. (2-tailed)	0.746	0.226	0.308	0.931	0.071
n	*12*	*12*	*12*	*12*	*12*

To further evaluate model performance based on proximity to land, the *Se* of each vertical profile was plotted based on distance away from land as well as with distance inland (Figure 5.3). Although not statistically significant, a notable relationship between the *Se* of wind direction and proximity to land exists (Figure 5.3). The *Se* increased for each ICE profile *(F13* case), as it approached the terrain. This trend also appears in other cases (*F3* and *F5*) but to a lesser extent. For example, in *F3* the *Se* for two profiles < 50 km away from terrain was small ~ 5° but increased to 30° in a profile within 2 km of terrain. This demonstrates the propensity for model error along topographic boundaries. Though not entirely unexpected, the small-scale variability of wind direction is evident.

The *Se* of other variables did not show relationships with distances inland or away from land. However it was clear that model performance for some variables, varied by case and synoptic forcing at times The *Se* of specific humidity, taken from profiles during cyclonically driven events shows a degree of clustering. Over OW, the *Se* from *F4* were ~0.2 g kg^{-1}, but closer to 0.7 g kg^{-1} for *F3* and *F5*, yet the same large *Se* of moisture was not present over land in these cases. This indicates that large upstream errors in humidity can be present in cyclonically driven events.

Figure 5.3: Standard error of GEM-LAM 2.5 vertical profiles plotted based on proximity to land. Data information - Colour denotes surface environment - Open-water (blue), land (cyan), sea ice > 8/10s coverage (grey), land with sea ice 8/10s coverage upstream (pink). Shape identifies STAR case study – F3 (circle), F4 (triangle), F5 (diamond with cross), and F13 (square).

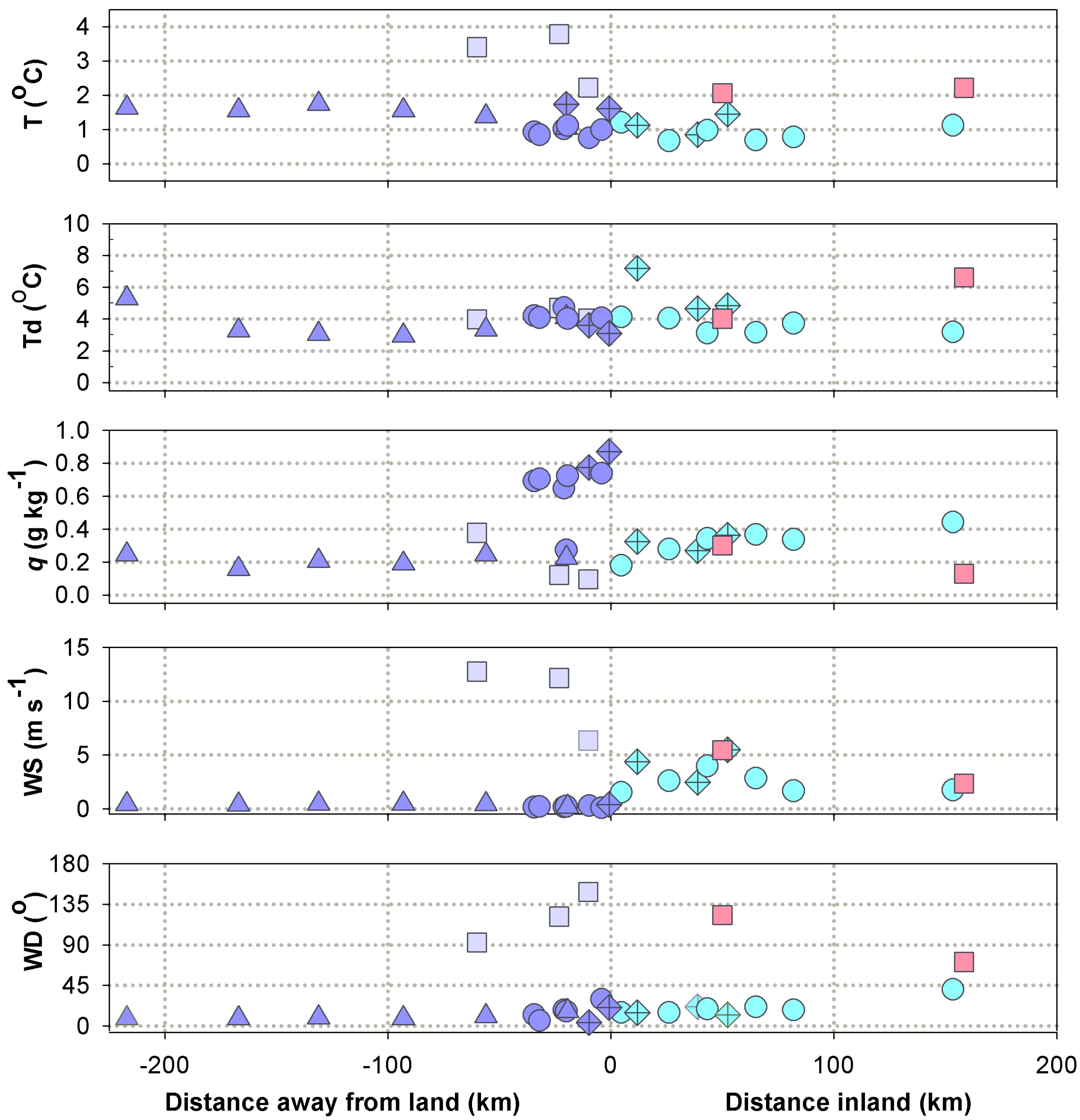

5.3.3 Distribution of error in the vertical profile

5.3.3.1 Sounding profile comparisons

A comparison of all dropsondes and modelled sounding profiles is provided in Appendix B. Key findings are outlined using the eight profiles shown in Figure 5.4. The model commonly overestimated temperature by ~ 1 to 2°C. This occurred between 900 hPa and the surface in all but one profile. Over OW, the model environment was usually too warm in most profiles up to ~600 hPa (a, d, & e in Figure 5.4). However, model performance over LD was variable, both cold and warm inaccuracies could be identified in the same profiles (commonly ±1°C) at altitudes above 900 hPa (b,c, & f in Figure 5.4). Over ICE the model was unable to capture a thermal inversion present in the observational data (Figure 5.4h), with the exception of one profile over LD-ICE (Figure 5.4g). Consequently, over ICE temperatures were warmer near the surface by ~2 °C but colder than observed near the height of inversion (by -8 to -12°C).

Overall the model overestimated moisture content. Dew-point temperature was generally over-predicted by 2 to 4°C in most profiles. Model soundings also frequently indicated the near surface saturation of the atmosphere over land (b & c in Figure 5.4), which was not observed. The model therefore has a tendency to indicate an environment conducive to hydrometeor growth. Model error in the temperature-dew-point spread in some profiles suggests that clouds occurred in different locations than observed and the depth of layers were inconsistent. This phenomenon will be addressed in more detail in section 5.3.4.

Figure 5.4: Comparison of dropsonde data (black) and GEM-LAM 2.5 sounding profiles (red). Temperature (solid line) and dew-point temperature (dashed line). Profiles are labelled with case ID, release time (UTC), and surface environment.

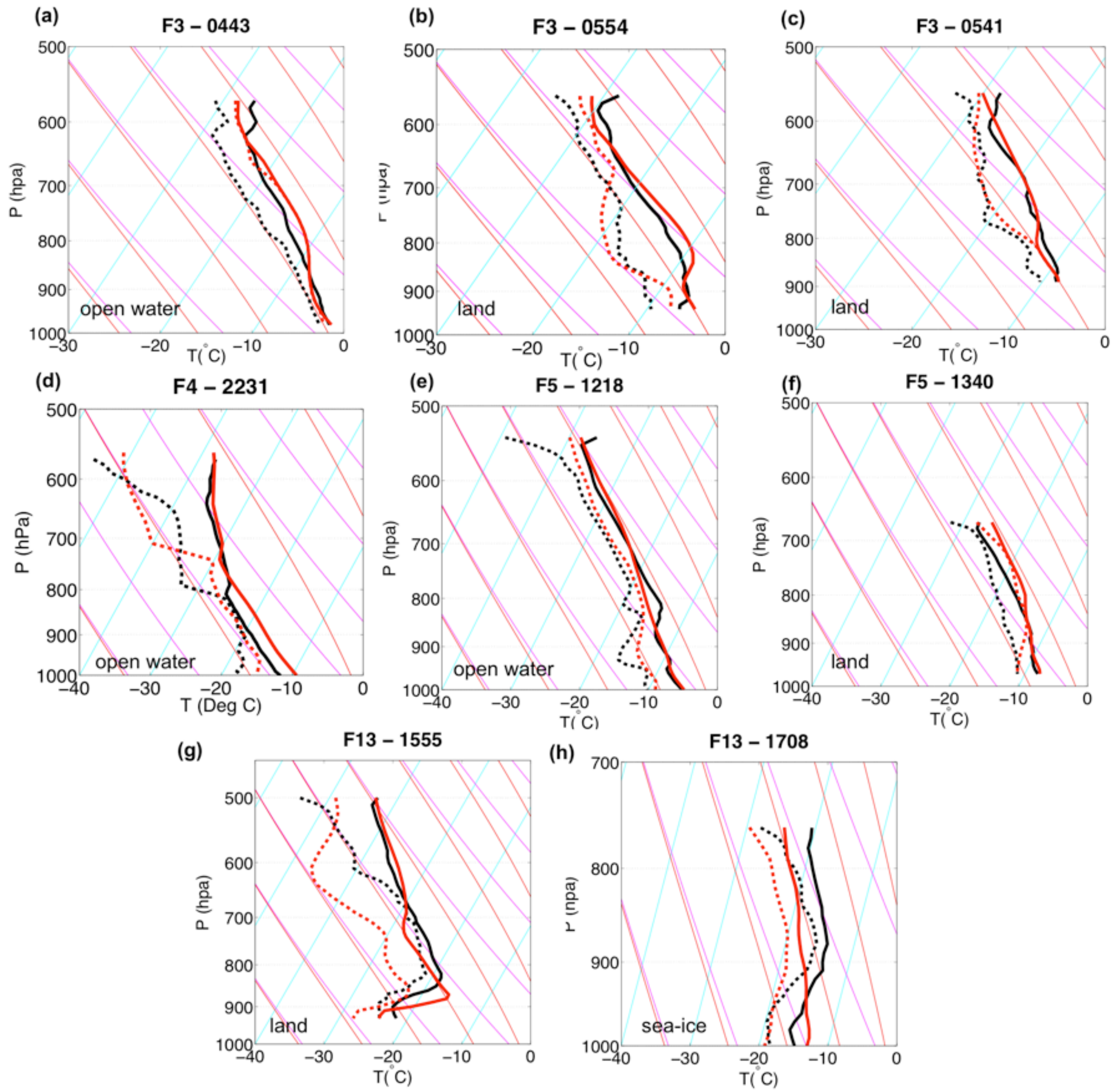

5.3.3.2 Bias and residual range

Overall model bias, determined as the average vertical profile bias from all 28 dropsondes, is shown in Figure 5.5. Considerable inter-dropsonde variability was present, so the residual range has also been included. Residuals for all meteorological variables and individual vertical profiles can be found in Appendix B. Key findings from these data are summarized here.

Vertical profile bias was generally inconsistent, with both positive and negative bias for most variables (Figure 5.5). For temperature, error was positively biased, between 0.5 and 2°C at altitudes lower than 800 hPa, with a gradual shift to negative biases between 700 to 800 hPa, and at altitudes greater than 600 hPa. Overall, the residual profiles were similar over all surface types to within ±2°C with the exception of differences between modeled and observed temperatures over ICE which were closer to 4°C, with the largest residual errors around 800 hPa due to the inability of the model to represent the temperature inversion. Temperature was overestimated near the surface in all profiles, independent of the environment. Lastly, examination of individual profiles showed that at altitudes lower than 800 hPa, the residual error was commonly ~ 1°C smaller for cyclone driven events (*F3*, *F5*), compared to events with a weak synoptic forcing (*F4*, *F13*).

Figure 5.5: Overall GEM-LAM 2.5 model bias (all dropsondes). Residual range shaded in light grey (model minus observation).

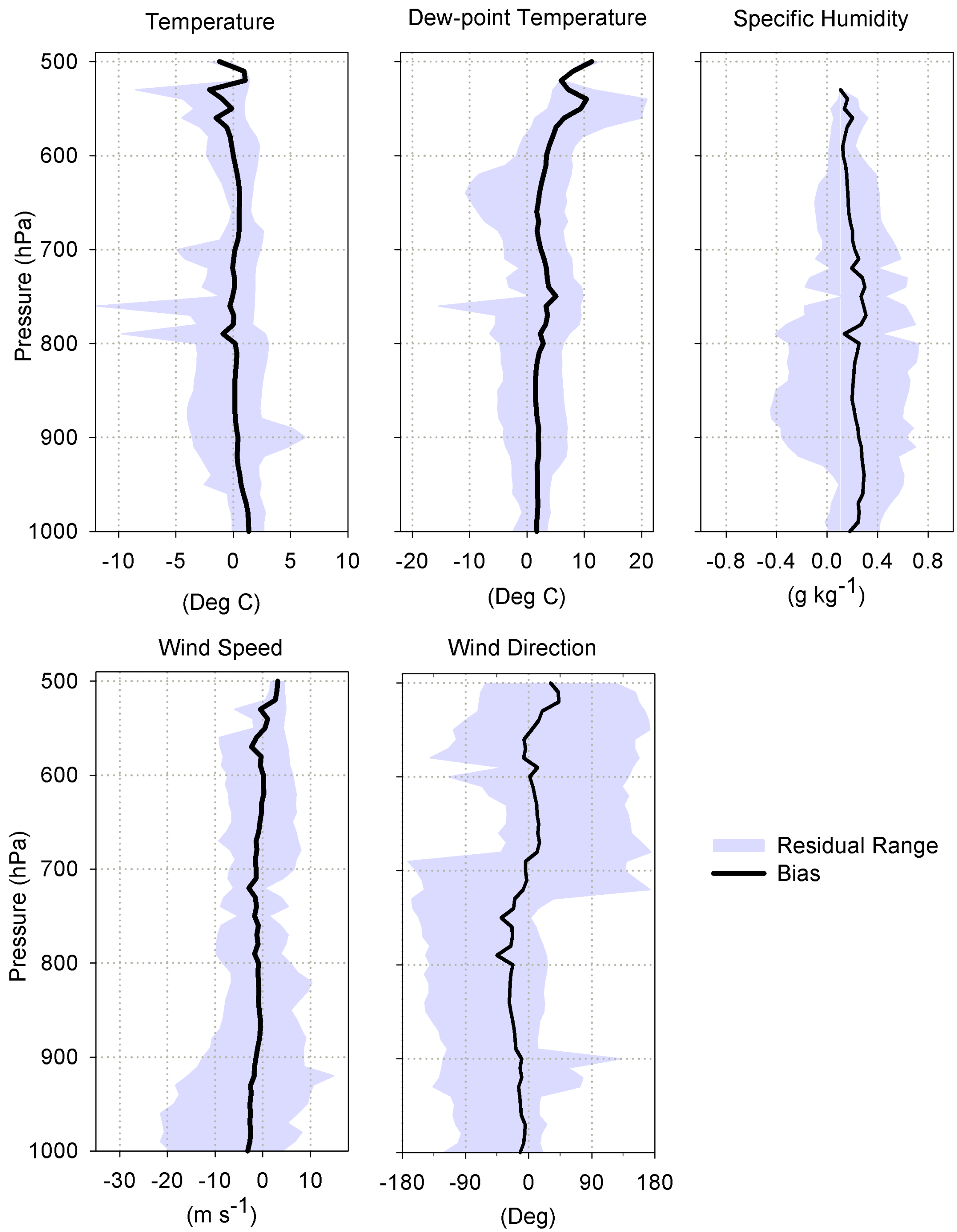

Overall dew-point temperature bias remained positive between the surface and 500 hPa, but the bias magnitude increased with increasing altitude. At 1000 hPa bias was 1.6 °C and increased to 11.3 °C at 500 hPa (Figure 5.5). Examination of individual profiles revealed variability specific to case study and surface environment, e.g. over OW where residual error for cyclone driven events (*F3*, *F5*) consistently increased with altitude. However, the residual errors over OW for *F4* was more variable with height and intermittently negative.

Bias for specific humidity confirms that GEM-LAM 2.5 overestimated moisture (between 0.1 to 0.3 g kg^{-1}). The residual range shows that despite the overall positive bias between 700 and 900 hPa, a large dry bias was also possible. The examination of individual profiles showed that negative bias between these altitudes occurred during two separate circumstances. First, the model was too dry aloft over ice. While, secondly, the model under-predicted moisture when dry layers were present in some profiles over the terrain. This result is not entirely unexpected, as the microphysical scheme in the model does not allow for sublimation, which would add moisture to the atmosphere.

Bias for wind speed was underestimated between the surface (-3 m s^{-1}) and 600 hPa (-1 m s^{-1}), with the error magnitude decreasing with height (Figure 5.5). According to the residuals, wind speed was most variable between the surface and 900 hPa, but the magnitude of the error was generally within ± 10 m s^{-1}. Bias over ICE was -20 m s^{-1} near the surface for all three vertical profiles. In contrast to wind speed, wind direction bias was lowest (< 20˚) below 850 hPa and rarely exceeded 30° above this altitude (Figure 5.5). Individual profiles indicated consistent model performance for all vertical profiles from *F3*, *F4* and *F5*. As previously mentioned, errors were extremely large (>90˚) in vertical profiles from *F13*.

5.3.3.3 Frequency distribution of bias

The distribution of average model bias throughout the vertical profiles for each surface environment is examined (Figure 5.6) along with the frequency distribution of the bias for each meteorological variable (Figure 5.7 to Figure 5.11). Results indicate that bias in the model shows similarities and differences between surface environments.

Figure 5.6: Average GEM-LAM 2.5 model bias for the different surface environments.

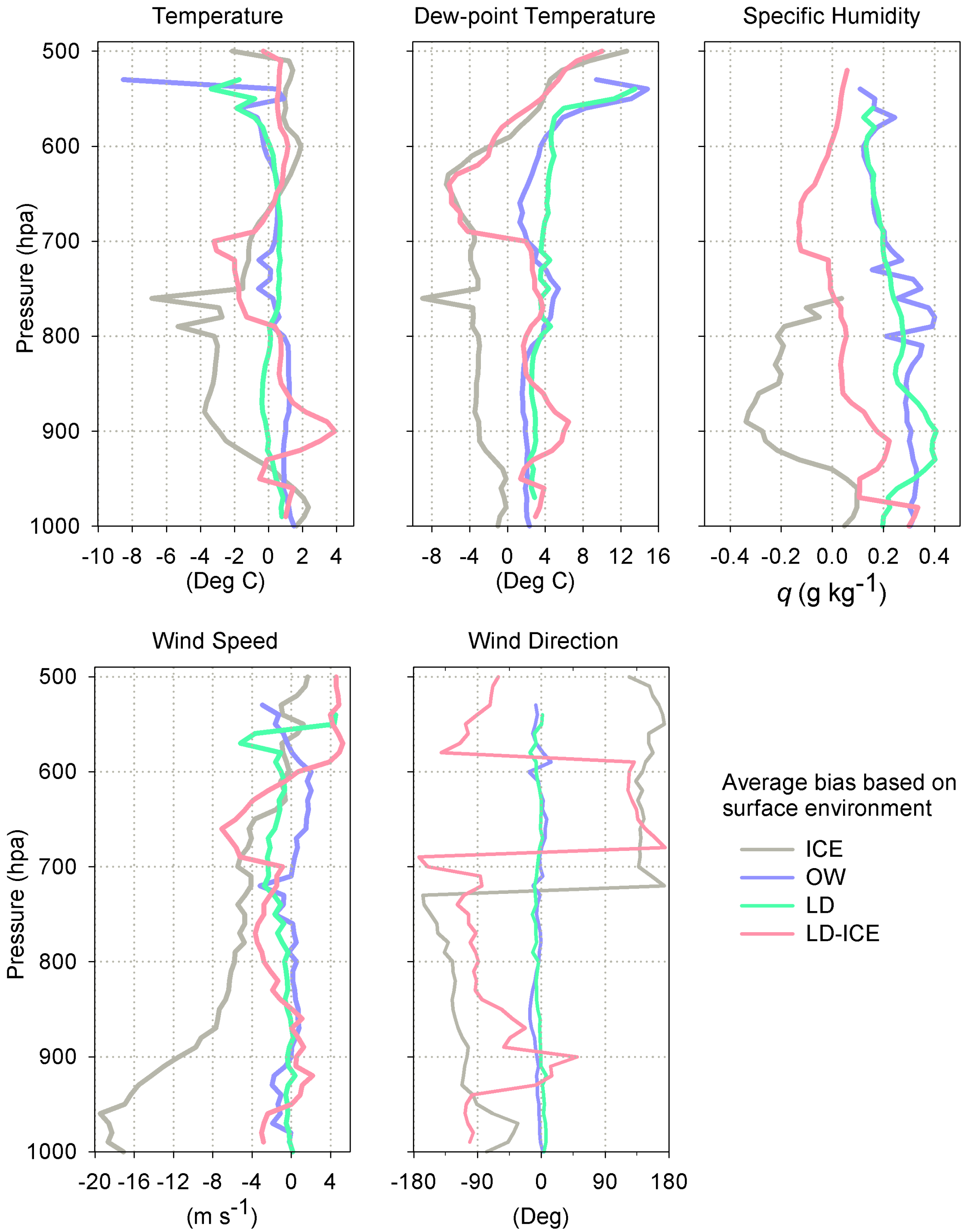

The model was more likely to overestimate temperature over all surface types, but a large underestimation of this variable over surfaces with proximity to sea ice was possible (Figure 5.7). The frequency of bias for dew-point temperature and specific humidity shows model most frequently overestimated moisture for three surface types: OW, LD and LD-ICE (Figure 5.8 and Figure 5.9). Over ICE the model had a greater tendency to be too dry, and exhibited more variability compared to other surfaces. The distribution of wind speed showed a bias typically to within ± 5.0 m s^{-1} (Figure 5.10). Over OW the model frequently underestimated speed and while overestimating speed over LD. Winds were shown to be too weak over ICE and bias was large. Average wind direction bias over OW and LD was generally contained between ± 10° (Figure 5.11). Direction was poorly represented over ICE and LD-ICE, where error usually exceeded 90° (Figure 5.11). Further testing is required to establish the role of sea ice and bias.

Figure 5.7: The frequency distribution of average temperature bias (grouped by surface environment) through the vertical atmospheric profile (500 and 1000 hPa).

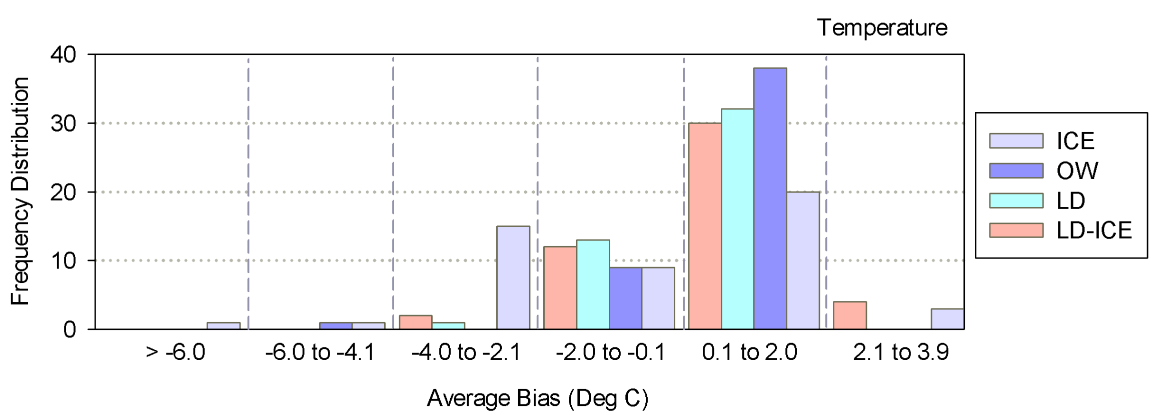

Figure 5.8: Same as Figure 5.7 but for dew-point temperature (°C)

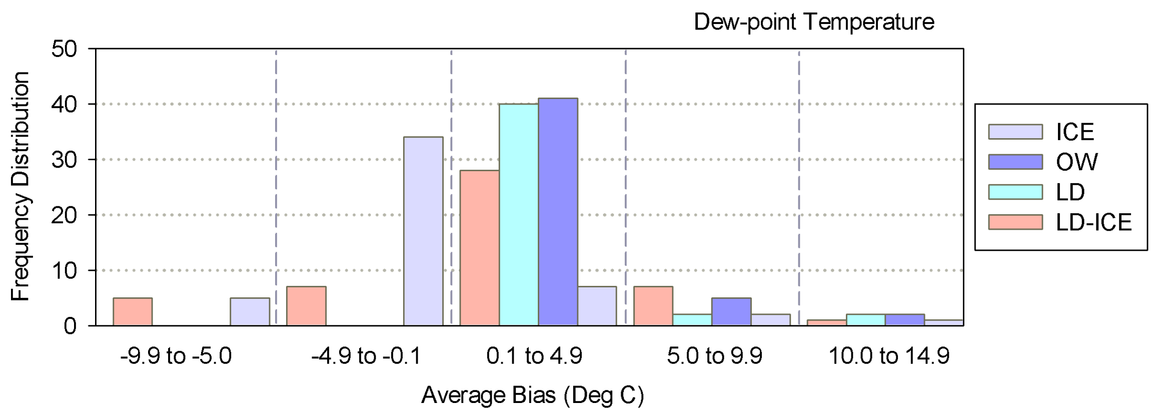

Figure 5.9: Same as Figure 5.7 but for specific humidity (g kg $^{-1}$).

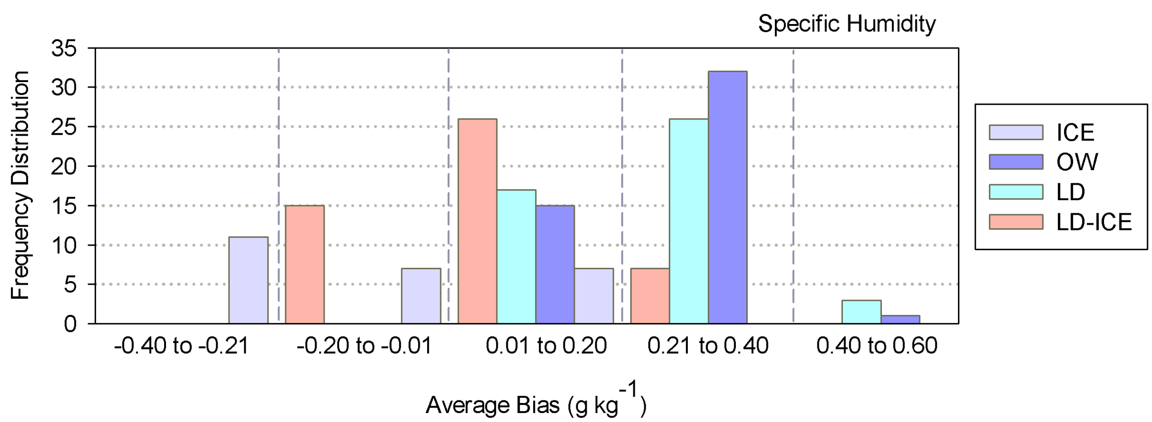

Figure 5.10: Same as Figure 5.7 but for wind speed (m s $^{-1}$).

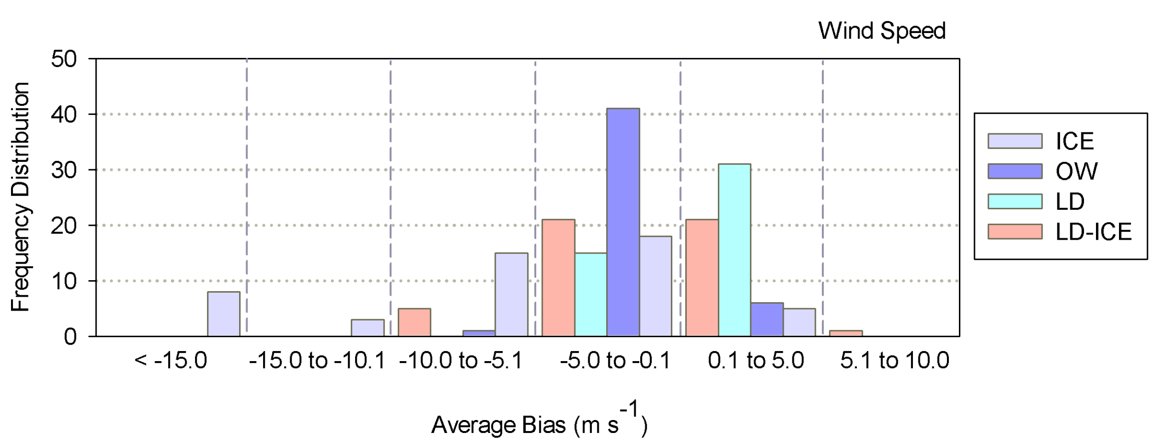

Figure 5.11: Same as Figure 5.7 but for wind direction (Deg).

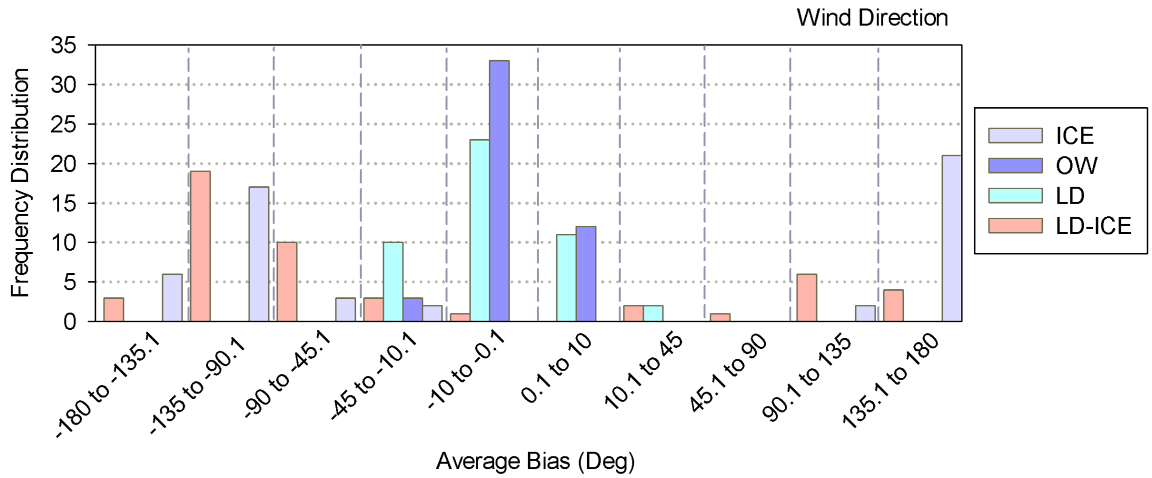

5.3.4 Cloud features

The presence of clouds in each profile is plotted in Figure 5.12. During the *F3* case study, dropsondes were released in cloud and therefore do not provide an estimate of cloud-top height; instead, W-band radar data was used. Radar-derived cloud-top heights were added to Figure 5.12 for all cases showing that height estimates from dropsondes and radar were nearly identical. This indicates the equilibrium level from the GEM-LAM 2.5 soundings and dropsondes is a reasonable estimate of cloud-top height, and that the substitution of W-band radar data for *F3* dropsondes provides a sufficient replacement for the missing data.

5.3.4.1 Cloud layers

In cases where multiple cloud layers were present, GEM-LAM 2.5 was able to capture these features most of the time (Figure 5.12). However, due to errors in modelled temperature and moisture, the dry layer depth was often too deep (200 to 800 m). These errors are prominent in the *F3* case over the terrain (Figure 5.12). In contrast there were some instances where GEM-LAM 2.5 suggested multiple layers in the profile, not confirmed by observations. This was more common in *F4* and *F13* profiles (weak synoptic forcing).

Figure 5.12: The presence of clouds inferred from dropsonde data (blue) and model soundings (speckle). Data information – W-band radar derived cloud-top height (m) red line; terrain height under dropsonde shown in brown.

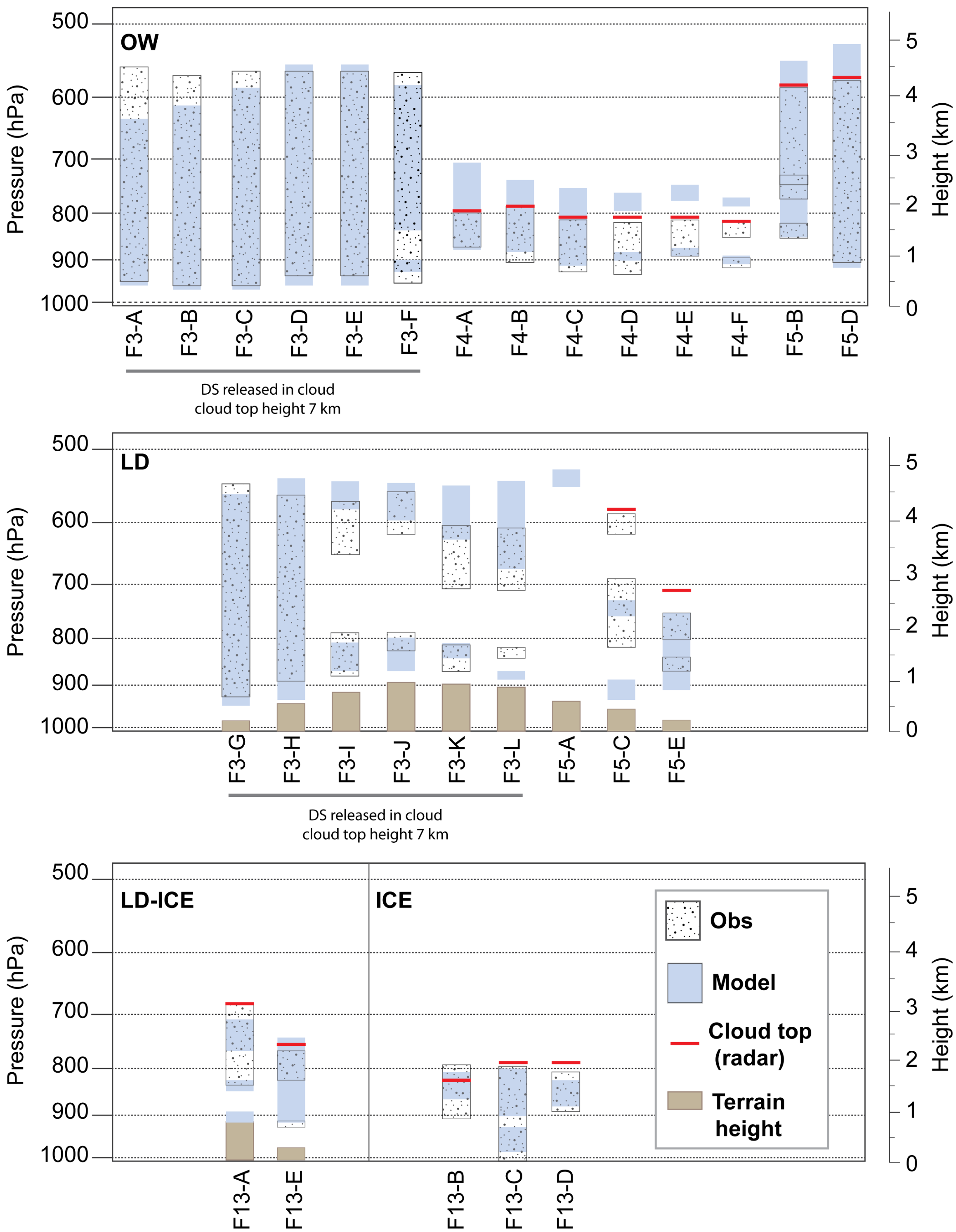

Table 5.4: Description of dropsonde labels used in Figure 5.12.

STAR Case ID	Release time (UTC)	Dropsonde ID	Surface Environment
F3	0427	F3-A	OW
	0431	F3-B	OW
	0435	F3-C	OW
	0439	F3-D	OW
	0443	F3-E	OW
	0447	F3-F	OW
	0531	F3-G	LD
	0535	F3-H	LD
	0538	F3-I	LD
	0541	F3-J	LD
	0544	F3-K	LD
	0554	F3-L	LD
F4	2208	F4-A	OW
	2215	F4-B	OW
	2231	F4-C	OW
	2233	F4-D	OW
	2239	F4-E	OW
	2250	F4-F	OW
F5	1208	F5-A	LD
	1218	F5-B	OW
	1225	F5-C	LD
	1340	F5-D	OW
	1351	F5-E	LD
F13	1555	F13-A	LD-ICE
	1614	F13-B	ICE
	1326	F13-C	ICE
	1708	F13-D	ICE
	2210	F13-E	LD-ICE

5.3.4.2 Cloud-top and cloud-base estimates

Generally cloud-tops were too high in the model (Figure 5.13). The mean error for cyclonically driven events was 300 m, and the range was large, between -1675 and 4750 m. The maximum error occurred in an *F5* profile where the model identified cloud, a feature not present in the observations (Figure 5.13). Inspection of the W-band radar profile at the coincident time of the dropsonde release shows a similar shallow middle-level cloud layer present, but approximately 35 km upstream. This shows that GEM-LAM 2.5 has the ability to predict similar cloud features, but error in location may occur. Cloud-top errors for events with weak synoptic forcing were also too high, but less variable. The surface environment played a role in cloud-top and base estimates. Cloud-tops were on average higher over OW and LD, with a mean value of ~400 m for each. Cloud-top height was always overestimated above OW, but both positive and negative errors were present above other surface types.

Cloud-bases for cyclonically driven events were generally too low, with the error commonly between -100 to -500 m (Figure 5.13). In contrast, errors from events with weak synoptic forcing were distributed more evenly above and below the observations (Figure 5.13). When the results were evaluated based on surface environment, cloud-base height was usually between -50 and -500 m too low, but results from LD-ICE and ICE were variable.

Figure 5.13: Box-and-whisker plot showing median distribution of cloud-top (top) and cloud-base (bottom) data grouped by surface environment and event forcing. The box size is defined by the upper and lower quartiles (25% and 75%) of data (shaded area) and contains the median (black line) value. The red line indicated the mean value; the whiskers represent the maximum and minimum values, excluding outliers. Outliers (black circles) are more (less) than 3/2 times the upper (lower) quartile. There was insufficient data to create a plot for LD-ICE, mean value (red line), maximum and minimum (black dots) are shown.

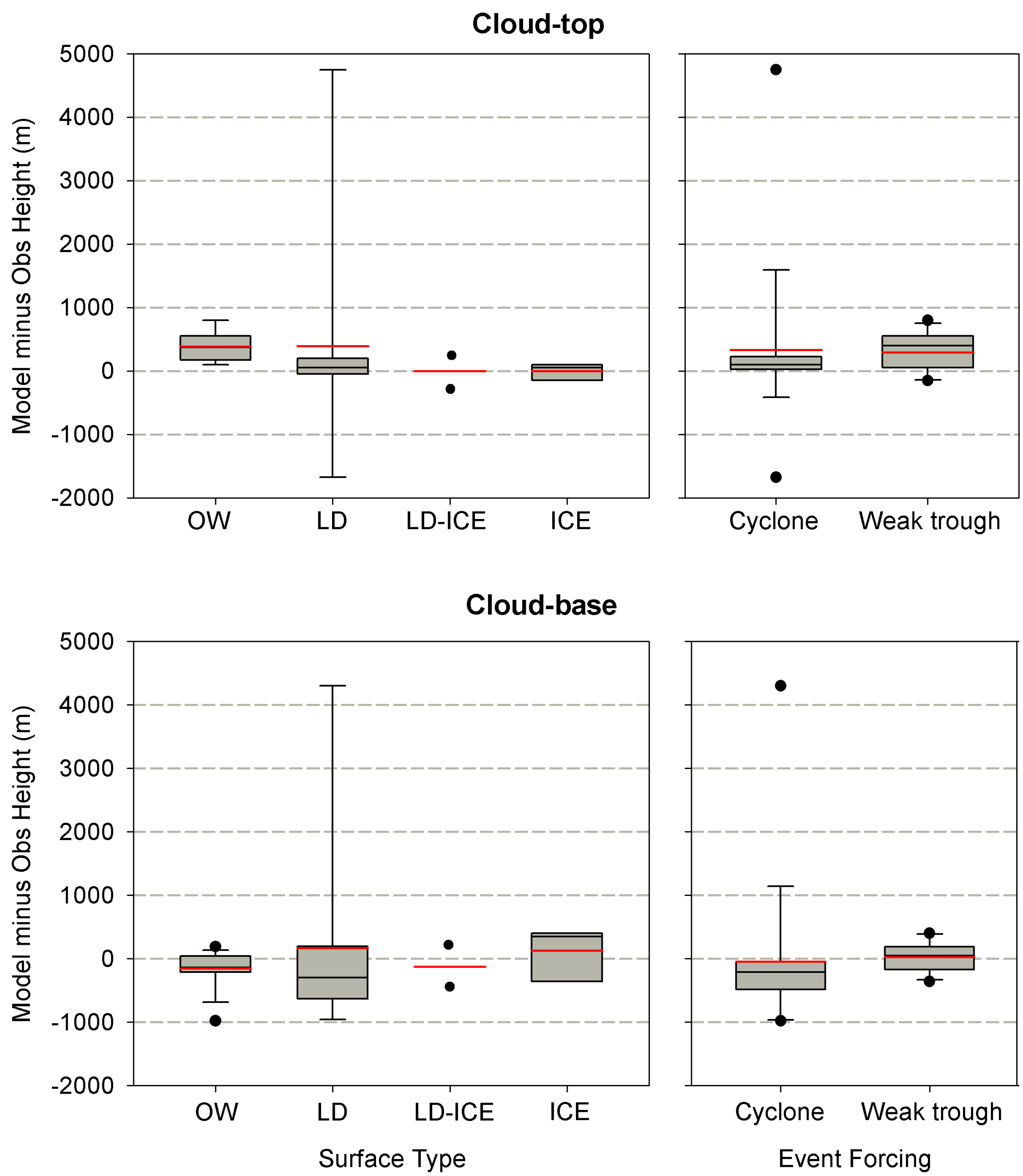

5.4 Discussion

5.4.1 Summary of model performance

The accuracy of the GEM-LAM 2.5 model around southern Baffin Island was examined for 28 vertical profiles during autumn 2007. Results facilitate an evaluation of how the model performed under variable synoptic conditions and over different surface types.

In general the model overestimated temperature by 1 to 2˚C between the surface and 900 hPa. At altitudes above 900 hPa, temperature error was variable but predominantly positive. Examination of individual profiles showed errors ~ 1°C smaller for cyclone driven events (*F3*, *F5*) compared to events with a weak synoptic forcing (*F4*, *F13*). Model predictions were most variable over LD, where it was not uncommon to have both cold and warm bias in the same profiles (~ ±1°C). Over ICE, during the *F13* case, the model was unable to capture the thermal inversion present in the observational data.

Dew-point temperature was frequently overestimated between 2 and 4˚C, and specific humidity levels were too high (0.2 to 0.4 g kg^{-1}). In contrast, in an environment with high sea ice cover the model showed a greater tendency to underestimate moisture content (-0.1 to -0.2 g kg^{-1}). Over open water, standard errors for moisture were much larger for cyclonically driven events (~0.7 g kg^{-1}) compared to weakly forced events (~0.2 g kg^{-1}). This might indicate an increased tendency for the model to overestimate precipitation during cyclonically driven events when the moist air is advected over the terrain but this needs to be confirmed.

In addition, error in specific humidity was shown to correlate with proximity to the coastline. Error increased with increasing distance inland. *Fargey et al*. [2014] found that cloud and precipitation structure over the terrain was more variable than over the adjacent ocean upstream, which may account for some difficulties in accurate simulation of this variable over the terrain.

In general wind speed was under-predicted near the surface (~3 m s^{-1}), with error improving with height (~1 m s^{-1} around 600 hPa). The residual range shows that winds were most variable between the surface and 900 hPa, but error was generally contained between ± 5 m s^{-1}. Examination of individual residual profiles showed that it was common for both negative and positive residuals error to be present within the same case study. Inter-dropsonde variability was higher over OW than LD, and model performance was more variable for events with large scale cyclonic forcing.

Wind direction was poorly represented over ICE and LD-ICE. Standard errors over these surface environments exceeded 90° showing considerable error in the dynamical flow regime in the model during *F13*. Wind direction standard error was comparably low for other cases and surface environments (≤ 20°). There is a general relationship between wind direction error and proximity to land, as indicated by the increased standard error for all cases approaching the terrain. This shows that, along topographic boundaries, errors may be large in the model. This error is not unexpected because of terrain smoothing in the model, and the fact that model soundings data comes from a 2.5 km grid cell, but shows that the ability to represent wind direction can vary considerably over small spatial scales.

In cases where multiple cloud layers were present the model captured this feature most of the time. However, due to errors in temperature and moisture, the dry layer depth was often too deep (up to 800 m) compared to observations over land. Individual profiles also showed instances where the model underestimated moisture in the dry layers (close to -0.2 g kg^{-1}) over land. In contrast, there were some instances where the model indicated multiple layers not actually observed. This was more common in profiles associated with weakly forced synoptic events (*F4* and *F13*).

Overall, cloud-tops were commonly overestimated (~ 300 m) and cloud-bases were underestimated (-50 to -500 m) by the model. This result was fairly common for cyclonically driven events. Cloud-tops were also overestimated with similar error for events with weak synoptic forcing, but cloud-base errors were inconsistent.

5.4.2 Implications for prediction of clouds and precipitation

5.4.2.1 Sublimation

In the model, the atmosphere was usually saturated or super-saturated with respect to ice near the surface over land. When combined with the fact that modelled cloud-tops were usually too high (~300 m) and cloud-bases were too low (-50 to -500 m) might suggest the model environment was more conducive to hydrometeor growth, rather than enhanced loss from sublimational processes thereby increasing the probability of precipitation in the model pending further verification. However, these results are complicated by the errors in temperature and moisture over land, particularly in the *F3* case where the dry layer depth was often too deep (up to 800 m). These errors may result in less precipitation by the model if snow sublimates (partially or fully) in the sub-saturated layer.

In *Fargey et al.* [2014a] and *Fargey et al.* [2014b], sublimation below cloud base and between cloud layers reduced or eliminated precipitation reaching the surface in all the case studies used in this study. During the cold season, persistent low temperatures and moisture supply, combined with the predominant presence of solid precipitation, increases the probability that hydrometeors will sublimate before they reach the ground even if microphysical processes aloft are efficient at precipitation production. This process in an important factor in determining whether precipitation will reach the surface and how much will accumulate. Consequently humidity and temperature variables need to be more accurately represented. In addition, microphysical schemes and conversion processes may need to be adjusted or further generalized to better characterize the Arctic environment.

5.4.2.2 Errors in a high sea ice extent environment

Considerable model errors were shown to exist in the presence of sea ice. Major errors included the inability of the model to capture the observed thermal inversion feature; consequently temperature was overestimated (~2°C) near the surface and underestimated between 800 and 900 hPa (-8 to -12°C). This also led to errors in estimated moisture, with overestimations near the surface and, in some cases, underestimations aloft (-0.2 to -0.4 g kg^{-1}). In addition, wind speeds were up to ~20 m s^{-1} too low near the surface and direction was poorly represented, with *Se* > 90° revealing error in the dynamical flow regime in the model.

Fargey et al. [2014a] showed that the presence of sea ice aided in the development of a thermal inversion, which resulted in low-level blocking and reduced lift of surface winds over the terrain. Wind speed was high (~21 m s^{-1}) and channelled parallel to the topography of Cumberland Peninsula as a result. Consequently, inability of the model to capture the thermodynamic character of the environment may have also impacted the dynamics. Without extensive model sensitivity tests this is not verifiable here.

Errors above sea ice may have further implications for cloud and precipitation production in the region. In this case, the atmosphere above the thermal inversion was conditionally unstable and moist, suggesting that where parcels were lifted due to the terrain there may have been embedded convection [*Fargey et al.,* 2014a]. The model soundings were stable and dry, which resulted in less vertical development (-300 m) impacting cloud and precipitation production on the windward slopes of the Cumberland Peninsula.

As the analysis of a high sea ice extent environment is from a single case study, further research is required to determine conclusively whether or not errors of this magnitude are common in the model or it they are case specific. The ice fraction included in the model was consistent with observations so there is some confidence that these errors are not the result an inaccurate surface mosaic.

5.4.2.3 Weakened upslope processes

Fargey et al. [2014a] showed that the most dramatic precipitation enhancement over the orography in the southern Baffin Island region occurred coincident to upslope flow at all levels. Results from this study showed a tendency in the model to underestimate wind speed at altitudes lower than 900 hPa upstream of the terrain. This altitude is similar to the heights of the orography of the Hall and Meta Incognita Peninsulas, which suggests that upslope processes may be weakened in the model below terrain height and thereby influence precipitation over the orography in the region.

To evaluate the behaviour of the atmospheric flow impinging on the topography of the Meta Incognita Peninsula, *Fargey et al.* [2014b] calculated the Froude number (*Fr*). The *Fr* for both the model and observations were high (>1) confirming that a strong upslope component existed for both, however the *Fr* in the model was smaller than the observations in part due to the weaker flow strength. Applying the same methodology for this study, the *Fr* for the model was calculated following a similar procedure to *Medina and Houze* [2003] to examine the behaviour of flow for *F3*, a case in which *Fargey et al.* [2014] also showed a strong upslope component (*Fr* >1). Similarly, the *Fr* was smaller than observed. These results show that reduced upslope flow may reduce condensation and precipitation processes over the terrain in the model.

5.4.3 Comparison with other studies

Results from this work show some similarities with other studies in the Arctic. They include a propensity for GEM-LAM 2.5 to overestimate temperature between the surface and 600 hPa [*Paquin-Ricard, et al.*, 2010; *Simjanovski et al.,* 2011], overestimate specific humidity between the surface and 900 hPa [*Simjanovski et al.,* 2011] and under-predict wind speed in some cases [*Hanesiak et al.*, 2013]. However, results from this study also showed some differences. The general character of moisture varied between this study and the ones from the western Arctic. *Simjanovski et al.* [2011] showed that the model was too dry between 600 and 900 hPa, where as GEM-LAM 2.5 was generally too moist at similar altitudes for STAR cases, with the exception of a few profiles. The differences may be the result of the microphysical scheme used between studies. In *Simjanovski et al.* [2011] GEM-LAM 2.5 was run with the Sundqvist scheme [*Sundqvist,* 1978]. Like the Kong-Yau scheme, it is an explicit grid-scale condensation scheme, but differences in prescribed temperature dependant cloud water content parameterizations exist.

Stewart et al. [2004] compared the GEM model to radar observations in the Fort Simpson, Northwest Territories to investigate cloud field representation. The GEM model over-predicted cloud height by more than 3000 m at times and showed a slight overestimation of the number of cloud layers. In this study the GEM-LAM 2.5 also overestimated cloud height but errors were less, and cloud layers were fairly well represented, but the model did overestimate the number of cloud layers in some profiles especially in weakly forced events. Results from this work show that the GEM-LAM 2.5 shows some improvement over the GEM model in cloud height estimates in an Arctic environment, but errors in the number of cloud layers exist in both.

Model performance during STAR cases was also compared to relevant results from mid-latitude research in a mountainous environment. During the Science and Nowcasting of Olympic Weather for Vancouver 2010 project [SNOW-V10; *Isaac et al.,* 2012] two limited area versions of the GEM model (2.5 and 1-km resolutions) were evaluated using a number of special surface observations over the coastal mountain range around Whistler in British Columbia [*Mailhot et al.*, 2012]. Standard error for temperature was around 2°C for both versions of the limited area model, with a general cold bias. Corresponding to errors in temperature was that the models were too dry (*Td* bias around -2°C). These results are dissimilar to how the model performed at the surface around southern Baffin Island. In comparison the model environment was too warm and moist in STAR cases.

In SNOW-V10 all model resolutions were shown to have difficulty forecasting wind direction. Standard errors were large, between 40° to 50°. In all but one case study wind direction was better represented in STAR cases near the surface (<20°). In contrast, wind speed was well represented overall during SNOW-V10. The *Se* was ~1.4 m s^{-1} and bias values were small with no indication of systematic errors [*Mailhot et al.,* 2012]. In STAR cases, the *Se* for wind speed was approximately twice that value. These results confirm regional variation in GEM-LAM 2.5 performance.

There were differences in how cloud microphysics and precipitation were parameterized between SNOW-V10 and STAR, which may account for some of the differences between studies. For SNOW-V10, GEM-LAM 2.5 used the two-moment version of the Milbrandt-Yau bulk microphysical scheme [*Milbrandt & Yau*, 2005]. The scheme predicts the mass mixing ratio and total number concentration of six different hydrometeor categories, which includes ice (pristine crystals), snow (large crystals/aggregate), graupel (heavily rimed snow) and hail (frozen drops and hail) for solid precipitation types. Over the southern Ontario GEM-LAM 2.5 domain, the Milbrandt-Yau scheme was shown to notably improve precipitation forecast for summer and mixed precipitation events in the winter over the Kong-Yau scheme [*Milbrandt et al.,* 2008]. However, the performance of the Milbrandt-Yau scheme was not significantly different from the Kong-Yau scheme for the prediction of small accumulation events in winter. Further investigation should be conducted with this updated microphysical scheme in the Arctic.

5.5 Concluding remarks

Data collected during the STAR project provided a unique opportunity to evaluate the Canadian operational limited area model (GEM-LAM 2.5) in a region of complex topography and where observational data are scarce. Results from this study confirm regional variation in GEM-LAM 2.5 performance in the Arctic, along with variability in its ability to characterize high and mid-latitudes mountainous environments.

Based on evidence from the four case studies, the model typically overestimated temperature, with the exception of profiles over sea ice. The model frequently indicated near surface saturation of the atmosphere over land, which was not observed, along with a large overestimation of moisture for cyclonically driven events over open water. Cloud-tops were usually too high and cloud-bases too low and in cases where multiple cloud layers were present the model was able to represent this feature, but dry layer depth was often inaccurate. Combined these errors suggest the model environment may be more conducive to hydrometeor growth and result in an overestimation of precipitation in some cases, particularly over open water and during cyclonic events but this needs to be confirmed.

Results from this study showed a tendency in the model to underestimate wind speed at altitudes below the height of the orography of southern Baffin Island. This suggests that upslope processes may be weakened in the model and thereby also impact orographic cloud and precipitation processes in the region. Precipitation production would likely be further impacted over land, because dry layer depth was too deep.

The presence of sea ice was associated with significant model error and it is important to learn if these errors are common over that surface type. In proximity to ice the model typically underestimated moisture content and had difficulties simulating the thermal inversion feature represented in the observations, influencing the stability and dynamics in that case. The model soundings were stable and dry compared to observations, which resulted in less vertical development impacting cloud and precipitation production on the windward slopes of the terrain.

The results presented in this study stem from single vertical profile comparisons. Future work should also include vertical profiles from neighbouring grid cells to provide a more in depth evaluation of the models spatial representation of the environment. The analysis in this study would have also benefited from a more comprehensive temporal investigation of the model performance during each event had the additional GEM-LAM 2.5 data been available.

In summary this study evaluated the accuracy of the Canadian operational limited area model during four STAR case studies around southern Baffin Island, in the south-east Canadian Arctic. Descriptions of model errors and proficiencies were examined for different synoptic forcing and surface environments, including orography, open water and sea ice. GEM-LAM 2.5 data was only available for aircraft flight times of the four cases providing the opportunity to compare 28 vertical profiles from dropsondes but not from other STAR observations at Iqaluit (such as rawionsondes) during IOPs. However, despite the limited number of observations, this study is an important step towards understanding errors in the model and their implications for cloud and precipitation production and their forecast. Based on evidence from this study, it is crucial that further improvements are made in the ability to simulate the Arctic environment to make reliable estimates of future climate conditions, and short-term forecasts.

5.6 References

Air Weather Service. (1979). The use of the skew-T, log p diagram in analysis and forecasting. AWS/TR=79/006 revised, p. 157 [Available from U.S. Air Force Weather Service, Scott Air Force Base, II, 62225-5008].

Arctic Monitoring and Assessment Programme (AMAP). (2011). Snow, Water, Ice and Permafrost in the Arctic (SWIPA): Climate Change and the Cryosphere. Oslo, Norway. 538 pages.

Belair, S., Mailhot, J., Girard, J., and Vaillancourt, P. (2005). Boundary layer and shallow cumulus clouds in a medium-range forecast of a largescale weather system. *Monthly Weather Review, 133,* 1938–1960. doi:10.1175/MWR2958.1.

Burford, J.E., and Stewart, R.E. (1998). The sublimation of falling snow over the Mackenzie River Basin. *Atmospheric Research, 49*, 289-214.

Cassano, J.J., Box, J.E., Bromwich, D.H., Li, L., and Steffen, K. (2001). Evaluation of Polar MM5 simulations of Greenland's atmospheric circulation. *Journal of Geophysical Research. 106,* 33867–33889.

Chapman, W.L. and Walsh, J.E. (2007). Simulations of Arctic Temperature and Pressure by Global Coupled Models. *Journal of Climate. 20,* 609-632.

Côté, J., Gravel, S., Méthot, A., Patoine, A., Roch, M., and Staniforth, A. (1998). The operational CMC-MRB global environmental multiscale (GEM) model. Part I: Design considerations and formulation. *Monthly Weather Review, 126,* 1373-1396.

Curry, J.A., Rossow, W.B., Randall, D.A., and Schramm, J.L. (1996). Overview of Arctic cloud and radiation characteristics. *Journal of Climate, 9,* 1731–1764.

Deacu, D., Zandra. A., and Hanesiak, J. (2010). Simulating wind channelling over Frobisher Bay and its interaction with downslope winds during the 7-8 November 2006 Wind Event. *Atmosphere-Ocean. 48*, 101-121. doi:10.3137/AO1109.2010.

Erfani, A., Mailhot, J., Methot, A., Gravel, S., Desgagne, M., Plante, A., Sills, D., King, P., and Ashton, A. (2006). The 2.5 km horizontal resolution limited area version of the Global Environmental Multiscale model over southern Ontario and Quebec. *In: Abstracts of 15th International Great Lakes Operational Meteorology Workshop, 25–27 October 2006*, Niagara Falls, Ontario, Canada.

Fargey, S., Hanesiak, J., Stewart, R., and Wolde, M. (2014a). Aircraft observations of orographic cloud and precipitation features over southern Baffin Island, Nunavut, Canada. *Atmosphere-Ocean*. *52,* 54-76. doi:10.1080/07055900.2013.855624.

Fargey, S., Henson, W., Hanesiak, J., and Goodson, R. (2014b). Characterization of an unexpected snowfall event in Iqaluit, Nunavut during the Storm Studies in the Arctic Project. *Journal of Geophysical Research-Atmos*. *119,* 5492-5511 doi: 10.1002/2013JD021176

Garand, L. and Mailhot, J. (1990). The influence of infrared radiation on numerical weather forecasts. *In: Proceedings of the seventh Conference on Atmospheric Radiation, 23–27 July 1990*, San Francisco, USA.

Goodson, R. (2008). Which way blows the winds at Pangnirtung – the Answer Revealed, November 17 -18, 2007. Hydrometeorology and Arctic Laboratory, Environment Canada, Edmonton, Alberta, Canada.

Hanesiak, J., Stewart, R.E., Taylor, P., Moore, K., Barber, D., McBean, G., Strapp, J.W. Wolde, M., Goodson, R., Hudson, E., Hudak, D., Scott, J., Liu, G., Gilligan, J., Biswas, S., Desjardins, D., Dyck, R., Fargey, S., Field, R., Gascon, G., Gordon, M., Greene, H., Hay, C. Henson, W., Hochheim, K., Laplante, A., Martin, R., Melzer, M.A., and Zhang, S. (2010). Storm Studies in the Arctic: The meteorological field project. *Bulletin of the American Meteorological Society, 91,* 47-68. doi:10.1175/2009BAMS2693.1

Hanesiak, J.M., Brimelow, J.C., Zadra, A., Goodson, R., and Liu, G. (2013). Structure and predictive skill of strong northeasterly wind events using a limited area numerical weather prediction model at Iqaluit, Canada. *Tellus A, 65,* 1-16

Hock, T. and Franklin, J.L. (1999). The NCAR GPS dropwindesonde. *Bulletin of the American Meteorological Society, 80,* 407-420.

IPCC. (2013). Climate Change 2013: The Physical Science Basis. Contribution of Working Group I to the Fifth Assessment Report of the Intergovernmental Panel on Climate Change [Stocker, T.F., D. Qin, G.-K. Plattner, M. Tignor, S.K. Allen, J. Boschung, A. Nauels, Y. Xia, V. Bex and P.M. Midgley (eds.)]. Cambridge University Press, Cambridge, United Kingdom and New York, NY, USA, 1535 pp.

Isaac G.A., Joe, P. Mailhot, J., Bailey, M., Belair, S., Boudala, F., Brugman, M., Campos, E., Carpenter, R., Crawford, R.W., Cober, S., Denis, B., Doyle, C., Reeves, H., Gultepe, I., Heiden, T., Heckman, I., Huang, L., Milbrandt, J.A., Mo, R., Rasmussen, R., Smith, T., Stewart. R.E., and Wang, D. (2012). Science of nowcasting Olympic weather for Vancouver 2010 (SNOW-V10): A world weather research programme project**.** *Pure and Applied Geophysics, 169*, doi:10.1007/s00024-012-0579-0

Kirtman, B., Power, S.B., Adedoyin, J.A., Boer, G.J., Bojariu, R., Camilloni, I., Doblas-Reyes, F.J., Fiore, A.M., Kimoto, M., Meehl, G.A., Prather, M., Sarr, A., Schär, C., Sutton, R., van Oldenborgh, G.J., Vecchi G., and Wang, H.J. (2013) Near-term Climate Change: Projections and Predictability. In: Climate Change 2013: The Physical Science Basis. Contribution of Working Group I to the Fifth Assessment Report of the Intergovernmental Panel on Climate Change [Stocker, T.F., Qin, D., Plattner, G.-K., Tignor, M., Allen, S.K., Boschung, J., Nauels, A., Xia, Y., Bex V., and Midgley, P.M. (eds.)]. Cambridge University Press, Cambridge, United Kingdom and New York, NY, USA

Kong, F., and Yau, M.K. (1997). An explicit approach to microphysics in MC2. *Atmosphere-Ocean, 35,* 257–291.

Lachlan-Cope, T. (2010). Antarctic clouds. *Polar Research*. 29, 150-158.

Mailhot, J. 1994. The Regional Finite-Element (RFE) Model Scientific Description – Part 2: Physics. Meteorological Service of Canada Internal Science Report. Atmospheric Environment Service, Dorval, Quebec. March, 1994.

Mailhot, J., Belair, S., Lefaivre, L., Bilodeau, B., Desgagne, M.,Girard, C., Glazer, A., Leduc, A.-M., Methot, A., Patoine, A., Plante, A., Rahill, A., Robinson, T., Talbot, D., Tremblay, A.,Vaillancourt, P., Zadra, A., and Qaddouri, A. (2006). The15-km version of the Canadian regional forecast system. *Atmosphere-Ocean, 44*, 133–149.

Mailhot, J., Milbrant, J.A., Ciguere, A., McTaggart-Cowan, R., Erfani, A., Denis, B., Glazer, A., and Vallee, M. (2012). An experimental high-resolution forecast system during the Vancouver 2010 Winter Olympic and Paralympic Games. *Pure and Applied Geophysics*. doi10.1007/s00024-012-0520-6.

Medina, S. and Houze, R.A. (2003). Air motions and precipitation growth in Alpine Storms. *Quarterly Journal of the Royal Meteorological Society, 129*, 345-371.

Meehl, G.A, Boer, G.I., Covey, C., Latif, M., and Stouffer, R.J (2000). The coupled intercomparison project (CMIP). *Bulletin of the American Meteorological Society, 81,* 313-318.

Milbrandt, J. A. and Yau, K.Y (2005). A multimoment bulk microphysics parameterization. Part I: Analysis of the role of the spectral shape parameter. *Journal of Atmospheric Sciences, 62,* 3051-3064

Milbrandt, J., Mailhot, J., and Efrani, A. (2008). A new cloud microphysics scheme for the GEM-LAM 2.5. *In: Abstracts of Water, Weather and Climate: Science Informing Decisions 42nd Canadian Meteorological and Oceanographic Society Congress, 25–29 June 2008,* Kelowna, British Columbia, Canada.

Morrison, H.C., Shupe, M., and Curry, J.A. (2003). Modeling clouds observed at SHEBA using a bulk microphysics parameterization implemented into a single-column model. *Journal of Geophysical Research.* 108: 4255, doi:10.1029 2002JD002229

Paquin-Ricard, D., Jones, C., and Vaillancourt, P.A. (2010). Using ARM observations to evaluate cloud and clear-sky radiation processes as simulated by the Canadian regional climate model GEM. *Monthly Weather Review, 138,* 818–838.

Rinke, A. and Dethloff, K. (2000). On the sensitivity of a regional Arctic climate model to initial and boundary conditions. *Climate Research*, *14,* 101-113.

Rogerson. P. (2006). Statistical Methods for Geography (2nd Edition). SAGE Publications Ltd. 2455 Teller Road, Thousand Oaks, California.

Serreze, M.C., Barrett, A.P. and F. Lo (2005). Northern high-latitude precipitation as depicted by atmospheric reanalyses and satellite retrievals. *Monthly Weather Review*, *133*, 3407-3430. doi:10.1175/MWR3047.1.

Simjanovski, D., Girard, E., and Du, P. (2011). An evaluation of arctic cloud and radiation processes simulated by the limited-area version of the Global Multiscale Environmental Model (GEM-LAM). *Atmosphere-Ocean, 49,* 219-234.

Stewart, R.E., Burford, J.E., Hudak, D.R., Currie, B., Kochtubajda, B., Rodriguez, P., and Liu, J. (2004). Weather systems occurring over Fort Simpson, Northwest Territories, Canada, during three seasons of 1998–1999: Part 2. Precipitation features. *Journal of Geophysical Research, 189,* 1984-2012.

Sundqvist, H. (1978). A parameterization scheme for non-convective condensation including prediction of cloud water content *Quarterly Journal of the Royal Meteorological Society, 104,* 677-690.

Taylor, N. M., Sills, D. M., Hanesiak, J. M., Milbrandt, J. A., Smith, C. D., Strong, G. S, Skone, S.H., McCarthy, P.J., and Brimelow, J.C. (2011). The Understanding Severe Thunderstorms and Alberta Boundary Layers Experiment (UNSTABLE) 2008. *Bulletin of the American Meteorological Society*, *92,* 739-763.

Tjernstrom, M., Zagar, M., Svensson, G., Cassano, J.J., Pfeifer, S., Rinke, A., Wyser, K., Dethoff, K., Jones, C., Semmler, T., and Shaw, M. (2004). Modelling the Arctic boundary layer: an evaluation of six ARCMIP regional-scale models using data from the SHEBA project. *Boundary-Layer Meteorology, 117*, 337-381. DOI 10.1007/s10546-004-7954-z.

Uttal, T.U., Curry, J.A., McPhee, M.G., Perovich, D., Moritz, R.E., Maslanik, J.A., Guest, P.S., Stern, H.L., Moore, J.A., Turenne, R., Hieberg, A., Serreze, M.C., Wylie, D.P., Persson, O.G., Paulson, C.A., Halle, C., Morison, J.A., Wheeler, P.E., Makshtas, A., Welch, A., Shupe, M.D., Intrieri, J.M., Stamnes, K., Lindsey, R.W., Pinkel, R., Pegau, W.S., Stanton, T.P., and Grenfeld, T.C. (2002). Surface heat budget of the Arctic Ocean *Bulletin of the American Meteorological Society, 82***,** 255-275.

Wyser, K., Jones, G., Du, P., Girard, E., Willen, U, Cassamp, J., Christensen, J.H., Curry, J.A., Dethloff, K., Haugen J-E., Jacob, D., Koltzow, M., Laprise, R., Lynch, A., Pfeifer, S., Rinke, A., Serreze, M., Tjernstrom, M., and Zagar, M. (2008) An evaluation of Arctic cloud and radiation processes during the SHEBA year: simulation results from either Arctic regional climate models. *Climate Dynamics*, *30,* 203-223.

Yang, D., Ritchie, H., Desjardins, S., Pearson, G., MacAfee, A., and Gultepe, I. (2010). High-resolution GEM-LAM application in marine fog predictions: evaluation and diagnosis. *Weather and Forecasting*. *25,* 727-748. doi:10.1175/2009WAF2222337.1

Zhang, J., Gong, W., Leaitch, W.R., and Strapp, W. (2007), Evaluation of modeled cloud properties against aircraft observations for air quality applications. *Journal of Geophysical Research*, *112,* doi:10.1029/2006JD007596.

CHAPTER 6: SUMMARY AND CONCLUSIONS

Overall this thesis makes a significant contribution to improve the understanding of physical processes associated with orographic precipitation in high latitude mountain environments, and provides a number of key observations of cloud and precipitation features required to improve our modelling capabilities of these critical features.

6.1 Thesis Summary

- In Chapter 1, the motivation for this research was outlined and the objectives were stated.
- In Chapter 2, the importance and current state of knowledge of cold season orographic precipitation and the various controlling physical processes involved were discussed.
- In Chapter 3, orographic cloud and precipitation features over southern Baffin Island were characterized. A comparative analysis of how cloud and precipitation features from ocean regions upstream were modified by the orography, in addition to the variability of these features over diverse synoptic and sea ice conditions was performed.
- In Chapter 4, the processes controlling an unexpected small accumulation snowfall event in Iqaluit, Nunavut were examined. Analysis of the Global Environmental Multi-scale limited area model (GEM-LAM 2.5) showed that upstream convection and upslope processes were affected by model errors, which contributed to errors in its forecast.

- In Chapter 5, the accuracy of the GEM-LAM 2.5 model was further evaluated for 28 vertical profiles during STAR. Descriptions of model errors and proficiencies for different synoptic forcing and surface environments, including orography, open water and sea ice were shown. The skill of the model was also discussed in the context of its ability to accurately represent clouds and precipitation features.
- In this final Chapter (6), a summary of major findings from the three research chapters is provided, followed by a discussion of the limitations of this work, opportunities for future work in the subject area and general conclusions.

6.2 Summary of major findings

This study is the first to characterize cloud and precipitation over southern Baffin Island and surrounding area with a research aircraft. No comparable measurements aloft have been obtained in the region previously. Using high-resolution data collected on southern Baffin Island, Nunavut and surrounding area during the Storm Studies in the Arctic (STAR) field project the main scientific contributions and findings from this thesis are as follows.

1. Precipitation and cloud features over southern Baffin Island were shown to differ over orography compared to the adjacent ocean regions upstream. These features were also found to vary based on synoptic organization.

Results from Chapter 3 and Chapter 4 showed that precipitation enhancement occurred on the windward slopes of southern Baffin Island. Although this result is not unexpected, this study was able to provide specific details on cloud and precipitation features in the region, show how they are modified over the orography, in addition to the variability of these features over diverse synoptic and sea ice conditions.

Maximum reflectivity over the orography was ~18 dBZ, but reflectivity in the vertical profiles did not usually exceed 12 dBZ. When a high concentration of sea ice was present, maximum reflectivity was low (5 dBZ). Maximum reflectivities over the orography were found to be 3 to 10 dBZ higher than adjacent ocean regions upstream and the precipitation structure was more variable in all cases, regardless of synoptic organization or sea ice extent. Over the orography, fall streaks were common, compared to more uniform stratiform precipitation upstream. In addition, with increasing distance inland, the general characteristics of the profiles had higher reflectivities aloft with decreasing reflectivities towards the surface.

Events driven by large-scale cyclonic circulations were characterized by increased cloud depth, cloud height, total water content, particle concentrations and higher reflectivity values over the orography compared to weak synoptic forcing. This result, although not surprising, does imply that organized large-scale circulations may result in greater precipitation enhancement over the terrain in the region. However, results from Chapter 3 and Chapter 4 showed that weakly organized synoptic systems are also important for precipitation production and enhancement over the orography in the region and should receive more attention in the literature.

2. Precipitation enhancement over the orography on southern Baffin Island was found to be strongly associated with gravity waves, terrain shape, atmospheric stability, upslope flow at all levels, and low sea ice extent upstream of the topography.

The results in Chapter 3 revealed that a number of factors caused precipitation enhancement over the orography in the region. These results contribute to the existing body of knowledge on cloud systems and precipitation processes in northern regions, but are uniquely focused on the influence of the orography on these critical features. Gravity waves and upslope flow at all levels of the atmosphere (no low-level blocking) were the main factors associated with the greatest precipitation enhancement. This study is the first to show vertical radar profile of a gravity wave feature in the Arctic. Low sea ice extent (< 3/10s) upstream of regional topography, in conjunction with a strong temperature gradient between the atmosphere and ocean, were shown to result in upward exchanges of heat and moisture and the initiation of convection, creating an environment conducive to hydrometeor growth, prior to orographic lifting.

3. Sublimation, low-level blocking and high sea ice extent upstream, were strongly associated with decreasing precipitation over the orography of southern Baffin Island.

Sublimation below cloud base and between dry layers was shown to reduce or eliminate precipitation reaching the surface in all cases. Although this result is not unique and has been shown to occur in the Arctic in other studies [*Laplante et al*., 2012; *Henson et al*., 2011; *Roberts et al.,* 2008; *Stewart et al.,* 2004; *Burford and Stewart*, 1998], this study illustrated where sublimation was likely to take place in the region. Results showed that with increasing distance from the coast (30 to 60 km), particles were more susceptible to sublimation. Results also showed that sublimation was more common over the orography than over adjacent ocean regions. Lower concentrations of small (100 to 800 μm) particles existed over the orography compared to upstream regions. This may suggest that smaller particles over the orography are sublimating before reaching the ground due to their low density and low fall velocities. It is likely that the lower concentration of small particles over the orography is also the result of particle aggregation that is occurring. Without aggregation or accretion, it is probable that more ice particles would have sublimated before reaching the ground.

The presence of sea ice also influenced precipitation over the orography. High ice extent (>8/10s) contributed in part to low total water content and liquid water content throughout the cloud profile by limiting upward exchanges of heat and moisture. The presence of sea ice also aided in development of a thermal inversion, which resulted in low-level blocking and reduced lift of surface winds over the terrain. Consequently, there was less chance for enhanced condensation and precipitation by reducing upslope flow.

4. The nature of precipitating hydrometeors over the orography of southern Baffin Island was variable. Accretion and aggregation were identified as important determinants of whether precipitation reached the ground.

Results from Chapter 3 were the first to characterize hydrometeors in clouds over the orography of southern Baffin Island. Aircraft measurements showed that mid-to-upper clouds were characterized by a combination of irregularly shaped particles, polycrystalline particles, and bullet and column rosettes. Fragmented particles were also present, suggesting that hydrometeors were additionally formed through secondary processes not involving nucleation.

Hydrometeors with light to moderate accretion were present and more frequent particle aggregation was identified over the orography. Previous ground-based studies have noted the occurrence of accretion and aggregation at the surface in Iqaluit [*Roberts et al.* 2008; *Henson et al.*, 2011] but this study was able to offer a more comprehensive explanation of why there was enhanced particle growth over the terrain. Dynamic and thermodynamic factors, such as gravity waves and embedded convection over the orography contributed to increased deposition and precipitation generation aloft, in addition to increasing the potential for particle collisions. This resulted in a higher concentration of large hydrometeors (1000 to 2600 μm) over the orography compared to similar heights over the adjacent ocean upstream. Without aggregation or accretion, it is probable that more ice particles would have sublimated before reaching the ground.

Despite environmental differences between mid-latitude regions and the Arctic, hydrometeors observed over Baffin Island and surrounding area were not substantially different from observations during field projects in mid-latitude regions [*Stoelinga et al.,* 2001; *Rotunno & Houze,* 2005; *Isaac et al.,* 2012; among others]. Results from this study also showed similarities with other observations from the western Canadian Arctic despite differences in orography [*Korolev et al.* 1999; *Morrison et al.,* 2011; among others].

5. The complexity of small accumulation snowfall events over southern Baffin Island may represent a significant challenge for forecasting and modelling.

Results from Chapter 4 were the first to use a combination of ground-based and airborne radar, along with surface and upper air observations to characterize a precipitation event in the eastern Canadian Arctic. These results contribute to the existing body of knowledge on cloud systems and precipitation processes in northern regions, but the use of multiple sensors offered a uniquely comprehensive assessment of these features. In addition, the processes controlling small accumulation events in the region had not been investigated in sufficient detail, despite their important contribution in the moisture cycling in the region and the STAR data provided a relevant opportunity to improve our understanding of these types of events.

In this case study, the arrangement of cold atmospheric temperatures over a relatively warm ocean (near 0°C) generated low-level convective instability where energy was actively being released in the atmosphere. Strong upslope flow of the unstable air promoted cloud and precipitation production over the terrain. The passing of the trough was shown to provide additional convergence aloft, that when combined with orographic forcing resulted in an environment conducive to thicker cloud (up to 900 m higher) and enhanced hydrometeor growth. With the combined influence of these factors, cloud development and precipitation generation were forced to the altitudes required for these features to penetrate over the terrain, which resulted in precipitation at Iqaluit.

A lack of snow in the model (50% lower than observations) was attributed in part to its representation of the upstream environment. At lower altitudes, the model consistently overestimated temperature (~ 2 °C) and moisture (dew-point temperature between 0.5 and 3 °C higher than observations), indicating reduced exchange between ocean and atmosphere, which may have limited convection. Further errors were shown in the dew-point depression profiles, cloud-bases were too high and dry layers were present in some profiles. The combination of these factors reduced the potential for hydrometeor growth and therefore the amount of precipitation that reached Iqaluit.

Wind speed errors were also a factor. At altitudes lower than 900 hPa, the model winds were under-predicted (by 1 to 4 m s^{-1}), which reduced upslope processes (lower Froude number). It is also possible that due to a general positive wind speed bias at altitudes above 900 hPa (up to 5 m s^{-1}), smaller hydrometeors would have been advected downstream, further reducing accumulation at the Iqaluit site. Results showed that the model was skilful in its ability to pick up the passage of the trough over Iqaluit but approximately 3-hours later than observations, delaying precipitation onset.

6. Further improvements and verification of the GEM-LAM 2.5 model are required to better represent and simulate the Arctic environment.

Results from Chapter 5 of this thesis contribute to an improved understanding of the accuracy of the GEM-LAM 2.5 model around southern Baffin Island. Based on evidence from the four case studies, results from this study confirm some regional variation in its performance in the Arctic [*Paquin-Ricard, et al.*, 2010; *Simjanovski et al.,* 2011; among others] along with variability in its ability to characterize high and mid-latitudes mountainous environments [*Yang et al.*, 2010; *Malihot et al.,* 2012; among others].

In Chapter 5, the model was shown to generally overestimate temperature (1 to 2˚C too warm) compared to observations. This consistently occurred between the surface and 900 hPa. At altitudes above 900 hPa, temperature errors were more variable, but usually remained positive. Differences in errors were found based on synoptic forcing and surface environment. Errors were found to be ~ 1°C smaller for cyclone driven events, compared to events with weak synoptic forcing. The model was shown to be most variable over land, where it was not uncommon to have both cold and warm bias in the same profiles (~ ±1°C). Large errors were found over ice.

Dew-point temperature was frequently overestimated between 2 and 4˚C, and specific humidity levels were too high (0.2 to 0.4 g kg^{-1}). Over open water, standard errors for moisture were much larger for cyclonically driven events (~0.7 g kg^{-1}) compared to weakly forced events (~0.2 g kg^{-1}), which may have implications for accurate precipitation simulation in the model. In an environment with high sea ice cover the model showed a greater tendency to underestimate moisture content (-0.1 to -0.2 g kg^{-1}) and was unable to simulate the thermal inversion feature represented in the observations, influencing the stability and dynamics in that case.

In all case studies the model showed a tendency to underestimate winds at altitudes lower than 900 hPa (~ -3 m s^{-1}). This altitude is similar to the heights of the orography of the Hall and Meta Incognita Peninsulas on Baffin Island, which suggests that upslope processes may be weakened in the model. Wind direction was also poorly represented over the ice-covered surface case, where error usually exceeded 90˚.

However, wind direction standard error values were comparably low for other cases and surface environments (≤ 20°). A general relationship was shown with respect to wind direction error and proximity to land. Standard error increased for all cases when profile location approached the terrain.

The ability to represent clouds was variable. In cases where multiple cloud layers were present GEM-LAM 2.5 captured this feature most of the time. However, due to errors in temperature and moisture, the dry layer depth was often too deep (up to 800 m). In contrast, there were some instances where GEM-LAM 2.5 suggested multiple layers in the profile, not confirmed by observations. This was more common in profiles from weakly forced synoptic events. Generally cloud-tops were too high in the model (~ 300 m) and cloud-bases were too low (-50 to -500 m). This was fairly consistent for cyclonically driven events. Cloud-tops were also overestimated with similar error for events with weak synoptic forcing, but cloud-base errors were more variable.

6.3 Limitations and future work

Although Chapter 3 and Chapter 4 contain significant results on the characterization of cold season cloud and precipitation features in the south-east Canadian Arctic, and some of the first and most comprehensive to be reported, these results are limited by the number of case studies over a short period of time used in this analysis. Due to aforementioned challenges and the cost of acquiring data in a high latitude environment with complex terrain, it is not uncommon for datasets, such as the one collected during STAR, to be non-continuous, regionally specific and case study focused. As a consequence, the dataset is inadequate to make generalizations on the climatology of these critical features and assess changes overtime without continued monitoring. However, even if broad generalizations are not possible, this thesis is an important step towards an improved understanding of the factors that influence cloud and precipitation in Arctic regions with complex topographies.

Additional limitations of the work relates to the sampling constraints of the research aircraft. In Chapter 3, data collection on particle habit and size spectrum could only occur above a certain altitude because of safety requirements, resulting in no in situ data below a critical altitude. In the case of STAR this altitude was two-times the height of the underlying terrain. As a result, the characteristics of cloud and precipitation features presented in this thesis do not necessarily represent the general characteristics at altitudes closer to the terrain. Microphysical characteristics were assessed at the surface at Iqaluit, but the hydrometeors sampled had already passed over considerable topographies and may not have provided the best representation of the character of these features over higher elevation. The use of a helicopter, if one had been available, could have supplemented the data collection at altitudes closer to the terrain.

Results from Chapter 5 were limited by the relatively small amount of data used to evaluate the model. Of the 14 Intensive Observation Periods (IOPs) during STAR, only four IOPs corresponded to events where GEM-LAM 2.5 data were available for comparison. The acquisition of data over entire IOP time periods rather than just aircraft flight times would have provided the opportunity to include other STAR observations at Iqaluit (such as rawionsondes) in the analysis. The analyses would have also benefited from a more comprehensive temporal investigation of the model performance during each event, in addition to including more case studies to strengthen the statistical analysis had additional GEM-LAM 2.5 data been available. If time and resources had allowed, output from the regional and global model should have also been acquired to allow for the evaluation of the model at different resolutions. The analysis would have also been improved with a more spatial evaluation of the model.

The comparison between the model and the observations in Chapter 5 took place along single dropsonde vertical profiles. The GEM-LAM 2.5 model is a high-resolution model but still over generalizes and simplifies areas that may or may not be homogeneous with respect to terrain height and surface environment. Vertical profiles from neighbouring grid cells could have supplemented the analysis. This would have resulted in a comprehensive evaluation of the models spatial representation of the environment as well. In particular, this may have been an improved methodology when evaluating the Froude number between observation and model.

Although it is not uncommon to evaluate models using observations from an individual storm or case study, it is clear from the results of Chapter 5 that future work should include an assessment of the GEM-LAM 2.5 model in the Arctic over a longer time period. A similar evaluation of model performance to the one performed during the Science and Nowcasting of Olympic Weather for Vancouver 2010 (SNOW-V10) project could be completed at the Iqaluit Environment Canada site because of the existing infrastructure and sounding program. The comparison would also benefit from some automatic stations on the elevated terrain in the region to continue progress on understanding model performance in complex topographies. During the cold season, this evaluation would be further advanced with automatic stations located on sea ice around southern Baffin Island.

To continue working towards a more advanced characterization of cloud and precipitation in the region requires enhanced observations at the surface by gauges at increased sampling densities and higher elevation sites. Ground-based radars, macro-photography and other special surface instrumentation that can provide information on the total amount and microphysical composition of precipitation such as shape, particle size spectrums, concentration and phase are also required. The data were not only necessary to address continued issues related to impacts of anticipated climatic changes, but also weather forecasting. Realistically, the installation/maintenance challenges and costs associated with monitoring in the Arctic and in complex terrain means that we must do the best we can with the resources/instrumentation currently available but the scientific community should continue intensive field programs when funding is available.

Because monitoring and data collection remain an ongoing challenge in the Arctic, there will likely be an increased reliance and focus on alternative techniques such new satellite radar technologies like the one a part of the Global Precipitation Mission (GPM), launched March 2014. This satellite carries a precipitation profiling radar with a 5 km by 5 km horizontal sampling resolution and a 250 to 500 m vertical resolution, which are larger than ideal for sampling cloud and precipitation processes but is an improvement over current data. However, results from this thesis show that the minimum reflectivity detected by the GPM satellite is inadequate for precipitation detection in this region (12 dBZ). Further validation will be required to assess its utility in monitoring precipitation in the Arctic.

Future field projects should collect data comparable to STAR with a greater focus on enhanced sampling strategies over the orography. Specifically, I would like to see the installation of an automatic gauge network over one of the peninsulas on Baffin Island. Gauges could be installed in a linear format, from the coast of the windward slope over the orography of the peninsula, to the coast of the leeside. This would allow for a relevant assessment of actual accumulation over the orography during events and an invaluable opportunity to examine accumulation in the GEM model over the terrain.

Future research in the region should also include a series of model sensitivity studies. Both topographical features and atmospheric conditions could be modified. For example if a sensitivity study was performed on the F4 case, the removal, lowing and raising of the orography of the Meta Incognita Peninsula may provide more details on the role of topography in the Iqaluit snowfall event. Results would likely provide more details on the influence of this factor (and others) on precipitation and its distribution over the region. In addition the model showed a consistent over-prediction of temperature near the surface (too warm). It would be interesting to apply a false temperature modification of approximately +2°C below 900 hPa to see if convective processes were still weakened in the upstream environment. A sensitivity study to further investigate the influence of sea ice on cloud and precipitation production would also be useful.

6.4 Conclusions

The overarching objective of this thesis was to better understand the physical processes associated with orographic cloud and precipitation in a high latitude mountainous region. A unique, highly detailed and extensive dataset collected during the Storm Studies in the Arctic field project in the south-east Canadian Arctic formed the basis of the research carried out to address this objectives of this work proposed in Chapter 1.

Key findings summarized in section 6.2 show that cloud and precipitation were enhanced over the complex terrain of southern Baffin Island. The characteristics of these critical features were shown to differ over the orography compared to the adjacent ocean regions upstream of the terrain, but also with variable event forcing and sea ice extent. Multiple factors were shown to influence the characteristics of cloud and precipitation in the study region by either enhancing or reducing them over the orography. An evaluation of the Canadian operational limited area model provided insights into why some precipitation events are not well forecast by the model. The evaluation also demonstrated both deficiencies and proficiencies in model performance during STAR case studies.

An improved understanding of cold season high latitude cloud and precipitation processes and their characteristics has been achieved. The capacity of both operational and climate models to use this information will depend on their resolution range and the sensitivity of the parameterization schemes including microphysics. As computing power improves, so should our ability to incorporate more advanced and computationally demanding parameterization schemes into these models, allowing for improved simulations of the environment.

Although these results show progress, future work can expand upon the analysis presented through the continued collection of high-resolution data and a more comprehensive assessment of limited area models in the region. Considerable changes are occurring in the Arctic in response to global climate change. The impact of these changes on cloud and precipitation in the region will likely have profound effects on local ecosystems as well as effect many communities across the region. This necessitates continued monitoring of these critical features and understanding their role in the hydrological cycle and the region's climate.

6.5 References

Burford, J.E. and Stewart, R.E. (1998). The sublimation of falling snow over the Mackenzie River Basin. *Atmospheric Research, 49*, 289-214.

Hanesiak, J., Stewart, R.E., Taylor, P., Moore, K., Barber, D., McBean, G., Strapp, J.W. Wolde, M., Goodson, R., Hudson, E., Hudak, D., Scott, J., Liu, G., Gilligan, J., Biswas, S., Desjardins, D., Dyck, R., Fargey, S., Field, R., Gascon, G., Gordon, M., Greene, H., Hay, C., Henson, W., Hochheim, K., Laplante, A., Martin, R., Melzer, M.A., and Zhang, S. (2010). Storm Studies in the Arctic: The meteorological field project. *Bulletin of the American Meteorological Society, 91,* 47-68. doi:10.1175/2009BAMS2693.1

Henson, W., Stewart, R., and Hudak, D. (2011). Vertical reflectivity profiles of precipitation over Iqaluit, Nunavut during Autumn 2007. *Atmospheric Research*, *99*, 217-229. doi: 10.1016/j.atmosres.2010.10.009.

Korolev, A.L., Issac, G.A., and Hallett, J. (1999). Ice Particle habits in Arctic Clouds. *Geophsyical Research Letters, 26*, 1299-1302.

Laplante, A., Stewart, R., and Henson, W. (2012). Characterization of cloud and precipitation features over southern Baffin Island and adjacent areas during STAR. *Atmosphere-Ocean*, *50*, 54-69. doi:10.1080/07055900.2011.646535.

Mailhot, J., Milbranbt, J.A., Ciguere, A., McTaggart-Cowan, R., Erfani, A., Denis, B., Glazer, A., and Vallee, M. (2012). An experimental high-resolution forecast system during the Vancouver 2010 Winter Olympic and Paralympic Games. *Pure and Applied Geophysics*. doi10.1007/s00024-012-0520-6.

Paquin-Ricard, D., Jones, C., and Vaillancourt, P.A. (2010). Using ARM observations to evaluate cloud and clear-sky radiation processes as simulated by the Canadian regional climate model GEM. *Monthly Weather Review, 138,* 818–838.

Roberts, E., Nawri. N., and Stewart, R.E. (2008). On the storms passing over southern Baffin Island during Autumn 2005. *Arctic,* 61, 309-321.

Simjanovski, D., Girard, E., and Du, P. (2011). An evaluation of arctic cloud and radiation processes simulated by the limited-area version of the Global Multiscale Environmental Model (GEM-LAM). *Atmosphere-Ocean, 49,* 219-234.

Stewart, R.E., Burford, J.E., Hudak, D.R., Currie, B., Kochtubajda, B., Rodriguez, P., and Liu, J. (2004). Weather systems occurring over Fort Simpson, Northwest Territories, Canada, during three seasons of 1998–1999: Part 2. Precipitation features. *Journal of Geophysical Research, 189,* 1984-2012.

Woods, C.P., Stoelinga, M.T., Locatelli, J.D., and Hobbs, P.V. (2005). Microphysical processes and synergistic interactions between front and orographic forcing of precipitation during the 13 December 2001 IMPROVE-2 event over the Oregon Cascades. *Journal of Atmospheric Sciences, 62***,** 3492-3519.

Yang, D., Ritchie, H., Desjardins, S., Pearson, G., MacAfee, A., and Gultepe, I. (2010). High-resolution GEM-LAM application in marine fog predictions: evaluation and diagnosis. *Weather and Forecasting*. *25,* 727-748. doi:10.1175/2009WAF2222337.1

APPENDIX A: CONTRIBUTIONS OF AUTHORS TO THESIS CHAPTERS

Field data used in Chapter 3, Chapter 4 and Chapter 5 was collected in participation with STAR personal (principal investigators and students), along with Environment Canada and the National Research Council of Canada employees. I was involved in collecting much of the data used. In each Chapter the ideas for presenting the results and the ensuring discussion were largely my own. The contributions from co-authors to the manuscripts that make up this thesis are described below.

Chapter 3

Dr. John Hanesiak and Dr. Ronald Stewart provided expertise and discussion regarding cloud and precipitation characteristics, and logistical and financial support for the fieldwork. They also provided helpful comments on manuscript drafts. Dr. Mengistu Wolde provided technical support for the correction of the airborne Doppler radar data to remove aircraft motion effect and quality controlled the data.

Chapter 4

Dr. William Henson performed the ground-based X-band Doppler radar analysis (plotting and quality control) and helped with the interpretation of the data. He created Figures 5.8, 5.9, and 5.10. We worked in cooperation to create Figure 5.7. He also provided helpful comments on early manuscript drafts. Dr. John Hanesiak provided expertise and discussion regarding the results, and logistical and financial support for the fieldwork. Ron Goodson ran the GEM-LAM 2.5 in experimental mode and provided the model data used in analysis.

Chapter 5

Dr. John Hanesiak provided expertise and discussion regarding the model comparison results, and logistical and financial support for the fieldwork. He also provided helpful comments on early manuscript drafts that helped shape the presentation and discussion of results. Ron Goodson ran the GEM-LAM 2.5 in experimental mode and provided the model data used in this analysis.

APPENDIX B: SUPPLIMENTAL FIGURES

This appendix contains additional figures used in Chapter 5 analysis. Section B-1 contains all the dropsonde and model sounding profiles of temperature and dew-point temperature with height used for analysis in section 5.3.3.1. Section B-2 shows the residuals from the comparison of the dropsonde and model sounding profiles. Key findings from these figures are summarized in section 5.3.3.2 of this thesis.

B-1 Skew-T Diagrams

Figure B1-1: F3 - case study (released over open water). Comparison of dropsonde data (black) and extracted GEM-LAM 2.5 sounding profiles. Temperature (solid line) and dew-point temperature (dashed line). Profiles are labelled with case ID, release time (UTC November 8, 2007), and surface environment.

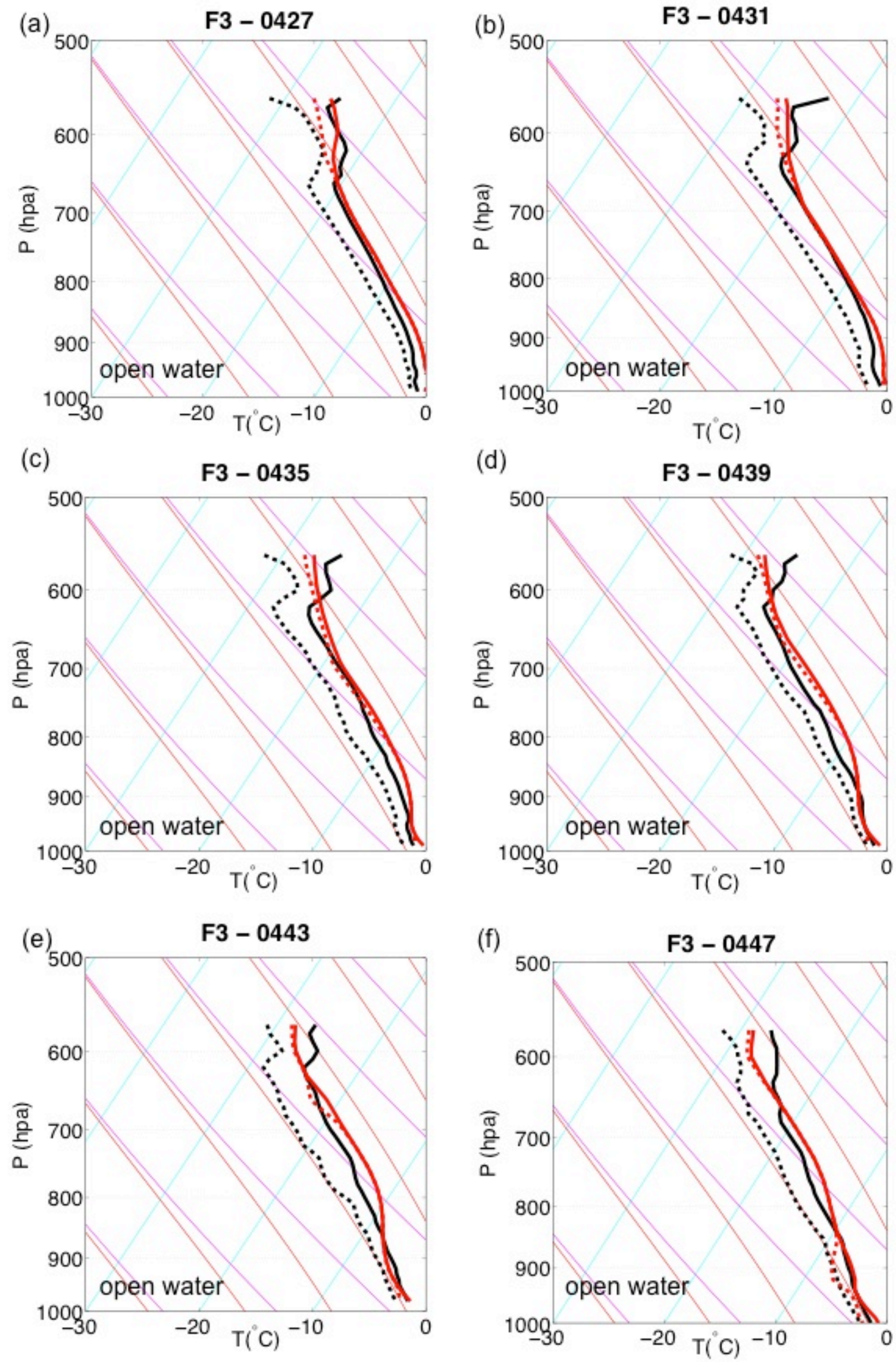

Figure B1-2: F3 - case study (released over land). Comparison of dropsonde data (black) and extracted GEM-LAM 2.5 sounding profiles. Temperature (solid line) and dew-point temperature (dashed line). Profiles are labelled with case ID, release time (UTC November 8, 2007), and surface environment.

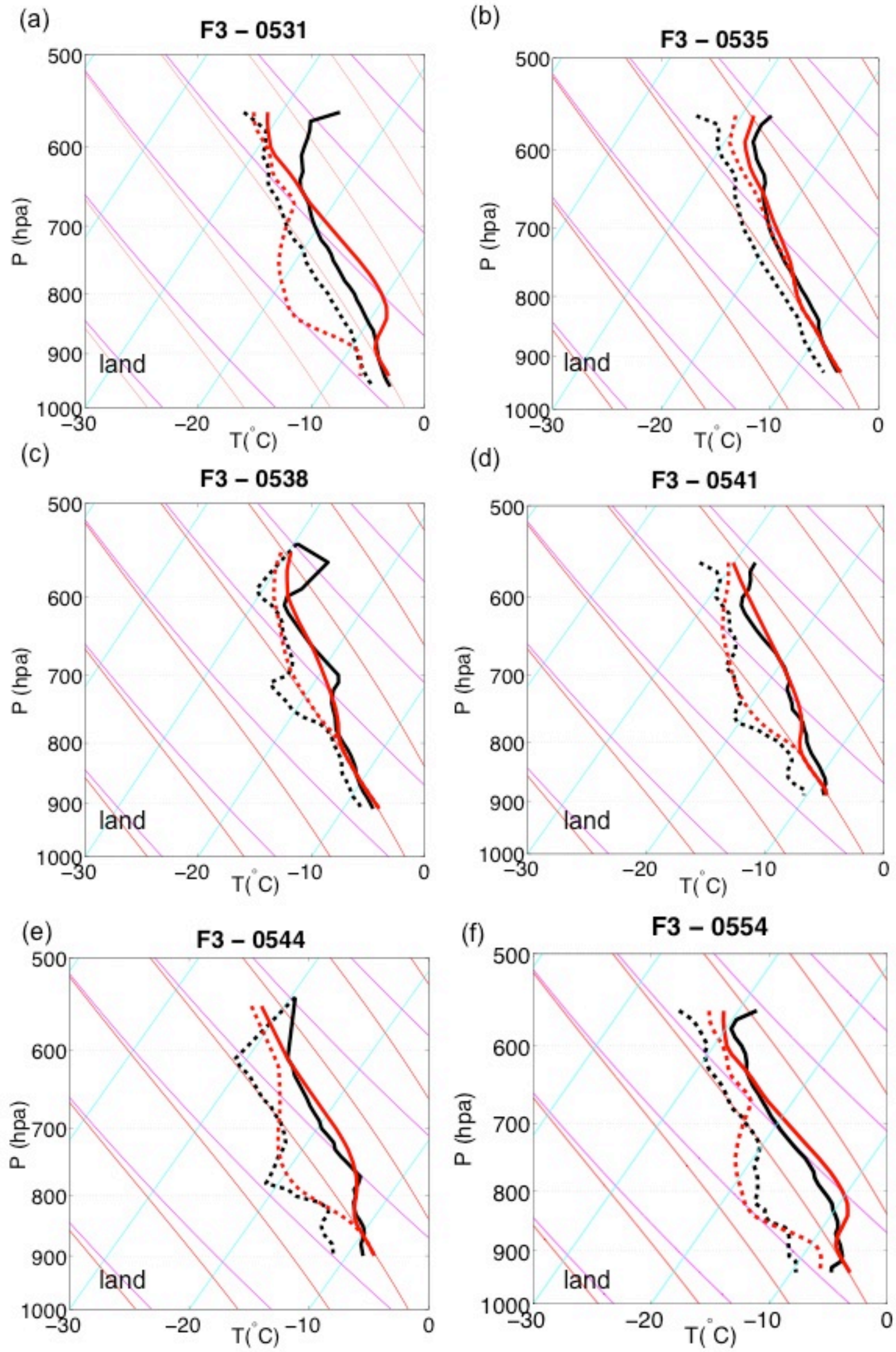

Figure B1-3: F4 - case study, modified from Figure 4.14 [Fargey et al., 2014b]. Comparison of dropsonde data (black) and extracted GEM-LAM 2.5 sounding profiles. Temperature (solid line) and dew-point temperature (dashed line). Profiles are labelled with case ID, release time (UTC November 9, 2007), and surface environment.

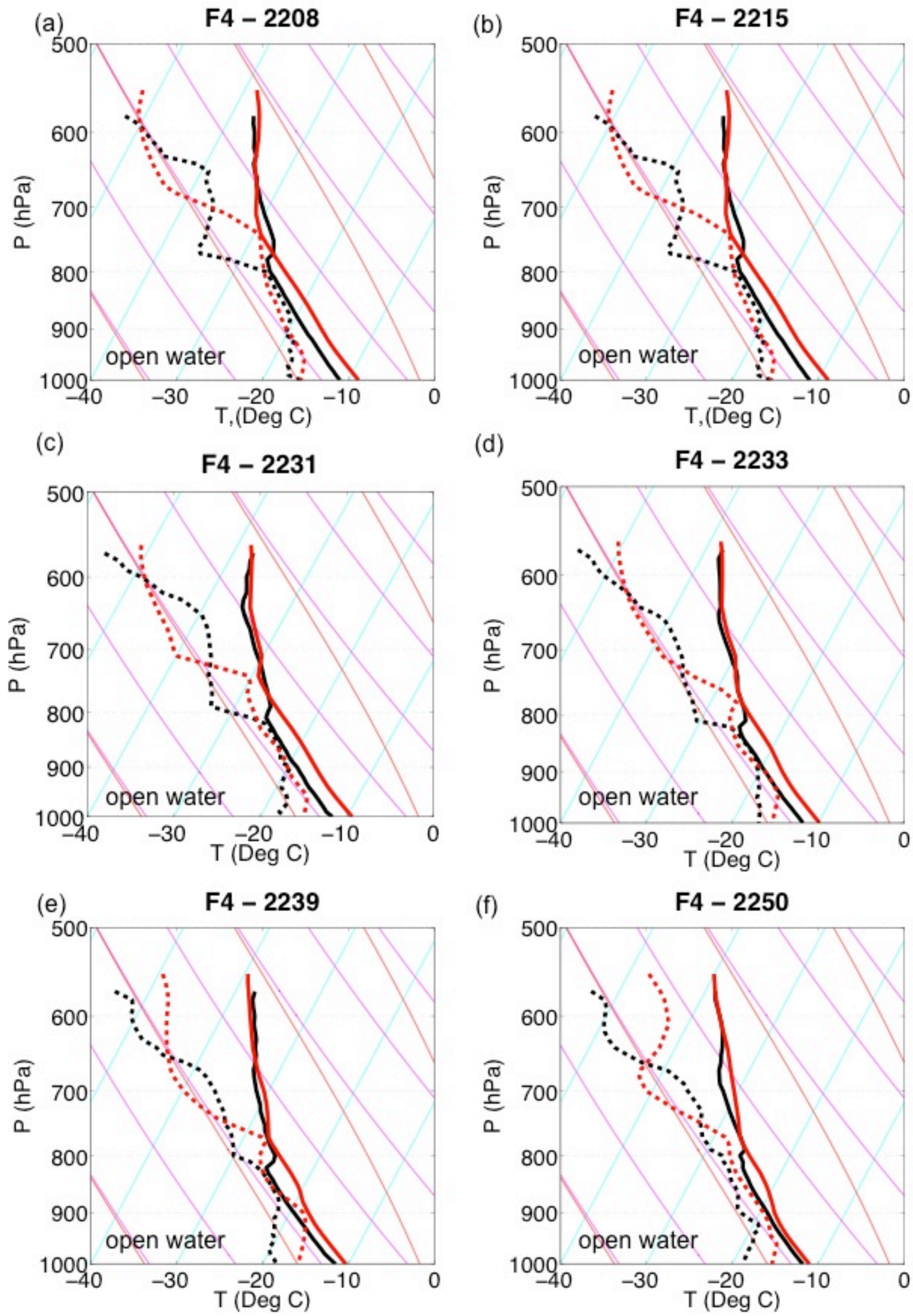

Figure B1-4: F5 - case study. Comparison of dropsonde data (black) and extracted GEM-LAM 2.5 sounding profiles. Temperature (solid line) and dew-point temperature (dashed line). Profiles are labelled with case ID, release time (UTC November 12, 2007), and surface environment.

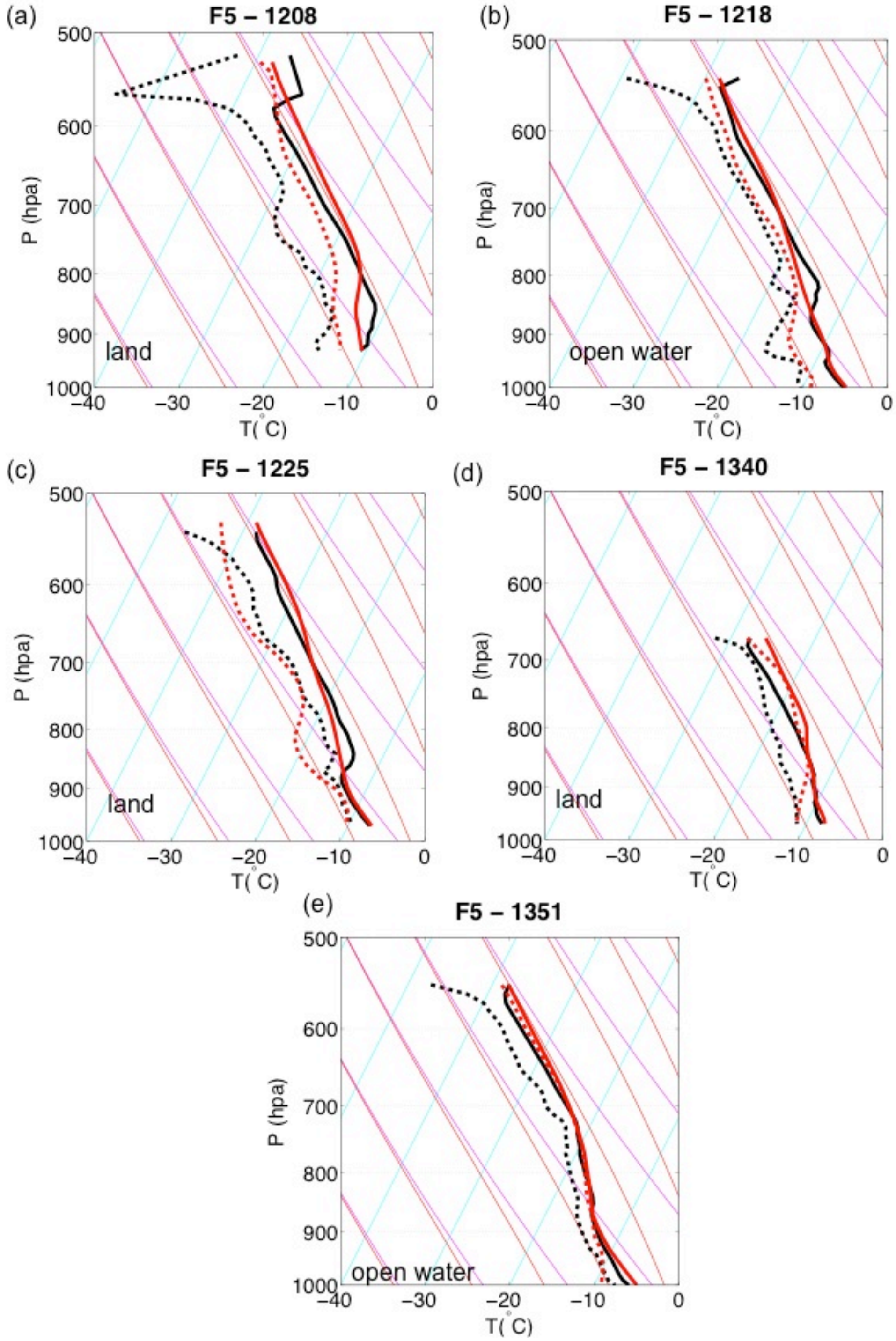

Figure B1-5: F13 - case study. Comparison of dropsonde data (black) and extracted GEM-LAM 2.5 sounding profiles. Temperature (solid line) and dew-point temperature (dashed line). Profiles are labelled with case ID, release time (UTC November 28, 2007), and surface environment.

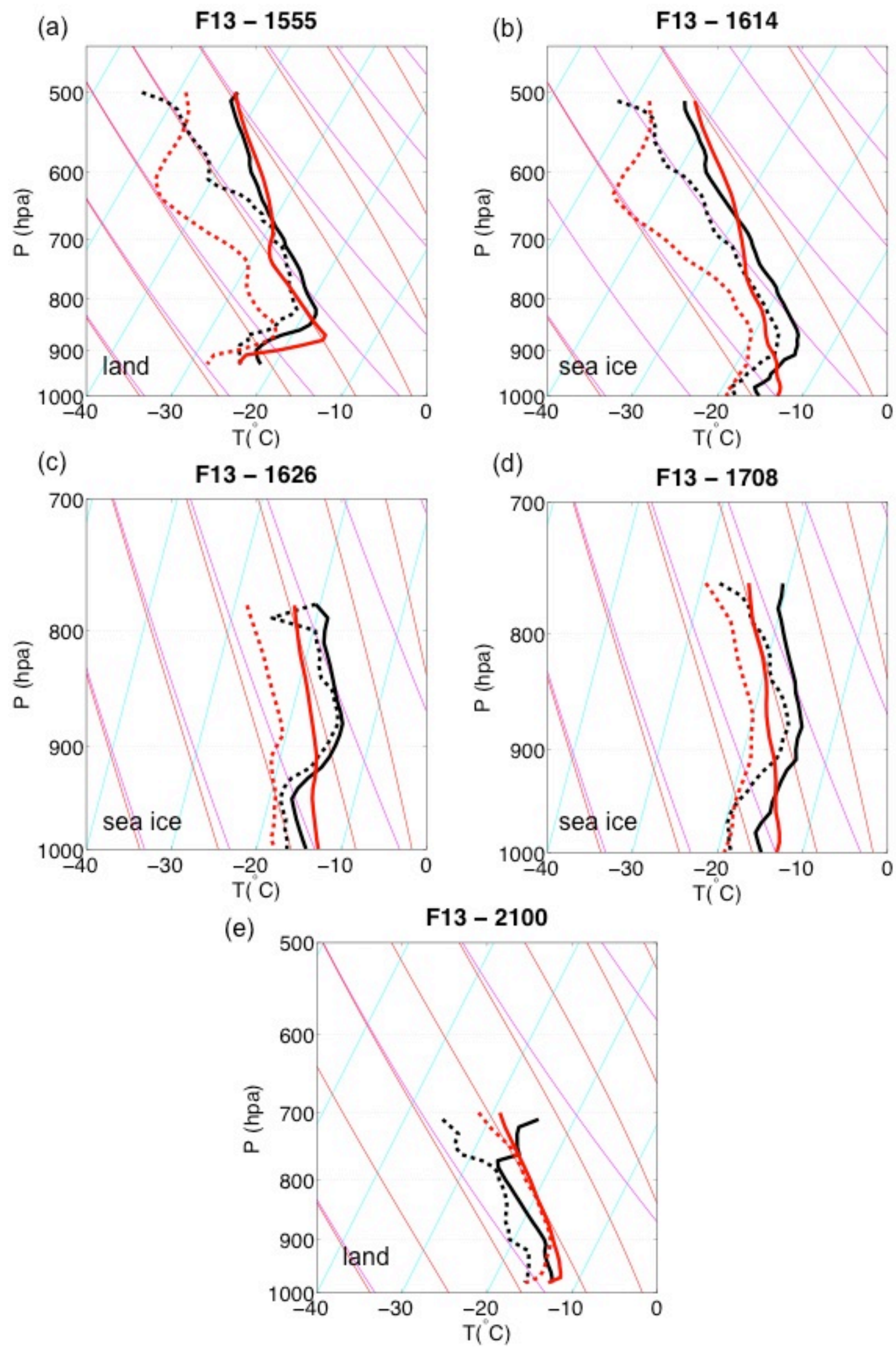

B-2 Residual analysis of vertical profiles

Figure B2-1: Bias (black line) and GEM-LAM 2.5 model residuals (coloured lines), from the comparison of extracted GEM-LAM 2.5 sounding profiles to dropsonde data for Temperature (Deg). Data is plotted by surface environment, and each case study is shown with a unique colour. Residual (model minus observation).

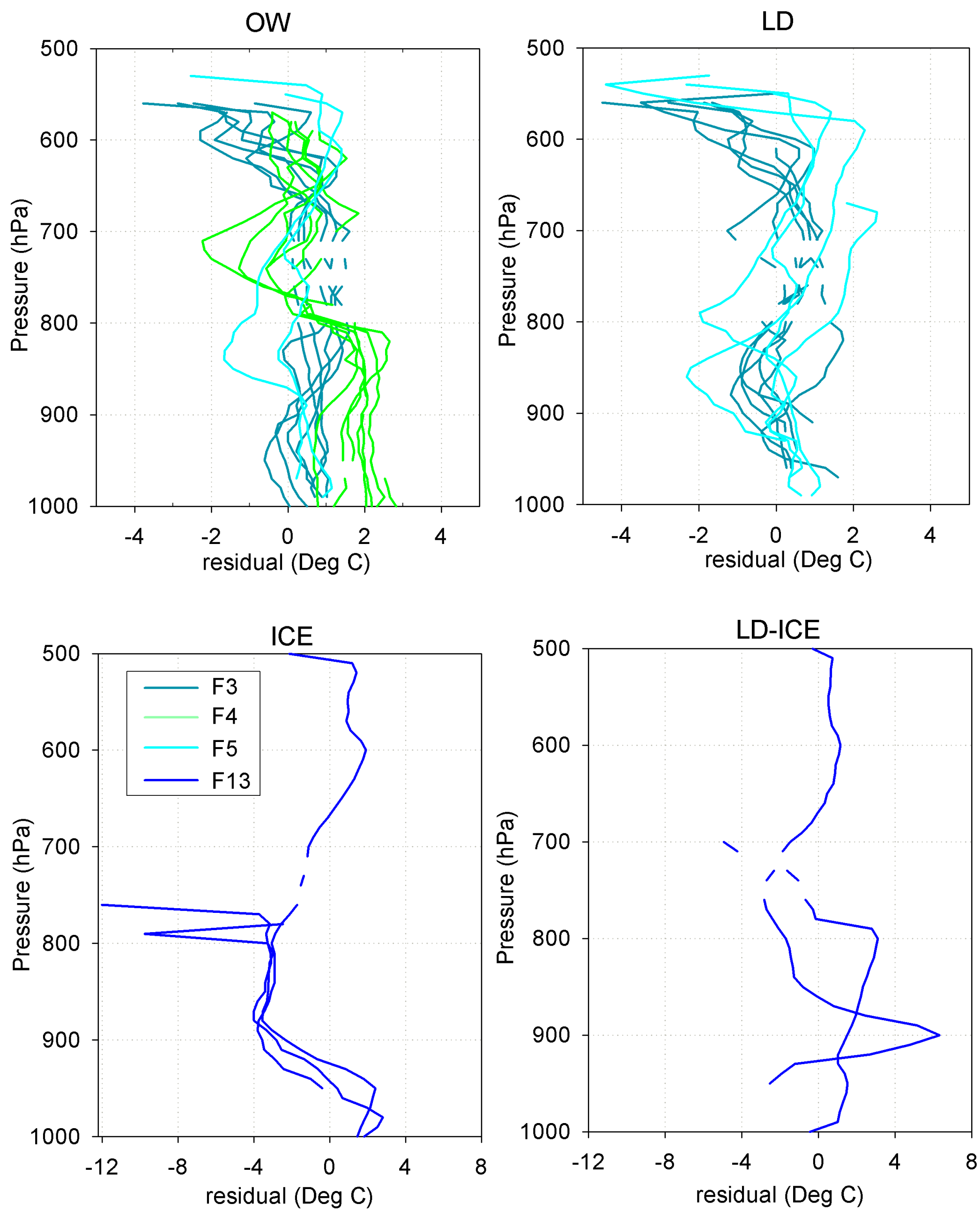

Figure B2-2: Bias (black line) and GEM-LAM 2.5 model residuals (coloured lines), from the comparison of extracted GEM-LAM 2.5 sounding profiles to dropsonde data for Dew-point temperature (Deg). Data is plotted by surface environment, and each case study is shown with a unique colour. Residual (model minus observation).

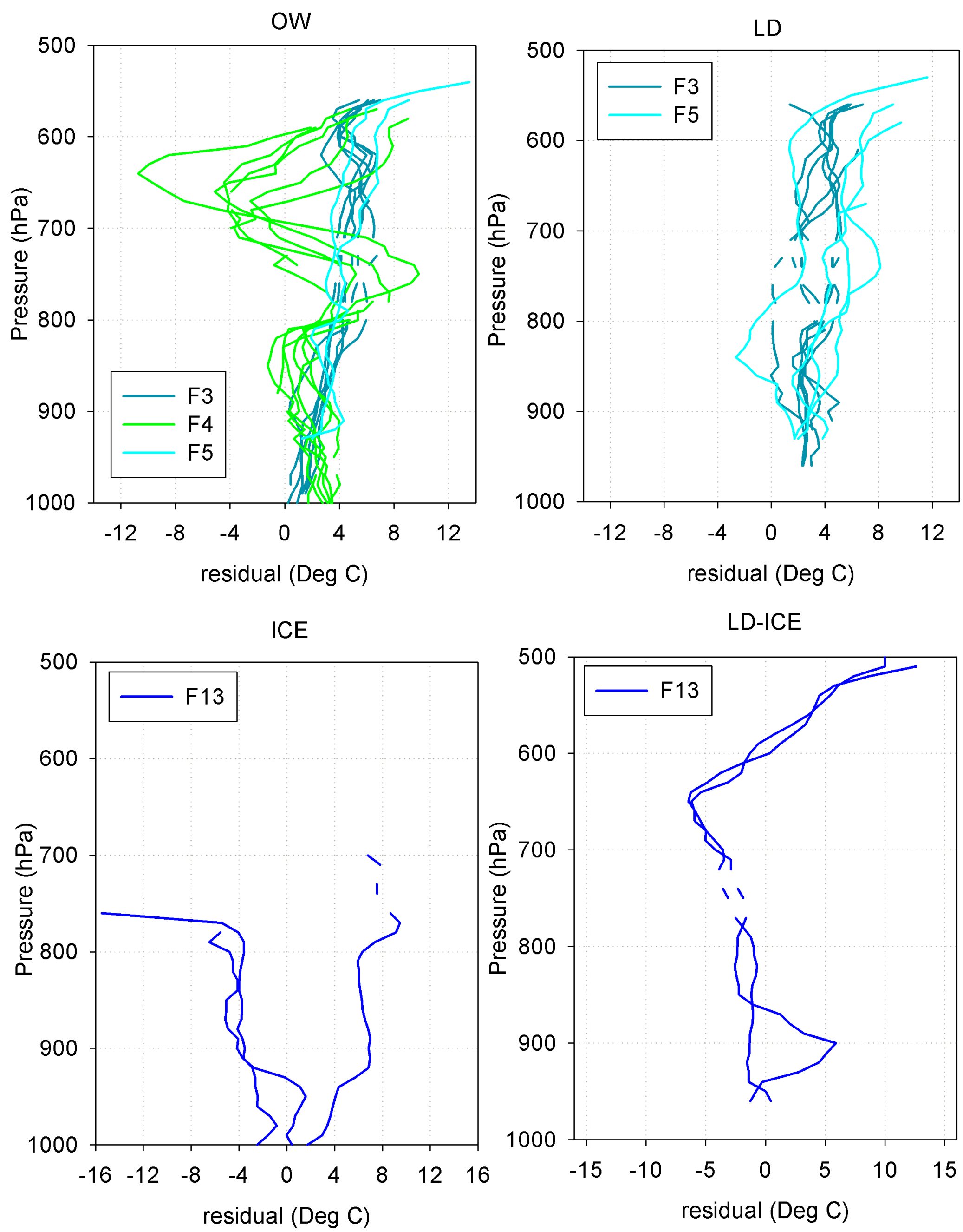

Figure B2-3: Bias (black line) and GEM-LAM 2.5 model residuals (coloured lines), from the comparison of extracted GEM-LAM 2.5 sounding profiles to dropsonde data for Specific humidity (g kg^{-1}). Data is plotted by surface environment, and each case study is shown with a unique colour. Residual (model minus observation).

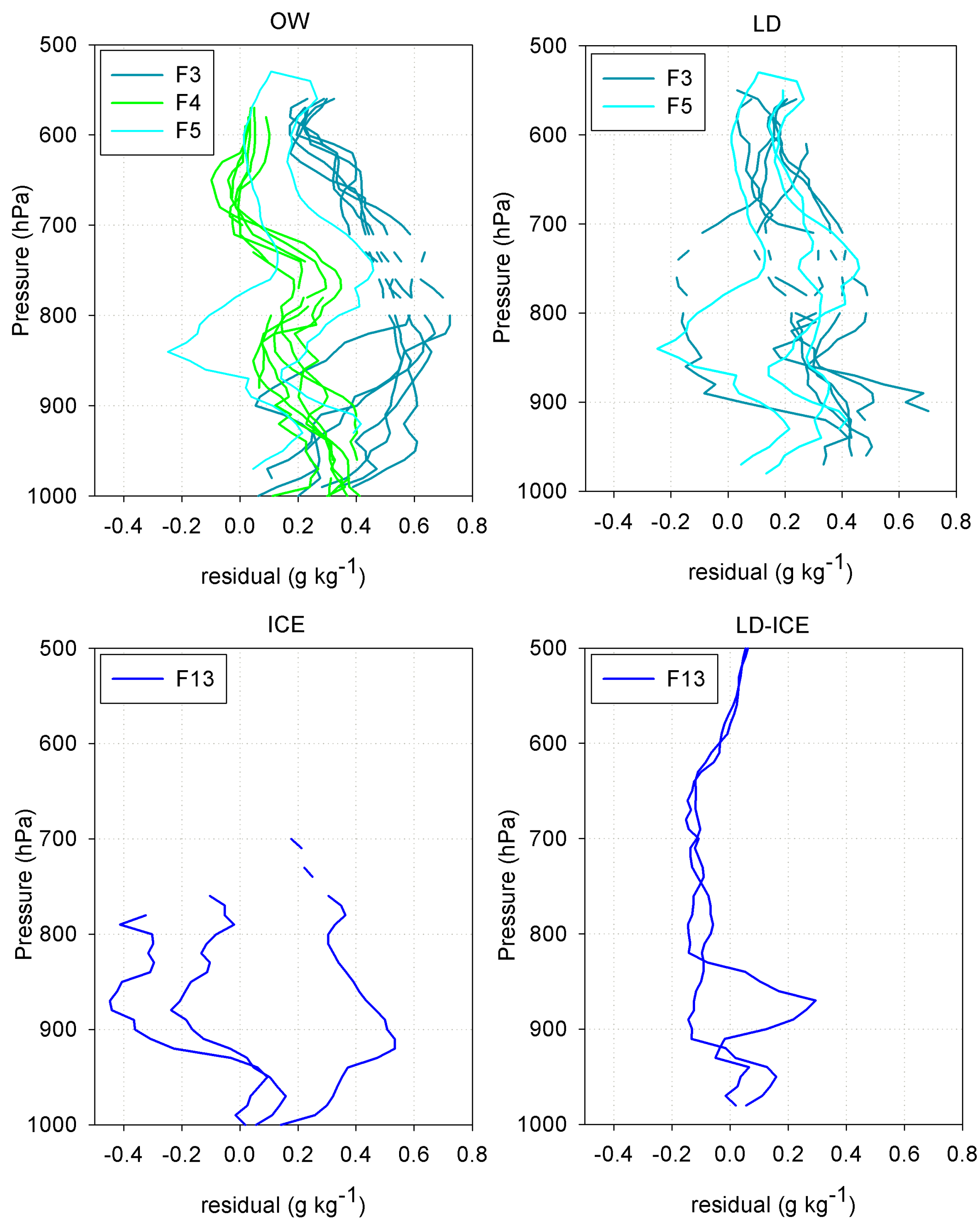

Figure B2-4: Bias (black line) and GEM-LAM 2.5 model residuals (coloured lines), from the comparison of extracted GEM-LAM 2.5 sounding profiles to dropsonde data for Wind Speed (m s^{-1}). Data is plotted by surface environment, and each case study is shown with a unique colour. Residual (model minus observation).

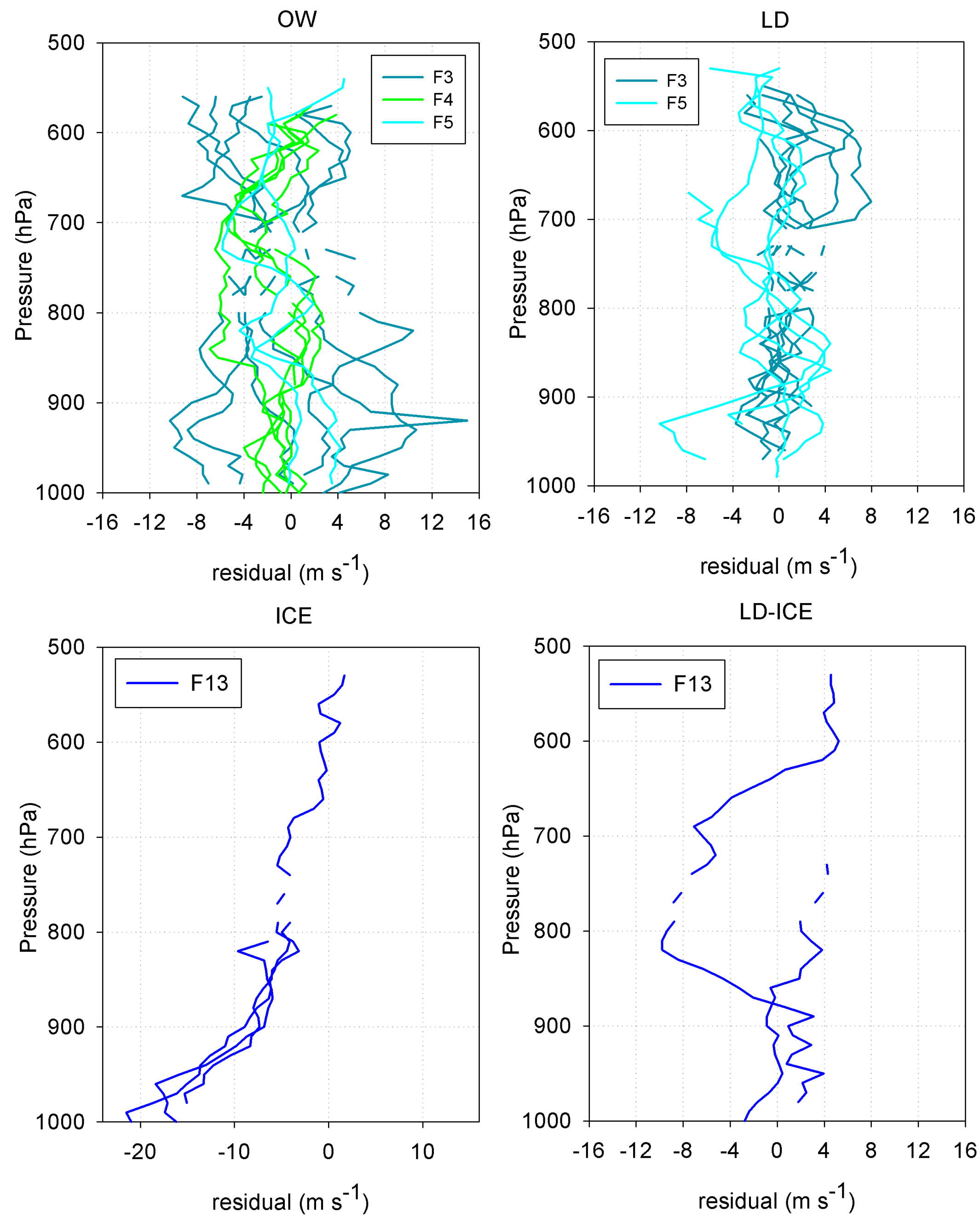

Figure B2-5: Bias (black line) and GEM-LAM 2.5 model residuals (coloured lines), from the comparison of extracted GEM-LAM 2.5 sounding profiles to dropsonde data for Wind Direction (Deg). Data is plotted by surface environment, and each case study is shown with a unique colour. Residual (model minus observation).

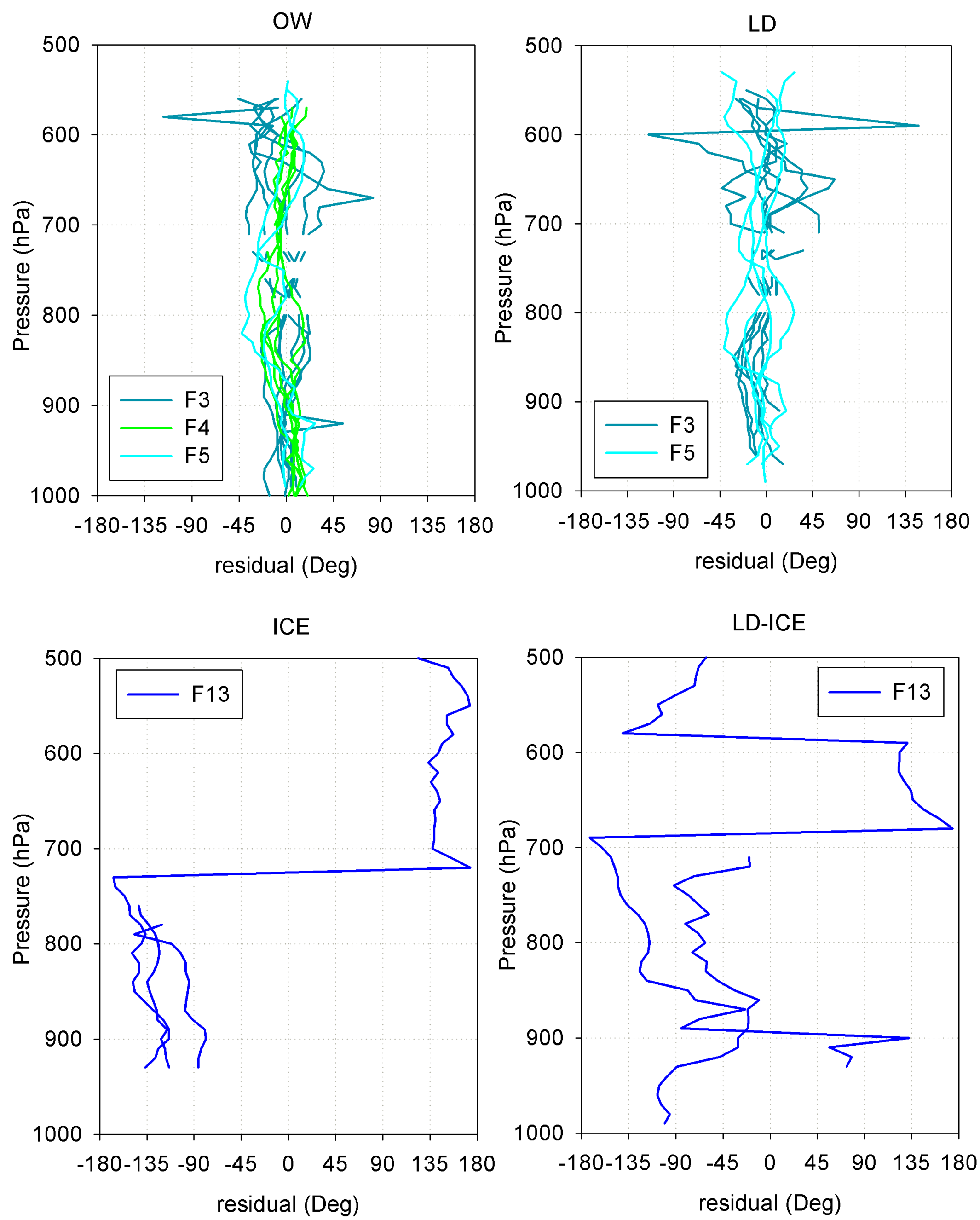

APPENDIX C: ADDITIONAL CONTRIBUTIONS

Publications and technical reports

In additional to the three papers contained in the body of this thesis, I also co-authored two peer-reviewed articles and was the lead author of the Storm Studies in the Arctic Data Report.

Gordon, M., Biswas, S., Taylor, P. A., Hanesiak, J., Albarran-Melzer, M., and Fargey, S. (2010). Measurements of drifting and blowing snow at Iqaluit, Nunavut, Canada during the star project. *Atmosphere-Ocean, 48,* 81-100. doi: 10.3137/AO1105.2010

In this paper, I assisted the lead author with field sampling and data collection.

Hanesiak, J., Stewart, R.E., Taylor, P., Moore, K., Barber, D., McBean, G., Strapp, J.W. Wolde, M., Goodson, R., Hudson, E., Hudak, D., Scott, J., Liu, G., Gilligan, J., Biswas, S., Desjardins, D., Dyck, R., Fargey, S., Field, R., Gascon, G., Gordon, M., Greene, H., Hay, C. Henson, W., Hochheim, K., Laplante, A., Martin, R., Melzer, M.A., and Zhang, S. (2010). Storm Studies in the Arctic: The meteorological field project. *Bulletin for the American Meteorological Society. 91,* 47-68. doi:10.1175/2009BAMS2693.1.

In this paper, I provided the lead author a summary of field data collected and other information related to intensive observation periods and aided in the composition two figures (one of the study and the other of data collection sites).

Fargey, S., Hanesiak, J., Liu, G., Gilligan, J., and Stewart, R. (editors) (2008). Storm Studies in the Arctic (STAR) Data Report. Centre for Earth Observation Science, 440 Wallace Building, University of Manitoba, Winnipeg, Manitoba, Canada, 75 pages.

In this technical report, I summarized the field data collected during STAR and other information related to intensive observation periods.

Conference Presentations

Fargey, S., Hanesiak, J. and R. Goodson (2014). An evaluation of vertical profiles using a limited area numerical weather prediction model over Baffin Island, Nunavut and surrounding area during autumn 2007. *American Meteorological Society 15th Mountain Meteorology Conference.* San Diego, CA, USA. August 18-22, 2014. (Interactive Presentation)

Fargey, S., Henson, W., Hanesiak, J. and R. Stewart (2012). Influence of topography on a snowfall event in Iqaluit, NU, with comparisons to GEM-LAM. *American Meteorological Society 14th Mountain Meteorology Conference.* Steamboat Springs CO, USA. August 20-24, 2012. (Oral Presentation)

Fargey, S., Hanesiak, J., Strapp, W., and M. Wolde. (2010). Measurements of Orographic Cloud and Precipitation over Southern Baffin Island. *American Meteorological Society Conference on Mountain Meteorology*. Squaw Valley, CA, USA. August 30 – September 3, 2010. (Oral Presentation)

Fargey, S., Hanesiak, J., Strapp, W., and M. Wolde. (2010). Characteristics of Orographic Cloud and Precipitation in the Arctic during STAR. *American Meteorological Society 13th Cloud Physics Conference.* Portland, Oregon, USA. June 28 - July 2, 2010. (Interactive Presentation)

Fargey, S., Hanesiak, J., Martin, R., Strapp, W., and M. Wolde. (2010). A Summary of Results: Characteristics of Upslope Precipitation in the Arctic during STAR. *STAR Final Workshop*. Winnipeg, MB, Canada. June 14-15, 2010. (Oral Presentation)

Fargey, S., Hanesiak, J., Martin, R., Strapp, W., and M. Wolde. (2010). Characteristics of Upslope Precipitation in the Arctic during STAR. *Canadian Meteorological and Oceanographic Society 43rd Annual Congress,* Ottawa, ON, Canada. May 30-June 4, 2010. (Oral Presentation)

Fargey, S.E. and J.M. Hanesiak. (2009). Upslope Precipitation Features in the Canadian Arctic. *MOCA - International Association of Meteorology and Atmospheric Sciences (IAMAS),* Montreal, QC, Canada. July 19-29, 2009. (Oral Presentation)

Fargey, S.E. and J.M. Hanesiak. (2009). Characterization of Upslope Precipitation in the Eastern Canadian Arctic, using a Research Aircraft. UK Polar Network, Atmospheric Workshop, Cambridge, England. April 28-May 1, 2009. (Interactive Presentation)